

**A Comparison of 1D Beam-element and 3D Solid-element based Modelling  
Approaches based on a Developed Tool for the Nonlinear Analysis of  
Reinforced Concrete Structural Components**

Clément Uwitonze

**A Thesis in**

**The Department**

**of**

**Building, Civil and Environmental Engineering**

**Presented in Partial Fulfillment of the**

**Requirements for the Degree of Master of Applied**

**Science (Civil Engineering) at Concordia University**

**Montréal, Québec, Canada**

March 2024

©Clément Uwitonze, 2024

# CONCORDIA UNIVERSITY

School of Graduate Studies

This is to certify that the thesis prepared

By: Clément Uwitonze

Entitled: **A Comparison of 1D Beam-element and 3D Solid-Element Based Modelling, Approaches based on a Developed Tool for the Nonlinear Analysis of Reinforced Concrete Structural Components**

and submitted in partial fulfillment of the requirements for the degree of

**Master of Applied Science (Civil Engineering)**

complies with the regulations of this University and meets the accepted standards with respect to originality and quality.

Signed by the Final Examining Committee:

\_\_\_\_\_  
*Prof. Khaled E. Galal* Chair

\_\_\_\_\_  
*Prof. Khaled E. Galal* Examiner

\_\_\_\_\_  
*Prof. Ahmed Soliman* Examiner

\_\_\_\_\_  
*Dr. Emre Erkmen* Supervisor

Approved by

\_\_\_\_\_  
Dr. Samuel Li, Chair of Department of Building, Civil and Environmental Engineering

March 2024

\_\_\_\_\_  
Dr Mourad Debbabi, Dean of  
Faculty of Engineering and Computer Science

# **Abstract**

## **A Comparison of Beam and Solid Element Based Modelling**

### **Approaches based on a Developed Tool for the Nonlinear Analysis of Reinforced Concrete Structural Components**

Clement Uwitonze

Nonlinear material models are needed for the capacity analysis of structural components. Often, 1D-beam element-based models are preferred over more sophisticated solid element-based modeling approaches due to their efficiency. However, their reliance on uniaxial material representations often overlooks the crucial influence of shear stresses, potentially leading to inaccuracies in predicting structural responses. In response, this study introduces a novel approach by integrating a multi-axial 3D concrete model within a 1D finite element framework, effectively capturing the effects of shear stresses. The proposed multi-axial elasto-plastic concrete model offers a comprehensive representation of concrete behavior under both tension and compression, thus enhancing the predictive capabilities of the analysis. By adopting a 1D beam-type finite element formulation, the research enables a detailed examination of shear wall behavior under lateral loading conditions. The main purpose of the thesis is to validate the developed finite element analysis tool which employs a sophisticated 3D concrete material model. The inelastic material behaviour of steel reinforcements bars has also been considered in the analysis. For the beam-type finite element, a 2-node formulation was adopted based on the Timoshenko theory so that the shear deformation effects are also considered in the analysis. For the modelling of the concrete bulk with 3D material model, the 8-node solid element with 6-degrees-of-freedom per node including the nodal rotations was adopted. The numerical formulation is then used for pushover analysis of beams and shear walls and compared with experimental results from literature for validation purposes. Five different structural components are tested. Validation efforts include comparisons with experimental data from existing literature and alternative modelling approaches. Parametric studies are conducted by changing the span sizes of the structural components.

## Dedication

I cannot express enough Dr Emre Erkmen's impact on my life, Dr Emre Erkmen accepted openhandedly to be my master's supervisor. His unwavering support, knowledge, dedication, and invaluable guidance were instrumental throughout this research program. Your presence and assistance have been a constant source of inspiration. May God bless and fulfill your dreams.

I would also like to express my profound gratitude to the Almighty Jesus Christ for guiding me through this journey and providing me with the strength and wisdom to persevere. His grace has been a constant source of comfort and hope. If it wasn't you, I wouldn't have done anything.

I am deeply indebted to my life partner, Prisca, for being my rock, my confidante, and my source of unwavering support and encouragement. Her love and belief in me have been the driving force behind my success. Her sacrifices, understanding, and unwavering faith in my endeavors have been the foundation upon which I built my academic and professional journey. It would not be possible for me to accomplish this challenge without your love. May God bless You abundantly.

My gratitude also goes to my parents and siblings, whose unconditional love, support, and inspiration have been my pillars of strength. Despite the physical distance, their prayers and well-wishes have accompanied me every step of this journey, without which I would not have achieved this milestone. I would like to offer a special acknowledgment to my father for his enduring motivation and financial support. May you be eternally blessed and have your faith only strengthen in Jesus Christ

Lastly, I want to express my appreciation to my uncle Francois, my brothers and sisters for their prayers and all those who provided words of encouragement. Your kindness has been a source of motivation, and I am truly thankful for your presence in my life.

# Table of Contents

<b>List of Figures .....</b>	<b>ix</b>
<b>Chapter 1 Introduction .....</b>	<b>1</b>
1.1. Overview.....	1
1.2. Problem Statement.....	2
1.3. Objective.....	2
1.4. Scope.....	2
1.5. Outline of the Thesis.....	3
<b>Chapter 2 Literature review.....</b>	<b>4</b>
2.1. Introduction.....	4
2.2. FRP reinforced members .....	5
2.3. Modelling of Structural Components.....	8
2.3.1. Introduction.....	8
2.3.2. Concrete Modelling.....	14
2.3.3. Computational Plasticity .....	18
2.4. Uni-axial material models.....	28
2.5. Multi-axial material models.....	30
2.6. Case studies.....	36
<b>Chapter 3 Material FORTRAN code model.....</b>	<b>38</b>
3.1. Introduction.....	38
3.2. Non-associative Multi-surface Plasticity .....	39
3.2.1. Plastic Flow Rule .....	39
3.2.2. Plastic Consistency Condition.....	40

3.3.	Computational Algorithm .....	42
3.3.1.	Plastic deformation.....	43
3.3.2.	Possible Scenarios of the Return Algorithm .....	48
3.3.3.	Parameters Considering Viscosity update .....	50
3.3.4.	Material Definition in Heigh-Westergaard Coordinates.....	51
3.4.	Material Model Specifics.....	55
3.4.1.	Menetrey-Willam Yield Surface for Compression.....	55
3.4.2.	Potential Function for Compression.....	58
3.4.3.	Rankine Yield Surface for Tension Cut-off .....	58
3.5.	Solution of the Global Equilibrium Equations.....	59
3.5.1.	Variational Form of the Equilibrium Equations .....	59
3.5.2.	Linearization of the Equilibrium Equations .....	59
3.5.3.	Selected Finite Element Types .....	61
3.5.4.	Uni-axial Sugano Model for 1D Beam-Type Analysis .....	61
<b>Chapter 4</b>	<b>Description of the finite element models .....</b>	<b>64</b>
4.1.	ABAQUS Model.....	64
4.1.1.	Concrete model in ABAQUS .....	64
4.1.2.	Reinforcements in ABAQUS .....	65
4.1.3.	Finite Element Types and Meshing in ABAQUS .....	65
4.1.4.	Boundary Condition and Loading in ABAQUS.....	66
4.2.	Model properties .....	66
4.2.1.	Beams.....	66
4.2.2.	Shear walls .....	71
<b>Chapter 5</b>	<b>Numerical results.....</b>	<b>76</b>
5.1.	Introduction.....	76

5.2.	Validation of the Numerical Model .....	76
5.2.1.	Beams.....	76
5.2.2.	Shear walls .....	78
5.3.	Parametric Studies on Shortened members.....	79
5.3.1.	Beams.....	80
5.3.2.	Shear walls .....	81
5.4.	Parametric Studies on Elongated members.....	83
5.4.1.	Beams.....	83
5.4.2.	Shear walls .....	86
5.5.	Limitations .....	88
	<b>Conclusions .....</b>	<b>89</b>
	<b>Future work recommendation .....</b>	<b>90</b>
	<b>References .....</b>	<b>91</b>
	<b>APPENDIX 1 SE_Plasticity_Plane User Guide.....</b>	<b>108</b>
A1.1.	Data entry and solutions.....	108
A1.1.1.	Input files for static 1D Beam-Type model .....	108
A1.1.2.	Output files for static 1D Beam-Type model.....	108
A1.2.	Input files .....	109
A1.3.	Example 1. Beam Analysis .....	113
A1.3.1.	Input files.....	113
A1.3.2.	Input check .....	122
A1.3.3.	Output files .....	128
<b>A1.4.</b>	<b>Example 2. Shear Wall Analysis .....</b>	<b>148</b>
<b>A1.4.1.</b>	<b>Input files.....</b>	<b>148</b>
<b>A1.3.2.</b>	<b>Input check.....</b>	<b>155</b>

<b>A1.3.3. Output files</b> .....	163
<b>APPENDIX 2 ReinCon3D6DOF User Guide</b> .....	<b>176</b>
A2.1. Data entry and solutions.....	176
A2.1.1. Input files for static 3D model.....	176
A2.1.2. Output files for static 3D model .....	177
A2.2. Input files .....	177
A2.3. Example 1. Beam Analysis .....	182
A1.3.1. Input files.....	182
A1.3.2. Input check .....	191
A1.3.3. Output files .....	224



# List of Figures

Figure 2-1. Euler-Bernoulli beam theory.....	10
Figure 2-2. Timoshenko beam theory .....	11
Figure 2-3. Plane-frame element .....	11
Figure 2-4. Multi-fiber beam model .....	12
Figure 2-5. Unloading to the origin (Jirasek & Bazant, 2002) .....	21
Figure 3-1. Comparison between the Associative Flow rule and the Non-associative Flow rule.....	39
Figure 3-2. Two surface model in Rendulic Plane .....	52
Figure 3-3. Deviatoric Plane Menetrey & Willam (1995) .....	56
Figure 4-1. Reinforcement configuration in ABAQUS. ....	65
Figure 4-2. Shallow S-C1-9 beam test setup and dimensions (units in mm) .....	67
Figure 4-3. ABAQUS Depiction of S-C1-9 beam (top: meshed beam, bottom: reinforcement) .....	67
Figure 4-4. Shallow S-C1-9 beam FEAVIEWER configuration .....	67
Figure 4-5. Deep D-C1-9 beam test setup and dimensions (units in mm) .....	68
Figure 4-6. ABAQUS Depiction of D-C1-9 beam (top: meshed beam, bottom: reinforcement) .....	68
Figure 4-7. Deep D-C1-9 beam FEAVIEWER configuration .....	68
Figure 4-8. Reinforcement details of ISO30-1 beam (Benmokrane et al. (1995) .....	69
Figure 4-9. ABAQUS Depiction of ISO30-1 beam (top: meshed beam, bottom: reinforcement) .....	69

Figure 4-10. ISO30-1 beam FEAVIEWER configuration .....	70
Figure 4-11. Top view dimensions and reinforcement details of SW-1 .....	71
Figure 4-12. Elevation of SW-1 .....	72
Figure 4-13. ABAQUS Depiction of SW1 shear wall (Left: meshed beam, Right: reinforcement) .....	72
Figure 4-14. SW-1 Shear wall FEAVIEWER configuration .....	73
Figure 4-15. G-15 concrete dimensions and details of reinforcement configuration .....	74
Figure 4-16. ABAQUS Depiction of shear wall G15 (Left: meshed version, Right: reinforcement) .....	74
Figure 4-17. G15 Shear wall FEAVIEWER configuration.....	75
Figure 5-1. Force – Displacement curve for shallow CFRP beam (S-C1 × 9).....	77
Figure 5-2. Force - Displacement curve for Deep CFRP beam (D-C1 × 9).....	77
Figure 5-3. Force – Displacement for ISOROD GFRP beam (ISO30-1).....	78
Figure 5-4. Force – Displacement curve for G15 shear wall.....	79
Figure 5-5. Force - Displacement curve for SW-1 shear wall.....	79
Figure 5-6. Depiction of the Shortened D-C1-9 (Right: meshed version, Left: reinforcement) .....	80
Figure 5-7. Load - deflection curve for the Shortened D-C1-9 .....	80
Figure 5-8. Depiction of Shortened S-C1-9 (Left: meshed version, Right: reinforcement).....	80
Figure 5-9. Load - deflection curve for the Shortened S-C1-9.....	81
Figure 5-10. Depiction of the Shortened SW-1 (Left: meshed version, Right: reinforcements).....	81
Figure 5-11. Load - deflection curve for the Shortened SW-1 .....	82

Figure 5-12. Depiction of the Shortened G15(Left: meshed version, Right: reinforcements) ..... 82

Figure 5-13. Load - deflection curve for the Shortened G15 ..... 83

Figure 5-14. Depiction of the elongated D-C1-9 (Top: meshed version, Bottom: reinforcement) ..... 83

Figure 5-15. Load - deflection curve for the elongated D-C1-9..... 84

Figure 5-16. Depiction of elongated S-C1-9 (top: meshed version, bottom: reinforcement)..... 84

Figure 5-17. Load - deflection curve for the elongated S-C1-9 ..... 85

Figure 5-18. Depiction of the elongated ISO30-1(Left: meshed version, Right: reinforcements) ..... 85

Figure 5-19. Load - deflection curve for the elongated ISO30-1 ..... 86

Figure 5-20. Depiction of the elongated SW-1 (Left: meshed version, Right: reinforcements) ..... 86

Figure 5-21. Load - deflection curve for the elongated SW-1..... 87

Figure 5-22. Depiction of the elongated G15(Left: meshed version, Right: reinforcements)..... 87

Figure 5-23. Load - deflection curve for the elongated G15 ..... 88

# Chapter 1

## Introduction

### 1.1.Overview

In the vast majority of civil engineering applications, reinforced concrete beams are used as flexural structural components to span distances. On the other hand, Reinforced Concrete Columns and Shear walls are also commonly used in building design, where those members are dominantly subjected to compressive stresses.

To forecast their response, analytical and numerical techniques can be adopted. However, analytical solutions can only be applied to limited number of cases. For example, analytical solutions of deformations and internal forces of a statically determined homogeneous beam can be obtainable only if concrete does not crack. To completely describe the "problem," it is required to take into account the sources of cross-sectional heterogeneity, including the influence of reinforcement, material non-linearity due to concrete damage, and the relative slip between constitutive materials.

Since the problem is no longer statically determinate or linear elastic, a non-linear analysis technique must be adopted to obtain the solution that satisfies equilibrium and compatibility conditions along with the constitutive material laws.

In the context of phenomenological material modeling, the inelastic response of materials is associated with two distinct mechanical phenomena: plasticity, involving dislocations along slip planes, and damage, which entails the nucleation and coalescence of cracks. Phenomenological models grounded in coupled elastoplastic-damage theory exhibit the ability to capture both the enduring deformations caused by the plastic component and the reduction in elastic moduli resulting from the damage component.

## **1.2.Problem Statement**

Understanding the failure behavior of reinforced concrete structural components is very important in order to ensure the safety, durability, and good performance of civil engineering structures. To conduct accurate and reliable failure analyses, engineers and researchers rely on advanced computer modeling approaches.

The modelling approaches for the analysis of structural components made of reinforced concrete are based on both beam-element and solid-element modelling. Beam-element models are widely used for the study of structural components where uni-axial material models are commonly used due to their computational efficiency. However, the significance of shear stresses on the behavior of the material is ignored by such material models.

## **1.3.Objective**

The objective of this study is a multi-axial elasto-plastic material model for concrete and adopt it for both 3D solid-element as well as 1D beam-element type modelling to integrate the impacts of confinement pressure and shear stresses. In order to do this, a multi-axial elasto-plastic material model for concrete is suggested and used for modelling 1D beam elements in along with 3D solid elements.

To achieve this objective, the following specific goals will be pursued:

- **Examine the approaches employed in conducting a 3D structural analysis of reinforced concrete structural elements, integrating a multi-surface elasto-plastic material model.**
- **Validate the developed modelling techniques using the ABAQUS program.**
- **Check the correctness of the numerical technique by comparing the findings to prior work's experimental results.**

## **1.4.Scope**

To achieve the objective of this research, computational technology is adopted. The FORTRAN programming language is used to implement the numerical procedures. This program offers a user-friendly interface that simplifies the process from pre-processing to post-processing. It requires minimal input and

the user is guided with keywords throughout the process. The 1D user-guide is described in [Appendix 1](#) and the 3D user-guide is in [Appendix 2](#).

Comparisons are made between Beam and solid type modelling approaches with the purpose of identifying the confinement effects. To capture the behavior of concrete beyond elasticity, the material model based on the plasticity theory is used. Both steel and FRP reinforced concrete beams will be investigated. Various failure mechanisms are identified.

To ensure the reliability of the developed tool, its results with those based on experimental data were compared. Additionally, a finite element model is crafted within the ABAQUS software platform to analyze reinforced concrete beams and shear walls comprehensively. ABAQUS offers versatile capabilities for analyzing such structures, accommodating steel or FRP reinforcements. Consequently, employing ABAQUS provides a reliable means to corroborate the findings obtained from the numerical approach.

## **1.5. Outline of the Thesis**

The thesis is structured across six chapters, with each contributing distinct insights and analysis to the overarching research endeavor.

- Chapter 2 offers a comprehensive review of modelling techniques, delving into existing formulations and models pertinent to reinforced concrete structures. It also provides a succinct overview of prior literature and publications in the field, including discussions on finite element modelling. Furthermore, this chapter concludes with a detailed presentation of the case study.
- Chapter 3 elucidates the intricacies of the multi-surface Elasto-Plastic Material Model, outlining the behavior of elasto-plastic materials and expounding upon the components of plasticity models.
- Chapter 4, the finite element model within the ABAQUS software is meticulously delineated, encompassing concrete, reinforcement, and FRP elements.
- Chapter 5 serves as the focal point for presenting the primary findings and results derived from the numerical methodology, encompassing both FORTRAN code and ABAQUS simulations. This chapter meticulously validates the 3D and 1D material models against ABAQUS simulations and experimental data from prior studies.
- The conclusion and future work recommendation

# Chapter 2

## Literature review

### 2.1.Introduction

The development of extremely powerful computers and sophisticated non-linear numerical analysis software, however, as well as the challenges in finding a prognostic solution for complex structural cases have all encouraged the adoption of numerical methods for the majority of engineering applications. The most used numerical method right now is the finite element method. If used correctly, it offers quick, efficient solution schemes with the accuracy the user specifies, based on the specific instance.

The adoption of the finite element approach in the given research is decided by a variety of parameters, including:

- a. **The size of the construction, whether it is a single member or the full structure**
- b. **The problem's difficulty (one dimension, two dimensions, or three dimensions)**
- c. **The desired outcomes (global or local features)**
- d. **The degree of accuracy**
- e. **The model's limitations (material or mathematical non-linearity, computational apparatuses available)**

When performing a limited component examination, the examiner's main pressing concern is usually the balance between precision and computational expense. For the global investigation of a huge structure, a full model would most likely be computationally "expensive" or even superfluous. When looking at simple geometries or structural components, on the other hand, a more sophisticated model that can describe more complicated phenomena is often possible and necessary. Non-linearity types that arise from either the material manner of behaving or the calculation of the example, as well as nearby scale impacts. To capture the aforementioned properties, advanced computational approaches must be created. The term "advanced"

can refer to more sophisticated constitutive models for materials or to additional components that must be incorporated in addition to the structural components that comprise the majority of the model.

In structural engineering practice, beam-type one-dimensional finite element formulations are frequently utilized as analysis and design tools for structural components. These models offer computational efficiency, which is particularly crucial in nonlinear analysis scenarios, and facilitate easier interpretation of results for design purposes. Among the various modeling approaches employed for the nonlinear analysis of reinforced concrete buildings, the lumped plasticity approach stands out as one of the simplest and most commonly adopted methods. This approach leverages the predicted moment distribution in frame buildings subjected to earthquake-induced lateral loads, allowing engineers to effectively assess the structural response and design appropriate reinforcement strategies.

## **2.2. FRP reinforced members**

High-strength synthetic or organic fibers encased in a resin matrix typically make up FRPs. For applications in civil engineering, carbon (CFRP), aramid (AFRP), and glass (GFRP) are the FRPs that are most frequently utilized. In the real world, they are used as ground anchors, reinforcement for reinforced and prestressed concrete elements, and for strengthening or repairing existing concrete structures. Due to a dearth of research information and design guidelines, its extensive application in reinforced concrete structural engineering has been severely constrained.

These materials' strong corrosion resistance, high tensile strength, and light weight are advantages. According to the kind of FRP product and surface treatment, other typical features of FRP materials include their relatively low modulus of elasticity, linear stress-strain relationship till failure, and varied bond properties ([Galati et al., 2006](#)). Both the bond performance of reinforcement and the shear strength of FRP materials are impacted by their anisotropic behavior. Additionally, splitting cracks and concrete cover failure may result from the anisotropic behavior of FRP bars and the high transverse coefficient of thermal expansion with respect to concrete ([Aiello et al., 2001](#)).

In comparison to steel bars, FRP bars typically have a lower elastic modulus and a higher tensile strength. In order to meet the restrictions of deflection and crack width, FRP reinforced concrete beams must thus be over reinforced ([Jaeger et al., 1997](#)). As a result, the serviceability limit states frequently determine the



design. As a result, numerous research projects have been focused on developing accurate analytical, numerical, and design methods for the prediction of deflections and crack width (Gao et al., 1998) as well as theoretical advancements regarding specific models of composite structures (Barretta et al., 2015; Barretta & Luciano, 2014). Some of the suggested techniques (Gravina & Smith, 2008) make use of the local bond slip relationship that distinguishes the FRP-concrete interface and is a distinctive quality of every single FRP product. Other studies (Kara et al., 2013) are aimed to calibrate the coefficients of a simple equation for the prevision of the deflection in the frame of the Branson's method (Branson, 1977).

When it comes to FRP and steel bars, the bond to concrete shear stress transmission phenomena is different. This is caused by the FRP bars' lower modulus of elasticity, the resin matrix's lower shear strength compared to steel, and the different coefficient of thermal expansion. Additionally, in the case of FRP and steel bars, the impact of transversal stresses and the size of the concrete cover are also different (Seo et al., 2013). There have been several experimental investigations on this subject (Cosenza et al., 1997); some of these were based on pull-out tests, which seem inappropriate for examining the bending behavior of concrete parts (Oh et al., 2007). To assess the relationship between concrete strength and bond properties, additional investigations were carried out. According to Achillides and Pilakoutas (2006), the strength of the concrete has no bearing on the binding of FRP bars to it. Concrete with strengths ranging from 29 to 60 MPa was used in Okelo and Yuan's (2005) study of the bond behavior of FRP reinforced parts. They discovered that when the concrete grade rises, bond performance is better. According to some research, a strong connection is not necessarily desired in FRP bars since it may cause localized overstress and an early failure of the member (Darby et al., 2007).

The absence of plastic deformations in FRP bars indicates that the reinforcements are incompatible with ductile behavior, which is needed, for example, in main members (beams and columns) of earthquake-resistant frame structures. Due to this, the majority of applications for FRP reinforcing bars have focused on structural components in many nations, such as floor structures, concrete slabs, and concrete members supporting hollow-tile floors, for which ductility is not a major concern (Rizkalla et al., 2003).

Utilizing FRP bars in the building of bridge decks is another useful usage for them. In this instance, the static redundancy of the structure and the FRP bars' superior corrosion resistance properties play a major

role in limiting deflections. Additionally, these structures frequently lack transverse reinforcement, leaving them vulnerable to a shear-related early collapse (Tureyen & Frosch, 2002).

In order to resist lateral stresses brought on by wind or seismic occurrences, multistory structures must have a suitable amount of stiffness. In compared to alternative lateral-resisting systems, reinforced concrete shear walls, which have a high in-plane stiffness, have been shown to provide good, cost-effective lateral resistance (Cardenas et al. 1973; Wyllie et al. 1986; Fintel 1995). Shear-wall constructions have the advantages of reduced deformation and nonstructural element damage as compared to frame-type structures.

Despite this, the weather conditions that lead to the extensive use of deicing salts during the winter months typically speed up the rusting of steel reinforcement, resulting in the degradation of reinforced concrete buildings, particularly bridges and multistory garages.

One of the various methods proposed to improve the corrosion resistance of reinforced concrete structures is the use of fibre reinforced plastic (FRP) rebars in place of steel rebars (Clarke, 1993). Particularly in situations where traditional steel-reinforced concrete has produced poor service, FRP rebar provides tremendous promise for application in reinforced concrete construction (Neale & Labossière, 1992).

Due to these circumstances, other forms of reinforcement were required to solve the corrosion issues. ACI 440R (ACI 2007; Fédération Internationale du Béton (fib) 2007; ISIS Canada 2007) states that the effective application of fiber-reinforced polymer (FRP)-reinforcing bars as concrete reinforcement in a wide range of building elements has achieved an acceptable level. FRP bars have been used into a variety of building elements, including beams, one-way and two-way slabs, and columns (Kassem et al. 2011; Bakis et al. 2002; El-Salakawy et al. 2005; Sharbatdar and Saatcioglu 2009; Tobbi et al. 2012). This is because of their benefits. More than 20 years ago, the initial use of FRP bars in reinforcing beams demonstrated how expensive they were compared to steel bars. Although FRP materials are more expensive than steel, they also have cheaper shipping and handling expenses as a result of the smaller weight of the components. In addition, compared to steel-reinforced structures, FRP-reinforced structures require far less long-term maintenance. Investigation of the inelastic behavior of shear walls completely reinforced with FRP is required in order to construct a multistory building with acceptable stiffness employing FRP reinforcement.

[Yamakawa and Fujisaki \(1995\)](#) examined seven carbon-FRP (CFRP) grid-reinforced, one-third scale shear walls with dimensions of 800 mm by 950 mm by 80 mm. The walls have double-layered CFRP grid reinforcement with 100 mm meshes, giving them a 0.8% reinforcement ratio. When 1% drift and minimal energy dissipation were attained, the specimens quickly lost their ability to support lateral loads. This decrease in capacity was caused by three major flaws:

- (1) The CFRP grids could not support compressive stress and broke under low compressive stresses;**
- (2) Adequate development lengths needed to be designed to prevent the reinforcing bars from pulling out of the wall base; and**
- (3) The CFRP grid reinforcement did not provide concrete confinement.**

According to research on concrete shear walls reinforced with steel bars, factors affecting the behavior of shear walls, such as wall aspect ratio and configuration, axial load, shear-stress demand, and wall reinforcement ratios, have received the majority of attention ([Barda et al. 1977](#); [Wallace and Moehle 1992](#); [Sittipunt et al. 2001](#)). The design of reinforced concrete shear walls is governed by code provisions such as CSA A23.3 (CAN/CSA 2004) and ACI 318 (ACI 2008), which place emphasis on providing the necessary strength and stiffness to prevent or reduce damage from frequent earthquakes while ensuring adequate wall-deformation capacity ([Massone and Wallace, 2004](#)).

Therefore, this study focused on the behavior of shear walls with a medium aspect ratio, which are typical in parking garages and medium-rise structures. According to [Jiang and Kurama \(2010\)](#), the majority of shear walls built in the US and Canada are classed as medium rise structures with wall aspect ratios that generally range from 2 to 4. The lateral response of such shear walls is greatly influenced by nonlinear flexural and nonlinear shear deformations ([Massone et al., 2006](#)).

## **2.3. Modelling of Structural Components**

### **2.3.1. Introduction**

The process of creating a three-dimensional representation of an object or system using computer software is referred as 3D modeling. It allows the visualization and analyze of complex structures in a virtual environment. Simplified models or reduced-order models (ROMs) also known as reduced models, are

approximations of complex systems. They aim to capture essential behavior while minimizing computational effort. applying a single axial load (force or displacement) along one direction to a structure, the Sugano model is a uni-axial model that considers axial stress-strain relations along the longitudinal fiber. This modeling approaches determine material properties and behavior under simple loading conditions.

Since 3D solid components demand more computing work than 1D structural elements or 2D continuum elements, beams are often not simulated with them. The use of 3D features has several benefits. They are able to detect failure modes that other types of elements cannot, such as spalling and anchoring failure in support zones. Various modelling techniques may be used to represent the reinforcement in 3D solid parts. Each bar is represented by one 3D solid element with a different constitutive relation in a 3D solid element. With this approach, it is feasible to represent the reinforcement as embedded, allowing for complete interaction between the two materials, or to put an interface layer between the concrete and steel. The interface layer needs to be defined using a constitutive model in order to be able to prescribe the bond-slip action between the two materials. The reinforcement can alternatively be described as a 1D truss with each bar's cross section defined within a 3D solid or as a 2D plane with an equivalent thickness of reinforcement layer. According to [Lykidis et al. \(2008\)](#) in both situations, it is possible to represent the bond-slip relation in commercial software using specific interface components, such as embedded reinforcement or line-solid interfaces for 1D and plane-solid interfaces for 2D.

In general, a line with a specific cross-sectional area represents a one-dimensional element. It can be composed of a single material, which would make it homogeneous, or of multiple materials, which are then homogenized across the cross-section. The simplest FE model that can be implemented, which consists of two-node bar or truss elements with one or two translational degrees of freedom per node. Higher order 1D elements are also used when capturing more complex phenomena, which contain more than two nodes and higher order approximating functions. Beam or structural elements occupy a unique position within the 'family' of 1D elements.

As depicted in Figure 2-1, they exist in their simplest form as two-node elements with a vertical translational and rotational degree of freedom per node. It is likely the most well-known and extensively used finite element, owing primarily to the simplifications that typically underlie its constitutive theories and its

minimal computational cost, which make it very user-friendly. The principle that "plane sections remain plane and perpendicular to the reference axis of the beam," also known as the Euler-Bernoulli beam theory, covers an important section of such theories (Ottosen and Petersson, 1992). When the global response of a structure as a whole is desired, or when structural cases of extreme deformation are examined, they could be employed.

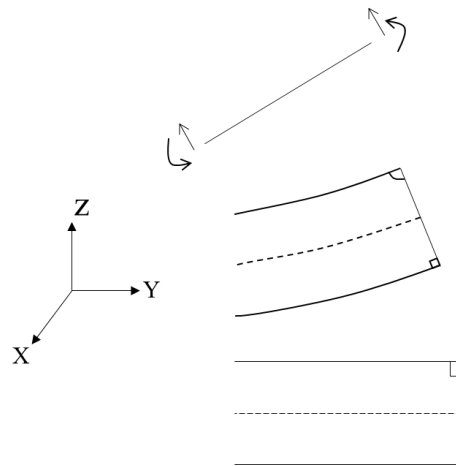
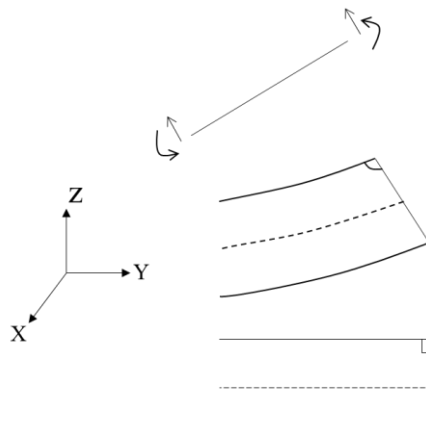


Figure 2-1. Euler-Bernoulli beam theory

The Timoshenko beam theory is also often used (Hjelmstad, 2005). This theory says that plane parts stay flat, but they don't have to be perpendicular to the reference line. Timoshenko bar component models are also employed for the global primary analysis; they offer benefits comparable to those of Euler-Bernoulli components, but their major usage is when shear activity is believed to be crucial for the prediction of the reaction of the part viable (Figure 2-2).



*Figure 2-2. Timoshenko beam theory*

The plane-frame element can be used with either of the two beam theories talked about so far, and it also takes into account the axial shift of the element's reference axis (Figure 2-3). The pertinent component is typically used in applications where the hub movement of the framework is important, such as recreations of plane casing structures. Consideration of the axial displacement degree of freedom is beneficial for modelling effects and geometries that occur and exist in the axial direction of the model, such as the reinforcement effect and the bold-slip in reinforced concrete members.

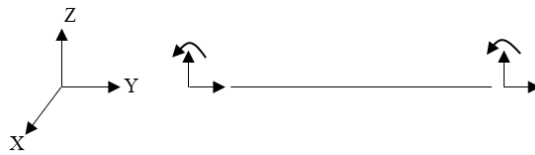


*Figure 2-3. Plane-frame element*

In addition to the previously mentioned fundamental structural elements, more advanced 1D beam-type models have been created. These are typically composed of multiple materials, homogenized across the cross-section, and modelled using more specialized techniques. The development of such models was necessitated by the need to account for more complex tasks in a simplified but nonetheless representative manner. These tasks may involve several localized phenomena that would be impossible to capture using the Euler-Bernoulli or Timoshenko beam theory alone.

As previously mentioned, simulating large civil engineering structures may be challenging. Therefore, a simplified technique has been developed. As a result, a method that has been developed has been provided (Spacone et al., 1996; Mazars et al., 2004; Kotronis and Mazars, 2005). Specifically, the assembly under consideration is discretized into beam elements that adhere to Euler-Bernoulli or Timoshenko beam theory. Typically, beams and other flexural members are analyzed using the Euler-Bernoulli beam theory. When shear effects are stronger, the Timoshenko theory for beams is used for understanding them. The unique aspect of the applicable method is the subdivision of the cross-section into fibres (Figure 2-4). In Figure 2-4, (i) Reinforced concrete specimen (ii) Discretization into elements, nodes, degrees of freedom (iii) Separation of the cross-section into fibers. Each fibre represents a finite cross-sectional area and is created from one of the constituent materials, concrete or steel.

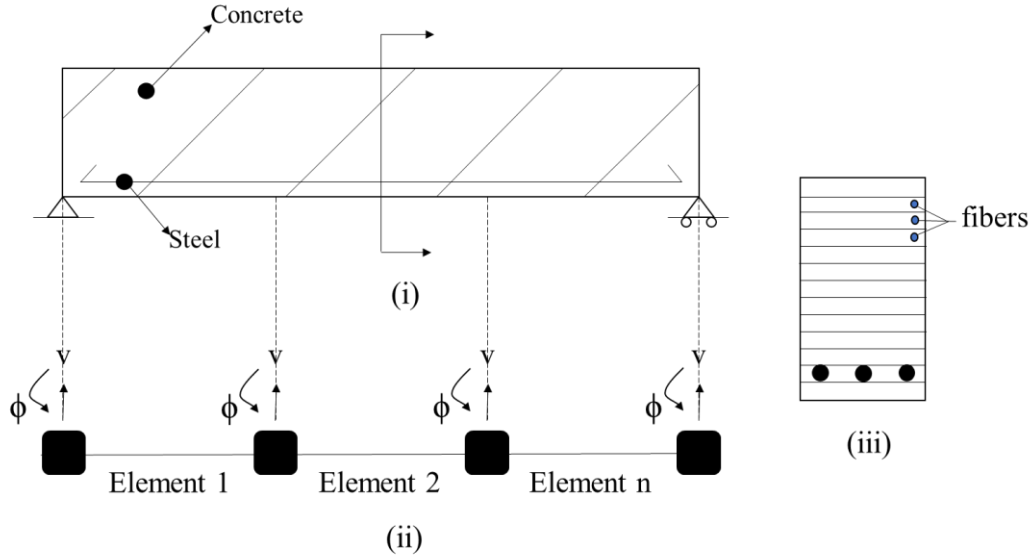


Figure 2-4. Multi-fiber beam model

The basic presumption that plain portions stay planar stays true in the suggested method's implementation strategy. The well-known beam theories discussed in the preceding paragraph are relevant based on that supposition.

The model's calculation is carried out at three different levels:

- a) the element level;
- b) the sectional level; and
- c) the fiber levels. The nodal displacements of the simulated member are connected to the normal strains (in the case of the Euler-Bernoulli beam theory) through the fundamental beam theories using a connection of the form.

$$\varepsilon_{xx} = \frac{\partial u^o}{\partial x} + z \frac{\partial^2 w}{\partial x^2} \quad \text{Eq. 2.1}$$

Where,  $\partial u^o / \partial x$ , accounts for the axial deformation of the reference axis of the beam,  $\partial^2 w / \partial x^2$  is the curvature, and  $z$  denotes the position of the fiber along the cross-section of the beam. In order to determine the stress at the location where the fiber resides along the cross-sectional height, the sectional strain of each

fibre as determined by Eq. 2.1 is then placed into the constitutive law that is allocated for the material of the fibre.

Composites in the infrastructure sector have the potential to offer considerable cost and durability reductions if used properly. High strength-to-weight and stiffness-to-weight ratios, chemical and corrosion resistance, adjustable thermal expansion and damping properties, and electro- magnetic neutrality are additional benefits. These benefits might result in improved safety and life expectancy as well as cost savings for equipment, fabrication, and maintenance.

Although Galileo's simple theories may have inspired early plasticity theories ([Jirásek & Bazant, 2002](#)), the linear-elastic model, which takes Hooke's rule as a given, has become the most widely used material model. But as processing power has increased and numerical analysis methods have been developed, nonlinear material models and analysis methodologies have advanced. The two primary methodologies created for the investigation of nonlinear material behavior can be seen to be the theory of plasticity and damage theory.

The idea of plasticity, which first emerged in the late nineteenth century, has been the preeminent framework for studying material nonlinearity. However, the method's predictive capability was not as great for brittle materials (like concrete and rock) as it was for ductile materials (like metals).

The continuum damage theory was first published by [Kachanov \(1958a\)](#), in which a damage variable was used to describe the flaws in the material matrix. Although defects can be studied at the micro, meso, and macroscale levels, the mechanical behavior of various materials, such as metals and rocks, is similar enough that their common mesoscopic properties by using a few energy mechanisms in the context of damage mechanics can be understood. ([Lemaitre, 1985](#)).

Although they are very effective methodologies, plasticity and damage theories can capture various aspects of a material's inelastic response. For instance, whereas damage models might take material moduli deterioration into account, plasticity models are founded on the idea of persistent (irreversible) deformation.

One can account for both persistent deformations and the degradation of material moduli brought on by inelastic processes by coupling the plastic and damage models. A number of coupled elastoplastic-damage



models have been used to simulate the non-elastic mechanical behavior of a variety of materials, including steel, concrete, porous metals, and geomaterials.

### **2.3.2. Concrete Modelling**

The field of constitutive modelling in concrete is a complex and diverse area of study, encompassing numerous proposed methodologies. The primary objective of this work is to examine the modelling of concrete through the utilization of plasticity and continuum damage theories.

Concrete is a material that exhibits sensitivity to pressure, with distinct variations in its behavior when subjected to compressive and tensile forces. When subjected to uniaxial tensile loading, the initiation of tensile cracks occurs in a direction perpendicular to the primary tensile stress. These cracks have the potential to merge together, resulting in the formation of bigger cracks.

As a result, once the tensile strength threshold is attained, a decline in strength becomes evident by a pronounced decrease in stiffness on the stress-strain curve. Moreover, the existence of tensile cracks also leads to a decline in material moduli. In order to incorporate the aforementioned attributes of concrete inside the plastic-damage constitutive modelling framework, the process of softening is typically represented by the progressive development of yield criteria. Additionally, the deterioration of material moduli is accounted for by incorporating damage factors. It is important to acknowledge that instead of being distributed uniformly over the entire volume, inelastic strains tend to concentrate in the proximity of macro fractures.

Therefore, it may be inferred that plasticity and damage models, which are grounded in the continuum framework, can only offer imprecise predictions.

The inelastic behavior of concrete under uniaxial compression loading is typically characterized by the formation of compression cracks that frequently emerge in a direction parallel to the applied compressive stress. The tangential stiffness of a material decreases as it is subjected to increasing deformation beyond its elastic limit, ultimately leading to a reduction in its ability to resist tangential forces. Additionally, the compression stress experienced by the material reaches its maximum value at the point of compressive strength. Under conditions of continuous loading, a regime of softening occurs. Just like in the case of tensile strength, the moduli of materials also experience degradation due to inelastic processes.

The behavior of concrete can undergo considerable changes, particularly in the case of multiaxial stress, with a notable impact observed in triaxial compressive loading scenarios. The strength and ductility of concrete exhibit a significant rise as the confining pressure is elevated. Hence, it is crucial to consider and incorporate this particular attribute of concrete in constitutive models, especially where confinement pressure plays a key role. In the context of multiaxial tensile testing, it is observed that the inelastic behaviour is mostly influenced by the maximum tensile stress.

The aforementioned factors lead to the prevalence of Rankine-type yield surfaces, characterised by triangular shapes in the deviatoric plane, in tensile modelling. Conversely, Drucker-Prager type yield surfaces, which exhibit round shapes in the deviatoric plane, offer superior performance in compressive modelling of concrete. Simultaneous utilisation of several yield criteria, such as the Rankine criterion for tension and the Drucker-Prager criterion for compression, is a prevalent practice in order to get a more precise representation of both compressive and tensile features. The utilisation of a multi-surface technique enables the incorporation of distinct damage evolutions in both tension and compression, hence enhancing the model's capacity to accurately represent the observed behaviour.

The authors [Feenstra and de Borst \(1996\)](#) proposed a multi-surface plasticity model to analyse the behaviour of plain and reinforced concretes subjected to monotonic biaxial loading. The composite yield surface is comprised of the Rankine criterion for tension and the Drucker-Prager criterion for compression. As previously stated, the corners resulting from the junction of various yield requirements were addressed through the use of Koiter's rule. The authors place significant emphasis on the fact that their model does not take into account the loss of rigidity.

Although the yield requirements and hardening/softening formulas exhibit variations, [Erkmen & Sarikaya \(2019\)](#) and [Feenstra & de Borst \(1996\)](#) demonstrate certain similarities. The utilisation of two distinct surfaces to represent tension and compression, and their ability to undergo distinct hardening or softening processes, has enabled enhanced control in the simulation of concrete. The model proposed by [Feenstra & de Borst \(1996\)](#) is appealing due to its incorporation of connection between various damage variables.

The hardening plasticity model for planar concrete under multiaxial compression was developed by [Grassl, et al. in 2002](#). The yield surface proposed in the work of [Menetrey and Willam \(1995\)](#) was utilised by the study authors.

Subsequently, [Grassl and Jirásek \(2006a\)](#) proposed an integrated plastic-damage model to analyse the behaviour of concrete subjected to different types of stress, including tension, shear, and multiaxial compression. One notable aspect of the paper involves the examination of the requirements pertaining to local uniqueness in the context of coupled plasticity-damage. According to the paper, the assurance of local uniqueness was observed in cases where the plasticity component of the linked plasticity-damage model relied on the effective stress formulation. However, the authors assert that this was not consistently observed in the coupled scenario involving the nominal stress-based plasticity component.

According to the model proposed by [Grassl and Jirásek \(2006a\)](#), the process of hardening is influenced by the plastic hardening variable. Conversely, the softening behaviour is achieved by the evolution of the damage loading function, which is controlled by the damage-driving variable. One notable aspect of the model is the definition of the damage-driving variable, which is expressed as a function of plastic strain.

The model demonstrated a satisfactory level of accuracy in predicting the inelastic behaviour of concrete and reinforced concrete parts. The authors also said that the model shown greater suitability for monotonic loadings compared to tension-compression cyclic loadings, primarily because it employed a single damage variable for all loading regimes.

Subsequently, [Grassl et al. \(2013\)](#) made enhancements to their prior model ([Grassl & Jirásek 2006a](#)), referred to as 'Concrete Damage Plasticity Model 1' (CDPM1), while introducing a new model known as 'Concrete Damage Plasticity Model 2' (CDPM2). One notable enhancement was the implementation of distinct damage variables for tension and compression, enabling the modelling of varying stiffness properties of concrete during tension-compression loading cycles. In addition, the authors have addressed the mesh-dependency problem that is inherent in CDPM1 by incorporating complete plasticity in the post-peak area. The authors incorporated the concept of hardening plasticity into the post-peak regime within the CDPM2 model. The significance of employing distinct damage criteria in concrete models, particularly

during tension-compression cycles, is exemplified by the contrast between CDPM1 and CDPM2 ([Sarikaya et al., 2021](#)).

The proposition of employing distinct damage factors has been put forth in various other scholarly investigations. [Lee and Fenves \(1998\)](#) introduced a coupled plasticity-damage model that incorporates changes in the compressive and tensile stiffness of concrete through the utilization of distinct damage variables for compression and tension.

One notable feature of the model is the coupling of the tension and compression damage variables. The phenomenon of tensile fracture closure can be observed by the recovery of stiffness when switching from tensile loading to compressive loading.

In their study, [Červenka and Papanikolaou \(2008\)](#) put out a model that combines plasticity and fracture. The fracture component of the analysis is derived from the Rankine criterion, and a smeared crack technique is utilised in the analysis. The plasticity component, however, relies on the Menetrey-Willam yield surface that was previously examined. The Rankine criterion and the yield surface given by [Menetrey and Willam \(1995\)](#) were utilised by the writers. The study conducted by [Sarikaya and Erkmen \(2019\)](#) utilises various aspects of the concrete model proposed by [Červenka and Papanikolaou \(2008\)](#), as well as its earlier iteration by [Papanikolaou and Kappos \(2007\)](#). However, the expression for hardening was altered as a result of the infinite derivative produced after the onset of hardening.

In several prior models, the consideration of degradation in material characteristics, such as a decrease in strength or material moduli, was achieved by implementing external reduction factors, rather of deriving these reductions as a result of the model. Subsequent studies introduced plasticity-based models as a means to effectively represent the strength, as exemplified by the work of [Ulm et al. \(2002\)](#). In a similar vein, many scholars have employed damage-based models to effectively represent the decrease in material moduli, as demonstrated by the work of [Comi et al. \(2009\)](#).

In recent studies, researchers have employed coupled plastic-damage models, as demonstrated by [Grimal et al. \(2008a\)](#) and [Morenon et al. \(2019\)](#). The plasticity-damage model proposed by [Sarikaya et al. \(2021\)](#) in their thesis might also be included in the aforementioned category. The inclusion of the plasticity component allows for the simultaneous analysis of both the development of permanent displacements and the evolution

of material strength. The damage component, however, enables the capture of the deterioration in the material moduli. When these two components are integrated, they form a precise analysis tool that is applicable in circumstances where the behaviour is governed by inelastic material characteristics.

In the context of plasticity theory, it is necessary to have a yield function and a flow rule in order to establish the permissible stresses and plastic (permanent) strains. In contrast, beliefs pertaining to damage exhibit a greater degree of diversity. However, [Armero and Oller \(2000a\)](#) demonstrated that many damage mechanisms can be consolidated and incorporated into the conventional plasticity approach. The incorporation of damage strain as an additional component of total strains facilitated the attainment of this outcome. Given the overall independence of plasticity and damage components, it becomes imperative to establish distinct yield functions for each component. [Sarıkaya and Erkmén \(2019\)](#) introduced a novel direct connection technique that enables the utilisation of a shared yield surface for both plasticity and damage.

Concrete is a multifaceted substance that exhibits a stress-strain relationship that is not linear in nature. The observed data reveals a notable disparity in the compressive and tensile strengths, with the strength being contingent upon the applied pressure, specifically influenced by the confinement pressure. In order to discuss the aforementioned aspects, [Sarıkaya et al. \(2020-2022\)](#) formulated an innovative composite yield surface and conducted an analysis of the stress integration circumstances.

### **2.3.3. Computational Plasticity**

In general, engineering problems present difficulty in geometry, boundary conditions, actions, and constitutive behavior that is extremely challenging to address analytically. Computational methods like the finite element method (FEM) are used to solve these difficult problems. The FEM can be used to solve the overall problem of determining strains and stresses (thus, forces and displacements) in the framework of continuum mechanics. However, in order to link strains and stresses, the FEM needs the constitutive model to be implemented. The constitutive relations make up the local component of the issue in the context of plasticity.

#### ***2.3.3.1. Integration schemes***

Integration schemes are commonly categorized into two main types: explicit and implicit. In the explicit situation, the present solution is dependent on the prior solutions, but in the implicit case, the current answer

is found to be self-dependent. Within the realm of algorithmic stability, implicit schemes exhibit a higher level of superiority due to their reduced susceptibility to the influence of step size. In the case of fully implicit schemes, stability is guaranteed regardless of the step size, thereby rendering them unconditional in their stability. Conversely, explicit systems typically possess conditional stability. In contrast, explicit schemes are more computationally efficient as they do not necessitate an additional step of solving a system of equations, which is typically required for implicit systems.

Moreover, the categorization of integration schemes can be determined by the quantity of steps incorporated in the integration process (Scalet & Auricchio, 2018). For example, if the variables at time  $tn+1$  are calculated only based on the variables obtained at the previous step  $tn$ , the process can be considered as a single step. If the process involves multiple steps, it can be classified as a multi-step method. One-step or multi-step frameworks can be utilised to design both implicit and explicit schemes.

The seminal research conducted by Wilkins (1963) can be regarded as a forerunner to contemporary integration methods. The radial return approach was developed for J2 elastoplasticity in the study. Subsequently, the scholarly contributions of Simo and Taylor (1985) and Ortiz and Popov (1985) have emerged as very significant exemplars of one-step integration techniques within the realm of plasticity theory.

The study conducted by Ortiz and Popov (1985) extensively examines the precision and reliability of two integration algorithms, specifically the generalised trapezoidal and generalised mid-point rules. Their work demonstrated that the generalised trapezoidal and mid-point algorithms had the ability to combine explicit and implicit strategies. The authors demonstrated that, in circumstances involving ideal plasticity and certain no associative flow scenarios, the mid-point algorithm exhibited higher stability performance compared to the trapezoidal rule.

In a significant study, Simo and Taylor (1985) established the concept of algorithmically consistent tangent moduli, which effectively maintained the quadratic rate of convergence of the implicit integration scheme. Subsequently, Simo and Taylor (1986) demonstrated the necessity of imposing the consistency constraint on the generalized mid-point state in order to maintain the symmetry of the consistent tangent moduli (Eq. 2.2).

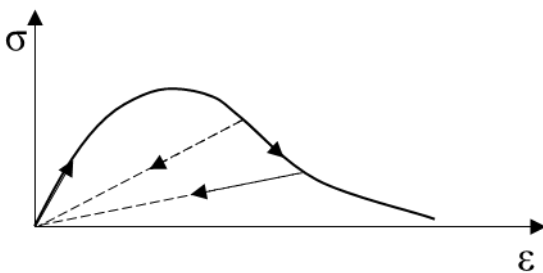
$$f_{n+\theta} = f(\sigma_{n+\theta}, q_{n+\theta}) \quad \text{Eq. 2.2}$$

Subsequently, [Ortiz and Martin \(1989\)](#) demonstrated that just the fully implicit variant of [Simo and Taylor's \(1985\)](#) approach could guarantee the symmetry of the consistent tangent moduli. The researchers conducted an investigation into the criteria that preserve symmetry in algorithmic moduli within return mapping techniques. In their work, [Simo and Govindjee \(1991\)](#) introduced a set of algorithms that rely on fully associative models. These algorithms aim to achieve symmetry and enforce the consistency criterion, as described in Eq. 2.2 mentioned before, which pertains to consistency upon reaching the mid-point state.

### 2.3.3.2. Plastic-Damage Coupling

The development of coupled plastic-damage constitutive models has been undertaken in order to ascertain the mechanical behavior of materials that demonstrate both persistent deformations and degradation of material moduli. These models have been utilized for the purpose of simulating the inelastic behavior of many materials, including concrete, geomaterials, and metals. An example of this may be seen in the work of [Jason et al. \(2006\)](#), where they proposed a linked plastic-damage model that effectively accounts for the irreversible deformations and stiffness degradation observed in concrete materials. As elucidated in their scholarly publication, neither a purely damage-based nor a purely plasticity-based model is capable of accurately representing the stiffness of a concrete element experiencing inelastic deformations. The underlying factors can be attributed to the fact that in a purely damage-based model, the stress-strain curve is centered around the origin, while in a purely plasticity-based model, the initial stiffness remains constant during the unloading process. However, as illustrated in Figure 2-5, a connected model has the ability to address these limitations.

a. strain fully reversible



b. strain partially irreversible

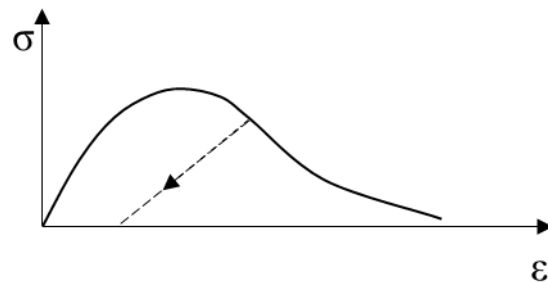


*Figure 2-5. Unloading to the origin (Jirasek & Bazant, 2002)*

In contrast to the prevailing plasticity hypothesis, the methodologies within the damage mechanics framework exhibit a notable degree of diversity. One of the strategies utilised in damage modelling is founded on the effective stress notion, which can be dated back to.

The introduction of a continuous damage variable to account for the impact of microscale faults on the macroscale was initially proposed by [Kachanov in 1958b](#). In the scenario of isotropy, the scalar damage variable  $\varphi$ , ranging from 0 to 1, quantifies the proportion of areas that have undergone damage in relation to the areas that remain undamaged (intact) under the influence of stress. Based on the aforementioned observations, it is possible to create the idea of effective stress, which corresponds to the stress exerted on the undisturbed surface. Theories that are grounded in the concept of effective strain have also been formulated in a comparable manner. [Simo and Ju \(1987, 1989\)](#), [Lubliner et al. \(1989\)](#), and [Luccioni et al. \(1996\)](#) represent notable instances of damage formulations that rely on the effective stress notion.

The incorporation of spatial orientation as a factor in the effective stress/strain approach leads to the consideration of damage tensors in the characterization of anisotropic damage. Several examples of relevant literature include [Murakami's \(1993\)](#) work, [Chaboche's](#) publication from 1984, and the study conducted by [Voyiadjis and Park](#) in 1997.

Models that employ the fourth-order compliance tensor as the primary internal variable represent a distinct category within the field of continuum damage mechanics. The derivation of the evolution of the compliance tensor often follows a thermodynamically consistent framework, such as the principle of maximal damage dissipation. There are numerous similarities seen between the aforementioned technique and the associative plasticity framework. In the current study, it is aimed to establish a coupled damage-plasticity model by leveraging this similarity. [Ortiz \(1985\)](#) and [Simo and Ju \(1987\)](#) can be regarded as pioneer exemplifications utilising the compliance tensor methodology. Additional examples of relevant studies in the field include the works of [Hansen and Schreyer \(1994\)](#), [Govindjee et al. \(1995\)](#), [Ibrahimbegović, et al. \(2003\)](#), [Ibrahimbegović and Markovič \(2003\)](#), [Ibrahimbegović et al. \(2008\)](#), as well as [Brancherie and Ibrahimbegovic \(2009\)](#).



The literature also presents an alternative class of models, known as smeared crack damage models, which address the formation and advancement of macrocracks resulting from the commencement and progression of microcracks. In the earlier studies, such as the one conducted by [Rashid \(1968\)](#), it was thought that the direction of the crack would remain constant. The introduction of the idea of fracture rotation was observed in subsequent investigations ([Gupta & Akbar, 1984](#)). Subsequently, [Jirásek and Zimmermann \(1998\)](#) demonstrated that the rotating crack model exhibited the stress locking phenomenon previously seen in models utilising a non-aligning finite element mesh with crack orientation.

In relation to the smeared crack approach, it is important to highlight the kinematic decomposition, which involves separating the total strain into elastic and inelastic components. This decomposition is expressed as follows:

$$\varepsilon = \varepsilon_e + \varepsilon_c \quad \text{Eq. 2.3}$$

Here,  $\varepsilon$  represents the total strain tensor, which consists of the elastic strain tensor  $\varepsilon_e$  and the crack strain tensor  $\varepsilon_c$ . The crack strain tensor is specifically associated with the inelastic deformations, as described by [Jirásek and Zimmermann \(1998\)](#).

In the context of classical plasticity, the primary strategy involves the additive decomposition of the strain tensor  $\varepsilon$  into its elastic  $\varepsilon_e$  and plastic  $\varepsilon_p$  components, as expressed by the Eq. 2.4.

$$\varepsilon = \varepsilon_e + \varepsilon_p \quad \text{Eq. 2.4}$$

One of the primary differentiating factors among the several alternative damage models lies in the manner in which kinematic decomposition is implemented. Hence, many formulations emerge within the context of coupled damage-plasticity frameworks. In several studies, the overall strain is divided exclusively into elastic ( $\varepsilon_e$ ) and plastic ( $\varepsilon_p$ ) components, as demonstrated by [Lemaitre \(1985\)](#), [Ju \(1989\)](#), [Hansen & Schreyer \(1994\)](#), [Cicekli et al. \(2007\)](#), [Grassl et al. \(2013\)](#), and [Alfarah et al. \(2017\)](#). In certain literature, however, an additional component known as the damage strain ( $\varepsilon_d$ ) has been incorporated into the strain decomposition, represented as

$$\varepsilon = \varepsilon_e + \varepsilon_p + \varepsilon_d \quad \text{Eq. 2.5}$$

Previous studies have explored the division of total strain into elastic, plastic, and damaging strains. Notable contributions in this area include the research conducted by [Klisiński & Mróz \(1988\)](#), as well as the work of [Yazdani & Schreyer \(1990\)](#). Subsequently, several research have incorporated coupled constitutive models that incorporate a damage strain component. These studies include [Armero and Oller \(2000a\)](#), [Al-Rub and Voyiadjis \(2003\)](#), [Ibrahimbegović et al. \(2008\)](#), [Ayhan et al. \(2013\)](#), and [Wu and Cervera \(2016\)](#).

In addition to the aforementioned sources, [Sarıkaya et al. \(2021\)](#) conducted a detailed examination of the works by [Armero & Oller \(2000a\)](#) and [Armero & Oller \(2000b\)](#) in order to provide a more comprehensive analysis of their plastic-damage coupling method within the context of the current study. [Armero and Oller \(2000a\)](#) proposed a novel conceptual framework that allows for the integration of various alternative damage therapies, as previously stated, into a coherent approach. The central significance in their architecture is attributed to the concept of damage strain, which allows for the inclusion of various damage mechanisms. The authors of the study have adopted the additive decomposition of the strain tensor, which is consistent with the formulation presented in Eq. 2.5. The damage strain, denoted as  $\varepsilon_d$ , is composed of various contributions originating from different damage mechanisms.

$$\varepsilon_d = \sum_{d_i=1}^{n_{dam}} \varepsilon_{d_i} \quad \text{Eq. 2.6}$$

Each damage mechanism is represented by  $d_i$ , where  $i$  is the corresponding number assigned to the mechanism. The overall number of damage mechanisms is denoted as  $n_{dam}$ .

It is worth mentioning that [Armero and Oller \(2000a\)](#) classify the damage strains as recoverable. The recoverability of damage strains can be attributed to the correlation between each damage mechanism and its corresponding damage energy potential. Based on the aforementioned information, the stored energy function  $W$  was expressed by [Sarıkaya et al. \(2021\)](#) by incorporating the damage terms,

$$W = W^e(\varepsilon_e) + \mathfrak{I}^p(K_p) + \sum_{d_i=1}^{n_{dam}} W^{d_i}(\varepsilon_{d_i}, K_{d_i}) \quad \text{Eq. 2.7}$$

The variables  $W^e$  and  $W^d$  represent the stored energy associated with elasticity and damage, respectively. The symbol  $\Psi^p$  is used to denote the potential related to the plastic hardening process, which is influenced by the development of the internal plastic hardening variable  $K_p$ . Likewise,  $K_d$  denotes the variable associated with damage hardening.

One notable aspect of [Armero & Oller's \(2000b\)](#) work is the similarity between the stress return algorithms for plasticity and damage models. Furthermore, the modular treatment of the numerical integration problem is facilitated by representing each damage mechanism according to its contribution to the total damage strain.

Subsequently, [Ibrahimbegovic et al. \(2003, 2008\)](#) incorporated the coupled plasticity-damage framework proposed by [Armero and Oller \(2000a\)](#) and its numerical implementation ([Armero and Oller 2000b](#)) in several studies, including [Ibrahimbegović et al. \(2003\)](#), [Ibrahimbegović and Markovič \(2003\)](#), [Ibrahimbegović et al. \(2008\)](#), and [Ayhan et al. \(2013\)](#). These studies focused on utilising this framework for constitutive modelling of concrete and other materials.

It is important to acknowledge that the concept of damage strain is employed in many ways within the existing body of literature.

In the studies conducted by [Armero & Oller \(2000a\)](#), [Ibrahimbegović \(2009\)](#), and [Wu & Cervera \(2016\)](#), the damage strain is found to be recoverable. However, in the works of [Al-Rub & Voyiadjis \(2003\)](#) and [Brünig & Michalski \(2017\)](#), the damage strain is associated with permanent deformations. The observed disparity arises as a result of variations in the conceptualization and operationalization of damage and strain.

The authors of the [Sarikaya et al. \(2021\)](#) study chose to utilise the linked plasticity-damage framework developed by [Armero & Oller \(2000a\)](#) and [Armero & Oller \(2000b\)](#) due to its straightforward nature and computational effectiveness. The authors proposed a direct coupling strategy to modify the framework developed by [Armero and Oller \(2000a\)](#), resulting in a more streamlined and computationally efficient algorithm. Instead of employing distinct yield (and potential) functions for plasticity and damage, the researchers developed a framework that use a single yield (and potential) function to encompass both plasticity and damage components. The research article by [Sarikaya and Erkmen \(2019\)](#) presents a study on

the direct coupling method and its utilization in analyzing the behavior of concrete subjected to compressive forces.

Other research in the literature have also recommended the utilisation of a solitary yield function to encompass both plasticity and damage. In the study conducted by [Meschke et al. \(1998\)](#), it was observed that both plastic and damage strains can be associated with a common yield surface. In contrast to employing distinct energy potentials for plasticity and damage, the formulation uses a single potential, hence restricting the ability to get individual plasticity and damage strains from the optimisation problem. The distinction between plastic and damage strains is established by incorporating a participation factor, denoted as  $\beta$ , which satisfies the condition  $0 \leq \beta \leq 1$ . This factor enables the consideration of three distinct scenarios: pure elastoplastic behaviour when  $\beta = 0$ , pure elastic-damage behaviour when  $\beta = 1$ , and coupled plastic-damage behaviour for intermediate values of  $\beta$ . The determination of the participation factor was achieved through calibration with experimental data. Subsequently, [Wu and Cervera \(2016\)](#) employed a comparable methodology to develop a cohesive elastoplastic-damage framework, serving as a foundation for the modelling of strain localizations characterised by pronounced discontinuities in quasi-brittle materials.

In relation to the utilisation of a singular yield function for plasticity and damage, it is pertinent to engage in a discourse concerning a specific category of interconnected plastic-damage modelling methodologies. These methodologies are founded upon the principles of thermodynamics, incorporating internal factors. In the pursuit of thermodynamic consistency, potential functions are commonly employed within the framework.

[Houlsby and Puzrin \(2000\)](#) developed a framework for a constitutive model that is thermodynamically consistent. This was achieved by incorporating two thermodynamic potentials, specifically the energy potential and the dissipation potential. These two potentials are the sole determinants of the constitutive behaviour, eliminating the requirement for any extra ad-hoc assumptions. The model is sometimes referred to as the hyperplasticity model, which suggests the significance of prospective functions. One notable aspect of the hyperplastic model is its ability to derive the yield surface directly using the Legendre transformation of the dissipation function. The historical data pertaining to the material is encapsulated inside the internal variables, such as the plastic strain.

The coupled and uncoupled plasticity damage model created by [Einav et al. \(2007\)](#) can be viewed as an expansion of the thermodynamically consistent hyper plasticity model proposed by [Houlsby and Puzrin \(2000\)](#) to incorporate the hyper-plastic-damage formulation. The introduction of damage as an internal variable is a key aspect in the development of both pure damage and coupled plastic-damage constitutive models. In this manner, it is possible to derive both the yield surface and the damage internal variable through the dissipation potential.

### ***2.3.3.3. Lumped plasticity***

Lumped Plasticity is a modeling technique used in structural analysis, particularly in the context of seismic performance assessment. This method leverages the simplicity of the plastic hinge by separating a line element into inelastic and elastic components. [Michael et al. \(2008\)](#) conducted an assessment of models applicable to Performance-Based Earthquake Engineering (PBEE) of bridge columns. Their evaluation encompassed novel formulations for effective elastic stiffness, plastic-hinge length, and strain thresholds for the onset of bar buckling. A dataset comprising 37 tests of large-scale circular bridge columns was utilized to refine and assess these models. The primary objective of this investigation was to formulate expressions compatible with existing lumped-plasticity models, thereby enhancing the efficacy of performance-based design methodologies for bridge columns. The findings underscored the viability of incorporating the proposed expressions, along with the recommended effective stiffness expressions and strain thresholds specific to the plastic-hinge length formulation, into existing models. Notably, the study concluded that the incorporation of existing expressions with the newly proposed parameters yielded satisfactory predictions of the force-displacement behavior and the corresponding displacements associated with various damage thresholds.

In their work, [Fablo and Mazza \(2010\)](#) introduced a lumped plasticity model (LPM) tailored for nonlinear static and dynamic analyses of three-dimensional reinforced concrete (r.c.) frames. The model incorporates a bilinear moment curvature law and an interaction surface axial force-biaxial bending moment relationship. For nonlinear dynamic analyses, a two-parameter implicit integration scheme coupled with an initial-stress like iterative strategy, following the Haar–Kàrmàn principle, was employed. The study revealed that the nonlinear seismic response, as predicted by the LPM, is highly sensitive to the selection of strength and stiffness input parameters, such as the reduction factor in flexural stiffness and the hardening ratio in the

bilinear moment-curvature law. These parameter choices significantly influence the maximum response parameters, waveform characteristics, and periodicity of the seismic response time histories. Comparative analysis with a refined fibre model demonstrated that the LPM adequately captures the flexural hysteretic behavior of r.c. frame elements, particularly in low- and medium-risk seismic regions, thereby offering a viable simulation approach for seismic performance assessment.

In the study conducted by [Mohammadreza et al. \(2019\)](#), the efficacy of the lumped plasticity model in predicting the nonlinear response of reinforced concrete frames subjected to gradually increasing vertical loads was studied. To this end, two full-scale RC frames featuring varying shear spans were fabricated and subjected to vertical loading applied through their beams. Finite element (FE) models of these experimental specimens were developed using SAP2000 software, enabling a comparison between numerical predictions and experimental findings. The investigation encompassed an analysis of the impact of different plastic hinge lengths, initial effective stiffness values, and plastic hinge locations on the accuracy of the FE models. It was observed that irrespective of the selected plastic hinge lengths, the FE models effectively approximated the yield and ultimate loads of the frames. However, discrepancies arose in accurately estimating the corresponding vertical displacements at yield and ultimate load stages. The study also highlighted the significant influence of chosen plastic hinge locations on the predicted yield and ultimate loads. Furthermore, the FE models tended to underestimate the damage levels at mid-span of beams compared to experimental observations upon reaching the ultimate load conditions.

[Chang et al. \(2021\)](#) conducted a study focusing on the parameter estimation of a lumped plasticity model designed to accurately replicate the nonlinear load-deformation behavior exhibited by circular reinforced concrete columns subjected to cyclic lateral loading. The calibration of model parameters relied on a comprehensive experimental dataset comprising 210 circular columns, each characterized by a variety of input parameters including material strength, reinforcement arrangement, specimen geometry, and testing configuration. Specifically, parameter values for initial stiffness, plastic rotation capacity, moment strength, and cyclic damage parameters were fine-tuned to match the first-cycle envelope of individual test datasets. To facilitate parameter estimation, empirical predictive equations were formulated, correlating model parameters with input parameters through four distinct regression techniques: stepwise, ridge, lasso, and elastic net regression. The implementation of the proposed lumped plasticity model yielded a notable

reduction in computational time, approximately 50% lower compared to the distributed plasticity model. Furthermore, as ground motion intensity escalated, disparities in response between the two models became more pronounced. The predictive accuracy of the bridge class response was significantly influenced by bent configuration and deck mass. Notably, due to the concentration of nonlinear response at column ends and the linear pre-yield behavior, the proposed lumped plasticity model demonstrated a lesser susceptibility to record-to-record variability compared to the existing distributed plasticity model.

## **2.4.Uni-axial material models**

When using beam-type 1D elements to accommodate various loading conditions, it becomes imperative to establish inelastic behavior at the stress-strain level, especially when dealing with arbitrary stress distributions. These one-dimensional generalized stress-strain relationships are contingent upon preconceived conditions, such as assumed confinement pressures, which must be defined prior to conducting the analysis.

The analytical model proposed by [Saatchioglou and Razvi \(1992\)](#) comprises a parabolic ascending segment followed by a linear descending portion described in Eq. 2.8. This model is rooted in the computation of lateral confinement pressure induced by both circular and rectilinear reinforcement, aiming to enhance the strength and ductility of confined concrete. Through meticulous analysis of extensive test data encompassing various levels of confinement, ranging from poorly confined to well-confined concrete specimens, the parameters of the analytical model were rigorously established. The strength and corresponding strain of confined concrete were characterized in relation to the equivalent uniform confinement pressure exerted by the reinforcement configuration. This equivalent uniform pressure was derived from the average lateral pressure determined based on sectional and material characteristics. The combined effect of different types of lateral reinforcement configurations was assessed by superimposing individual confinement effects. The stress-strain relationships delineated by the proposed methodology exhibited notable concordance with those derived from column tests featuring diverse geometries and reinforcement schemes, conducted under both concentric and eccentric loading conditions.

$$f_c = f'_{cc} \left[ 2 \left( \frac{\varepsilon_c}{\varepsilon_1} \right) - \left( \frac{\varepsilon_c}{\varepsilon_1} \right)^2 \right]^{1/(1+2K)} \leq f'_{cc} \quad \text{Eq. 2.8}$$

Where  $K = k_1 f_{le} / f'_{co}$ ,  $k_1 = 6.7 (f_{le})^{-0.17}$ ,  $f_{le}$  being the effective uniform confining pressure in Mpa

$f'_{co}$  and  $f'_{cc}$  unconfined and confined strengths of concrete in a member respectively.

$\varepsilon_1$  is peak stress

The ductility of ultra-high-strength concrete columns undergoes substantial influence from both axial compression levels and the effectiveness of lateral reinforcement. A pertinent indicator for assessing ductility is the capacity of lateral reinforcement normalized by concrete strength. To gauge displacement ductility, [Sugano \(1996\)](#) introduced empirical Eq. 2.9, derived from a comprehensive regression analysis of available column data for high-strength concrete. Despite the inherently brittle nature of ultra-high-strength concrete, effective confinement can still be achieved through the utilization of high- or ultra-high-strength lateral reinforcement. It is noteworthy that achieving adequate ductility in ultra-high-strength concrete demands a relatively greater capacity of lateral reinforcement compared to lower-strength concrete scenarios.

$$\delta_f = 0.127 \frac{(\rho_c \times f_{yt})}{f_c} - 0.052 \left( \frac{\sigma_c}{f_c} \right) + 0.041 \quad \text{Eq. 2.9}$$

Where  $\rho_c$  is the Area ratio of ties,  $f_{yt}$  is the Yield strength of ties,  $f_c$  is the compressive strength of concrete cylinder and  $\sigma_c$  is the axial stress.

In the study conducted by [Okan et al. \(2010\)](#), it was determined that augmenting the confinement ratio resulted in enhanced ultimate drift capacities for reinforced columns subjected to strengthening measures. They introduced a drift-based equation incorporating key parameters such as longitudinal reinforcement ratio, axial load level, and confinement ratio. Through this equation, the drift capacities of the columns within the experimental dataset were accurately estimated, aligning closely with standard engineering expectations.

[Fabio et al. \(1991\)](#), [Enrico et al. \(1996\)](#), [Bulent and Donald \(2005\)](#), [Ashraf \(2006\)](#), [Erkmen and Attard \(2011\)](#), [Saritas and Filippou \(2013\)](#), and [Pisca et al. \(2017\)](#) have extensively explored beam element-based



modeling approaches employing inelastic uni-axial stress-strain relations. These formulations, commonly referred to as fibre elements in academic discourse, operate under the assumption that plane sections remain plane and normal to the longitudinal axis. Within this framework, the intricate interplays of shear and bond-slip phenomena are often disregarded, reflecting a simplified representation of structural behavior.

## **2.5. Multi-axial material models**

Multi-surface plasticity techniques are widely employed in various engineering disciplines, encompassing the characterization of concrete and geomaterials in constitutive modelling, as well as in crystal plasticity scenarios involving multiple slip planes. The concept revolves around the introduction of multiple plasticity yield functions, each corresponding to distinct surfaces within the principal stress space. This approach aims to more accurately capture the material's response under various conditions, such as disparities in compressive and tensile behavior.

The existence of several yield surfaces is a hurdle due to the occurrence of discontinuities in the stress space at specific spots. In situations when two surfaces cross in a non-smooth manner, it is commonly observed that the normal at the point of intersection lacks a well-defined value. Therefore, it is necessary to expand both the rate and incremental forms of plasticity equations in order to address non smooth sections, sometimes referred to as corners.

One of the techniques suggested in scholarly literature for addressing non smooth regions involves the incorporation of smoothing functions to mitigate sharp edges. In the study conducted by [Nayak and Zienkiewicz \(1972\)](#), a straightforward averaging method was utilized in the proximity to singularities. In numerous instances, the substitution of a segment of a criterion with an alternative lead to the introduction of additional corners at the points of intersection ([de Borst, 1987](#)).

The authors of [Abbo & Sloan \(1995\)](#) utilized a hyperbolic approximation to address the singularity issue associated with the apex point in the Mohr-Coulomb criterion. Furthermore, it should be noted that a yield criterion may exhibit discontinuous gradients at certain points, resulting in distinct boundaries in the major stress space. This phenomenon is observed in many criteria such as Tresca, Mohr-Coulomb, and Rankine criteria.

[Menetrey and Willam \(1995\)](#) suggested a failure criterion that includes common strength assumptions for a range of engineering materials and captures the key characteristics of triaxial concrete strength. The verification cases showed that the suggested failure criterion may capture information on biaxial and triaxial strength. They established that the von-Mises, Drucker-Prager, and Rankine criteria can all be included in a framework that uses the three-parameter failure criterion. The linear Mohr-Coulomb criterion's extension and compression meridians are also where the generalized failure envelope degenerates. It also reduces to the approximate parabolic two-invariant form of the Leon criteria. The unified formulation has the benefit of include several well-known failure criteria as special instances. Their proposed criterion integrated the traditional Rankine criterion for maximum tensile strength with the Mohr-Coulomb hypothesis governing shear strength. This amalgamation offered a balanced depiction of both the tensile/cohesive strength of cementitious materials and the shear strength of frictional materials. The three-parameter failure criterion devised for concrete is expressed as a function of the three stress invariants and is formulated using the Haigh-Westergaard coordinates, facilitating straightforward geometric interpretation. Notably, its cohesion and friction parameters are decoupled, enabling direct manipulation for hardening/softening extensions. Moreover, the criterion simplifies to the parabolic two-invariant approximation of the Leon criterion. The unified nature of this formulation proves advantageous as it encompasses numerous well-established failure criteria as special cases, consolidating diverse theoretical frameworks into a cohesive conceptual model.

As previously stated, the occurrence of corners can be attributed to the simultaneous utilization of many yield criteria. For example, the utilization of distinct yield requirements for compression and tension has been implemented in many concrete models, such as the ones proposed by [Feenstra and de Borst \(1996\)](#) and [Červenka and Papanikolaou \(2008\)](#). Compression caps and tension cut-offs are frequently utilized in the modelling of geomaterials. Some models in the literature, such as [Dolarevic and Ibrahimbegovic \(2007\)](#), favored a seamless transition between distinct surfaces. However, numerous other models employed Koiter's rule, which explicitly addresses corners.

Numerous models have been developed in the literature, drawing upon Koiter's rule as a foundational principle. As an example, [de Borst \(1987\)](#) examined a specific scenario involving two yield surfaces and devised a comprehensive backward-Euler integration technique. This method was further expounded upon in relation to yield functions of the Mohr-Coulomb and Tresca types. The single-point integration method

does not require any iterations throughout the integration process. At the conclusion of the step, the consistency criterion was met. This was observed specifically in the scenario where hardening was modelled as a linear function solely dependent on the plastic strain. The author suggests use iterations for the case of nonlinear hardening. In order to ascertain the appropriate choice between the standard single-surface return method and the multi-surface return algorithm, de Borst devised a singularity indicator. Subsequently, an erroneous formula within his research was rectified in the study conducted by [de Borst et al. \(1991\)](#).

The classical work by [Simo et al. \(1988\)](#) is widely regarded as a significant contribution to the field of multi-surface plasticity. The researchers demonstrated that the Koiter's requirements are fundamentally identical to the optimality conditions of the corresponding convex mathematical programme. Additionally, they devised a comprehensive closest-point return mapping method for multi-surface plasticity that is associated with these circumstances. One notable aspect of their work involves the utilisation of the discrete formulation of Karush-Kuhn-Tucker (KKT) conditions.

One of the primary difficulties encountered when employing the elastic predictor-plastic corrector scheme is the limited availability of prior knowledge regarding the active surfaces for a particular trial stress state in multi-surface plasticity. This poses a significant difficulty when applying the discrete form of the Karush-Kuhn-Tucker (KKT) conditions.

This issue has been found in several investigations within the existing literature, such as the works of [Simo et al. \(1988\)](#) as well as [Simo and Hughes \(1998\)](#). In contrast, within the context of single-surface plasticity, the activation of the yield surface occurs directly when the trial stress exceeds the permissible stress. This characteristic of single-surface plasticity offers computational convenience.

In their classical work, [Simo et al. \(1988\)](#) put out a pair of methodologies, one conceptual and one practical, aimed at systematically identifying the active surfaces involved in the return mapping process. Both approaches were devised specifically for the instance of related plasticity.

The multi-surface plasticity algorithm established by [Simo et al. \(1988\)](#) remains widely recognized in the field because to its broad applicability. However, it is important to note that this method was specifically designed with associative plasticity in mind. The proposed approach systematically decreases the quantity of active surfaces until the resulting solution converges and meets the consistency criterion. [Pramono and](#)

Willam (1989) demonstrated that in instances of softening, there might be an increase in the quantity of active surfaces, contrary to the expected decrease. An alternative technique was proposed, wherein surfaces are engaged sequentially, beginning with the most dominant surface and subsequently including the next surface into the active set. Therefore, the collection of active surfaces expands until the consistency conditions are satisfied for all criteria.

In addition to the overarching multi-surface stress return methods, a substantial body of literature exists that examines specific criteria, such as the Tresca and Mohr-Coulomb yield surfaces. Pankaj and Bićanić (1997) devised a singularity indicator to assess if the trial stress conforms to the corner zone or not, specifically for the Mohr-Coulomb yield criteria with isotropic hardening. Perić and Neto (1999) introduced a stress-return algorithm for Tresca plasticity, utilising a geometrical perspective. This methodology was subsequently expanded upon by Neto et al. (2008) to encompass yield requirements of the Mohr-Coulomb type. In their study, Borja et al. (2003) examined the efficacy of integration algorithms in relation to smooth three-invariant representations of the Mohr-Coulomb model, such as the Lade-Duncan and Matsuoka-Nakai models.

Despite their higher computational demands, multi-axial material models offer the advantage of directly incorporating the influences of shear and confinement pressure, a capability stemming from the comprehensive nature of 3D analysis. Consequently, there has been substantial research interest and adoption of elasto-plastic material models for simulating concrete structural components.

In 1977, Ottosen introduced a failure criterion characterized by four parameters  $A, B, K_1, K_2$  encompassing all three stress invariants as shown Eq. 2.10.

$$f(I_1, J_2, \cos 3\theta) = A \frac{J_2}{\sigma_c^2} + \lambda \frac{\sqrt{J_2}}{\sigma_c} + B \frac{I_1}{\sigma_c} - 1 = 0 \quad \text{Eq. 2.10}$$

Where  $A$  and  $B$  are parameter and  $\lambda$  is a function of  $\cos 3\theta$ . It was suggested by the author that  $\lambda = \lambda(\cos 3\theta)$  could be represented as follow;

$$\lambda = K_1 \cos \left[ \frac{1}{3} \arccos (K_2 \cos 3\theta) \right] \quad \text{for } \cos 3\theta \geq 0 \quad \text{Eq. 2.11}$$

$$\lambda = K_1 \cos \left[ \frac{\pi}{3} - \frac{1}{3} \arccos (-K_2 \cos 3\theta) \right] \quad \text{for } \cos 3\theta \leq 0$$

In which parameters  $K_1$  and  $K_2$  are size and shape factor respectively ( $0 \leq K_2 \leq 1$ ). This criterion delineated a smooth convex failure surface with meridians curving in the negative direction of the hydrostatic axis. Additionally, the trace in the deviatoric plane transitioned from an almost triangular to a more circular shape as hydrostatic pressure increased. Empirical verification confirmed the criterion's validity under short-time monotonic loading conditions.

[Han et al. \(1987\)](#) introduced a constitutive model aimed at capturing the intricate behavior of concrete materials within elastic-plastic regimes. This model, rooted in a modified plasticity theory, effectively delineates strain-hardening through stress-space plasticity mechanisms and strain-softening via strain-space plasticity principles. Key attributes of Ottosen's model encompass the utilization of sophisticated failure criteria such as the Willam-Warnke five-parameter or Hsieh-Ting-Chen four-parameter model, incorporation of a closed-shape yield surface, implementation of a nonuniform hardening rule, and modulation of plasticity modulus dependent on hydrostatic pressure and Lode angle. Additionally, the model adopts a non-associated flow rule and employs a dual criterion based on stress and strain to discern various failure modes. It also features linear tensile softening to simulate cracking behavior and multiaxial softening to replicate mixed failure modes. They validated their innovative work-hardening model across a diverse spectrum of experimental data, consistently achieving commendable agreement between theoretical predictions and empirical observations.

Nevertheless, in simulating the concrete material behavior using plasticity theory, the adoption of a non-associative flow rule becomes imperative due to dilatation effects. Consequently, a potential function distinct from the yield surface is required to accurately determine the volumetric component of the plastic flow. Previous investigations into non-associative plasticity models, particularly those predicated on pressure-sensitive yield criteria for compressive concrete behavior, are exemplified in studies such as [Kang & Willam \(1999\)](#), [Grassl et al. \(2002\)](#), [Grassl \(2004\)](#), and [Bao et al. \(2013\)](#).

For a comprehensive structural analysis, it is imperative to define the tensile behavior of concrete material as well. The delineation between compressive and tensile behavior in concrete failure criteria, stemming from their disparate phenomenological characteristics, is well-documented in both experimental and

theoretical literature. Research focusing on developing concrete failure criteria primarily emphasizes compressive behavior, deeming tensile behavior relatively insignificant in reinforced concrete structural analysis. For tension failure, the adoption of Rankine's maximum tensile stress cut-off with strain softening is commonplace ([Jirasek & Bazant, 2001](#)).

In addressing the fluctuations of the carefully selected compressive yield surface of concrete under hardening and softening laws, the implementation of a tensile cut-off mechanism serves to mitigate unrealistic tensile strength. Numerous researchers such as [Wan \(1992\)](#), [Fuschi et al. \(1994\)](#), [Bao et al. \(2013\)](#), [Papanikolaou & Kappos \(2007\)](#) and [Yu et al. \(2010\)](#) have ventured into the development of multi-surface plasticity models for concrete.

The successful integration of elasto-plastic material modeling of concrete with multi-surface yield criteria into 3D structural level analyses has been achieved by various scholars, including [Červenka & Papanikolaou \(2008\)](#), [Galic et al. \(2011\)](#) and [Lu et al. \(2016\)](#). However, concerns regarding the robustness of numerical treatment have surfaced since the 1970s, as indicated by studies such as [Červenka \(1971\)](#) and [Bergan & Holand \(1979\)](#). Despite the extensive history of research in nonlinear finite element analysis, particularly concerning the 2D or 3D material nonlinear analysis of concrete structures, investigations into numerical robustness remain ongoing. Various aspects of numerical algorithms, including element and integration types, return mapping strategies at the material level, and adaptability of global equilibrium path-finding strategies, are known to impact convergence characteristics, especially when encountering softening and bifurcation points, as detailed in [Geers \(1999\)](#) and [Hofstetter & Valentini \(2013\)](#).

To address potential shear and volumetric locking issues, especially during plastic analysis of 3D solids, alternative numerical integration schemes have been developed, as seen in works such as [Hu & Nagy \(1997\)](#), [Liu et al. \(1994\)](#), and [Olovsson et al. \(2006\)](#). The introduction of multiple yield surfaces into material models necessitates specialized return mapping algorithms. For geo-materials and concrete specifically, multi-surface return mapping methodologies involving cut-off surfaces have been devised by researchers such as [Pramono & Willam \(1989\)](#), [Hofstetter et al. \(1993\)](#), [Feenstra & De Borst \(1996\)](#), [Dolarevic & Ibrahimbegovic \(2007\)](#), [Adhikary et al. \(2017\)](#) and [Pech et al. \(2021\)](#). Meanwhile, regularization techniques aimed at ensuring numerical stability in cases of softening have been proposed by [De Borst \(1987\)](#), [De Borst \(2001\)](#), [Dias da Silva \(2004\)](#), [Engen et al. \(2019\)](#) and [De Borst & Duretz \(2020\)](#).

## 2.6. Case studies

In order to perform numerical modeling to predict the behavior of beam and solid elements, experimental data were obtained from literatures [Focacci et al. \(2016\)](#), [Benmokrane et al. \(1995\)](#), [Mohamed et al. \(2014\)](#) and [Qian & Chen \(2005\)](#). The experimental program consisted of 3 beams and 2 shear walls. The choice of the beams, shear walls and FRP reinforcement is based on the fact that they generate tensile regions to test Multi-Surface Plasticity model and that the yielding occurs in concrete only when FRP rebars are used.

[Focacci et al. \(2016\)](#) investigated the response of FRP-reinforced members without shear reinforcement. Two series of specimens were tested in flexure, Shallow and deep rectangular cross section. All specimens were reinforced only in flexure with Steel, Carbon and Glass FRP bars. Over a clear span  $L$  of 2000 mm, the specimens were exposed to a one-point transverse force that was monotonically applied until failure. A response steel frame with a mechanical actuator to convey the displacement controlled transverse action was used for the tests. Shallow FRP-reinforced specimens failed in flexure and the deep FRP-reinforced specimens failed early due to shear.

[Benmokrane et al. \(1995\)](#) experimented span to depth ratio on glass fibre reinforced plastic concrete beams test to investigate their flexural behavior. This experimental program consisted of three series of reinforced concrete beams (Isorod, Kodiak GFRP and steel rebars) having different surface deformations. The beams were subjected to two equal symmetrical loads on a 3000 mm span. The research found that the span-to-height ratio would be crucial to consider when designing GFRP rebar-reinforced beams in order to manage deflection and fracture width. The GFRP rebars performed well and appeared to be a promising alternative to steel reinforcements. They claimed that GFRP rebars would work well in situations requiring long-term corrosion resistance, low conductivity to electrical and electromagnetic fields, high strength-to-weight ratios, and other similar qualities.

[Qian & Chen \(2005\)](#) conducted nine shear wall specimens experiment to verify the finite element-based macro model that the authors proposed. Two different sorts of elements made up the model: an RC column element for modelling boundary zones and an RC membrane element for modelling beams. Both elements' stiffness matrices were developed. Experimental findings for nine shear wall specimens confirmed the accuracy and applicability of the established analytical model. The analytical findings showed that the most

important factors affecting the load carrying capacity and deformation capacity of shear walls are the axial load ratio, the confinement index of the boundary zone, and the boundary zone length ratio. The higher the axial load ratio, the larger the confinement index of the boundary zone, and the greater the boundary zone length ratio should be in order to generate the necessary deformation capacity for a shear wall. It was advised that as the axial load ratio changes, not only the border zone length ratio but also the confinement index should change as well.

In order to meet the appropriate strength and drift criteria outlined in various codes, [Mohamed et al. \(2014\)](#) researched the applicability of reinforced concrete shear walls completely reinforced with glass fiber-reinforced polymer (GFRP) bars. Three GFRP-reinforced specimens, were tested to failure as part of the experimental program. To guarantee flexural dominance and prevent slide and shear failures, they were constructed with an appropriate quantity of distributed and concentrated reinforcement. Without any indication of early shear, sliding shear, bond and anchorage failure, or instability failure, all specimens reached their flexural strength. Shear walls with GFRP reinforcement may achieve high strength, deformation capacity, and adequate energy dissipation. This means that shear walls with GFRP reinforcement can be employed as lateral resisting systems.

The specimens that were selected in this research for validation purposes were subjected to monotonic compression load until failure. The mechanical properties of concrete, steel reinforcement and FRP reinforcements are discussed in section 4.2.



# Chapter 3

## Material FORTRAN code model

### 3.1.Introduction

In this chapter, the work of [Sarikaya et al. \(2020-2022\)](#) is presented. In order to model the mechanical behavior of concrete, they created a coupled plastic-damage multi-surface constitutive model. In their attempt to do this they introduced the direct coupling technique, in which they suggested connections between the plasticity and damage parts of the plastic-damage constitutive model. They created an explicit integration algorithm for a multi-surface plasticity framework. Then, in an effort to accurately portray concrete's behavior, they suggested the three-surface concrete plasticity model.

The infinitesimal framework was established by [Sarikaya et al. \(2021\)](#) through the utilization of Koiter's rule in conjunction with the linear complementarity problem (LCP). The need of utilizing the Linear Complementarity Problem (LCP) to derive uniqueness requirements was underscored. An explicit integration algorithm for multi-surface plasticity has been devised based on the infinitesimal formulation. One of the primary challenges posed by multi-surface plasticity is that the trial state alone is insufficient to fully characterize the conditions of inelastic loading and unloading, as is the case in single-surface plasticity. In the context of the incremental formulation of multi-surface plasticity, it is important to note that the presence of a yield function with a positive value does not automatically imply the activation of the corresponding surface. A method was devised to ascertain the borders of the corner zone for the incremental scenario. A proposal was put out to modify the plasticity multipliers in order to enhance the precision of the approach. According to [Pramono and Willam \(1989\)](#), the quantity of active surfaces can exhibit variability as a result of the occurrence of hardening or softening. The approach has the capability to analyze the active surfaces throughout each iteration, enabling it to track the progression of surfaces over time.

### 3.2. Non-associative Multi-surface Plasticity

In structural analyses involving materials exhibiting distinct strengths when subjected to tensile and compressive loads, employing multiple yield surfaces to delineate the stress-strain behavior for each loading condition proves advantageous. Multi-surface plasticity models offer a pragmatic solution as they are simpler to establish and calibrate in comparison to intricate single yield surfaces. Consequently, composite yield surfaces find widespread application in modeling various geomaterials such as soil, rock, and concrete. A fundamental principle involves the additive decomposition of the total strain increment,

$$d\varepsilon = d\varepsilon_e + d\varepsilon_p \quad \text{Eq. 3.1}$$

In the given expression,  $\varepsilon$  represents the overall strain experienced by the material, where  $\varepsilon_e$  denotes the elastic strain component and  $\varepsilon_p$  signifies the plastic strain component and  $d$  is the differential operator.

#### 3.2.1. Plastic Flow Rule

Plastic potential is a function used to determine the direction of plastic strain increment in the material under load. If the plastic potential is the same as the yield surface, the plastic flow rule is called an associated flow rule. Otherwise, it is called a non-associated flow (Figure 3-1).

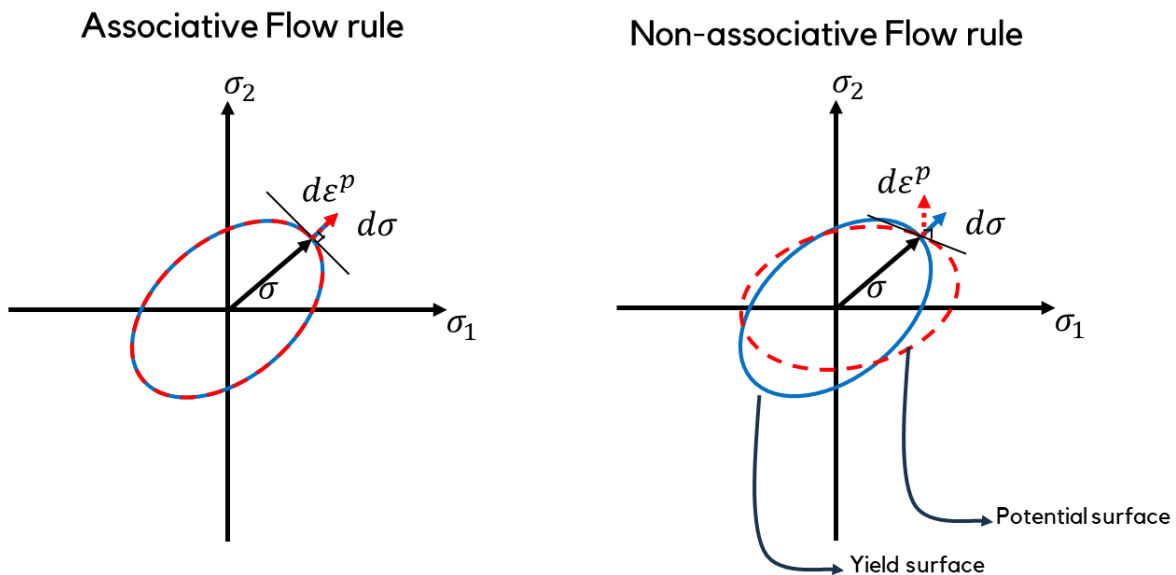


Figure 3-1. Comparison between the Associative Flow rule and the Non-associative Flow rule

Within the framework of non-associative mechanics, the plastic flow direction stems from the plastic potential function. In scenarios involving multi-surface plasticity, the flow rule extends its scope through the integration of multiple plastic functions. Thus, the increment in rate-independent plastic strain adheres to Koiter's rule (Warner, 1953), encapsulating the essence of plastic deformation mechanics.

$$d\varepsilon_p = \sum_{i=1}^M d\lambda_{p_i} \mathbf{g}_{p_i}, \boldsymbol{\sigma} \quad \text{Eq. 3.2}$$

In the presented formulation,  $\mathbf{g}_{p_i}(\boldsymbol{\sigma}, \kappa_{p_i})$  represents an active potential surface, while  $d\lambda_{p_i}$  signifies the associated proportionality factor, with  $M$  denoting the total number of active potential surfaces. The terms featuring indices separated by a comma, such as  $\mathbf{g}_{p_i}, \boldsymbol{\sigma} = \partial \mathbf{g}_{p_i} / \partial \boldsymbol{\sigma}$ , indicate partial differentiation, representing the gradient of the potential function regarding the stress tensor. In this discourse, each active yield surface is denoted as  $f_{p_i}(\boldsymbol{\sigma}, \kappa_{p_i})$ , and for an associative flow rule, the potential function  $\mathbf{g}_{p_i}$  aligns with the corresponding yield function  $f_{p_i}$ . Both the potential and hardening surfaces are dependent on the stress state  $\boldsymbol{\sigma}$  and a hardening function  $\kappa_{p_i}$ , which tracks the plasticity evolution for each active surface. Consequently, the increment in the plastic hardening function  $\kappa_{p_i}$  can be expressed in terms of the plastic proportionality factor.

$$d\kappa_{p_i} = d\lambda_{p_i} c_{p_i} \quad \text{Eq. 3.3}$$

$c_{p_i}(\boldsymbol{\sigma}, d\lambda_{p_i})$  is the equivalent hardening factor to be calibrated on physical basis.

### 3.2.2. Plastic Consistency Condition

The consistency condition should be assumed in order to obtain a whole relationship between stress and strain. For strain hardening solids, the consistency condition means that the stress remains on the new yield surface (expanded, contracted, or translated). In other words, plastic loading is known as a consistency condition where loading from a plastically deforming state leads to another plastically deforming state.

In the context of plastic deformations, it is imperative for stresses to remain confined within the yield surface. Consequently, the yield surface attains a value of zero during plastic flow to maintain this constraint.

Moreover, the proportionality factor, inherently non-negative, serves to prevent plastic unloading owing to the irreversible nature of plastic deformations. A proportionality factor of zero signifies exclusively elastic deformations. These principles, encapsulated within the Kuhn-Tucker conditions of plasticity, delineate the requisite conditions for plastic behavior and its constraints.

$$d\lambda_{p_i} \geq 0, \quad f_{p_i} \leq 0, \quad d\lambda_{p_i} f_{p_i} = 0, \quad 0 < i \leq N \quad \text{Eq. 3.4}$$

where  $N$  is the number of total surfaces out of which only  $M$  surfaces can be plastically active at a time but one of the Kuhn-Tucker conditions always apply. In a scenario where the initial  $M$  surfaces exhibit plastic activity, while the remaining surfaces remain inactive, one can derive the subsequent equations for each distinct group.

$$\begin{aligned} f_{p_i} = 0, \quad d\lambda_{p_i} > 0, \quad 0 < i \leq M \\ f_{p_i} < 0, \quad d\lambda_{p_i} = 0, \quad M < i \leq N \end{aligned} \quad \text{Eq. 3.5}$$

During a plastic process, when the yield surface function value remains at zero, the increase in the yield function is also zero, denoted as  $df_{p_i} = 0$ . This condition holds true as the yield surface is dependent on the stress state  $\boldsymbol{\sigma}$  and the corresponding hardening function  $\kappa_{p_i}$ . Consequently, the cumulative increment of each active yield surface during plastic deformations can be expressed as,

$$df_{p_i} = \frac{\partial f_{p_i}}{\partial \boldsymbol{\sigma}} : d\boldsymbol{\sigma} + \frac{\partial f_{p_i}}{\partial \kappa_{p_i}} d\kappa_{p_i} = 0, \quad , \quad 0 < i \leq M \quad \text{Eq. 3.6}$$

Both  $\partial f_{p_i}/\partial \boldsymbol{\sigma}$  and  $\boldsymbol{\sigma}$  represent second-order tensors, denoted by the symbol (:), indicating the tensorial product. Assuming that stress increments are solely elastic, expressed as  $d\boldsymbol{\sigma} = \mathbf{E} : d\boldsymbol{\varepsilon}_e$ , and leveraging equations Eq. 3.1 and Eq. 3.2 along with Eq. 3.6, results in the derivation of Eq. 3.7.

$$d\boldsymbol{\sigma} = \mathbf{E} : \left( d\boldsymbol{\varepsilon} - \sum_{j=1}^M d\lambda_{p_j} \mathbf{g}_{p_j} \boldsymbol{\sigma} \right) \quad \text{Eq. 3.7}$$

$\mathbf{E}$  is the fourth order elasticity tensor. By using Eq. 3.3 and Eq. 3.6 in Eq. 3.7, the consistency condition can be re-written as

$$df_{p_i} = \frac{\partial f_{p_i}}{\partial \boldsymbol{\sigma}} : \mathbf{E} : \left( d\boldsymbol{\varepsilon} - \sum_{j=1}^M d\lambda_{p_j} \mathbf{g}_{p_j}, \boldsymbol{\sigma} - d\boldsymbol{\varepsilon}_p \right) + \frac{\partial f_{p_i}}{\partial \kappa_{p_i}} d\lambda_{p_i} c_i = 0, \quad 0 < i \leq M \quad \text{Eq. 3.8}$$

Eq. 3.8 represents the formulation for each of the  $M$  active surfaces, necessitating the determination of  $M$  proportionality factors,  $d\lambda_{p_i}$ . Consequently, these proportionality factors,  $d\lambda_{p_i}$ , assume the role of primary unknowns, as they dictate the increments in plastic strain and the hardening function as depicted in Eq. 3.2 and Eq. 3.3 respectively. Once established, these factors enable the determination of stresses as updated in Eq. 3.7. However, it's worth noting that Eq. 3.8 poses a non-linear differential equation, typically necessitating a numerical approach for resolution.

### 3.3. Computational Algorithm

In formulating the numerical algorithm, express the equations in finite incremental form as indicated by Eq. 3.9:

$$\boldsymbol{\sigma}_{(n)} = \mathbf{E}(\boldsymbol{\varepsilon}_{(n)} + \boldsymbol{\varepsilon}_{p(n)}) \quad \text{Eq. 3.9}$$

Here, the subscript  $(n)$  denotes the last converged step of the material level stress return algorithm, signifying  $\boldsymbol{\sigma}_{(n)}$  as the last converged stress. It is essential to recognize that algorithm-related indices are denoted within parentheses. Step subscripts and iteration superscripts are employed accordingly. Moving forward to the subsequent step  $(n + 1)$ , following convergence, extract the strain  $\boldsymbol{\varepsilon}_{(n+1)}$  from the global algorithm. Initially, presume the strain increment  $\Delta\boldsymbol{\varepsilon}_{(n+1)} = \boldsymbol{\varepsilon}_{(n+1)} - \boldsymbol{\varepsilon}_{(n)}$  to be fully elastic. Consequently, establish the trial stress assuming a complete elastic increment, expressed as:

$$\boldsymbol{\sigma}_{(n+1)}^{trial} = \boldsymbol{\sigma}_{(n)} + \mathbf{E}\Delta\boldsymbol{\varepsilon}_{(n+1)} \quad \text{Eq. 3.10}$$

In the numerical computations, opt to utilize the Voigt notation, thus simplifying the treatment of stress, strain, and elastic tensors as vectors and matrices. When assessing the trial stress outlined in Eq. 3.10, should it fall within the elastic boundaries of the yield surface—potentially occurring during unloading or re-loading—accept this trial stress as the converged stress. Conversely, if the trial stress state surpasses the elastic threshold, indicating plastic deformation, trigger the plastic return mapping algorithm. This algorithm facilitates the adjustment of stress according to Eq. 3.11.

$$\boldsymbol{\sigma}_{(n+1)} = \boldsymbol{\sigma}_{(n)} + \mathbf{E}(\Delta\boldsymbol{\varepsilon}_{(n+1)} - \Delta\boldsymbol{\varepsilon}_{p(n+1)}) \quad \text{Eq. 3.11}$$

In the context provided,  $\boldsymbol{\sigma}_{(n+1)}$  denotes the stress subsequent to the plastic return mapping convergence at the conclusion of the present step ( $n + 1$ ). Eq. 3.11 delineates  $\Delta\boldsymbol{\varepsilon}_{p(n+1)}$  as the cumulative total of plastic strain accrued during step ( $n + 1$ ), typically necessitating iterative computations.

$$\Delta\boldsymbol{\varepsilon}_{p(n+1)}^{(k)} = \Delta\boldsymbol{\varepsilon}_{p(n+1)}^{(k-1)} + \delta\boldsymbol{\varepsilon}_{p(n+1)}^{(k)} \quad \text{Eq. 3.12}$$

In the iterative process ( $k$ ), the symbol  $\delta$  represents the increment within each iteration, distinguished from the symbol  $\Delta$ , which denotes the total increment within the step ( $n + 1$ ). Upon achieving convergent mapping after the final iteration, the updated strain produces  $\Delta\boldsymbol{\varepsilon}_{p(n+1)} = \Delta\boldsymbol{\varepsilon}_{p(n+1)}^{(k_{final})}$ .

### 3.3.1. Plastic deformation

The total plastic strain accumulated within step ( $n + 1$ ) have already been determined, the next step is to determine the plastic strain increment, denoted as  $\delta\boldsymbol{\varepsilon}_{p(n+1)}^{(k)}$ , within each iteration ( $k$ ) of the current step ( $n + 1$ ). To achieve this, recall Eq. 3.2,

$$\delta\boldsymbol{\varepsilon}_{p(n+1)}^{(k)} = \sum_{j=1}^{N=2} \delta\lambda_{p_j}^{(k)} \mathbf{g}_{p_j}^{(k)}, \boldsymbol{\sigma} \quad \text{Eq. 3.13}$$

The subscript ( $n + 1$ ) is omitted from the right-hand side of Eq. 3.13 for the sake of notation simplicity. Nevertheless, it is implicit that the iterations consistently occur within the current step ( $n + 1$ ). In Eq. 3.13, both the proportionality factor and the gradient of the potential function are denoted with the superscript ( $k$ ), signifying that their values are refreshed in each iteration. The iterative proportionality factor stands as the primary unknown, which is determined from the iterative incremental expression of Eq. 3.8, expressed as

$$\delta\mathbf{f}^{(k)} = \delta\mathbf{b}^{(k)} - \mathbf{A}^{(k)}\delta\boldsymbol{\lambda}^{(k)} \quad \text{Eq. 3.14}$$

In accordance with the consistency condition,  $\delta\mathbf{f}^{(k)}$  is a zero vector. Eq. 3.14 facilitates the determination of the proportionality factor  $\delta\boldsymbol{\lambda}^{(k)}$ .

$$\delta\boldsymbol{\lambda}^{(k)} = \mathbf{A}^{(k)-1} \delta\mathbf{b}^{(k)} \quad \text{Eq. 3.15}$$

In order to delineate the constituents outlined in Eq. 3.15 with precision, introduce the premise that the total count of active surfaces is limited to a maximum of two. Subsequently, in Section 3.4, elaborated is multi-surface plasticity framework tailored for concrete, wherein the system incorporates solely two surfaces, denoted as  $N = 2$ . In the context of a broad two-surface plasticity framework, the matrix  $\mathbf{A}^{(k)}$  articulated in Eq. 3.14 can be explicitly expressed as such:

$$\mathbf{A}^{(k)} = \begin{bmatrix} a_{11}^{(k)} & a_{12}^{(k)} \\ a_{21}^{(k)} & a_{22}^{(k)} \end{bmatrix} = \begin{bmatrix} \mathbf{n}_1^{(k)T} \mathbf{R}^{(k)} \mathbf{m}_1^{(k)} + f_{p_1, \kappa_1}^{(k)} c_1^{(k)} & \mathbf{n}_1^{(k)T} \mathbf{R}^{(k)} \mathbf{m}_2^{(k)} \\ \mathbf{n}_2^{(k)T} \mathbf{R}^{(k)} \mathbf{m}_1^{(k)} & \mathbf{n}_2^{(k)T} \mathbf{R}^{(k)} \mathbf{m}_2^{(k)} + f_{p_2, \kappa_2}^{(k)} c_2^{(k)} \end{bmatrix} \quad \text{Eq. 3.16}$$

Where

$$\mathbf{m}_i^{(k)} = \mathbf{g}_{p_i, \sigma}^{(k)}, \quad 0 < i \leq 2 \quad \text{Eq. 3.17}$$

$$\mathbf{n}_i^{(k)} = \mathbf{f}_{p_i, \sigma}^{(k)}, \quad 0 < i \leq 2 \quad \text{Eq. 3.18}$$

$$\mathbf{R}^{(k)} = (\mathbf{E}^{-1} \mathbf{Q}^{(k)})^{-1} \quad \text{Eq. 3.19}$$

The hardening functions in Eq. 3.16 are assumed uncoupled. The matrix  $\mathbf{Q}_i$  is

$$\mathbf{Q}^{(k)} = \left( \mathbf{I} + \mathbf{E} \sum_{j=1}^{N=2} \Delta\lambda_{p_j}^{(k)} \mathbf{H}_j^{(k)} \right) \quad \text{Eq. 3.20}$$

where  $\mathbf{I}$  represents the identity matrix and  $\mathbf{H}_i$  denotes the Hessian matrix of the active potential surface.

$$\mathbf{H}_i^{(k)} = \mathbf{m}_{i, \sigma}^{(k)}, \quad 0 < i \leq 2 \quad \text{Eq. 3.21}$$

On the other hand, the vector  $\delta\mathbf{b}^{(k)}$  in Eq. 3.14 can be written as

$$\delta\mathbf{b}^{(k)} = \mathbf{f}^{(k)} - \mathbf{h}^{(k)} \quad \text{Eq. 3.22}$$

in which  $\mathbf{f} = \langle f_{p1} \ f_{p2} \rangle^T$  and the superscript  $(k)$  indicates that the yield surface values used in Eq. 3.22 are updated in each iteration, i.e.

$$f_{p_i}^{(k)} = f_{p1}(\boldsymbol{\sigma}_{(n+1)}^{(k)}, \kappa_{p_i}^{(k)}) \quad 0 < i \leq 2 \quad \text{Eq. 3.23}$$

Where

$$\boldsymbol{\sigma}_{(n+1)}^{(k)} = \boldsymbol{\sigma}_{(n)} + \mathbf{E}(\Delta \boldsymbol{\varepsilon}_{(n+1)} - \Delta \boldsymbol{\varepsilon}_{p(n+1)}^{(k)}) \quad \text{Eq. 3.24}$$

And

$$\kappa_{p_i}^{(k)} = \kappa_{p_i}^{(k-1)} + \delta \kappa_{p_i}^{(k)} \quad 0 < i \leq 2 \quad \text{Eq. 3.25}$$

In Eq. 3.22 the vector  $\mathbf{h}^{(k)}$  is defined as

$$\mathbf{h}^{(k)} = \begin{Bmatrix} h_1^{(k)} \\ h_2^{(k)} \end{Bmatrix} \quad \text{Eq. 3.26}$$

whose components can be written as

$$h_i^{(k)} = \mathbf{n}_i^{(k)T} \mathbf{R}_i^{(k)} \mathbf{E}^{-1} \mathbf{r}_i^{(k)} \quad 0 < i \leq 2 \quad \text{Eq. 3.27}$$

To derive vector  $\delta \mathbf{b}^{(k)}$  in Eq. 3.14 in finite incremental form, the consistency condition,  $d\mathbf{b} = \mathbf{f}_{,\sigma} : \mathbf{E} : d\boldsymbol{\varepsilon}$  is replaced with the finite incremental form of the consistency condition. For this purpose, first refer to the finite form of the yield condition i.e.  $f_{p_i}^{(k)} = 0$ , which is then truncated using first order Taylor series approximation in the neighbour of the trial stress  $\boldsymbol{\sigma}_{(n+1)}^{(trial)}$ . From Eq. 3.11, the converged stress state that satisfies the consistency condition can be written in terms of the trial stress as

$$\boldsymbol{\sigma}_{(n+1)} = \boldsymbol{\sigma}_{(n+1)}^{trial} - \mathbf{E} \Delta \boldsymbol{\varepsilon}_{p(n+1)} \quad \text{Eq. 3.28}$$

Backward-Euler finite difference procedures derived from the first order Taylor series expansion are commonly adopted as time-stepping procedures in, (Pramono and Willam, 1989), which in our context lead to Eq. 3.14. Furthermore, two of the most commonly adopted time stepping procedures for plasticity are



Closest Point Projection and Cutting Plane Algorithms. Both are Elastic-Prediction-Plastic-Correction procedures in which, when triggered the return mapping to yield surface is performed after a full elastic assumption, for which the second term on the right of Eq. 3.28 is pursued. Thus, plastic strain is assumed zero for the initial iteration, i.e.  $\delta\varepsilon_{p(n+1)}^{(0)} = \mathbf{0}$ . On the other hand, the stress state in the gradients of the potential and yield surfaces in Eq. 3.17 and Eq. 3.18, respectively determine whether the algorithm is Cutting Plane or Closest Point Projection. For calculating the gradients, while the former algorithm uses the stress state at the end of the previous iteration, i.e.  $\boldsymbol{\sigma}_{(n+1)}^{(k-1)}$ , the later uses the updated stress state, i.e.  $\boldsymbol{\sigma}_{(n+1)}^{(k)}$ . To implement the Cutting Plane Algorithm, one enforces the satisfaction of the yield condition in iterations i.e.,  $f_{p_i}^{(k)} < tol$ . In addition, the Closest Point Projection Algorithm employs the first order Taylor approximation of the finite form of the flow rule so that the direction between the trial and the converged stress is enforced to be the closest-point projection direction from the trial stress point  $\boldsymbol{\sigma}_{(n+1)}^{trial}$  towards the last updated stress  $\boldsymbol{\sigma}_{(n+1)}^{(k)}$ , i.e.

$$\mathbf{r}^{(k)} = \boldsymbol{\sigma}_{(n+1)}^{(k)} - \boldsymbol{\sigma}_{(n+1)}^{trial} + \mathbf{E} \sum_{j=1}^{N=2} \Delta\lambda_{p_j}^{(k)} \mathbf{m}_j^{(k)} \quad \text{Eq. 3.29}$$

Where  $\mathbf{r}^{(k)}$  is a residual vector that should also vanish at the end of the iterations, i.e.  $\left\| \sum_{j=1}^{N=2} \Delta\lambda_{p_j}^{(k)} \mathbf{m}_j^{(k)} - \Delta\varepsilon_{p(n+1)}^{(k)} \right\| < tol$ . The proportionality factor components in Eq. 3.20 and Eq. 3.29 are updated as

$$\Delta\lambda_{p_i}^{(k)} = \Delta\lambda_{p_i}^{(k-1)} + \delta\lambda_{p_i}^{(k)} \quad 0 < i \leq 2 \quad \text{Eq. 3.30}$$

To find a solution that satisfies both conditions  $f_{p_i}^{(k)} = 0$  and  $\|\mathbf{r}^{(k)}\| = 0$  of Closest Point Projection Algorithm, one can implement the Newton-Raphson solution scheme. Thus, from the linearization of [Galic et al. \(2011\)](#) and  $f_{p_i}^{(k)} = 0$ , respectively one obtains

$$\mathbf{r}^{(k)} + \delta\boldsymbol{\sigma}^{(k)} + \mathbf{E} \sum_{j=1}^{N=2} \Delta\lambda_{p_j}^{(k)} \mathbf{H}_j^{(k)} \delta\boldsymbol{\sigma}^{(k)} + \mathbf{E} \sum_{j=1}^{N=2} \Delta\lambda_{p_j}^{(k)} \mathbf{m}_j^{(k)} = 0 \quad \text{Eq. 3.31}$$

And

$$f_{p_i}^{(k)} + \mathbf{n}_i^{(k)T} \delta \boldsymbol{\sigma}^{(k)} + f_{p_i, \kappa_i}^{(k)} c_{p_i}^{(k)} \delta \lambda_{p_i}^{(k)} = 0, \quad 0 < i \leq 2 \quad \text{Eq. 3.32}$$

where Eq. 3.3 was used in iterative-incremental form, i.e,  $\delta \kappa_{p_i} = \delta \lambda_{p_i} c_{p_i}$ . Solving for  $\delta \boldsymbol{\sigma}^{(k)}$  from Eq. 3.31 produces

$$\delta \boldsymbol{\sigma}^{(k)} = -\mathbf{Q}^{-1} \left( \mathbf{r}^{(k)} + \mathbf{E} \sum_{j=1}^{N=2} \Delta \lambda_{p_j}^{(k)} \mathbf{m}_j^{(k)} \right) \quad \text{Eq. 3.33}$$

Substituting Eq. 3.33 into Eq. 3.32 produces the vector of proportionality factors as in Eq. 3.15, i.e.

$$\delta \boldsymbol{\lambda}^{(k)} = \begin{Bmatrix} \delta \lambda_{p_1}^{(k)} \\ \delta \lambda_{p_2}^{(k)} \end{Bmatrix} \quad \text{Eq. 3.34}$$

The solutions of  $\delta \lambda_{p_1}^{(k)}$  are then used in Eq. 3.13 to update the plastic strain increment within the current step ( $n + 1$ ). On the other hand, to implement the Cutting Plane Algorithm as a special case, one needs to assume that the residual vector  $\mathbf{r}^{(k)}$  in Eq. 3.29 *a-priori* vanishes and  $\mathbf{R} = \mathbf{E}$  in all iterations, which bypasses the need for the calculation of the Hessian matrix  $\mathbf{H}_i$  of the active surfaces in Eq. 3.21, which might be difficult to obtain analytically if the potential surface function is complicated. Nevertheless, the potential surface's function adopted in this study conveniently vanishes, i.e.  $\mathbf{R} = \mathbf{E}$  is valid also for the Closest-Point Projection Algorithm by virtue of the concrete material model adopted in Section 3.4 due to the fact that selected potential functions are low order. Thus, which of the algorithms used in this study is only a matter of whether the vanishing of the residual vector  $\mathbf{r}^{(k)}$  is adopted as a condition or not.

It is also important to note that to obtain a unique solution for  $\delta \boldsymbol{\lambda}^{(k)}$  from Eq. 3.15, the matrix  $\mathbf{A}^{(k)}$  should be invertible. In associative perfect plasticity, the uniqueness conditions are automatically met. For the case with associative plasticity with hardening, hardening-related terms enforce a limit on uniqueness of the solution (Simo & Hughes, 2006).

On the other hand, for the general case, where plastic flow is non-associative and hardening takes place, the uniqueness of the solution relies on all terms of the matrix  $\mathbf{A}^{(k)}$ . For the matrix  $\mathbf{A}^{(k)}$  to be invertible, the conditions can be written as

$$a_{11}^{(k)} > 0, \quad a_{22}^{(k)} > 0, \quad \det(\mathbf{A}^{(k)}) = |\mathbf{A}^{(k)}| = a_{11}^{(k)} a_{22}^{(k)} - a_{12}^{(k)} a_{12}^{(k)} > 0 \quad \text{Eq. 3.35}$$

in which the first two conditions are related to the single-surface plasticity while the third condition arises when both surfaces are active. If any of the three conditions in Eq. 3.35 is not satisfied due to the fact that  $f_{p_1, \kappa_1}^{(k)} c_1^{(k)} < 0$  or  $f_{p_2, \kappa_2}^{(k)} c_2^{(k)} < 0$  in the softening regions, then assign  $f_{p_1, \kappa_1}^{(k)} c_1^{(k)} = 0$  and/or  $f_{p_2, \kappa_2}^{(k)} c_2^{(k)} = 0$ , where necessary to prevent premature convergence failures.

### 3.3.2. Possible Scenarios of the Return Algorithm

When both surfaces are active, refer to it as the first scenario, which is when the non-converged stresses are in the corner zone region of the stress space. On the other hand, during the return mapping process at the intermediate iterations, if the stress state is outside of the corner zone, then it yields to the classical single-surface plasticity problem. When only the first surface is active, refer to it as the second scenario and when only the second surface is active, refer to it as the third scenario. Finally, when no surface is active and thus, the stress is in the elastic region, refer to it as scenario zero. Figure 3-2, the boundaries between corner zone and single-surface zones are denoted with the symbols  $\partial C_1$  and  $\partial C_2$  on both sides. In the following, introduce the criteria for the selection of the active surface.

#### 3.3.2.1. Scenario 1 – Both surfaces are Active

When both surfaces are active at the initial iteration, the Kuhn-Tucker conditions given in Eq. 3.5 for  $M = 2$  produces

$$\begin{aligned} f_1^0 > 0 \quad \delta \lambda_1^0 > 0 \\ f_2^0 > 0 \quad \delta \lambda_2^0 > 0 \end{aligned} \quad \text{Eq. 3.36}$$

It should be noted that Eq. 3.36 is implemented in a finite incremental fashion therefore, before convergence is achieved both yield conditions are violated which makes the surfaces active during the iterations. As

mentioned above, select the scenario to implement out of the four possible scenarios after evaluating the yield surface values of the initial iteration, i.e.  $f_i^0 > 0$ . On the other hand, from, Eq. 3.15 requirement of a solution for positive proportionality factors, i.e.,  $\delta\lambda_i^0 > 0$ , produces

$$\delta\lambda_1^0 = \frac{a_{22}^0 \delta b_1^0 - a_{12}^0 \delta b_2^0}{|\mathbf{A}^0|} \quad \text{Eq. 3.37}$$

$$\delta\lambda_2^0 = \frac{-a_{21}^0 \delta b_1^0 + a_{11}^0 \delta b_2^0}{|\mathbf{A}^0|}$$

From Eq. 3.37, the criteria to activate Scenario 1 can be obtained as

$$a_{22}^0 f_1^0 \geq a_{12}^0 f_2^0 \quad \text{Eq. 3.38}$$

$$a_{11}^0 f_2^0 \geq a_{21}^0 f_1^0$$

which are in addition to the uniqueness conditions provided in Eq. 3.35 and violation of yield conditions in Eq. 3.36 for the initial iteration.

### 3.3.2.2. Scenario 2 – Only Surface 1 is Active

When only the first surface is active at the initial iteration, the Kuhn-Tucker conditions given in Eq. 3.5 produces

$$f_1^0 > 0 \quad \delta\lambda_1^0 > 0 \quad \text{Eq. 3.39}$$

$$f_2^0 = 0 \quad \delta\lambda_2^0 > 0$$

From, Eq. 3.15 requirement of a solution for positive proportionality factor for  $i = 1$ , i.e.,  $\delta\lambda_1^0 > 0$ , produces

$$a_{22}^0 f_1^0 \geq a_{12}^0 f_2^0 \quad \text{Eq. 3.40}$$

$$a_{21}^0 f_1^0 > a_{11}^0 f_2^0 \quad \text{Eq. 3.41}$$

It is also interesting to note that, in this case the return point is affected by whether the algorithm is Closest-Point Projection or Cutting-Plane.

### 3.3.2.3. Scenario 3 – Only surface 2 is Active

For when only the second surface is active, the Kuhn-Tucker conditions produces

$$f_2^0 = 0 \quad \delta\lambda_1^0 > 0 \quad \text{Eq. 3.42}$$

$$f_1^0 > 0 \quad \delta\lambda_2^0 > 0$$

From, Eq. 3.15 requirement of a solution for positive proportionality factor for  $i = 2$ , i.e.,  $\delta\lambda_2^0 > 0$ , produces

$$a_{12}^0 f_2^0 > a_{22}^0 f_1^0 \quad \text{Eq. 3.43}$$

$$a_{11}^0 f_2^0 \geq a_{21}^0 f_1^0 \quad \text{Eq. 3.44}$$

Similar to Scenario 2, again the converged stress point is affected by whether the algorithm is Closest-Point Projection or Cutting-Plane.

### 3.3.2.4. Scenario 0 – No Surface is active

When the Kuhn-Tucker conditions at initial iterations are such that

$$f_1^0 < 0 \quad \delta\lambda_1^0 = 0 \quad \text{Eq. 3.45}$$

$$f_2^0 < 0 \quad \delta\lambda_2^0 > 0$$

then there is no active surface and accept the trial stress as the final stress within the incremental step ( $n + 1$ ).

### 3.3.3. Parameters Considering Viscosity update

The viscous behavior can be considered as a modification to the values obtained after the above time integration algorithm described based on the rate-independent plasticity assumption. This approach is often

referred to as Duvaut and Lions model (Ibrahimbegovic, 2009), in which the final value of stresses as well as hardening parameters are expressed as a linear combination of the trial elastic value and the converged stress of the rate independent algorithm, where the weighting factors are functions of the time step and the retardation time. Introducing viscous effects improves the numerical stability which may be required in the case of strain softening (Simo & Hughes, 2006). According to Duvaut and Lions model, the updated stress and evolution parameters can be written as

$$\boldsymbol{\sigma}_{(n+1)}^{final} = \boldsymbol{\sigma}_{(n)} e^{-\beta \Delta t} + \boldsymbol{\sigma}_{(n+1)} (1 - e^{-\beta \Delta t}) + \frac{(1 - e^{-\beta \Delta t})}{\beta \Delta t} \mathbf{E} \Delta \boldsymbol{\varepsilon}_{(n+1)} \quad \text{Eq. 3.46}$$

And

$$\kappa_i^{final} = \kappa_{i(n)} e^{-\beta \Delta t} + \kappa_{i(n+1)} (1 - e^{-\beta \Delta t}) \quad \text{Eq. 3.47}$$

in which  $\beta = 1/\tau$ , where  $\tau$  is the retardation time and  $\Delta t$  is the time increment of the step. The retardation time is a viscosity related material property which refers to the necessary time for complete stress relaxation to the final state. Thus, under the rate independent plasticity assumption of no relaxation, i.e.,  $\tau \rightarrow 0$ , for any  $\Delta t$ , Eq. 3.46 and Eq. 3.47 regenerate  $\boldsymbol{\sigma}_{(n+1)}$  and  $\kappa_{i(n+1)}$ , respectively, which are the last converged values of the rate-independent plasticity algorithm described above.

### 3.3.4. Material Definition in Heigh-Westergaard Coordinates

As isotropic material assumption is adopted, Heigh-Westergaard coordinates for its convenience will be used. The return mapping will take place in the Rendulic plane due to the fact that the plastic return direction being limited to Rendulic plane as a result of the selected potential functions. Figure 3-2 depicts a generic two surface model in Rendulic plane, where  $\xi$  is a measure of the volumetric component of the stress state and  $\rho$  is a measure of deviatoric component of the stress state, i.e.

$$\xi = \frac{1}{\sqrt{3}} \text{tr}(\boldsymbol{\sigma}) \quad \text{Eq. 3.48}$$

$$\rho = \sqrt{2J_2} \quad \text{Eq. 3.49}$$

Heigh-Westergaard coordinates are related to the principal stress components as

$$\begin{Bmatrix} \sigma_1 \\ \sigma_2 \\ \sigma_3 \end{Bmatrix} = \frac{1}{\sqrt{3}} \begin{Bmatrix} \xi \\ \xi \\ \xi \end{Bmatrix} + \sqrt{\frac{2}{3}} \rho \begin{Bmatrix} \cos \theta \\ \cos \left( \theta - \frac{2\pi}{3} \right) \\ \cos \left( \theta + \frac{2\pi}{3} \right) \end{Bmatrix} \quad \text{Eq. 3.50}$$

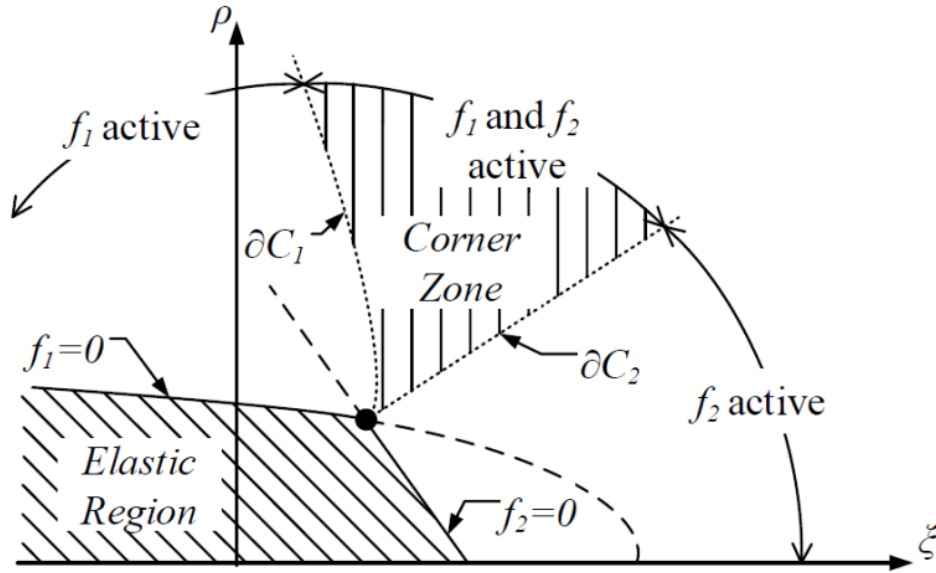


Figure 3-2. Two surface model in Rendulic Plane

in which  $\theta$  is the Lode angle that defines the orientation according to the polar coordinate system within the deviatoric plane of the Heigh-Westergaard space.

For further details about Heigh-Westergaard coordinate system one is referred to (Jirasek & Bazant, 2001).

The Lode angle  $\theta$  is related to the deviatoric stress tensor components as

$$\cos 3\theta = \frac{3\sqrt{3}}{3} \frac{J_3}{J_2^{3/2}} \quad \text{Eq. 3.51}$$

In Eq. 3.49, Eq. 3.53 and Eq. 3.51, the following stress tensor invariants have been used.

$$\sigma_v = \frac{I_1}{3} = \frac{1}{3} \text{tr}(\boldsymbol{\sigma})$$

$$J_2 = \frac{1}{2} \text{tr}(\mathbf{s}^2) \quad \text{Eq. 3.52}$$

$$J_3 = \frac{1}{3} tr(\mathbf{s}^3) = \det(\mathbf{s})$$

in which  $tr$  is trace operator,  $\sigma_V$  is the volumetric stress and  $\mathbf{s}$  is the deviatoric stress components of the stress tensor  $\boldsymbol{\sigma}$ , i.e.

$$\mathbf{s} = \boldsymbol{\sigma} - \sigma_V \boldsymbol{\delta} \quad \text{Eq. 3.53}$$

where  $\boldsymbol{\delta}$  is the Kronecker's delta

$$\delta_{ij} = \begin{cases} 1, & i = j \\ 0, & i \neq j \end{cases} \quad \text{Eq. 3.54}$$

### ***Material Parameters in terms of Bulk and Shear Moduli***

By virtue of the material model selected in Section 3.4, the matrix  $\mathbf{A}$  used in Eq. 3.15 for plastic stress return calculations can be conveniently expressed in terms of the bulk and shear moduli. For the alternative expression of  $\mathbf{A}$ , first refer to the elastic stress due to elastic strain. From Eq. 3.53, one obtains

$$\boldsymbol{\sigma} = \mathbf{s} + \sigma_V \boldsymbol{\delta} = \mathbf{E} : \boldsymbol{\varepsilon} = 3K\epsilon_V \boldsymbol{\delta} + 2G\mathbf{e} \quad \text{Eq. 3.55}$$

Where

$$K = \frac{E}{3(1 - 2\nu)} \quad \text{Eq. 3.56}$$

And

$$G = \frac{E}{2(1 + \nu)} \quad \text{Eq. 3.57}$$

written above in terms of the Elasticity Modulus  $E$  and Poisson's ratio  $\nu$  and in Eq. 3.55, volumetric strain



$$\epsilon_V = \frac{\text{tr}(\boldsymbol{\varepsilon})}{3} \quad \text{Eq. 3.58}$$

and deviatoric strain

$$\boldsymbol{e} = \boldsymbol{\varepsilon} - \epsilon_V \boldsymbol{\delta} \quad \text{Eq. 3.59}$$

definitions were used. From the definition in Eq. 3.55 to Eq. 3.59, one obtains the relation

$$\boldsymbol{\sigma}_V = 3K\epsilon_V \quad \text{Eq. 3.60}$$

$$\boldsymbol{s} = 2G\boldsymbol{e} \quad \text{Eq. 3.61}$$

Note that for shear stress-shear strain relations in Voigt vector notation Eq. 3.61 should be evaluated as

$$\boldsymbol{\tau} = G\boldsymbol{\gamma} \quad \text{Eq. 3.62}$$

This difference between the values in tensor and vector notations for shear strain components, i.e.  $\boldsymbol{\gamma} = 2\boldsymbol{e}$ , in which  $\boldsymbol{e}$  refers to the last three components of the six-dimensional deviatoric strain tensor. Thus, shear strains should be treated with caution in numerical calculations. By using Eq. 3.50, Eq. 3.60 and Eq. 3.61,  $f_{p,\sigma}^T \mathbf{E} g_{p,\sigma}$  can be written alternatively as

$$f_{p_i,\sigma}^T \mathbf{E} g_{p,\sigma} = 3K f_{p_i,\xi} g_{p_i,\xi} + 2G f_{p_i,\rho} g_{p_i,\rho} + \frac{2G}{\rho^2} f_{p_i,\theta} g_{p_i,\theta}, \quad 0 < i \leq 2 \quad \text{Eq. 3.63}$$

from which by substituting into Eq. 3.16, one obtains

$$\mathbf{A}^{(0)} = \begin{bmatrix} 3K f_{p_1,\xi}^0 g_{p_1,\xi}^0 + 2G f_{p_1,\rho}^0 g_{p_1,\rho}^0 + f_{p_1,\kappa_1}^0 c_1^0 & 3K f_{p_1,\xi}^0 g_{p_2,\xi}^0 + 2G f_{p_1,\rho}^0 g_{p_2,\rho}^0 \\ 3K f_{p_2,\xi}^0 g_{p_1,\xi}^0 + 2G f_{p_2,\rho}^0 g_{p_1,\rho}^0 & 3K f_{p_2,\xi}^0 g_{p_2,\xi}^0 + 2G f_{p_2,\rho}^0 g_{p_2,\rho}^0 + f_{p_2,\kappa_2}^0 c_2^0 \end{bmatrix} \quad \text{Eq. 3.64}$$

where  $g_{p_i,\theta} = 0$  for  $0 < i \leq 2$  was used to eliminate the last term in Eq. 3.63. In Eq. 3.64, the superscript indicates the initial iteration, i.e.,  $(k) = 0$ . Eq. 3.64 have been obtained for the initial iteration for the purpose of identifying the target yield surface. As it will be discussed next, in this algorithm the return surface have been selected at the initial iteration based on Eq. 3.64, after which the procedure explained in Section 3.3.1 above, is used to update the stresses. It should be noted that  $f_{p,\sigma}$  and  $g_{p,\sigma}$  are generally tensors,

however, all terms on the right-hand side of Eq. 3.63, e.g.  $f_{p,\xi}$ , are conveniently scalar quantities which are provided in Section 3.4.

### 3.4. Material Model Specifics

#### 3.4.1. Menetrey-Willam Yield Surface for Compression

The yield surfaces are described in terms of Haigh-Westergaard in stress space. Haigh-Westergaard coordinates are  $(\xi, \rho, \theta)$ , where  $\xi$  is the hydrostatic stress invariant,  $\rho$  is the deviatoric stress invariant,  $\theta$  is the deviatoric polar angle as described in Section 3.3.4. The yield surface proposed by [Menetrey & Willam \(1995\)](#) is given by the following equation:

$$f_{p_1}(\xi, \rho, \theta) = 1.5 \left( \frac{\rho}{f_c} \right)^2 + q_h(\kappa_p) m \left( \frac{\rho}{f_c \sqrt{6}} r + \frac{\xi}{f_c \sqrt{3}} \right) - q_h(\kappa_p) q_s(\kappa_p) \leq 0 \quad \text{Eq. 3.65}$$

where  $f_c$  is the uni-axial compressive strength. In Eq. 3.65,  $m$  is introduced as a measure of frictional strength in [Menetrey & Willam \(1995\)](#) and it can be written as

$$m = 3 \frac{f_c^2 - f_t^2}{f_c f_t} \frac{e}{e + 1} \quad \text{Eq. 3.66}$$

in which  $f_t$  is the uniaxial tensile strength and  $e$  is called eccentricity which describes the out-of-roundness of the yield surface in the deviatoric plane (Figure 3-3).

$$e = \frac{1 + \epsilon}{2 - \epsilon} \quad \text{Eq. 3.67}$$

Where

$$\epsilon = \frac{f_t f_b^2 - f_c^2}{f_b f_c^2 - f_t^2} \quad \text{Eq. 3.68}$$

In Eq. 3.65,  $r$  is the radius in the deviatoric plane which is a function of the deviatoric polar angle  $\theta$  and the eccentricity  $e$  i.e.

$$r(\theta, e) = \frac{v(\theta, e)}{s(\theta, e) - t(\theta, e)} \quad \text{Eq. 3.69}$$

Where

$$v(\theta, e) = 4(1 - e^2) \cos^2 \theta + (2e - 1)^2 \quad \text{Eq. 3.70}$$

$$s(\theta, e) = 2(1 - e^2) \cos \theta \quad \text{Eq. 3.71}$$

$$t(\theta, e) = (2e - 1)[4(1 - e^2) \cos^2 \theta + 5e^2 - 4e]^{1/2} \quad \text{Eq. 3.72}$$

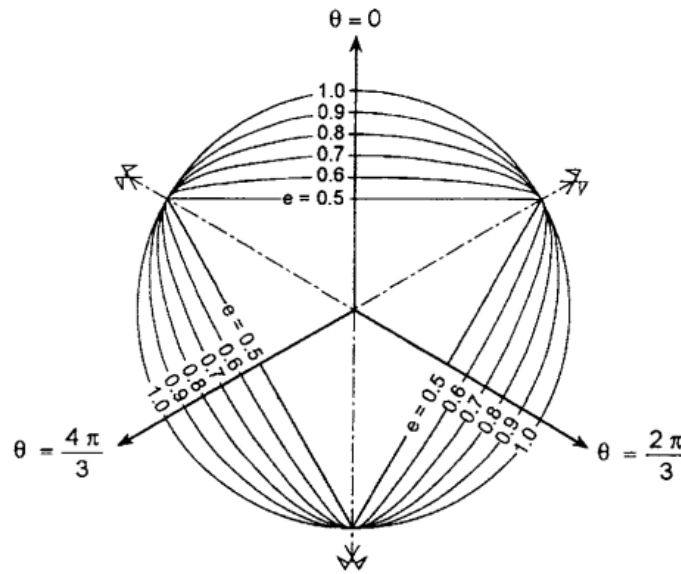


Figure 3-3. Deviatoric Plane *Menetrey & Willam (1995)*

### **Hardening and softening functions**

An isotropic hardening law based on which hardening and softening functions is adopted, i.e.,  $q_h$  and  $q_s$  respectively, only change the size of the yield surface, controlled by the hardening/softening parameter  $\kappa_{p1}$ .

Following [Grassl et al. \(2002\)](#), select the hardening parameter to be the plastic volumetric strain  $\epsilon_v^p$ . i.e.

$$\dot{\kappa}_{p1} = \dot{\epsilon}_v^p = \dot{\lambda}_p \frac{\sqrt{3}}{q_h q_s} \quad \text{Eq. 3.73}$$

where superimposed  $\cdot$  indicates rate. The function  $q_h$  is active in the hardening region and it is unity beyond the peak strain whereas  $q_s$  is active in the softening region. According to the hardening law in [Grassl et al. \(2002\)](#), the hardening function in Eq. 3.65 can be written as

$$q_h(\kappa_{p_1}) = q_h(\varepsilon_v^p) = k_0 + (1 - k_0) \sqrt{1 - \left( \frac{\varepsilon_{v0}^p - \varepsilon_v^p}{\varepsilon_{v0}^p} \right)^2} \quad \text{Eq. 3.74}$$

Where

$$k_0 = \sigma_{c_0} / f_c \quad \text{Eq. 3.75}$$

in which  $\sigma_{c_0}$  is the uniaxial concrete stress at the onset of plastic flow. In Eq. 3.74,  $\varepsilon_{v0}^p$  is the threshold value for the volumetric plastic strain at uniaxial concrete strength, i.e.

$$\varepsilon_{v0}^p = \frac{f_c}{E_c} (1 - 2\nu_c) \quad \text{Eq. 3.76}$$

where  $E_c$  and  $\nu_c$  are the Young's modulus and Poisson ratio for concrete, respectively.

$$q(\kappa_{p_1}) = q_h(\kappa_{p_1}) q_s(\kappa_{p_1}) \quad \text{Eq. 3.77}$$

The softening function  $q_s$  is unity during the hardening range and its value is updated only beyond the peak compressive strain, i.e.

$$q_s(\kappa_{p_1}) = \left( \frac{1}{1 + \left( \frac{n_1 - 1}{n_2 - 1} \right)^2} \right)^2 \quad \text{Eq. 3.78}$$

Where

$$n_1 = \frac{\varepsilon_v^p}{\varepsilon_{v0}^p} \quad \text{Eq. 3.79}$$

And

$$n_2 = \frac{\varepsilon_{v0}^p + t_c}{\varepsilon_{v0}^p} \quad \text{Eq. 3.80}$$

in which  $t_c$  is a calibrated parameter and considering MPa as the stress unit, it is recommended to use  $t_c = f_c/15000$ , (Papanikolaou & Kappos, 2007).

### 3.4.2. Potential Function for Compression

The linear potential function proposed in (Lee & Fenves, 1998) is adopted, which can be expressed in Haigh–Westergaard coordinates as

$$g_{p_1}(\xi, \rho) = -B\rho + \xi - a \quad \text{Eq. 3.81}$$

where  $B$  controls the slope in Rendulic Plane and it is chosen to give proper dilatancy. Lee & Fenves (1998) suggested a value between -6.6 and -5 in their case studies, which is adopted herein. The effect of slope  $B$  will be shown in Chapter 5 Numerical Results. It should be noted that more sophisticated potential functions that describe the confined concrete behaviour more accurately were discussed by Grassl et al. (2002) and Papanikolaou & Kappos (2007), which may cause some differences in results when the concrete is confined. However, in our experience the linear potential function selected herein performs well in numerical simulations as will be shown in Chapter 5, while other alternatives may cause convergence issues especially when tensile stresses are involved. It should also be noted that as the gradient of the potential function is used and not the potential function value itself, the value of  $a$  in Eq. 3.81 has no influence in the derivation of equations and results. It is a constant introduced to adjust the position of the potential function to be meaningful, i.e., to meet with the point of current stress state.

### 3.4.3. Rankine Yield Surface for Tension Cut-off

In tensile region, non-associative flow rule is also adopted to be able to use a potential function that is independent of the polar angle  $\theta$ , while using the Rankine yield surface to limit the maximum stress at the tensile strength. In Haigh–Westergaard coordinates the Rankine surface can be written as

$$f_{p_2}(\xi, \rho, \theta) = \sqrt{2}\rho \cos \theta + \xi - \sqrt{3}f_t \quad \text{Eq. 3.82}$$

On the other hand, the potential function is obtained by removing the dependence to angle  $\theta$  in Eq. 3.82 as

$$g_{p_2}(\xi, \rho) = \sqrt{2}\rho + \xi - b \quad \text{Eq. 3.83}$$

By adopting the potential function in Eq. 3.83, assure that the condition  $g_{p_2, \theta} = 0$ , which was used in the derivation of Eq. 3.64 is valid in the tension zone. Similar to the compressive potential surface constant  $a$ , the value of  $b$  in Eq. 3.83 has no influence in the derivation of the equations.

### 3.5. Solution of the Global Equilibrium Equations

#### 3.5.1. Variational Form of the Equilibrium Equations

To refer to difference in the finite element solution, first start with the general equilibrium equations based on the principle of virtual work i.e.

$$\delta\Pi = \delta\mathbf{W}^{int} - \delta\mathbf{W}^{ext} = 0 \quad \text{Eq. 3.84}$$

where  $\delta\mathbf{W}^{int}$  is the variation of the internal work, i.e.,

$$\delta\mathbf{W}^{int} = \int_V \delta\boldsymbol{\varepsilon}^T \boldsymbol{\sigma} dV \quad \text{Eq. 3.85}$$

And  $\delta\mathbf{W}^{ext}$  is the virtual work done by the external loads, i.e.,

$$\delta\mathbf{W}^{ext} = \delta\mathbf{d}^T \mathbf{P}^{ext} \quad \text{Eq. 3.86}$$

where  $\mathbf{P}^{ext}$  is the vector of the external nodal forces and  $\delta\mathbf{d}$  is the vector of the displacement variations. In the finite element form, refer to vector  $\delta\mathbf{d}$  as the nodal displacement vector. A relation can be directly built between the variations of strains and the variations of nodal displacements in the form of

$$\delta\boldsymbol{\varepsilon} = \mathbf{B}\delta\mathbf{d}_e \quad \text{Eq. 3.87}$$

where  $\mathbf{d}_e$  is the element displacement vector and matrix  $\mathbf{B}$  forms the element level discretized strain-displacement relations, which depends on the selected finite element interpolation field. For matrix  $\mathbf{B}$  geometrically linear small-strain assumptions have been adopted.

#### 3.5.2. Linearization of the Equilibrium Equations

Linearization of Eq. 3.84 produces

$$\delta \mathbf{d} \cdot \nabla_d \delta \Pi = \int_V \mathbf{B}^T \mathbf{C}_{ep} \mathbf{B} dV = \delta \mathbf{d}^T \mathbf{K}_{Gt} \delta \mathbf{d} \quad \text{Eq. 3.88}$$

Conventional displacement has been adopted based finite element formulations with standard assemblage procedures. Therefore, the formation of the nodal displacement vector  $\mathbf{d}$  as an assemblage of element displacements  $\mathbf{d}_e$  and all the relevant procedures are standard. Transition from the element level matrix  $\mathbf{B}$  to global level relations in Eq. 3.87 are not further elaborated herein and further details can be found in [Robert et al., \(2007\)](#). In Eq. 3.88,  $\mathbf{K}_{Gt}$  denotes the tangent stiffness matrix and  $\nabla_d$  is the gradient with respect to the nodal displacement vector. In Eq. 3.88,  $\mathbf{C}_{ep}$  is the material level tangent modulus which can be written as

$$\mathbf{C}_{ep} = \mathbf{E}[\mathbf{I} - \mathbf{m}_b \mathbf{A}^{-1} \mathbf{n}_a^T \mathbf{E}] \quad \text{Eq. 3.89}$$

Where

$$\mathbf{n}_a^T = \begin{Bmatrix} \mathbf{n}_1^T \\ \mathbf{n}_2^T \end{Bmatrix} \quad \text{Eq. 3.90}$$

$$\mathbf{m}_b^T = \begin{Bmatrix} \mathbf{m}_1^T \\ \mathbf{m}_2^T \end{Bmatrix} \quad \text{Eq. 3.91}$$

were used. In deriving Eq. 3.89, the differential equations  $d\boldsymbol{\lambda} = \mathbf{A}^{-1} \mathbf{n}_a^T \mathbf{E} d\boldsymbol{\varepsilon}$  and  $d\varepsilon_p = \mathbf{m}_b$  were substituted into  $d\boldsymbol{\sigma} = \mathbf{E}(d\boldsymbol{\varepsilon} - d\varepsilon_p)$ . The Newton-Raphson solution of the non-linear equilibrium equation in Eq. 3.84 produces

$$\begin{bmatrix} \mathbf{K}_{Gt} & -\mathbf{P}^{ext} \\ \mathbf{a}^{T(j)} & b^{(j)} \end{bmatrix} \begin{Bmatrix} \delta \mathbf{d}^{(j)} \\ \delta \boldsymbol{\Lambda}^{(j)} \end{Bmatrix} = - \begin{Bmatrix} \mathbf{r}_d^{(j)} \\ c^{(j)} \end{Bmatrix} \quad \text{Eq. 3.92}$$

where  $\boldsymbol{\Lambda}^{(j)}$  is a scaling factor that sets up the applied load level within each global iteration ( $j$ ) and  $\mathbf{r}_d^{(j)}$  is the residual of the global equilibrium condition in Eq. 3.84 calculated at the end of each iteration. To solve the above augmented system of equations more efficiently the iterative displacement vector can be decomposed as

$$\delta \mathbf{d}^{(j)} = \delta \Lambda^{(j)} \delta \mathbf{d}_p^{(j)} + \delta \mathbf{d}_r^{(j)} \quad \text{Eq. 3.93}$$

where  $\delta \mathbf{d}_p^{(j)} = \mathbf{K}_{Gt}^{-1} \mathbf{P}^{\text{ext}}$  and  $\delta \mathbf{d}_r^{(j)} = \mathbf{K}_{Gt}^{-1} \mathbf{r}_d^{(j)}$  From the second row of the augmented equation in Eq. 3.93 and using the displacement components, one obtains

$$\delta \Lambda^{(j)} = \frac{c^{(j)} - \mathbf{a}^{\text{T}(j)} \delta \mathbf{d}_r^{(j)}}{\mathbf{a}^{\text{T}(j)} \delta \mathbf{d}_p^{(j)}} \quad \text{Eq. 3.94}$$

In Eq. 3.93 and Eq. 3.94, the vector  $\mathbf{a}^{(j)}$  and the constant  $c^{(j)}$  enforces a constraint condition at each global iteration ( $j$ ), which allows selection of alternative control parameters while keeping the load scaling factor  $\Lambda$  a variable. It should be noted that the equations is solved in an incremental-iterative manner, where a modified Newton-Raphson procedure is adopted and thus, update the stiffness matrix only at the beginning of the initial iteration. Therefore,  $\mathbf{C}_{ep}$  and accordingly  $\mathbf{K}_{Gt}$  are presented without any reference to iteration ( $j$ ). However, they are updated after each converged increment. Adopted is the displacement control method to be able to trace the load-deflection curve beyond the peak strength. For the displacement-control method, the constraint conditions are such that the vector  $\mathbf{a}^{(j)}$  is composed of zero components except a unity at the controlled degree-of-freedom and the constant  $c^{(j)}$  takes the prescribed displacement value. Further details on the displacement-control algorithm can be found in the literature of [Batoz & Dhatt \(1979\)](#).

### 3.5.3. Selected Finite Element Types

In the modeling process of the concrete bulk utilizing a 3D material model, the 8-node solid element featuring 6-degrees-of-freedom per node is used, including nodal rotations, as outlined by [Ibrahimbegovic & Wilson \(1991\)](#). The steel reinforcement bars and stirrups are frame element type with 6-degrees-of-freedom and are represented using 2-node 1D elements. The beam type elements incorporating both translational and rotational degrees-of-freedom are adopted to ensure compatibility between solid and re-bar elements.

### 3.5.4. Uni-axial Sugano Model for 1D Beam-Type Analysis

In the realm of structural engineering, plain concrete exhibits a brittle behavior when subjected to uniaxial compression. However, the deformability of concrete experiences enhancement when subjected to confinement. Confinement effectively enables concrete to endure higher strains at the peak load, often



exhibiting minimal strength decay thereafter. The strain observed at peak stress is intricately tied to the effectiveness of the confinement mechanism. Building upon the work of previous researchers such as [Saatcioglu and Razvi \(1992\)](#) and [Mander et al. \(1988\)](#), an expression has been identified to yield accurate predictions of experimentally obtained strain values corresponding to peak stress  $\varepsilon_{cc}$ .

$$\varepsilon_{cc} = \varepsilon_{co} \left( 1 + 5 \left( \frac{f'_{cc}}{f'_{co}} - 1 \right) \right) \quad \text{Eq. 3.95}$$

Where

$$f'_{cc} = f'_{co} + \left( -1.254 + 2.254 \sqrt{1 + 7.94 \frac{f_l}{f'_{co}} - 2 \frac{f_l}{f'_{co}}} \right) \quad \text{Eq. 3.96}$$

It is imperative to note that  $\varepsilon_{co}$ , denoting the strain corresponding to peak stress of unconfined concrete, must be determined under the same rate of loading employed for the confined concrete. In instances where experimental data is lacking, a value of 0.002 may be deemed appropriate for  $\varepsilon_{co}$  under a slow rate of loading condition.

Eq. 3.96 denotes the compressive strength of confined concrete and was defined by [Mander et al. \(1988\)](#).

$$f_l = 0.5k_e\rho_c f_{yt} \quad \text{Eq. 3.97}$$

$f_l$  represents the effective lateral confining stress on the concrete ([Saatcioglu & Razvi, 1992](#)).  $k_e = \frac{A_e}{A_{cc}}$  is the confinement effectiveness coefficient.  $f_{yt}$  denotes the yield strength of transverse reinforcement.  $\rho_c = \frac{4A_{st}}{b_s s}$  is area ratio of transverse confinement reinforcement.  $A_{st}$  is the area of transverse reinforcement within spacing  $s$ .

$$f'_{co} = 0.85f_c \quad \text{Eq. 3.98}$$

where

$$f_c = \frac{1}{\delta_f - 0.041} (0.127f_{yt}\rho_c - 0.052\sigma_c) \quad \text{Eq. 3.99}$$

In which  $\delta_f$  is the ultimate displacement defined as the displacement angle at which 80% of the maximum strength is sustained in load versus displacement angle curve based on some experimental data carried out by [Sugano \(1997\)](#) thus Eq. 3.99 was acquired.

# Chapter 4

## Description of the finite element models

### 4.1.ABAQUS Model

#### 4.1.1. Concrete model in ABAQUS

The values of said parameters were utilized in accordance with the specifications outlined in the experimental data. The finite element software ABAQUS was used for comparison purposes, in which a coupled plastic damage model for concrete is available. The concrete damage plasticity (CDP) constitutive model is employed by ABAQUS to represent inelastic behavior. The model under consideration takes into account two primary failure processes, namely tensile cracking and compressive crushing (ABAQUS, 2008).

The CDP model in ABAQUS is derived from plastic behavior, compressive behavior, and tensile behavior. The investigation of the compressive behavior of concrete necessitates the establishment of a correlation between the yield stress and inelastic strain. The CDP model primarily focuses on the development of reinforced concrete structures. Therefore, the implementation of a stress-strain model for concrete, specifically the design-oriented model proposed by Milad et al. (2017), was carried out.

In order to establish the plasticity model of concrete, it is necessary to determine certain key parameters. The parameters under consideration include the dilation angle ( $\psi$ ), the plastic potential eccentricity ( $e$ ), the ratio of the initial equibiaxial compressive yield stress to the initial uniaxial compressive yield stress  $f_{b_0}/f_{c_0}$ , the ratio of the second stress invariant on the tensile meridian which governs the shape of the yield surface ( $k_c$ ), and the viscosity ( $u$ ). The dilation angle was selected as 31 degrees based on the calibration process. Milad et al. (2017) provided definitions for the eccentricity ( $e$ ), the ratio of the distance between

the foci to the length of the major axis ( $fb_0/fc_0$ ), the constant  $k_c$ , and the parameter ( $u$ ). Specifically, the values assigned to these variables were 0.1, 1.16, 2/3, and zero, respectively.

#### 4.1.2. Reinforcements in ABAQUS

The behavior of steel and FRP was modelled as elastic perfectly plastic model. The parameters which were used to define the model are modulus of elasticity, yield stress, and Poisson's ratio. Figure 4-1 illustrates the reinforcement arrangement for SW-1 in ABAQUS.

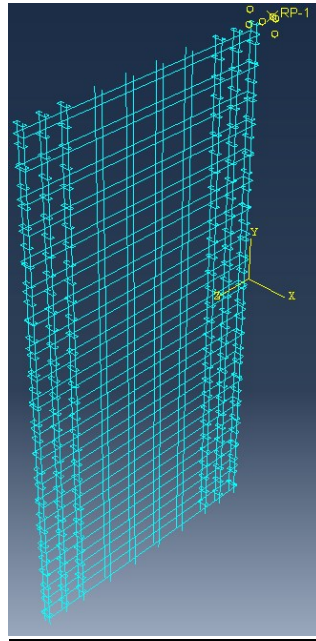


Figure 4-1. Reinforcement configuration in ABAQUS.

#### 4.1.3. Finite Element Types and Meshing in ABAQUS

To effectively simulate the concrete column in ABAQUS, distinct element types have been employed to represent the various components of the beams and shear walls. The primary materials included in the model are concrete, steel, and fiber-reinforced polymer (FRP). The primary material used for the concrete is represented in the model as a homogeneous 8-node 3D brick element, specifically the C3D8R element. Additionally, the longitudinal and transverse steel and FRP materials are represented in the model as linear truss elements, namely the T3D2 element.

In order to simulate the interaction between the concrete and the reinforcement, a constraint is applied to the embedded region. The purpose of the embedded contact region is to ensure that the number of

translational degrees of freedom (DOF) at a node on the embedded element is equivalent to the number of translational degrees of freedom at a node on the host element (referred to as Compatible DOF). The reinforcement was incorporated within the concrete, which is regarded as the host region. Hence, it can be observed that the concrete and reinforcement elements are interconnected at a common node, assuming an ideal link between them.

It is imperative that all elements possess a congruent degree of freedom and are interconnected via a common node. Consequently, in order to assure the accuracy of the results derived from the finite element model, all the utilized elements in the model were uniformly allocated the same mesh size. The model utilizes a mesh size of 25 mm in order to attain optimal outcomes while maintaining a suitable simulation pace.

#### **4.1.4. Boundary Condition and Loading in ABAQUS**

In the ABAQUS analysis, the shear walls were subjected to fixed boundary conditions at the bottom in all directions, while being freed at the top, except at the location where the load was applied. The beams, on the other hand, were supported using pinned connections (pin and roller). To determine the load-deflection characteristics of the simulated beams and shear walls, a static monotonic load was applied at the designated loading location. The displacement control approach was utilized to apply loading till failure. The displacement increments were modified to 1 millimeter for each successive step.

### **4.2. Model properties**

#### **4.2.1. Beams**

Three reinforced concrete beams were modelled, D-C1 × 9, S-C1 × 9 and ISO30-1. D-C1 × 9 and S-C1 × 9 were 2800mm long; the total length includes two parts of 400 mm beyond supports providing an additional bond length for the intrados reinforcing bars. ISO30-1 was 3000mm long; 200mm × 300 mm (width × depth). The first specimen S-C1 × 9 had a shallow rectangular cross section 200mm × 100 mm (width × depth) as described in Figure 4-2 to Figure 4-4. The second beam D-C1 × 9 had a deep cross section 100 mm × 200 mm (width × depth) as between Figure 4-5 and Figure 4-7. Given cube concrete strength values were converted into cylindrical concrete strength values by multiplying them with 0.83 (Focacci et al. 2016).  $f_c = 66.6$  MPa and the Modulus of elasticity of 38882 MPa are the material characteristics of deep and

shallow beams. FRP reinforcements with  $d_b = 9$  mm. Both the deep and shallow beams in ABAQUS were fixed in the bottom in all directions and released at the top except the top middle point where the load was applied.

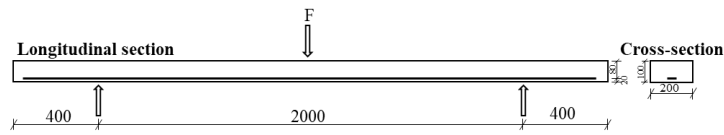


Figure 4-2. Shallow S-C1-9 beam test setup and dimensions (units in mm)

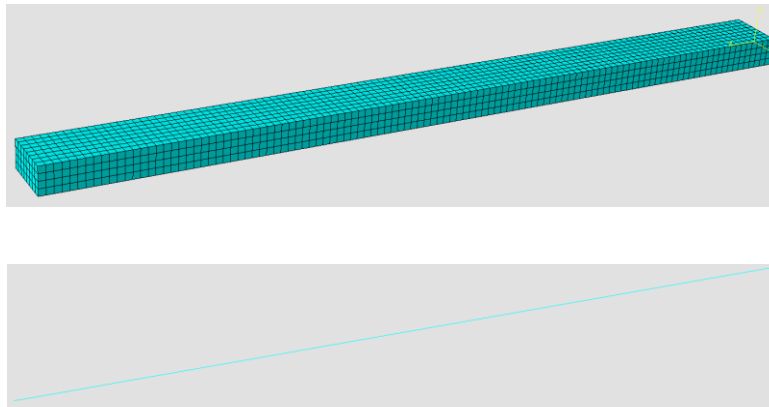


Figure 4-3. ABAQUS Depiction of S-C1-9 beam (top: meshed beam, bottom: reinforcement)

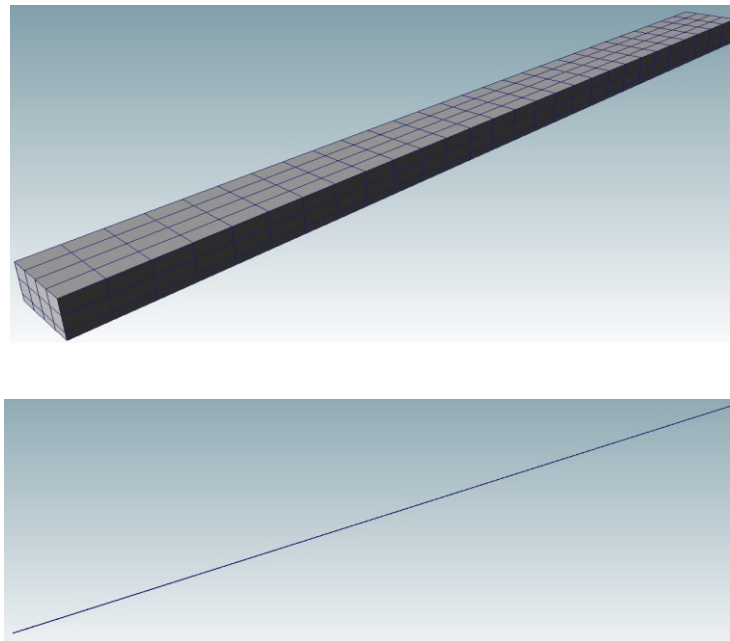


Figure 4-4. Shallow S-C1-9 beam FEAVIEWER configuration

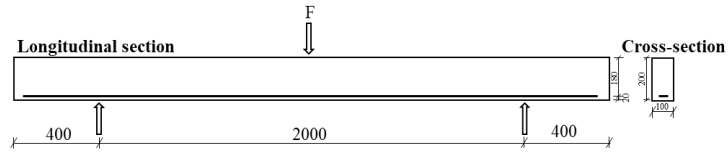


Figure 4-5. Deep D-CI-9 beam test setup and dimensions (units in mm)

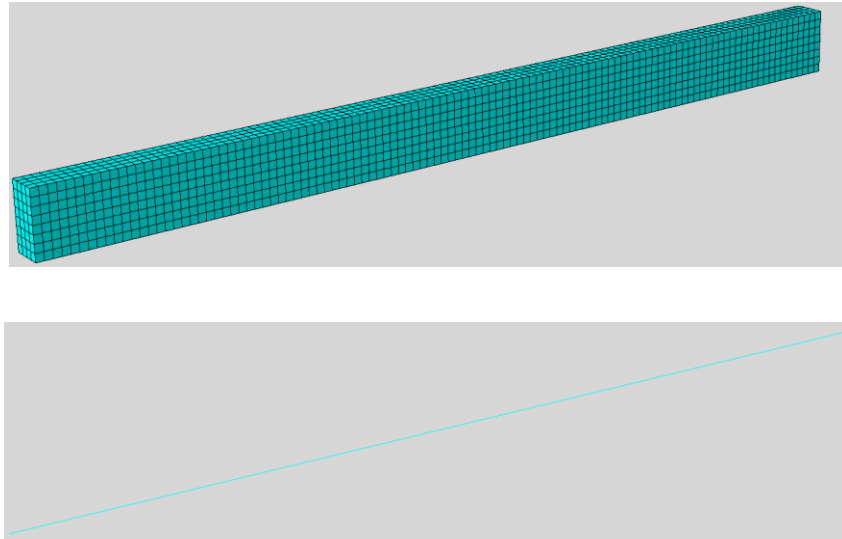


Figure 4-6. ABAQUS Depiction of D-CI-9 beam (top: meshed beam, bottom: reinforcement)

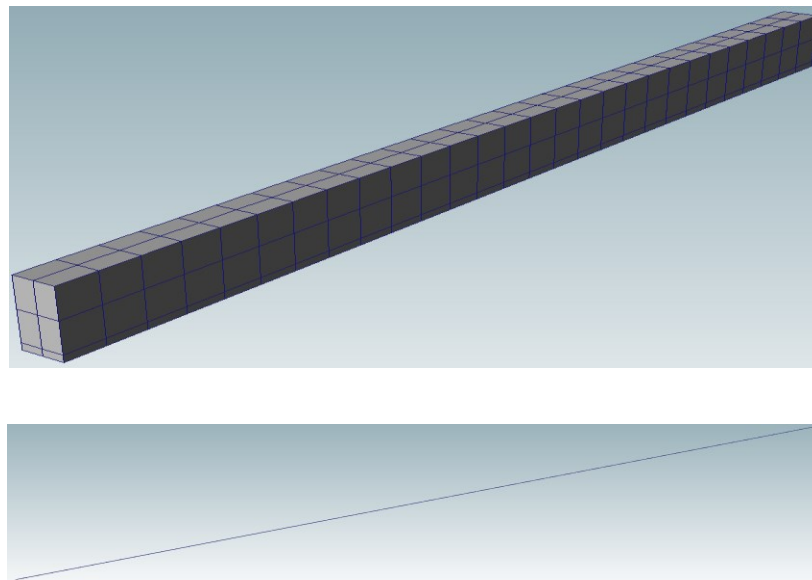


Figure 4-7. Deep D-CI-9 beam FEAViewer configuration

The third beam was 200 mm wide and 300 mm high [Benmokrane et al. \(1995\)](#). As shown in Figure 4-8 to Figure 4-10, it was simply supported on a span of 3000 mm and was subjected to two equal loads

symmetrically placed about the mid-span. The modulus of elasticity of concrete was 32 GPa and  $f_c=44$  MPa. Yielding stress for steel rebars was taken as 480 MPa, the ultimate strength was taken as 600 MPa and the modulus of elasticity was taken as 200 GPa. Conventional steel stirrups (10 mm diameter) were used in the non-constant moment zones, to prevent shear failure. The diameter of the reinforcement was maintained constant (19.1 mm diameter) and this beam was reinforced by two identical rebar as resumed in Figure 4-8.

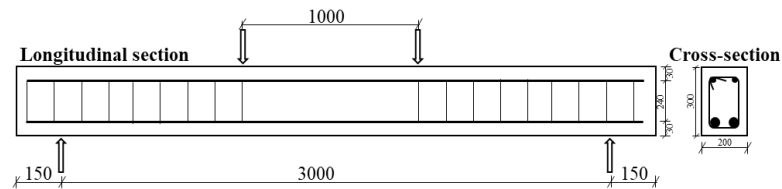


Figure 4-8. Reinforcement details of ISO30-1 beam (Benmokrane et al. (1995))

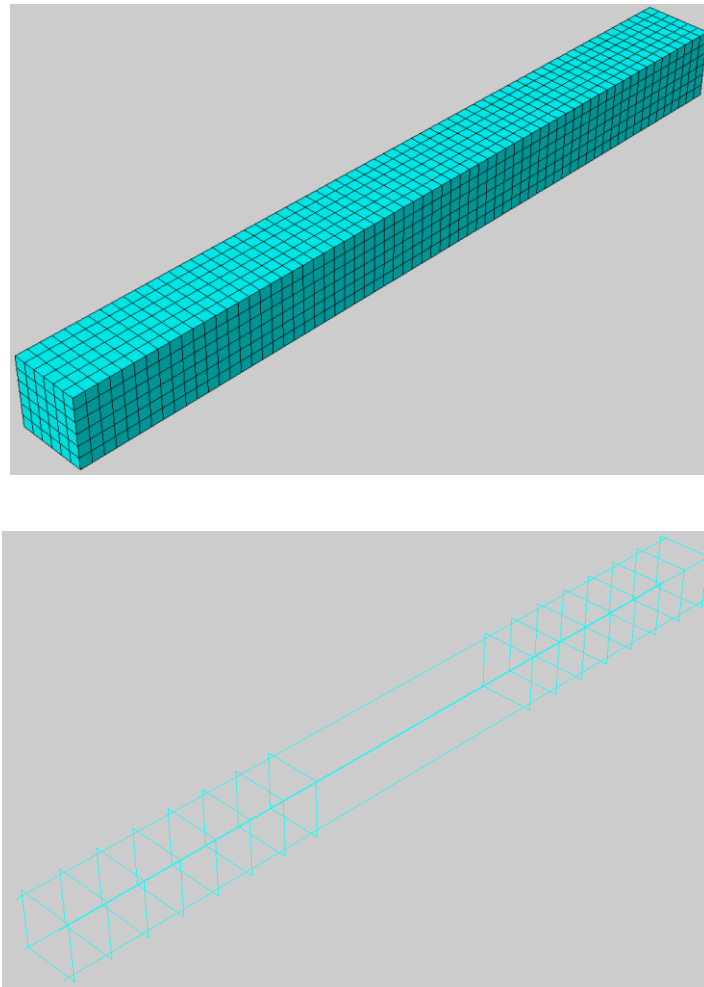
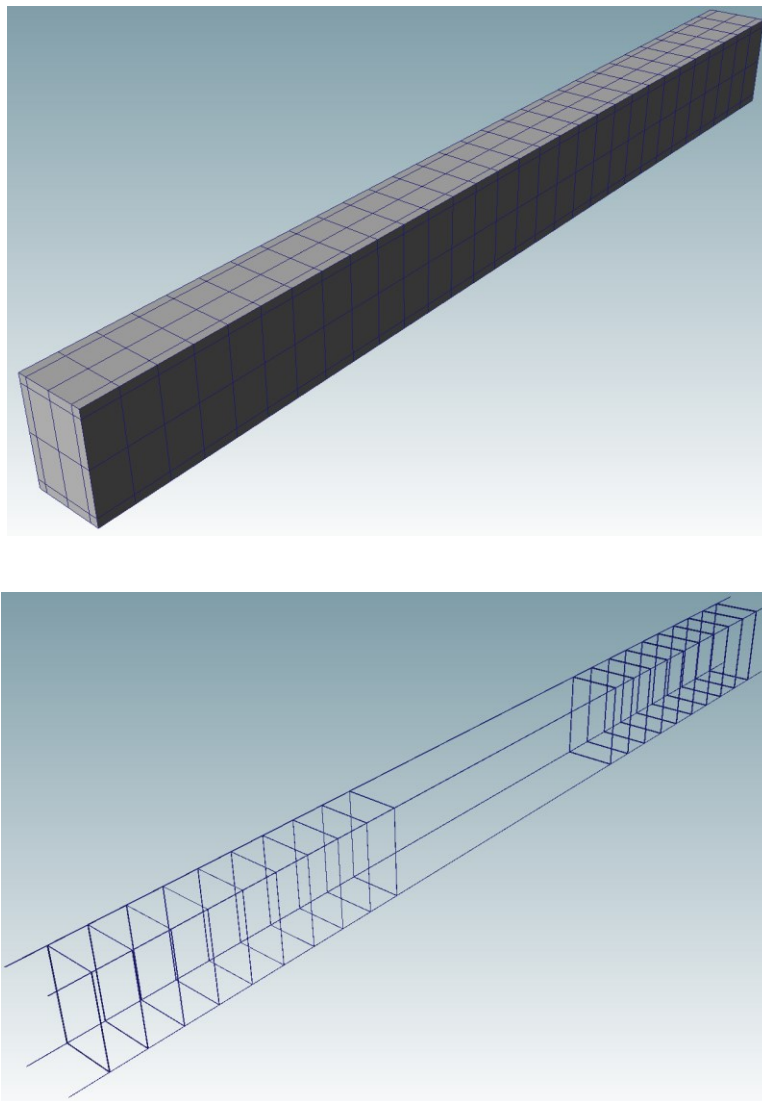


Figure 4-9. ABAQUS Depiction of ISO30-1 beam (top: meshed beam, bottom: reinforcement)



The elastic performance of concrete was determined based on the elastic modulus and Poisson's ratio. The values of those parameters were used as specified in the experimental data. For the inelastic behavior, ABAQUS uses the concrete damage plasticity (CDP) constitutive model. This model considers two main failure mechanisms, which are tensile cracking and compressive crushing [ABAQUS \(2008\)](#).

The CDP model in ABAQUS forms from plastic behavior, compressive behavior, and tensile behavior. The compressive behaviour of concrete requires determining the relationship between the yield stress and inelastic strain. The CDP model is primary developed for reinforced concrete structures. Thus, a design-oriented stress-strain model for concrete [Lam & Teng \(2003b\)](#) was implemented.



*Figure 4-10. ISO30-1 beam FEAVIEWER configuration*

#### 4.2.2. Shear walls

Two rectangular shear wall was modeled from the study of [Qian and Chen \(2005\)](#) – SW-1 and [Mohamed et al. \(2014\)](#) – G-15. The SW-1 wall by [Qian and Chen \(2005\)](#) was fixed at bottom and free at the top. The specimen had a height of 1900 mm and length of 1000 mm. The material properties of steel bars are listed in Table 4.1. welded hot-rolled steel bar (HRB400) fabrics, welded cold-rolled ribbed steel bar (CRB550) fabrics and CD, cold-drawn steel bar was used. The concrete cube compressive strength used 25.2 MPa, 774.4 kN as the axial load applied at top of specimen.

*Table 4.1. Properties of SW-1 reinforcements*

Grade of bar	Location	d: mm	$f_y$ :MPa	$f_u$ :MPa	$E_s$ : GPa
HRB 400	Distributed reinforcements	6	451.7	631.7	200
HRB 335	Vertical reinforcements in boundary zones	10	395	595	194
CD	Hoops in boundary zones	4	631.7	671.7	209

Reinforcement details of shear walls are given below from Figure 4-11 and Figure 4-14, all units are in millimeters

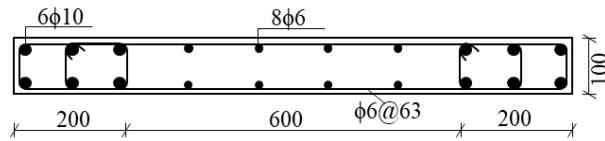


*Figure 4-11. Top view dimensions and reinforcement details of SW-1*

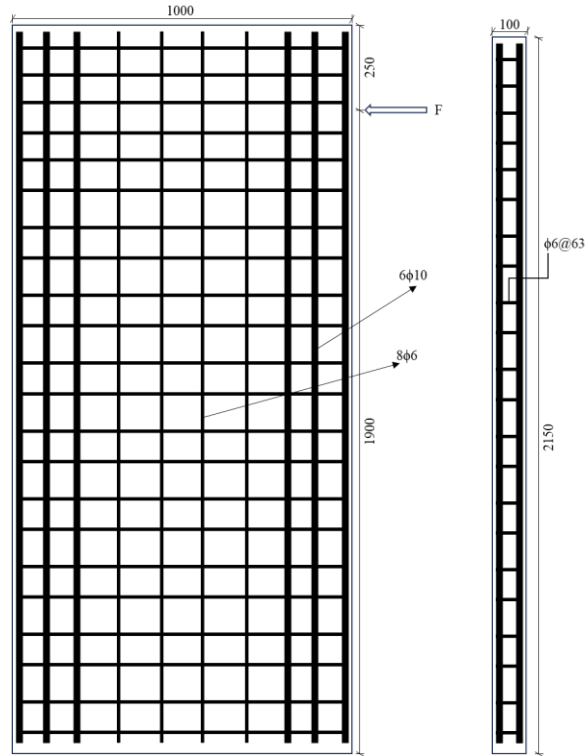


Figure 4-12. Elevation of SW-1

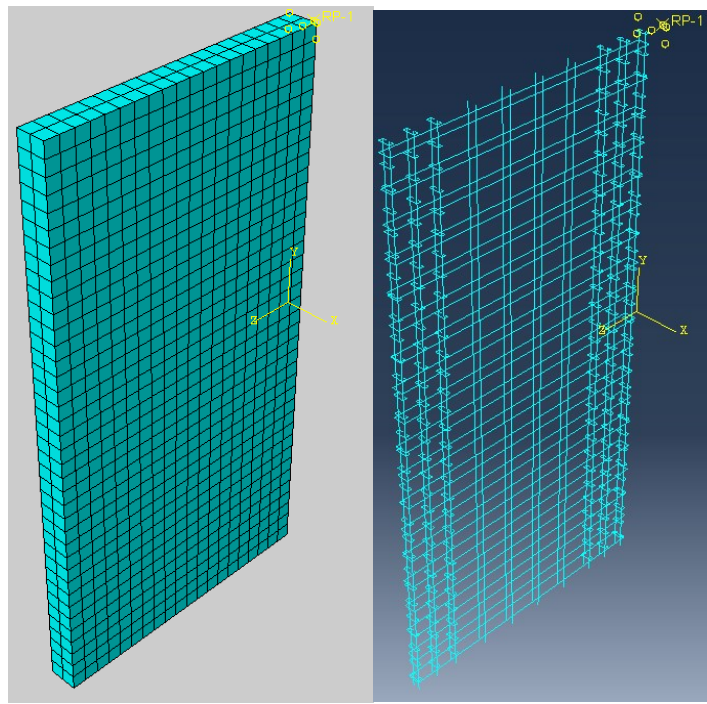


Figure 4-13. ABAQUS Depiction of SW1 shear wall (Left: meshed beam, Right: reinforcement)

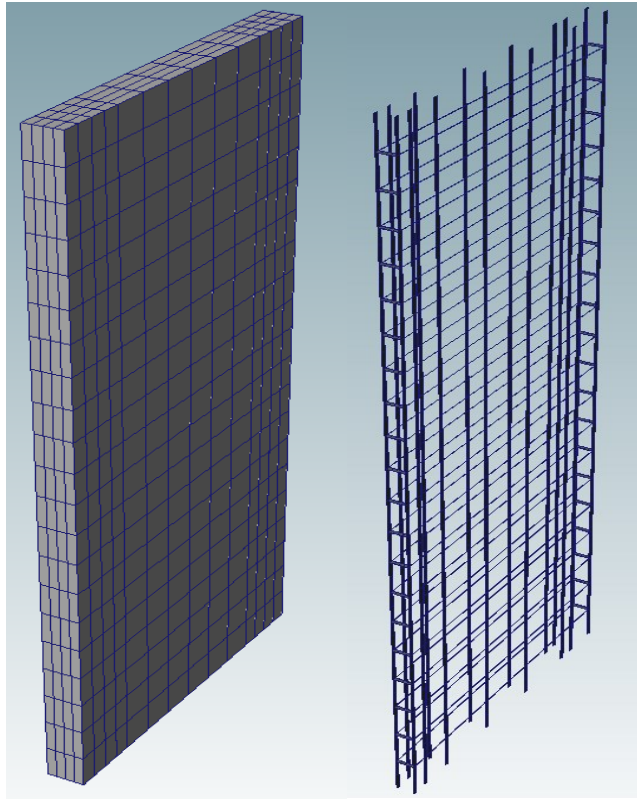
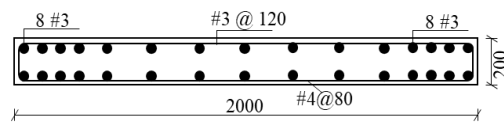


Figure 4-14. SW-1 Shear wall FEAVIEWER configuration

The specimen G-15 by Mohamed et al. (2015) represent a single shear wall complying with the special seismic requirements specified in CSA A23.3 (CAN/CSA 2004) and ACI 318 (ACI 2007) for the seismic-force resisting systems (SFRSs). The minimum thickness and reinforcement details were according to CSA S806 (CAN/CSA 2012) and ACI 440.1R-06 (ACI 2006) were applied for the GFRP-reinforced walls. The wall specimens were 3,500 mm in height, 200 mm thick and was 1,500 mm in length as shown in Figure 4-15. G-15 concrete dimensions and details of reinforcement configuration



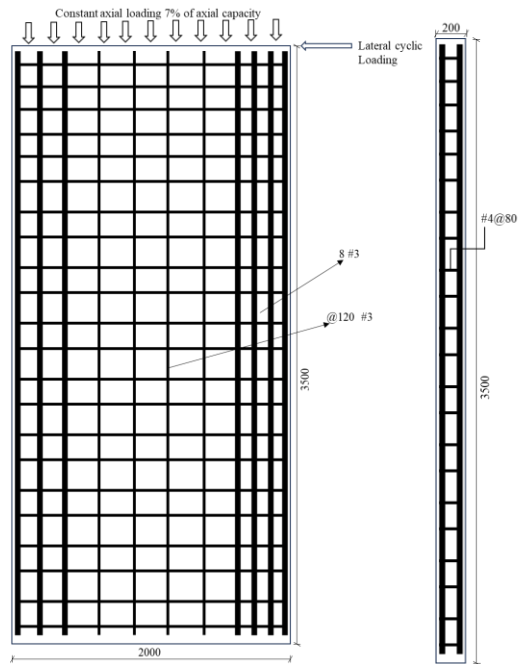


Figure 4-15. G-15 concrete dimensions and details of reinforcement configuration

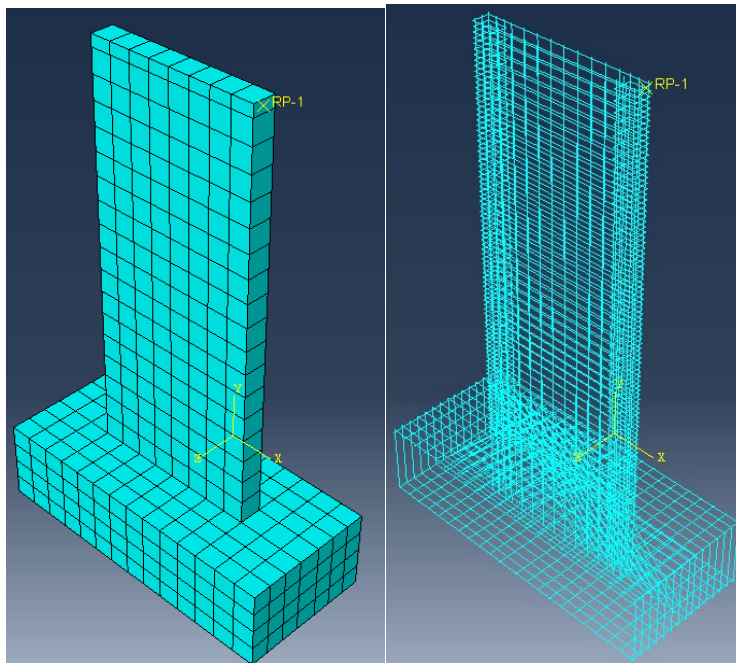
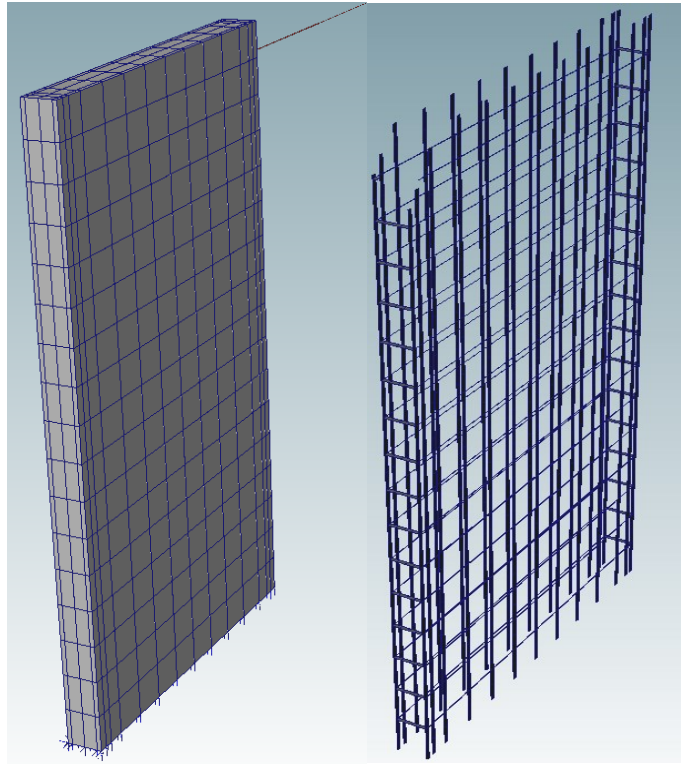


Figure 4-16. ABAQUS Depiction of shear wall G15 (Left: meshed version, Right: reinforcement)



*Figure 4-17. G15 Shear wall FEAVIEWER configuration*

The nominal concrete compressive strength used for G15 was 40 MPa. An axial load of  $0.07 \cdot b_w \cdot l_w \cdot f'_c$  was applied at the top of the wall. #3 for vertical bars ( $f_{fu} = 1,412 \text{ MPa}$ ,  $E_f = 66.9 \text{ GPa}$ ,  $\varepsilon_{fu} = 2.11\%$ ,  $A_f = 71.3 \text{ mm}^2$ ) and spiral ties (for straight portions  $f_{fu} = 962 \text{ MPa}$ ,  $E_f = 52 \text{ GPa}$ ,  $\varepsilon_{fu} = 1.85\%$ ,  $A_f = 71.3 \text{ mm}^2$ ; for bent portions:  $f_{fu} = 500 \text{ MPa}$  and #4 for horizontal bars ( $f_{fu} = 1,392 \text{ MPa}$ ,  $E_f = 69.6 \text{ GPa}$ ,  $\varepsilon_{fu} = 2\%$ ,  $A_f = 126.7 \text{ mm}^2$ ).

# Chapter 5

## Numerical results

### 5.1. Introduction

The results of the Beam and Solid element based finite element models, as well as those based on ABAQUS and experimental results in literature are presented in this chapter. With the help of load-displacement curves, all the data are graphically shown. In the load-deflection figures, the vertical axis is for the load and the horizontal axis for the displacement. In Section 5.2, the validation studies of the developed numerical technique are presented and comparisons with ABAQUS and those of experimental results. In Section 5.3, results of members whose span is half of the original length and in Section 5.4, doubled the spans.

### 5.2. Validation of the Numerical Model

#### 5.2.1. Beams

Figure 5-1 displays the force-displacement curves for a specimen of the ISOROD GFRP reinforced beam. The graphic clearly shows the good agreement between the results of the 1D and 3D material model, the experimental and ABAQUS models. The 1D and 3D model can therefore accurately reproduce the mechanical behavior of reinforced concrete columns.

The load-displacement curves for a deep section reinforced with one CFRP reinforcement in flexural and a shallow section reinforced with one CFRP beam are shown in Figures 5-2 and 5-3, respectively. The performance of the beams based on the 1D and 3D material models is well-aligned with the findings from ABAQUS and the experimental data. All approaches failed in flexural. The models behaved according to a load-displacement relationship consisting of two nearly linear branches representing the elastic uncracked phase and the elastic-cracked phase. Direct1DSugano was softer as it doesn't consider shear stress effects. It can be seen that all the models present similar stiffness in the uncracked phase. Due to high tensile strength of the GFRP the concrete failed in compression before the failure of the FRPs.

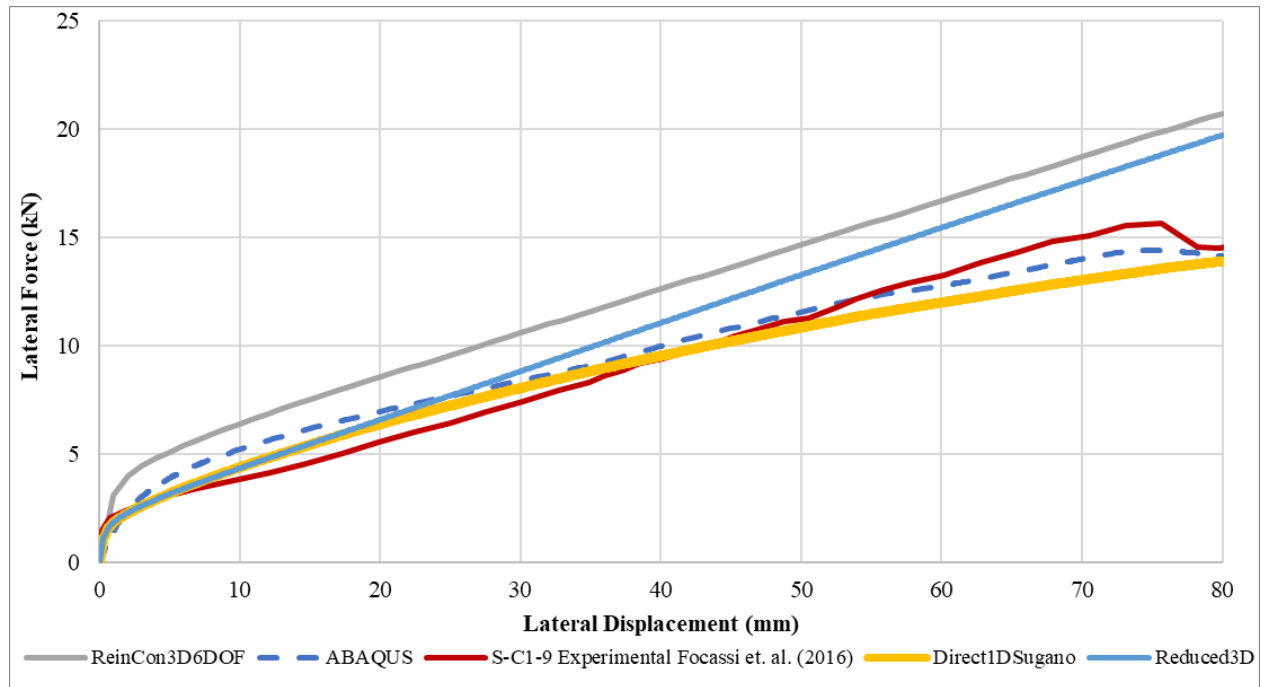


Figure 5-1. Force – Displacement curve for shallow CFRP beam (S-C1 × 9)

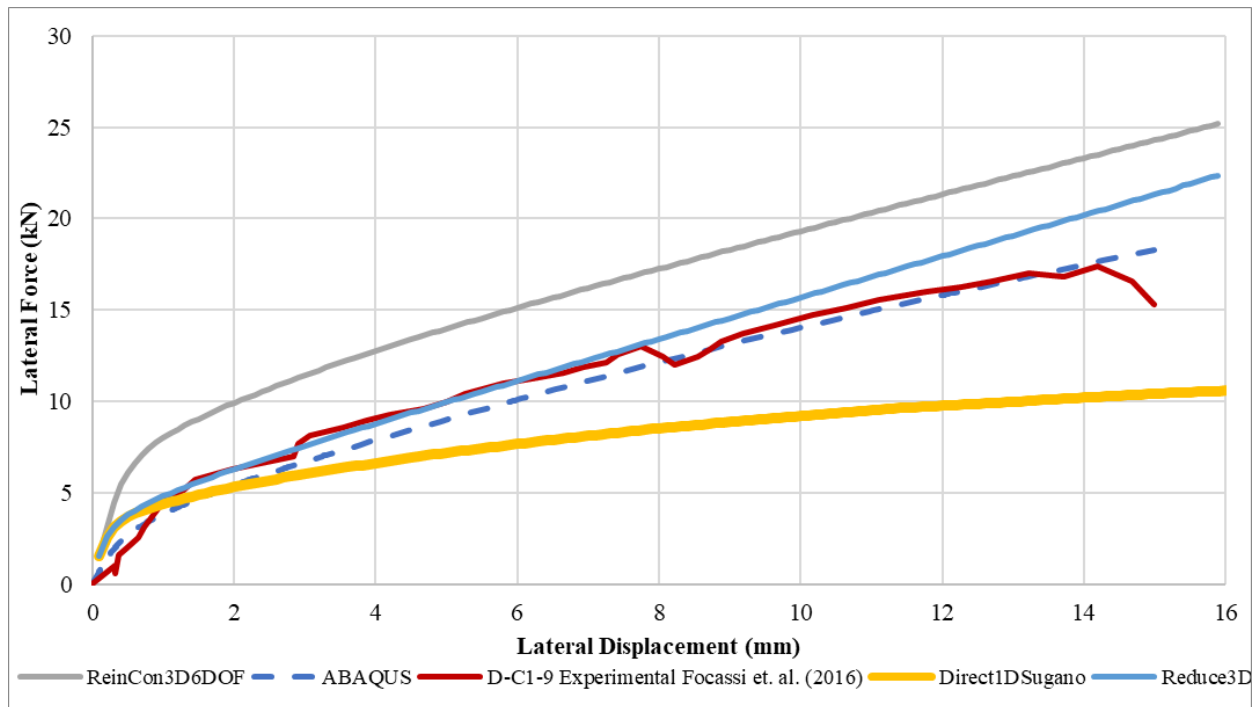


Figure 5-2. Force - Displacement curve for Deep CFRP beam (D-C1 × 9)



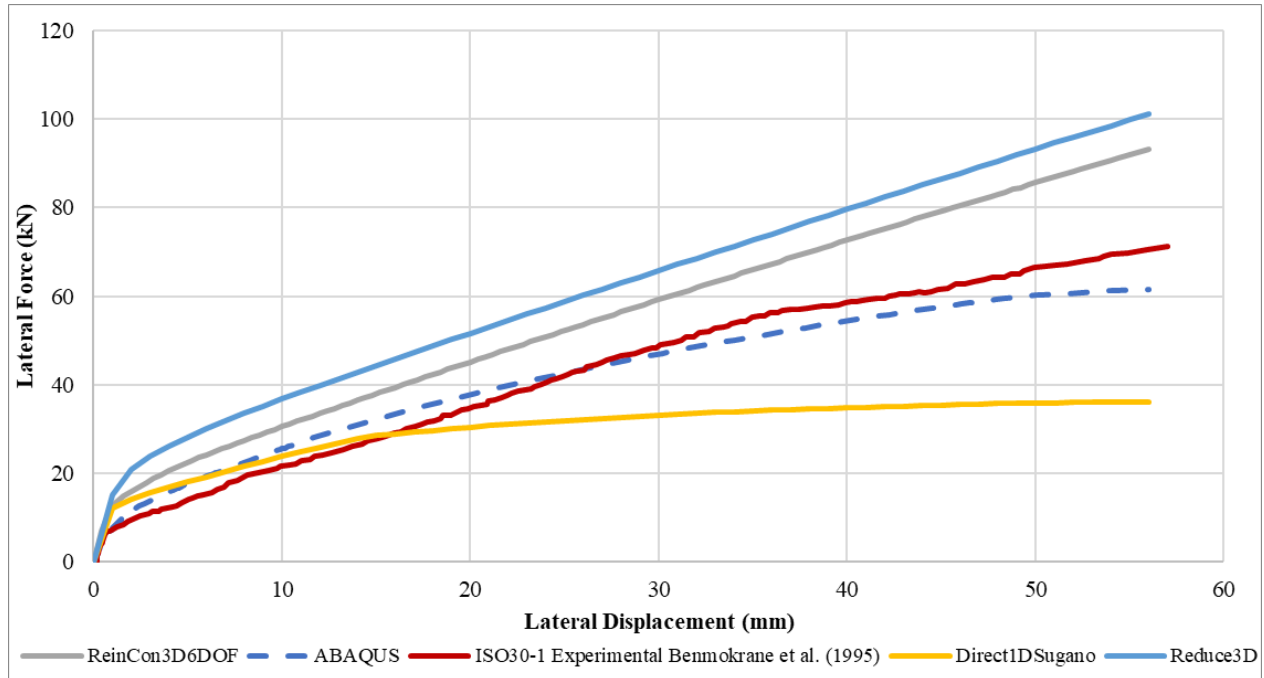


Figure 5-3. Force – Displacement for ISOROD GFRP beam (ISO30-1)

### 5.2.2. Shear walls

Figures 5-4 and 5-5 show the obtained monotonic curves of the lateral load against top lateral displacement of the shear walls. The 1D and 3D numerical models' performance are in good agreement with the results of the experiment and ABAQUS, which makes it evident from the data that it can accurately represent the behavior of reinforced walls. The initial stiffness until initial crack formation of G15 in the 3 proposed models is the same but higher than the literature and the ABAQUS. After the initial crack formation, there was a reduction of stiffness resulting in linear behavior until failure. For the SW-1, the 1D and literature were in good agreement up to the end unlike the fails earlier than the others. The 3D also fails before the other two though it behaved accordingly with the literature, ABAQUS and the 1D.

The use of several material models for concrete and various finite element types could account for any discrepancy in findings between the material model and ABAQUS.

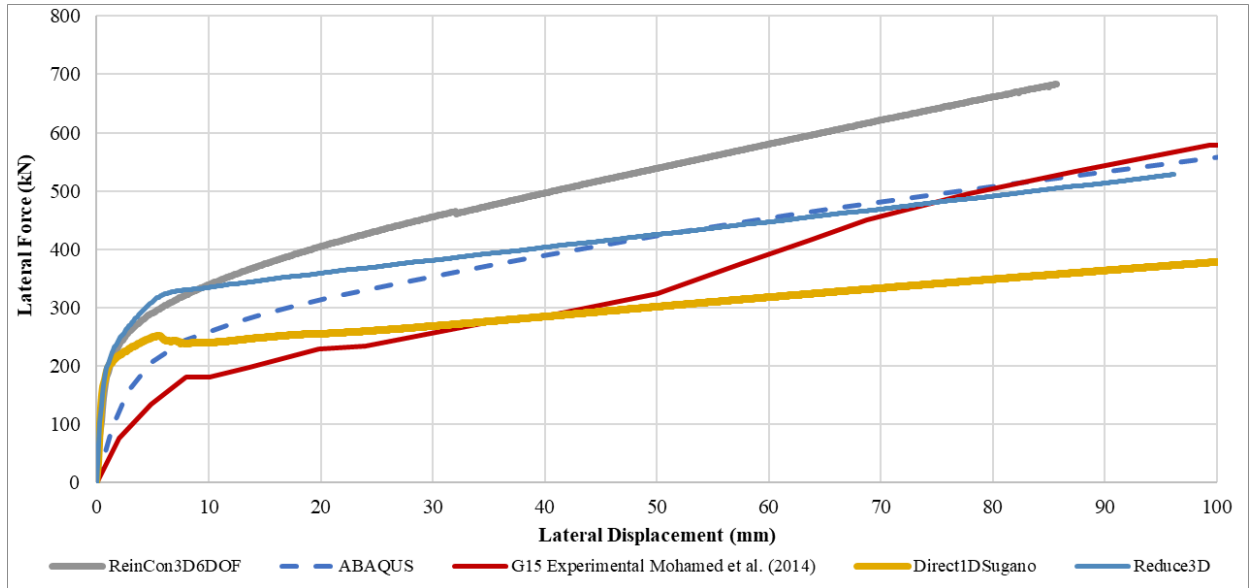


Figure 5-4. Force – Displacement curve for G15 shear wall

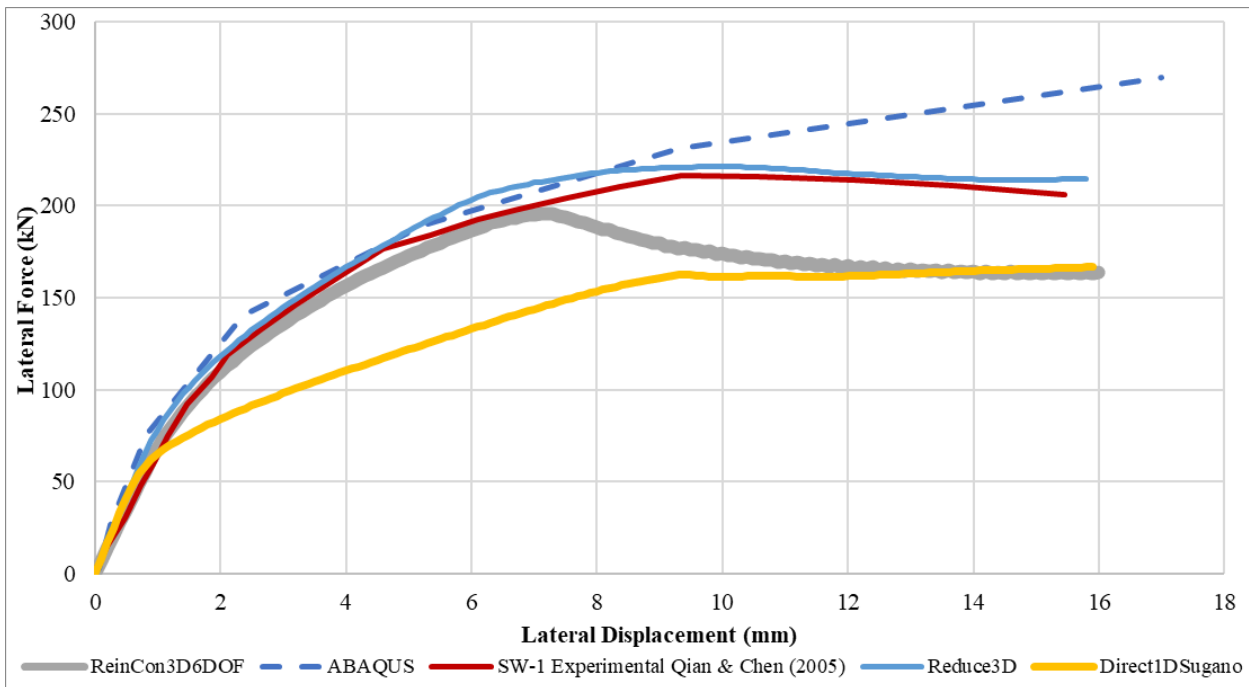


Figure 5-5. Force - Displacement curve for SW-1 shear wall

### 5.3. Parametric Studies on Shortened members

In this section, the above five cases used for validation purposes are changed by reducing the member sizes to half of their original length.

### 5.3.1. Beams

The beams analysed in Section 5.2.1 are re-analysed after reducing their spans to half to increase the effect of shear deformation.

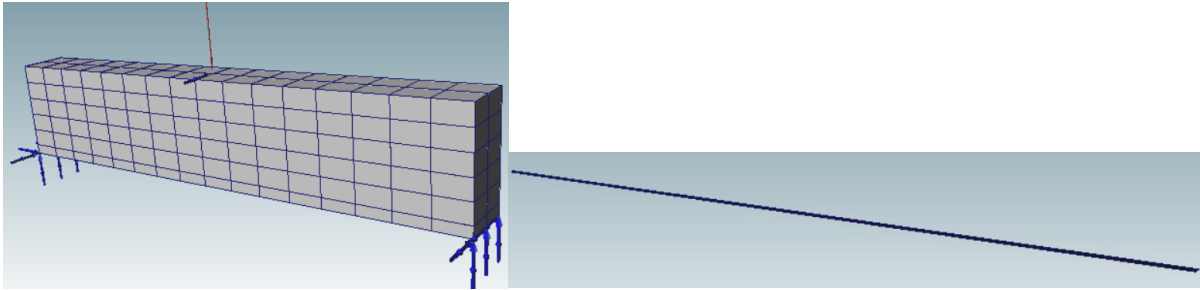


Figure 5-6. Depiction of the Shortened D-CI-9 (Right: meshed version, Left: reinforcement)

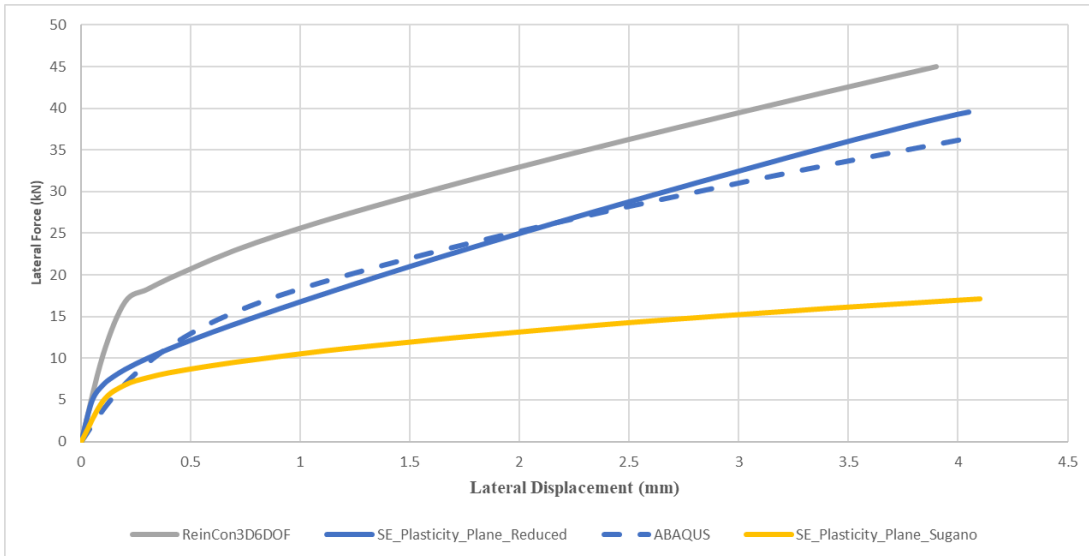


Figure 5-7. Load - deflection curve for the Shortened D-CI-9

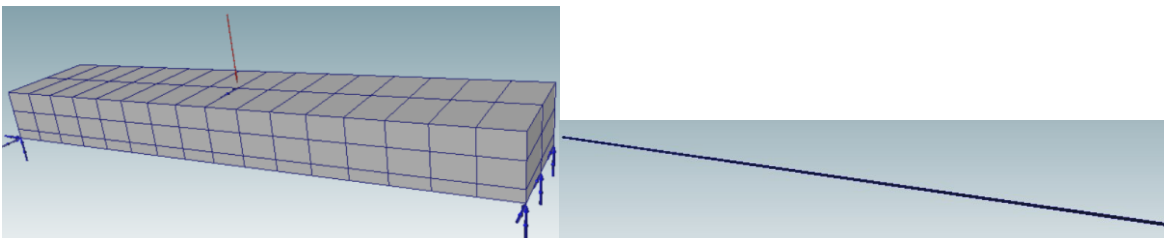


Figure 5-8. Depiction of Shortened S-CI-9 (Left: meshed version, Right: reinforcement)

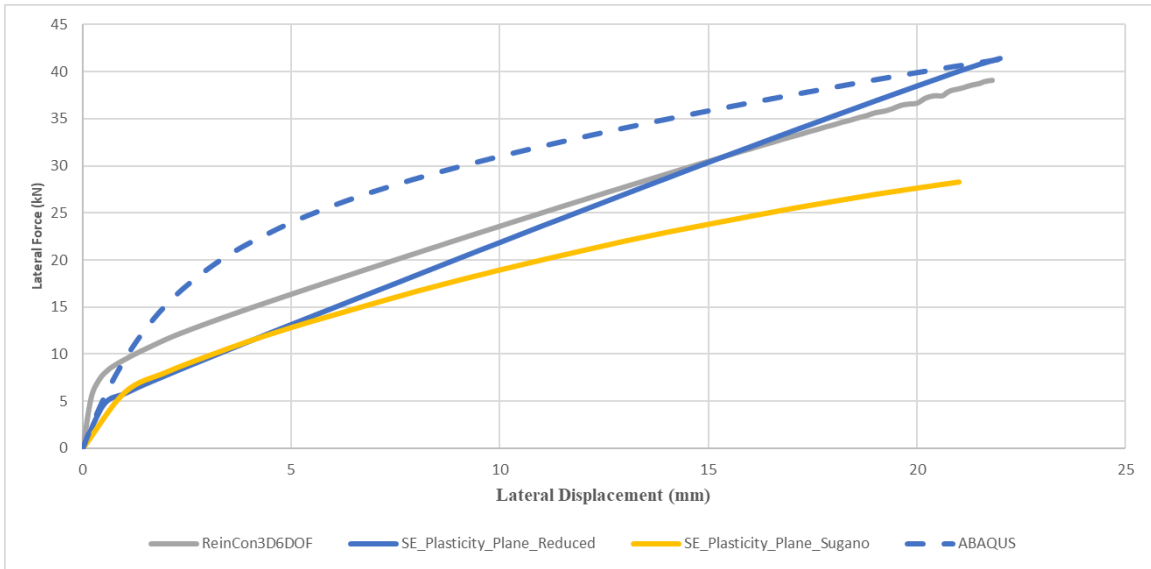


Figure 5-9. Load - deflection curve for the Shortened S-C1-9

### 5.3.2. Shear walls

In this example, the shear wall analysed in Section 5.2.2 are re-analysed after reducing their spans to half to increase the effect of shear deformation. When the spans of structural components are reduced, the 1D beam formulations become overly stiff compared to the 3D solid-element based formulation.

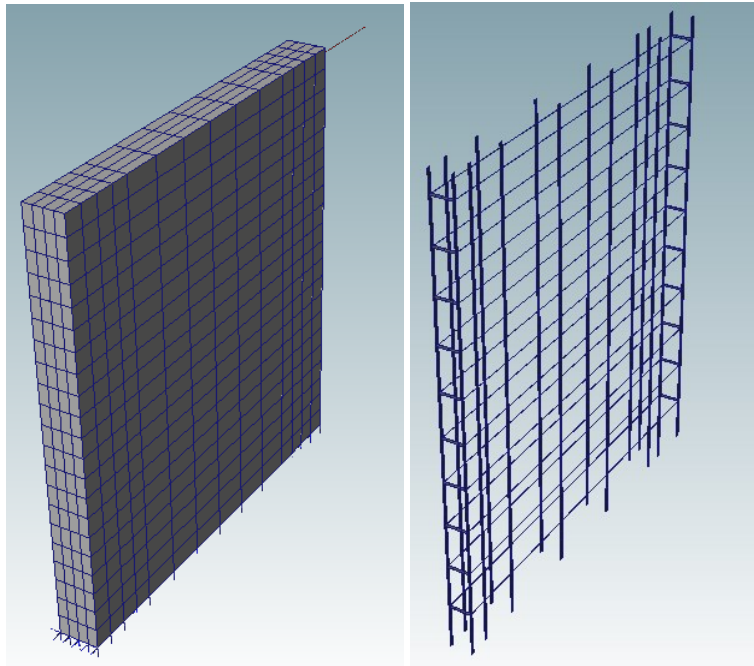


Figure 5-10. Depiction of the Shortened SW-1 (Left: meshed version, Right: reinforcements)

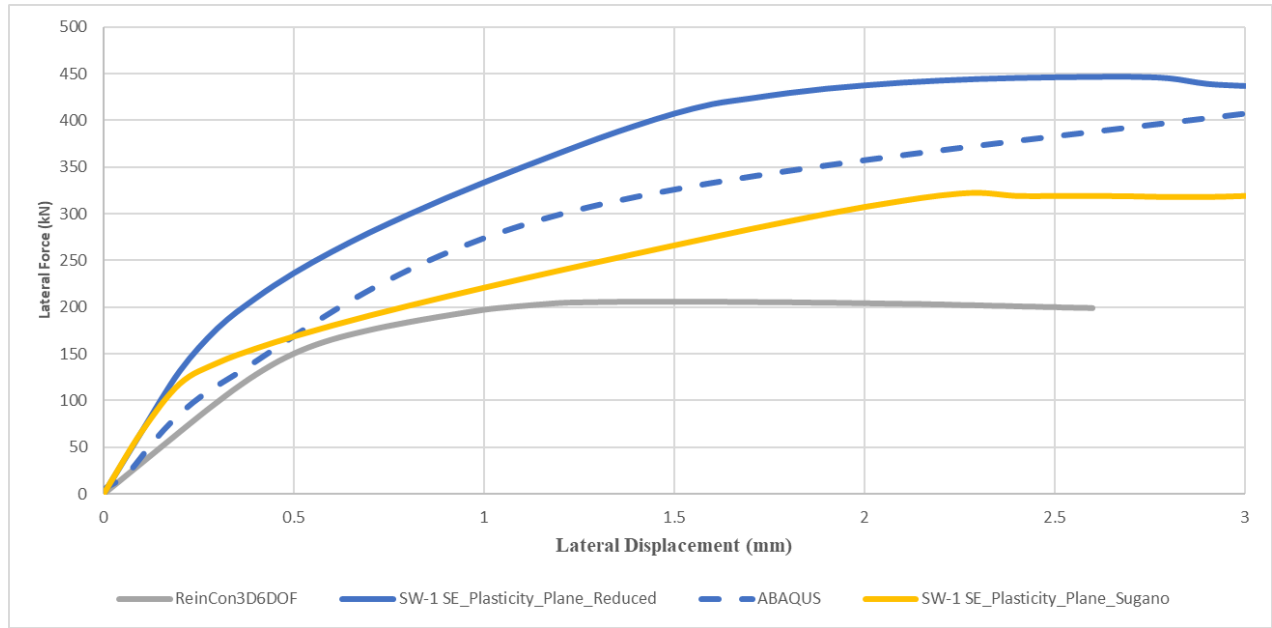


Figure 5-11. Load - deflection curve for the Shortened SW-1

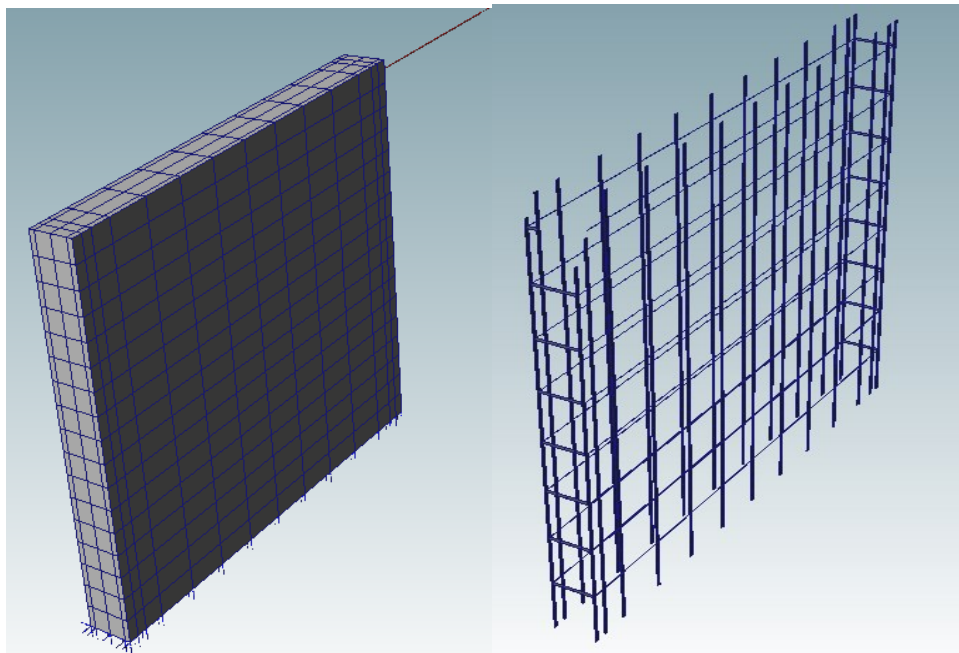


Figure 5-12. Depiction of the Shortened G15 (Left: meshed version, Right: reinforcements)

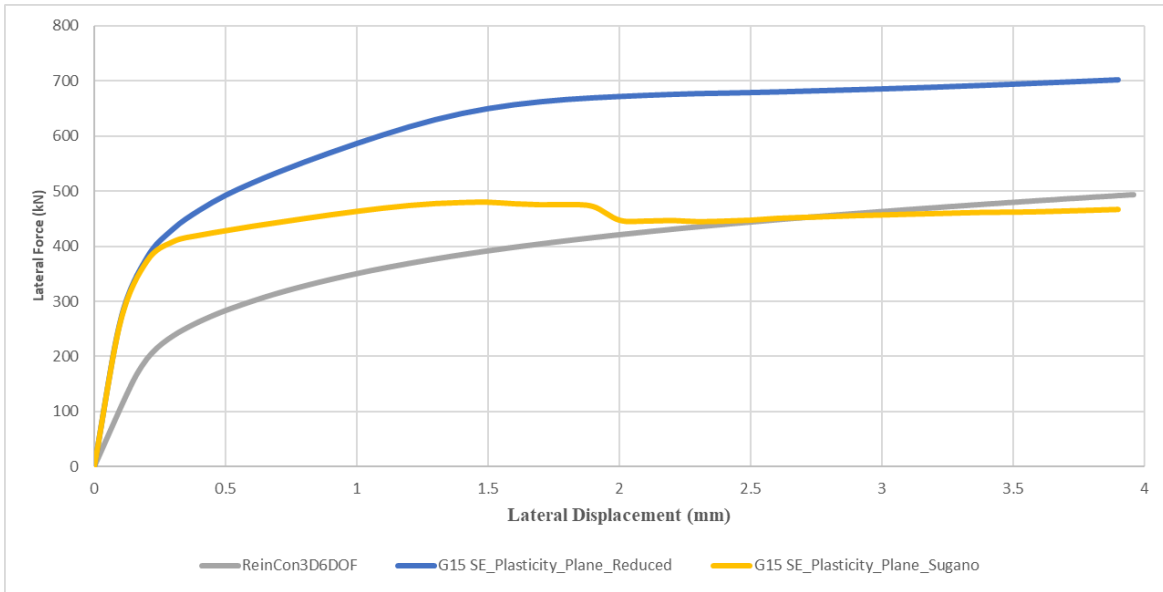


Figure 5-13. Load - deflection curve for the Shortened G15

## 5.4. Parametric Studies on Elongated members

### 5.4.1. Beams

The beams analysed in Section 5.2.1 are re-analysed after increasing their spans to double to decrease the effect of shear deformation.

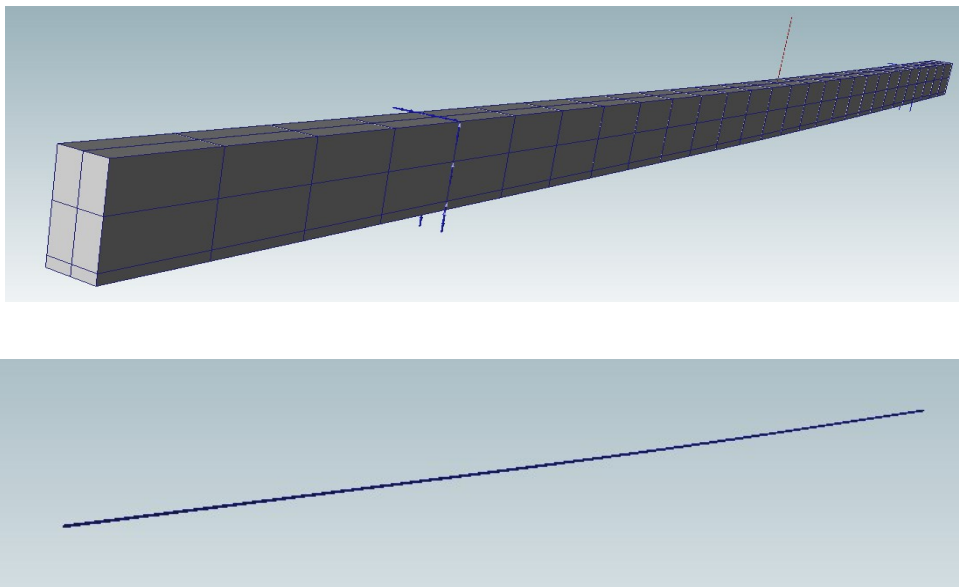


Figure 5-14. Depiction of the elongated D-C1-9 (Top: meshed version, Bottom: reinforcement)

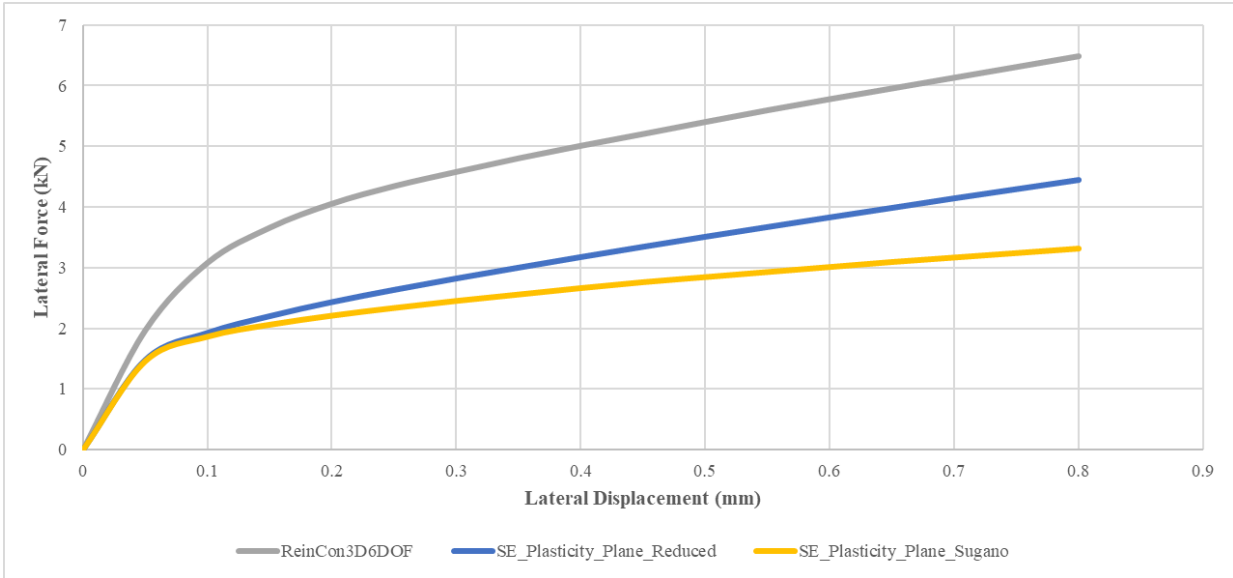


Figure 5-15. Load - deflection curve for the elongated D-C1-9

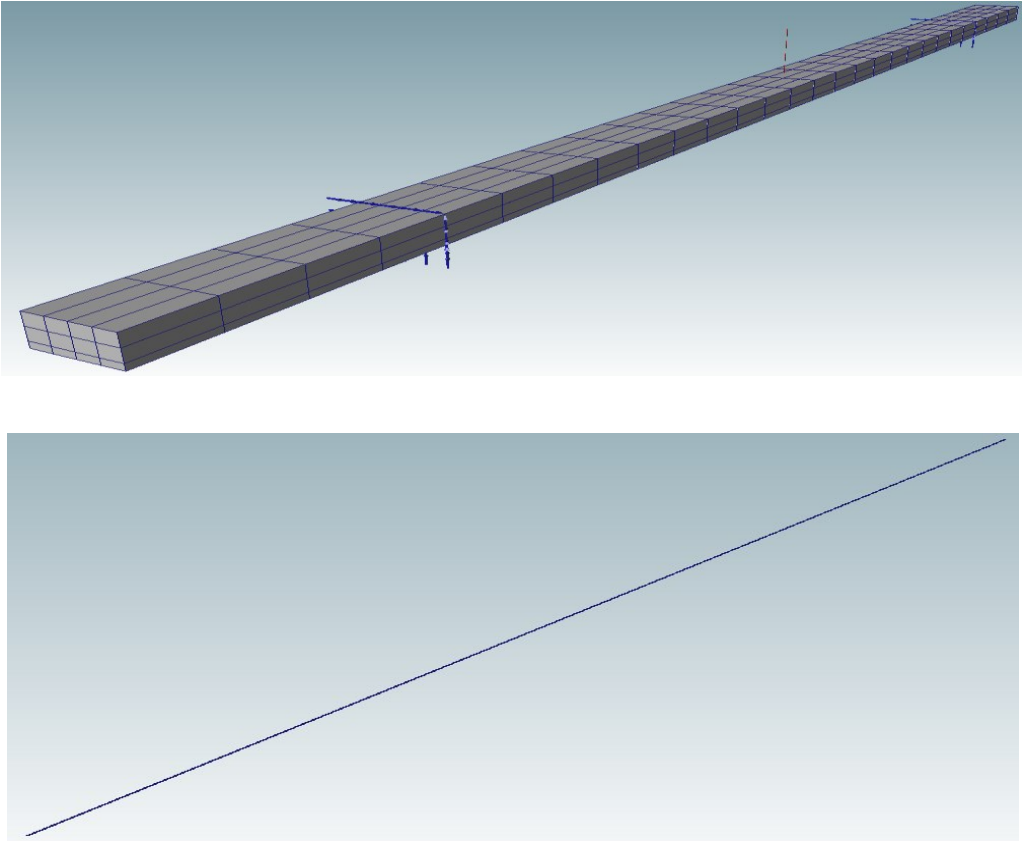


Figure 5-16. Depiction of elongated S-C1-9 (top: meshed version, bottom: reinforcement)

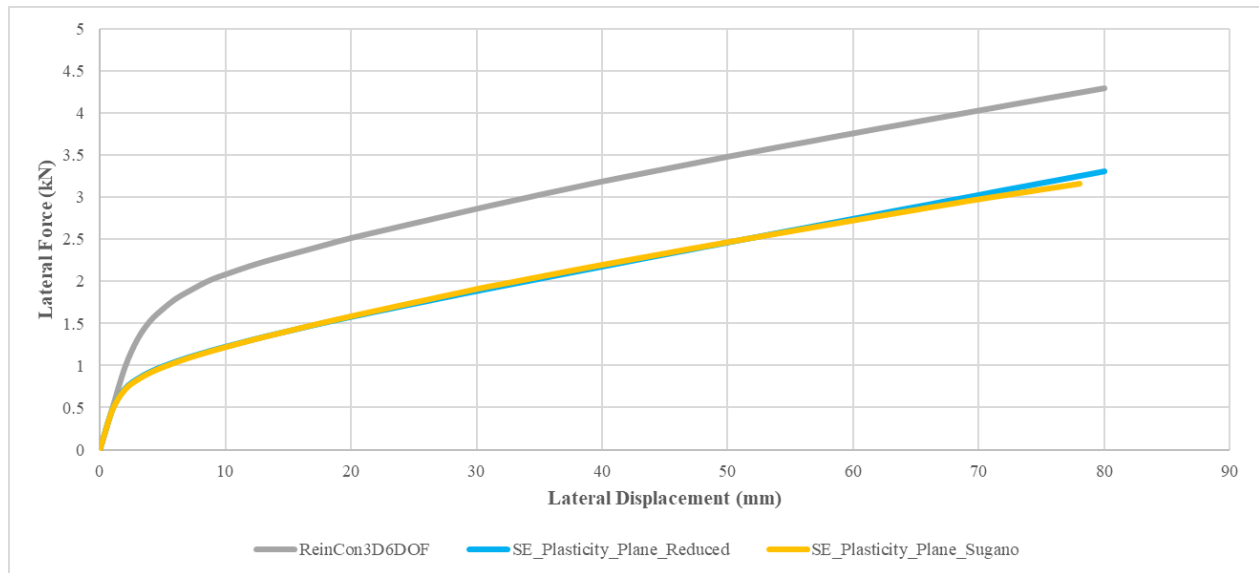


Figure 5-17. Load - deflection curve for the elongated S-C1-9

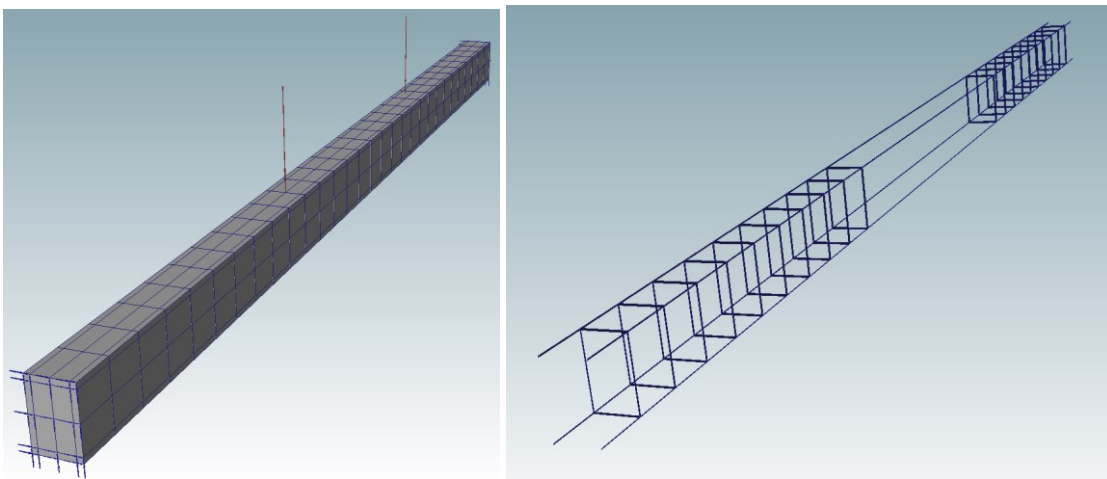


Figure 5-18. Depiction of the elongated ISO30-1 (Left: meshed version, Right: reinforcements)



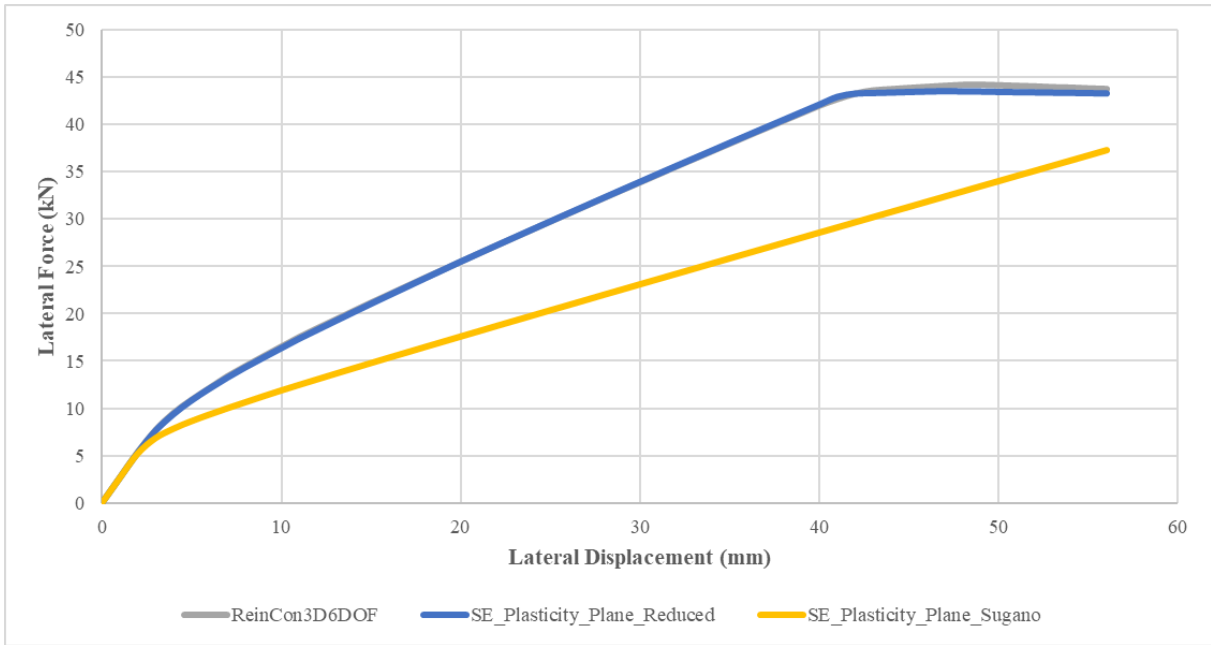


Figure 5-19. Load - deflection curve for the elongated ISO30-1

#### 5.4.2. Shear walls

In this example, the shear wall analysed in Section 5.2.2 are re-analysed after increased their spans to double to decrease the effect of shear deformation.

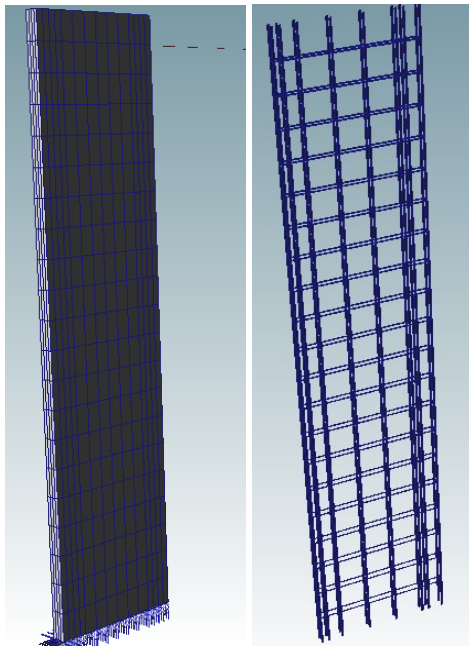


Figure 5-20. Depiction of the elongated SW-1 (Left: meshed version, Right: reinforcements)

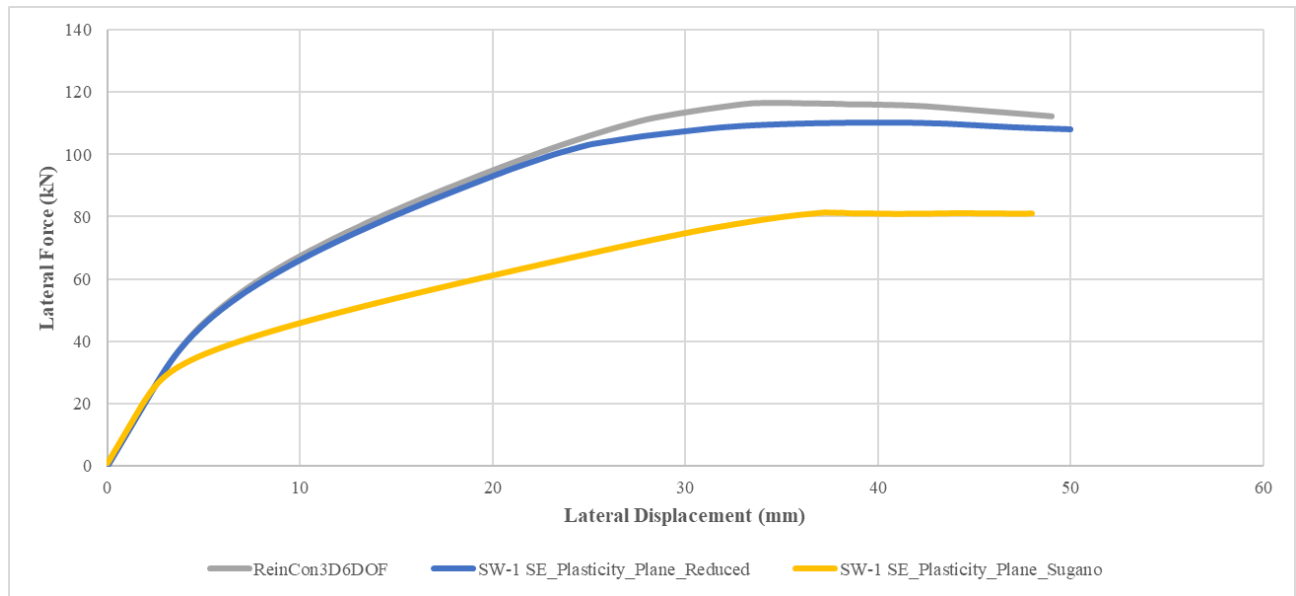


Figure 5-21. Load - deflection curve for the elongated SW-1

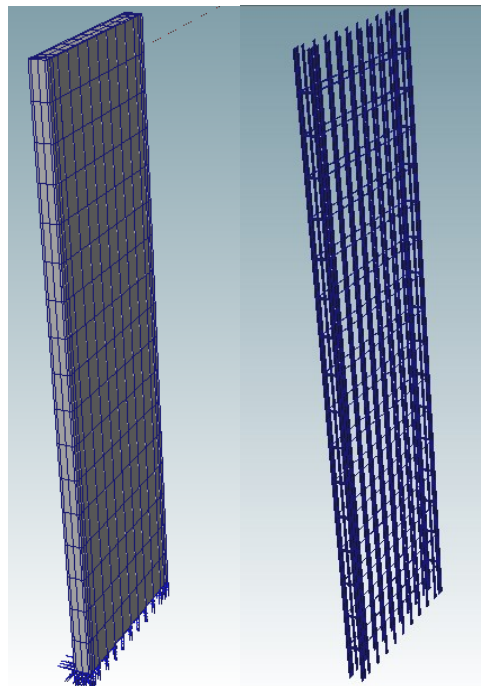


Figure 5-22. Depiction of the elongated G15 (Left: meshed version, Right: reinforcements)

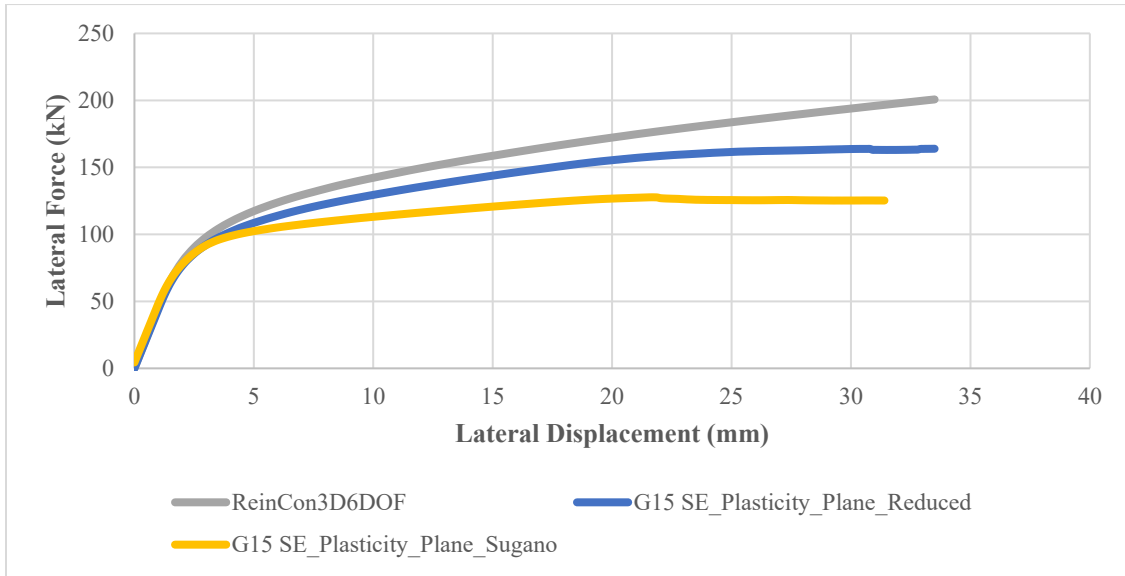


Figure 5-23. Load - deflection curve for the elongated G15

### 5.5.Limitations

As observed from section 5.2, the proposed modelling program has some limitation that need further investigation. calibration and sensitivity studies are needed to limit any discrepancy that was observed in this work.

# Conclusions

Two nonlinear structural analysis tools were developed. The first one employs 3D solid-type Finite Elements whereas the second one employs 1D 2-node Finite Elements for modelling of structural components. The tool was equipped with easy model generation and graphical representation options in order to reduce the risk of modelling errors. The inelastic material behaviour of steel reinforcements bars has also been considered in the analysis. Details of a proposed multi-axial elasto-plastic material model that can be used for the simulation of the concrete material under both tension and compression were described. The formulation for the material is implemented in the context of a 3D solid-element and 1D beam-element based formulations. 1D beam formulation was implemented using two alternative material models. The reduced model is obtained by removing all 3D stresses except the beams axial and vertical shear stress acting on the cross-section. On the other hand, what is referred to as the Sugano model is a uni-axial model which only considers the axial stress-strain relations along the longitudinal fibre. The modelling approach was used for simulating the behaviour of shear walls and beams under static loading causing tension and compression in various parts of the structural components. The model predictions were compared with three experimental results from literature as well as models developed in ABAQUS commercial software. Good agreement between the results were observed between the alternative modelling approaches.

# Future work recommendation

Future research work can be conducted in the following topics:

- **Alternative structural elements such as columns as well as stirrup and rebar arrangements can be tested to illustrate the performance of the developed tool.**
- **A sensitivity study on material parameters can be conducted to illustrate the effects on structural behaviour.**
- **Performance of alternative yield and potential surface types of the plasticity model can be tested.**
- **The elasto-plastic material model can be extended to include a damage component to be able to simulate structures under cyclic loads.**

# References

- ABAQUS, I. (2008). *Abaqus analysis user's manual, version 6.8*. ABAQUS Providence, RI
- Abbo, A.J. & Sloan, S.W. 1995, 'A smooth hyperbolic approximation to the MohrCoulomb yield criterion', *Computers & Structures*, 54(3), 427-441.
- Achillides, Z., Pilakoutas, K. (2006). FE modelling of bond interaction of FRP bars to concrete. *Structural Concrete*, 7(1), 7-16
- Adnan Ibrahimbegovic and Edward L Wilson. 1991. Thick shell and solid finite elements with independent rotation fields. *International journal for numerical methods in engineering*, 31(7):1393–1414.
- Aiello, M.A., F. Focacci, and A. Nanni. (2001) “Effects of Thermal Loads on Concrete Cover of FRP Reinforced Elements: Theoretical and Experimental Analysis,” *ACI Materials Journal*, 98(4), 332-339.
- Afsin Saritas and Filip C Filippou. 2013. Analysis of rc walls with a mixed formulation frame finite element. *Computers and Concrete*, 12(4):519–536.
- Alfarah, B., López-Almansa, F. & Oller, S. 2017, 'New methodology for calculating damage variables evolution in Plastic Damage Model for RC structures', *Engineering Structures*, 132, 70-86.
- Al-Rub, R.K.A. & Voyiadjis, G.Z. 2003, 'On the coupling of anisotropic damage and plasticity models for ductile materials', *International Journal of Solids and Structures*, 40(11), 2611-2643.
- American Concrete Institute (ACI) Committee 440. (2007). Report on fiber-reinforced polymer (FRP) reinforcement concrete structures (ACI 440R-07), ACI, Farmington Hills, MI, 100.
- Andrea A., A. D'Ambrisi, M.D. Stefano, Luciano F., F. Focacci, R. Nudo (2016). Experimental response of FRP reinforced members without transverse reinforcement: Failure modes and design issues, *Composites Part B: Engineering*, 89, 397-407.

Armero, F. & Oller, S. 2000a, 'A general framework for continuum damage models. I. Infinitesimal plastic damage models in stress space', *International Journal of Solids and Structures*, 37(48), 7409-7436.

Armero, F. & Oller, S. 2000b, 'A general framework for continuum damage models. II. Integration algorithms, with applications to the numerical simulation of porous metals', *International Journal of Solids and Structures*, 37(48), 7437- 7464.

Ashraf Ayoub. (2006). Nonlinear analysis of reinforced concrete beam–columns with bond-slip. *Journal of engineering mechanics*, 132(11): 1177–1186.

Ayhan, B., Jehel, P., Brancherie, D. & Ibrahimbegović, A. 2013, 'Coupled damage– plasticity model for cyclic loading: Theoretical formulation and numerical implementation', *Engineering Structures*, 50, 30-42.

B. Benmokrane, O. Chaallal, R. Masmoudi (1995). Glass fibre reinforced plastic (GFRP) rebars for concrete structures, *Construction and Building Materials*, 9(6): 353-364.

B. Piscesa, MM Attard, AK Samani, and S Tangaramvong (2017). Plasticity constitutive model for stress-strain relationship of confined concrete. *ACI Structural Journal*, 114(2).

Bakis, C. E., et al. (2002). “Fiber-reinforced polymer composites for construction—State-of-the-art review.” *J. Compos. Constr.*, 2(73), 73–87.

Barda, F., Hanson, J. M., and Corley, G. W. (1977). “Shear strength of lowrise walls with boundary elements.” *ACI Special Publication*, 53(8), 149–202.

Borja, R.I., Sama, K.M. & Sanz, P.F. 2003, 'On the numerical integration of threeinvariant elastoplastic constitutive models', *Computer Methods in Applied Mechanics and Engineering*, 192(9), 1227-1258.

Brancherie, D. & Ibrahimbegovic, A. 2009, 'Novel anisotropic continuum-discrete damage model capable of representing localized failure of massive structures: Part I: theoretical formulation and numerical implementation', *Engineering Computations*, 26(1/2), 100-127.

Branson, D. E. (1977). Deformation of concrete structures. (*No Title*).

Brünig, M. & Michalski, A. 2017, A stress-state-dependent continuum damage model for concrete based on irreversible thermodynamics, *International Journal of Plasticity*, 90, 31-43.

Bulent N Alemdar and Donald W White (2005). Displacement, flexibility, and mixed beam–column finite element formulations for distributed plasticity analysis. *Journal of structural engineering*, 131(12):1811–1819.

Byung Hwan Oh, Ji Cheol Kim, Young Cheol Choi (2007). Fracture behavior of concrete members reinforced with structural synthetic fibers, *Engineering Fracture Mechanics*, 74 (1): 243-257

Cardenas, A. E., Hanson, J. M., Corley, W. G., & Hognestad, E. (1973). Design provisions for shear walls. *ACI Journal*, 70(3), 221-230.

Červenka, J. & Papanikolaou, V.K. 2008, 'Three-dimensional combined fracture–plastic material model for concrete', *International Journal of Plasticity*, 24(12), 2192-2220.

Chaboche, J.L. 1984, 'Anisotropic creep damage in the framework of continuum damage mechanics', *Nuclear Engineering and Design*, 79(3), 309-319.

Chang Seok Lee, Yewon Park, and Jong-Su Jeon. (2021). Model parameter prediction of lumped plasticity model for nonlinear simulation of circular reinforced concrete columns. *Engineering Structures*, 245:112820.

Cicekli, U., Voyiadjis, G.Z. & Al-Rub, R.K.A. 2007, 'A plasticity and anisotropic damage model for plain concrete', *International Journal of Plasticity*, 23(10-11), 1874-1900.

Clarke, J.L. (ed.) *Alternative Materials for the Reinforcement and Prestressing of Concrete*, Blackie Academic and Professional, London, 1993

Comi, C., Fedele, R. & Perego, U. 2009, 'A chemo-thermo-damage model for the analysis of concrete dams affected by alkali-silica reaction', *Mechanics of Materials*, 41(3), 210-230.

Cosenza, E., Manfredi, G. and R. Realfonzo. 1997. “Behavior and Modeling of FRP Rebars to Concrete. *Compos. Struct.* 1 (1): 40-51.



Darby, AP., Ibell, T. J., Tallis, S., & Winkle, C. (2007). End Anchorage technique for internal FRP reinforcement. *Paper presented at Proceedings of Fibre-Reinforced Polymers for RC Structures (FRPRCS-8)*, Patras, Greece.

De Borst, R. 1987. Computation of post-bifurcation and post-failure behavior of strain softening solids. *Computers & Structures*, 25(2):211–224.

De Borst, R. 1987, 'Integration of plasticity equations for singular yield functions', *Computers & Structures*, 26(5), 823-829.

De Borst, R. 2001. Some recent issues in computational failure mechanics. *International Journal for Numerical Methods in Engineering*, 52(1-2):63–95.

De Borst, R., Pankaj & Bićanić, N. 1991, 'A note on singularity indicators for mohr-coulomb type yield criteria', *Computers & Structures*, 39(1), 219-220.

De Borst, R., and Thibault Duretz. 2020. On viscoplastic regularization of strain softening rocks and soils. *International Journal for Numerical and Analytical Methods in Geomechanics*, 44(6):890–903.

Deepak P Adhikary, Chandana T Jayasundara, Robert K Podgorney, and Andy H Wilkins. 2017. A robust return-map algorithm for general multisurface plasticity. *International Journal for Numerical Methods in Engineering*, 109(2):218–234.

Dechun Lu, Xiuli Du, Guosheng Wang, Annan Zhou, and Anke Li 2016. A three-dimensional elastoplastic constitutive model for concrete. *Computers & Structures*, 163:41–55.

DJ Han and Wai-Fah Chen. Constitutive modeling in analysis of concrete structures (1987). *Journal of engineering mechanics*, 113(4):577–593.

Dolarevic, S. & Ibrahimbegovic, A. 2007, 'A modified three-surface elasto-plastic cap model and its numerical implementation', *Computers & Structures*, 85(7), 419-430.

E. Spacone, F. Filippou, and F. Taucer. (1996). “Fibre beam-column model for non-linear analysis of R/C frames: Part I. Formulation”. In: *Earthquake Engineering and Structural Dynamics* 25.7 711–726.

Eddy Pramono and Kaspar Willam, 1989. Implicit integration of composite yield surfaces with corners. *Engineering Computations*, 6(3):186–197.

Einav, I., Houlsby, G.T. & Nguyen, G.D. 2007, 'Coupled damage and plasticity models derived from energy and dissipation potentials', *International Journal of Solids and Structures*, 44(7-8), 2487-2508.

El-Salakawy, E., Benmokrane, B., El-Ragaby, A., and Nadeau, D. (2005). “Field investigation on the first bridge deck slab reinforced with glass FRP bars constructed in Canada.” *J. Compos. Constr.*, 6(470), 470–479.

Enrico Spacone, Filip C Filippou, and Fabio F Taucer (1996). Fibre beam–column model for non-linear analysis of r/c frames: Part i. formulation. *Earthquake Engineering & Structural Dynamics*, 25(7):711–725.

Fabio Mazza and Mirko Mazza. (2010). ‘Nonlinear analysis of spatial framed structures by a lumped plasticity model based on the haar–kàrmàn principle’, *Computational Mechanics*, 45:647–664.

Fédération Internationale du Béton (fib). (2007). “FRP reinforcement in RC structures.” Task Group 9.3, Lausanne, Switzerland.

Fabio Taucer, Enrico Spacone, and Filip C Filippou (1991). A fiber beam-column element for seismic response analysis of reinforced concrete structures, *volume 91. Earthquake Engineering Research Center, College of Engineering, University.*

Feenstra, P.H. & de Borst, R. 1996, 'A composite plasticity model for concrete', *International Journal of Solids and Structures*, 33(5), 707-730.

Fintel, M., 1995, “Performance of Buildings with Shear Walls in Earthquakes of the Last Thirty Years,” *PCI Journal*, 40(3), 62-80.

G Hofstetter, B Valentini, 2013. Review and enhancement of 3d concrete models for large-scale numerical simulations of concrete structures. *International Journal for Numerical and Analytical Methods in Geomechanics*, 37(3):221–246.

G. C. Lykidis and K. Spiliopoulos. "3D Solid Finite-Element Analysis of Cyclically Loaded RC Structures Allowing Embedded Reinforcement Slippage". In: *Journal of structural engineering* 134.4 (2008), pp. 629–638.

Galati N, Nanni A, Dharanib LR, Focacci F, Aiello Ma (2006). Thermal effects on bond between FRP rebars and concrete. *Composites Part A*; 37.

Gao, D., Benmokrane, B., and Masmoudi, R., (1998), "A Calculating Method of Flexural Properties of FRP-Reinforced Concrete Beam: Part1: Crack Width and Deflection," Technical Report, Department of Civil Engineering, University of Sherbrooke, Sherbrooke.

Govindjee, S., Kay, G.J. & Simo, J.C. 1995, 'Anisotropic modelling and numerical simulation of brittle damage in concrete', *International Journal for Numerical Methods in Engineering*, 38(21), 3611-3633.

Grassl, P. & Jirásek, M. 2006a, 'Damage-plastic model for concrete failure', *International Journal of Solids and Structures*, 43(22-23), 7166-7196.

Grassl, P. & Jirásek, M. 2006b, 'Plastic model with non-local damage applied to concrete', *International Journal for Numerical and Analytical Methods in Geomechanics*, 30(1), 71-90.

Grassl, P., Lundgren, K. & Gylltoft, K. 2002, 'Concrete in compression: a plasticity theory with a novel hardening law', *International Journal of Solids and Structures*, 39(20), 5205-5223.

Grassl, P., Xenos, D., Nyström, U., Rempling, R. & Gylltoft, K. 2013, 'CDPM2: A damage-plasticity approach to modelling the failure of concrete', *International Journal of Solids and Structures*, 50(24), 3805-3816.

Grimal, É., Sellier, A., Le Pape, Y. & Bourdarot, É. 2008a, 'Creep, shrinkage, and anisotropic damage in alkali-aggregate reaction swelling mechanism-Part I: A constitutive model', *ACI Materials Journal*, 105(3), 227.

Grimal, É., Sellier, A., Le Pape, Y. & Bourdarot, É. 2008b, 'Creep, shrinkage, and anisotropic damage in alkali-aggregate reaction swelling mechanism-Part II: Identification of model parameters and application', *ACI Materials Journal*, 105(3), 236.

Günter Hofstetter, Juan C Simo, and Robert Leroy Taylor. 1993. A modified cap model: closest point solution algorithms. *Computers & Structures*, 46(2):203–214.

Gupta, A.K. & Akbar, H. 1984, 'Cracking in reinforced concrete analysis', *Journal of structural engineering (New York, N.Y.)*, 110(8), 1735-1746.

Hansen, N.R. & Schreyer, H.L. 1994, 'A thermodynamically consistent framework for theories of elastoplasticity coupled with damage', *International Journal of Solids and Structures*, 31(3), 359-389.

Hong D Kang and Kaspar J Willam (1999). Localization characteristics of triaxial concrete model. *Journal of engineering mechanics*, 125(8):941–950.

Houlsby, G.T. & Puzrin, A.M. 2000, 'A thermomechanical framework for constitutive models for rate-independent dissipative materials', *International Journal of Plasticity*, 16(9), 1017-1047.

I. F. Kara, Ashraf F. A., Cengiz D. 2013. Deflection of concrete structures reinforced with FRP bars. *Composites Part B: Engineering*, 44 (1), 375-384,

Ibrahimbegović, A. & Markovič, D. 2003, 'Strong coupling methods in multi-phase and multi-scale modeling of inelastic behavior of heterogeneous structures', *Computer Methods in Applied Mechanics and Engineering*, 192(28), 3089-3107.

Ibrahimbegović, A. 2009, *Nonlinear solid mechanics: Theoretical formulations and finite element solution methods*, 160, Springer Science & Business Media.

Ibrahimbegović, A., Jehel, P. & Davenne, L. 2008, 'Coupled damage-plasticity constitutive model and direct stress interpolation', *Computational Mechanics*, 42(1), 1-11.

Ibrahimbegović, A., Markovič, D. & Gatuingt, F. 2003, 'Constitutive model of coupled damage-plasticity and its finite element implementation', *Revue Européenne des Eléments Finis*, 12(4), pp. 381-405.

ISIS Canada. (2007). Reinforcing concrete structures with fiber-reinforced polymers—Design manual No. 3, ISIS Canada Corporation, Manitoba, Canada.

J. Mazars et al. “Numerical modelling for earthquake engineering: the case of lightly RC structural walls”. In: *International journal for numerical and analytical methods in geomechanics* 28.7-8 (2004), pp. 857–874.

Jaeger, L.G., Mufti, A.A., and Tadros, G. 1997. The concept of the overall performance factor in rectangular-section reinforced concrete members. *Proceedings of the 3rd International Symposium on Non-Metallic (FRP) Reinforcement for Concrete Structures*, 2, 551–559.

Jason, L., Huerta, A., Pijaudier-Cabot, G. & Ghavamian, S. 2006, 'An elastic plastic damage formulation for concrete: Application to elementary tests and comparison with an isotropic damage model', *Computer Methods in Applied Mechanics and Engineering*, 195(52), 7077-7092.

Jean-Louis Batoz and Gouri Dhatt. 1979. Incremental displacement algorithms for nonlinear problems. *International Journal for Numerical Methods in Engineering*, 14(8):1262–1267.

JQ Bao, X Long, Kang Hai Tan, and Chi King Lee. 2013. A new generalized drucker–prager flow rule for concrete under compression. *Engineering Structures*, 56:2076–2082.

Jiang, H., and Kurama, Y. C. (2010). “Analytical modeling of medium-rise reinforced concrete shear walls.” *ACI Struct. J.*, 107(4), 400–410.

Jirásek, M. & Bazant, Z.P. 2001, *Inelastic analysis of structures*, John Wiley & Sons, West Sussex, England.

Jirásek, M. & Zimmermann, T. 1998, 'Analysis of rotating crack model', *Journal of Engineering Mechanics*, vol. 124(8), 842-851.

Ju, J.W. 1989, 'On energy-based coupled elastoplastic damage theories: Constitutive modeling and computational aspects', *International Journal of Solids and Structures*, 25(7), 803-833.

Juan C Simo and Thomas JR Hughes. 2006. *Computational inelasticity, volume 7*. Springer Science & Business Media.

K. D. Hjelmstad. Fundamentals of structural mechanics. Springer, 2005.

Kachanov, L. 1958a, 'On the creep rupture time, Izv', AN SSSR, *Otd. Tekhn. Nauk*, 8, 26-31.

Kassem, C., Farghaly, A. S., and Benmokrane, B. (2011). "Evaluation of flexural behavior and serviceability performance of concrete beams reinforced with FRP Bars." *J. Compos. Constr.*, 682–695.

Klisiński, M. & Mróz, Z. 1988, 'Description of inelastic deformation and degradation of concrete', *International Journal of Solids and Structures*, 24(4), 391- 416.

L.M. Kachanov. On the creep fracture time. Izv. Akad. Nauk SSSR. Otd. Tekhn. Nauk. (8):26-31, 1958. (in Russian)

Lam, L., & Teng, J. (2003b). Design-oriented stress-strain model for frp-confined concrete in rectangular columns. *Journal of reinforced plastics and composites*, 22(13), 1149-1186.

Lars Olovsson, Kjell Simonsson, and Mattias Unosson (2006). Shear locking reduction in eight-noded trilinear solid finite elements. *Computers & structures*, 84(7):476–484.

Lee, J. & Fenves, G.L. 1998, 'Plastic-damage model for cyclic loading of concrete structures', *Journal of Engineering Mechanics*, 124(8), 892-900.

Lemaitre, J. (1985). A continuous damage mechanics model for ductile fracture.

Lublinter, J., Oliver, J., Oller, S. & Oñate, E. 1989, 'A plastic-damage model for concrete', *International Journal of Solids and Structures*, 25(3), 299-326.

Luccioni, B., Oller, S. & Danesi, R. 1996, 'Coupled plastic-damaged model', *Computer methods in applied mechanics and engineering*, 129, (1-2), 81-89.

Mander, J.B., Priestel, M.J.N, and Park, R., 1988, "Theoretical Stress-Strain Model for Confined Concrete," *Journal of Structural Engineering*, 114(8), 1804-1826.

Massone, L. M., and Wallace, J. W. (2004). "Load—deformation responses of slender reinforced concrete walls." *ACI Struct. J.*, 101(1), 103–113.

Massone, L. M., Orakcal, K., and Wallace, J. W. (2006). “Shear-flexure interaction for structural walls.” *ACI Special Publication, 236(7)*, 127–150.

Menetrey, P. & Willam, K.J. 1995, 'Triaxial failure criterion for concrete and its generalization', *Structural Journal*, 92(3), 311-318.

Meschke, G., Lackner, R. & Mang, H.A. 1998, 'An anisotropic elastoplastic-damage model for plain concrete', *International Journal for Numerical Methods in Engineering*, 42(4), 703-727.

MGD-b Geers. Enhanced solution control for physically and geometrically nonlinear problems. part ii—comparative performance analysis. 1999. *International Journal for Numerical Methods in Engineering*, 46(2):205–230.

Michel Samaan, Amir Mirmiran, and Mohsen Shahawy. 1998. Model of concrete confined by fiber composites. *Journal of structural engineering*, 124(9):1025–1031.

Michael P Berry, Dawn E Lehman, and Laura N Lowes. (2008). Lumped-plasticity models for performance simulation of bridge columns. *ACI Structural Journal*, 105(3):270.

Milad H., Farzad H., Ramin V., Mohd S. B. J. and Keyhan K. (2017). Simplified Damage Plasticity Model for Concrete, *Structural Engineering International*, 27:1, 68-78.

Mirela Galic, Pavao Marovic, and Zeljana Nikolic (2011). Modified mohr-coulomb–rankine material model for concrete. *Engineering computations*, 28(7):853–887.

Mohammadreza Vafaei, Sophia C Alih, and Ali Fallah. (2020). The accuracy of the lumped plasticity model for estimating nonlinear behavior of reinforced concrete frames under gradually increasing vertical loads. *Structural Concrete*, 21(1):65–80.

Morenon, P., Multon, S., Sellier, A., Grimal, E., Hamon, F. & Kolmayer, P. 2019, 'Flexural performance of reinforced concrete beams damaged by Alkali-Silica Reaction', *Cement and Concrete Composites*, 104, 103412.

Morten Engen, MAN Hendriks, Jan Arve Øverli, and Erik Áldstedt. 2019. Non-linear finite element analyses applicable for the design of large reinforced concrete structures. *European Journal of Environmental and Civil Engineering*, 23(11):1381–1403.

Murakami, S. 1983, 'Notion of continuum damage mechanics and its application to anisotropic creep damage theory', *Journal of Engineering Materials and Technology*, 105(2), 99-105.

Murat Saatcioglu and Salim R Razvi 1992. 'Strength and ductility of confined concrete'. *Journal of Structural engineering*, 118(6):1590–1607.

N. Ottesen and H. Pettersson. *Introduction to the finite element method*. Pearson Education Limited, 1992.

Nayak, G.C. & Zienkiewicz, O.C. 1972, 'Elasto-plastic stress analysis. A generalization for various constitutive relations including strain softening', *International Journal for Numerical Methods in Engineering*, 5(1), 113-135.

Nayera M. Ahmed S.F., B. Benmokrane, Kenneth W.N (2014). Experimental Investigation of Concrete Shear Walls Reinforced with Glass Fiber–Reinforced Bars under Lateral Cyclic Load, *Journal of Composites for Construction*, 18(3).

Neale, K.W. and Labossière, P. (eds.) In *Advanced Composite Materials on Bridges and Structures*, 1<sup>st</sup> Int. Conf, Sherbrooke, Québec, Canadian Society for Civil Engineering, 1992, p. 700

Neto, E.A.d.S., Owen, D.R.J. & Peric, D. 2008, *Computational Methods for Plasticity: Theory and Applications*, 1. Aufl. edn, Wiley, Chichester.

Niels Saabye Ottosen. A failure criterion for concrete. 1977. *Journal of the Engineering Mechanics Division*, 103(4):527–535.

Okan Ozcan, Baris Binici, and Guney Ozcebe (2010). Seismic strengthening of rectangular reinforced concrete columns using fiber reinforced polymers. *Engineering Structures*, 32(4):964–973.



Ortiz, M. & Martin, J.B. 1989, 'Symmetry-preserving return mapping algorithms and incrementally extremal paths: A unification of concepts', *International Journal for Numerical Methods in Engineering*, 28(8), 1839-1853.

Ortiz, M. & Popov, E.P. 1985, 'Accuracy and stability of integration algorithms for elastoplastic constitutive relations', *International Journal for Numerical Methods in Engineering*, 21(9), 1561-1576.

Ortiz, M. 1985, 'A constitutive theory for the inelastic behavior of concrete', *Mechanics of Materials*, 4(1), 67-93.

P Fuschi, M Dutko, D Perić, and DRJ Owen 1994. On numerical integration of the five-parameter model for concrete. *Computers & structures*, 53(4):825–838.

P. Kotronis and J. Mazars. “Simplified modelling strategies to simulate the dynamic behaviour of R/C walls”. In: *Journal of earthquake engineering* 9.02 (2005), pp. 285–306.

Pankaj & Bićanić, N. 1997, 'Detection of multiple active yield conditions for Mohr-Coulomb elastoplasticity', *Computers & Structures*, 62(1), 51-61.

Papanikolaou, V.K. & Kappos, A.J. 2007, 'Confinement-sensitive plasticity constitutive model for concrete in triaxial compression', *International Journal of Solids and Structures*, 44(21), 7021-7048.

Perić, D. & Neto, E.A.d.S. 1999, 'A new computational model for Tresca plasticity at finite strains with an optimal parametrization in the principal space', *Computer Methods in Applied Mechanics and Engineering*, 171(3), 463-489.

Peter Grassl (2004). Modelling of dilation of concrete and its effect in triaxial compression. *Finite elements in analysis and design*, 40(9-10):1021–1033.

Peter Grassl, Karin Lundgren, and Kent Gylltoft (2002). Concrete in compression: a plasticity theory with a novel hardening law. *International Journal of Solids and Structures*, 39(20):5205–5223.

Philippe Menetrey and KJ Willam (1995). Triaxial failure criterion for concrete and its generalization. *Structural Journal*, 92(3):311–318.

PG Bergan and I Holand. Nonlinear finite element analysis of concrete structures. 1979. *Computer Methods in Applied Mechanics and Engineering*, 17:443–467.

Pramono, E. & Willam, K. 1989, 'Implicit integration of composite yield surfaces with corners', *Engineering Computations*, 6(3), 186-197.

Pramono, E. & Willam, K. 1989, 'Implicit integration of composite yield surfaces with corners', *Engineering Computations*, 6(3), 186-197.

Qian J., Chen Q (2005). “A macro-model of shear walls for pushover analysis”, *Structures and Buildings*; 158: 119-132.

R. Barretta, L. Feo, R. Luciano. 2015. Some closed-form solutions of functionally graded beams undergoing nonuniform torsion, *Composite Structures*, 123, 132-136.

R. Barretta, R. Luciano. 2014. Exact solutions of isotropic viscoelastic functionally graded Kirchhoff plates, *Composite Structures*, 118, 448-454

R. Emre Erkmén and Mario M Attard (2011). Displacement-based finite element formulations for material-nonlinear analysis of composite beams and treatment of locking behaviour. *Finite elements in analysis and design*, 47(12):1293–1305.

R.J. Gravina, S.T. Smith. 2008. Flexural behaviour of indeterminate concrete beams reinforced with FRP bars. *Engineering Structures*, 30 (9), 2370-2380.

R.G. Wan. Implicit integration algorithm for hoek-brown elastic-plastic model. 1992. *Computers and Geotechnics*, 14(3):149–177.

Rashid, Y.R. 1968, 'Ultimate strength analysis of prestressed concrete pressure vessels', *Nuclear Engineering and Design*, 7(4), 334-344.

Rizkalla, S., Hassan, T. and Hassan, N. (2003), Design recommendations for the use of FRP for reinforcement and strengthening of concrete structures. *Prog. Struct. Engng Mater.*, 5: 16-28.

Robert D. Cook et al. *Concepts and applications of finite element analysis*. John Wiley & Sons, 2007.

Roman Okelo, A Robert L. Yuan. 2005. Bond Strength of Fiber Reinforced Polymer Rebars in Normal Strength Concrete. *Composites for Construction*. 9(3), 203-213.

Reddy JN (1997). "On Locking-free shear deformable beam elements", *Computer Methods in Applied Mechanics and Engineering* 149: 113-132.

SA Whyte, HJ Burd, CM Martin, and MJ Rattley. 2020. Formulation and implementation of a practical multi-surface soil plasticity model. *Computers and Geotechnics*, 117:103092.

Sarikaya, A., & Erkmen, R. (2019). A plastic-damage model for concrete under compression. *International Journal of Mechanical Sciences*, 150, 584–593.

Sarikaya, A., Erkmen, R.E., Gowripalan, N. & Sirivivatnanon, V. 2021, 'A plastic-damage model for concrete affected by alkali-silica reaction', paper presented to *the 16th International Conference on Alkali-Aggregate Reaction in Concrete (ICAAAR) 2020-2022*, Lisbon, Portugal, April 2021.

Scalet, G. & Auricchio, F. 2018, 'Computational methods for elastoplasticity: An overview of conventional and less-conventional approaches', *Archives of Computational Methods in Engineering*, 25(3), 545-89.

Sebastian Pech, Markus Lukacevic, and Josef Füssl. 2021. A robust multisurface returnmapping algorithm and its implementation in abaqus. *Finite Elements in Analysis and Design*, 190:103531.

Seo, S. Y., L. Feo, and D. Hui. 2013. "Bond strength of near surface-mounted FRP plate for retrofit of concrete structures." *Compos. Struct.* 95 (1): 719–727.

Sharbatdar, M. K., and Saatcioglu, M. (2009). "Seismic design of FRP reinforced concrete structures." *Asian J. Appl. Sci.*, 2(3), 211–222.

Shunsuke Sugano (1996). Seismic behavior of reinforced concrete columns which used ultra-high-strength concrete. *In Eleventh World Conference on Earthquake Engineering, Paper No. 1383*.

Simo, J.C. & Govindjee, S. 1991, 'Non-linear B-stability and symmetry preserving return mapping algorithms for plasticity and viscoplasticity', *International Journal for Numerical Methods in Engineering*, 31(1), 151-176.

Simo, J.C. & Hughes, T.J.R. 1998, *Computational Inelasticity*, Springer, New York.

Simo, J.C. & Ju, J.W. 1987, 'Strain- and stress-based continuum damage models—I. Formulation', *International Journal of Solids and Structures*, 23(7), 821-840.

Simo, J.C. & Ju, J.W. 1989, 'Strain- and stress-based continuum damage models—II. Computational aspects', *Mathematical and Computer Modelling*, 12(3), 378.

Simo, J.C. & Taylor, R.L. 1985, 'Consistent tangent operators for rate-independent elastoplasticity', *Computer Methods in Applied Mechanics and Engineering*, 48(1), 101-118.

Simo, J.C. & Taylor, R.L. 1986, 'A return mapping algorithm for plane stress elastoplasticity', *International Journal for Numerical Methods in Engineering*, 22(3), 649-670.

Simo, J.C., Kennedy, J.G. & Govindjee, S. 1988, 'Non-smooth multi-surface plasticity and viscoplasticity. Loading/unloading conditions and numerical algorithms', *International Journal for Numerical Methods in Engineering*, 26(10), 2161-2185.

Sittipunt, C., Wood, S. L., Lukkunaprasit, P., and Pattararattanakul, P. (2001). "Cyclic behavior of reinforced concrete structural walls with diagonal web reinforcement." *ACI Struct. J.*, 98(4), 554–562.

T Yu, JG Teng, YL Wong, and SL Dong 2010. Finite element modeling of confined concrete-ii: Plastic-damage model. *Engineering structures*, 32(3):680–691.

Tobbi, H., Farghaly, A. S., and Benmokrane, B. (2012). "Concrete columns reinforced longitudinally and transversally with glass fiber-reinforced polymer bars." *ACI Struct. J.*, 109(4), 551–558.

Tureyen, A. K., & Frosch, R. J. (2002). Shear tests of FRP-reinforced concrete beams without stirrups. *Structural Journal*, 99(4), 427-434.

Ulm, F.-J., Peterson, M. & Lemarchand, E. 2002, 'Is ASR-expansion caused by chemoporoplastic dilatation?', *Concrete Science and Engineering*, 4(13), 47-55.

V Dias da Silva (2004). A simple model for viscous regularization of elasto-plastic constitutive laws with softening. *Communications in Numerical Methods in Engineering*, 20(7):547–568.

Vassilis K Papanikolaou and Andreas J Kappos 2007. Confinement-sensitive plasticity constitutive model for concrete in triaxial compression. *International Journal of Solids and Structures*, 44(21):7021–7048.

Vladimir Cervenka. Inelastic analysis of reinforced concrete panels 1971. *Theory, Publ, Int. Assoc. Bridge Struc. Eng.*, 31:31–45.

Voyiadjis, G.Z. & Park, T. 1997, 'Anisotropic damage effect tensors for the symmetrization of the effective stress tensor', *Journal of Applied Mechanics*, 64(1), 106-110.

Wallace, J. W., and Moehle, J. P. (1992). “Ductility and detailing requirements of bearing wall buildings.” *J. Struct. Eng.*, (1625), 1625–1644.

Warner Tjardus Koiter. 1953. Stress-strain relations, uniqueness and variational theorems for elastic-plastic materials with a singular yield surface. *Quarterly of applied mathematics*, 11(3):350-354.

WF Chen. Concrete plasticity: Macro-and microapproaches (1993). *International journal of mechanical sciences*, 35(12):1097–1109.

Wilkins, M.L. 1963, 'Calculation of elastic-plastic flow', Series Calculation of elastic-plastic flow.

Wing Kam Liu, Yu-Kan Hu, and Ted Belytschko, 1994. Multiple quadrature underintegrated finite elements. *International Journal for Numerical Methods in Engineering*, 37(19):3263–3289.

Wu, J.-Y. & Cervera, M. 2016, 'A thermodynamically consistent plastic-damage framework for localized failure in quasi-brittle solids: Material model and strain localization analysis', *International Journal of Solids and Structures*, 88-89, 227-247.

Wyllie, L. A.; Abrahamson, N.; Bolt, B.; Castro, G.; and Durkin, M. E., 1986, "The Chile Earthquake of March 3, 1985—Performance of Structures," *Earthquake Spectra*, 2 (2), 93-371.

Yamakawa, T., and Fujisaki, T. (1995). "A study on elasto-plastic behavior of structural walls reinforced by CFRP grids." *Proc. of the Second Int. Symp. on Non-metallic (FRP) Reinforcement for Concrete Structures (FRPRCS-2)*, RILEM proc. 29, 267–274.

Yazdani, S. & Schreyer, H.L. 1990, 'Combined plasticity and damage mechanics model for plain concrete', *Journal of Engineering Mechanics*, 116(7), 1435- 1450.

Yu-Kan Hu and LI Nagy, 1997. A one-point quadrature eight-node brick element with hourglass control. *Computers & structures*, 65(6):893–902.

# APPENDIX 1

## SE\_Plasticity\_Plane User Guide

### A1.1. Data entry and solutions

Program accepts a group of input data files with .TXT extension and creates another group of output files with .DAC extension.

#### A1.1.1. Input files for static 1D Beam-Type model

The input files required for the 1D Beam-Type model analyses are:

- **CoorBOUNDSE**
- **CoorLoadSE**
- **GEOSE**
- **PROPERTY\_CONCRETE**
- **ReinforcementSE**
- **SEC**
- **Solution\_ParameterSE**
- **Step\_Guide**
- **SWITCHB**
- **Current\_PlasticDamageParam**

#### A1.1.2. Output files for static 1D Beam-Type model

The output files created after the 1D Beam-Type model static analysis

- **DEP\_X**
- **DEP\_Y**
- **ELEM\_MATRIX**
- **INPUT\_CHECK**

- **Lamda**
- **ROT\_Z**
- **STATIC\_DISPLACEMENTS**
- **TRANS**

## **A1.2. Input files**

- **CoorBOUNDSE.TXT: Support Information**

-EnterWithKeywords-

EnterNewBoundaryCoordinatesYorN: Y for a new boundary condition

BoundaryCoordinatesX-Y: Coordinates at which the support is applied

FixedDirection: 1 for horizontal and 2 for vertical

EnterNewBoundaryCoordinatesYorN: If there is no support information put N

- **CoorLoadSE.TXT: Nodal loads**

-EnterWithKeywords-

EnterNewLoadCoordinatesYorN: Y for a new load

LoadCoordinatesX-Y: Coordinate at which the node is applied

LoadDirection: Direction of the nodal loading (1 or 2)

LoadValue: Value of the nodal loading

EnterNewLoadCoordinatesYorN: If there is no loading information put N

- **GEOSE.TXT: Structural geometry information**

-EnterWithKeywords-

NumNodes:

NumElems:

NodeCoor: *X-Coordinate, Y-Coordinate*

ElemConnect:



- **PROPERTY\_CONCRETE.TXT: Properties of the concrete bulk**

-EnterWithKeywords-

ConcreteElasticityModulus: Modulus of elasticity, E

ConcretePoissonRatio: Poisson ratio,  $\mu$

ConcreteCompressiveStress: Compressive Stress,  $f_c$

OnsetRatioPlasticFlow:

CompressivePeakStrain:

ConcreteTensileStress:

TensionSofteningPower:

FactorIntersectTensionCompressionSurface:

PotentialSurfaceType:

SlopeLinearPotentialSurface:

TensionSurfaceType1Rankine\_2Mixed:

CornerReturnTypeAssociative0orNon1:

DamageEvolutionFactorCompression:

DamageEvolutionFactorTension:

AnalysisTypeIsotropic0Anisotropic1:

ConfinementCoefficientXdirection:

ConfinementCoefficientYdirection:

ProducePlasticReturnGraphAtSpecificPointYorN:

- **ReinforcementSE.TXT: Properties of the reinforcements**

-EnterWithKeywords-

NumberOfRebarProperties:

NumberOfRebarsInTheGroup:

RebarElasticityModulusOfTheGroup:

RebarYieldStressOfTheGroup:

RebarHardeningModulusOfTheGroup:

RebarAreaAndLocationInEachGroup:

ApplyAllElementsYorN:

EnterStirrupsYorN:

ReportReinforcementPlasticReturn:

- **SEC.TXT: Cross section of the concrete bulk**

-EnterWithKeywords-

EnterWidthDepthEachElement: The width and depth of the bulk

- **Solution\_ParameterSE.TXT: Parameters needed for running**

-EnterWithKeywords-

ElementType:

NumIntPoint:

SectionWidthIntegPoint:

SectionHeightIntegPoint:

AnalysisTypeNoShear0Shear1:

AnalysisTypeStatic1Dynamic2Both3:

ControlTypeLoad1Displacement2:

ControlNodeCoordinates:

ControlDirection:

StepSize:

StepNumberLimit:

HardeningType\_1volum\_2mixed:

HardeningUpdateLevel\_1GlobalStep\_2GlobalIteration\_3PlasticIteration:

PlasticReturnTypes\_1CuttingPlane\_2CPP:

AlgorithmStabilizationYorN:

PlasticReturnIterationLimit:

ViscosityRate\_0Independent\_1ViscoPlastic\_2ViscosRegularization:

GlobalAlgorithm\_ErrorMargin:

PlasticityAlgorithm\_ErrorMargin:

- **Step\_Guide.TXT: Setting the number of cycles**

-EnterWithKeywords-

NumberOfCycles:

ControlType1or2:

NumberOfStepsEachCycle:

- **SWITCHB.TXT: Activating option to consider during analysis**

-EnterWithKeywords-

LoadGenerateUsingCoordinatesYorN:

BoundaryGenerateUsingCoordinatesYorN:

MassGenerateUsingCoordinatesYorN:

- **Current\_PlasticDamageParam: Parameters of analysis**

-EnterWithKeywords-

MaterialModels\_1Reduce3D\_2Direct1DSugano\_3Direct1DSaatchi:

DirectUniaxialModelPostpeakCalibrationFactor:

CurrentCompressionPlasticityParameter:

CurrentTensionPlasticityParameter:

CurrentCompressionDamageParameter:

CurrentTensionDamageParameter:

*Solution\_ParameterSE*, *SWITCHB* and *Current\_PlasticDamageParam.txt* files are analysis information needed to smoothly run the program. The analysis type, the choice of solution control, Step size, Step number limit and stabilization parameters are defined. We didn't need them in this work. NumIntPoint: the number of integration points refers to the discretization of an element into smaller segments for numerical computation. In this program, integration is defined along the length of the element and on the cross section of the element. Analysis Type: is whether the run will be shear or non-shear based. In this work, the analysis type chosen is shear based.

Displacement control was employed for the analysis of structural elements in this work. Control Node Coordinates or Control Node Number is the coordinates of interest. The program gives the outputs based on this coordinate. In SWITCHB, that's where commands are activated or disactivated. There were introduced to give options to the user on how to use the program. There is a choice of using coordinates or nodes to apply load, supports or mass (in case it is dynamic analysis).

### **A1.3. Example 1. Beam Analysis**

The beam ISO30-1 is 200 mm wide and 300 mm high, as shown in Figure 4-8 to Figure 4-10, it is supported on a span of 3000 mm and is subjected to two equal loads symmetrically placed about the mid-span. The modulus of elasticity of concrete is 32 GPa and  $f_c=44$  MPa. Yielding stress for steel rebars is taken as 480 MPa, the ultimate strength is taken as 600 MPa and the modulus of elasticity is taken as 200 GPa. Conventional steel stirrups (10 mm diameter) is used in the non-constant moment zones, to prevent shear failure. The diameter of the reinforcement is maintained constant (19.1 mm diameter) and this beam is reinforced by two identical rebar as resumed in Figure 4-8.

#### **A1.3.1. Input files**

##### **GEOSE.TXT**

The geometry of the member to be analyzed is defined. The number of nodes, number of elements and each nodes' coordinates. For the example given, the member is 3000mm and is divided in 30 members (31 nodes). ElemConnect stands for the connection of each node.

```

GEOSE
File Edit View
-EnterWithKeywords-
NumNodes:
31
NumElems:
30
NodeCoord:
0.0000 , 0.0000
100.0000 , 0.0000
200.0000 , 0.0000
300.0000 , 0.0000
400.0000 , 0.0000
500.0000 , 0.0000
600.0000 , 0.0000
700.0000 , 0.0000
800.0000 , 0.0000
900.0000 , 0.0000
1000.0000 , 0.0000
1100.0000 , 0.0000
1200.0000 , 0.0000
1300.0000 , 0.0000
1400.0000 , 0.0000
1500.0000 , 0.0000
1600.0000 , 0.0000
1700.0000 , 0.0000
1800.0000 , 0.0000
1900.0000 , 0.0000
2000.0000 , 0.0000
2100.0000 , 0.0000
2200.0000 , 0.0000
2300.0000 , 0.0000
2400.0000 , 0.0000
2500.0000 , 0.0000
2600.0000 , 0.0000
2700.0000 , 0.0000
2800.0000 , 0.0000
2900.0000 , 0.0000
3000.0000 , 0.0000
ElemConnect:
1 , 2
2 , 3
3 , 4
4 , 5
5 , 6
6 , 7
7 , 8
8 , 9
9 , 10
10 , 11
11 , 12
12 , 13
13 , 14
14 , 15
15 , 16
16 , 17
17 , 18
18 , 19
19 , 20
20 , 21
21 , 22
22 , 23
23 , 24
24 , 25
25 , 26
26 , 27
27 , 28
28 , 29
29 , 30
30 , 31

```

## PROPERTY\_CONCRETE.TXT

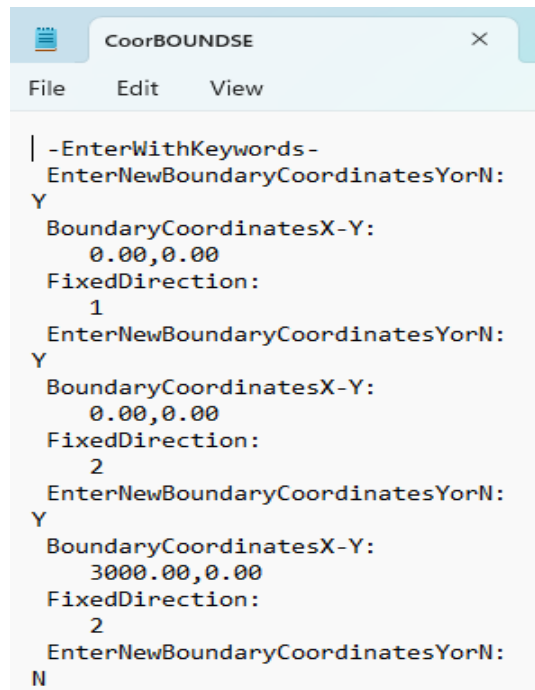
The solver requires the concrete material properties in order to analyze the system. Concrete Elasticity Modulus, Poisson Ratio, Compressive Stress, Tensile stress, peak strain and Onset ratio Plastic Flow are defined.

```
-EnterWithKeywords-
ConcreteElasticityModulus:
  32000.0000000000
ConcretePoissonRatio:
  0.150000000000000
ConcreteCompressiveStress:
  -46.0000000000000
OnsetRatioPlaticFlow:
  0.14
CompressivePeakStrain:
  -0.0022
ConcreteTensileStress:
  2.0
TensionSofteningPower:
  0.27
FactorIntersectTensionCompressionSurface:
  1.50000000000000
PotentialSurfaceType:
  1
SlopeLinearPotentialSurface:
  0.150000000000000
TensionSurfaceType1Rankine_2Mixed:
  XXX
CornerReturnTypesAssociative0orNon1:
  XXX
DamageEvolutionFactorCompression:
  XXX
DamageEvolutionFactorTension:
  XXX
AnalysisTypeIsotropic0Anisotropic1:
  XXX
ConfinementCoefficientXdirection:
  XXX
ConfinementCoefficientYdirection:
  XXX
ProducePlasticReturnGraphAtSpecificPointYorN:
  XXX
```

### CoorBOUNDSE.TXT

In order to analyse the system, the finite element solver requires boundary conditions to be defined. Boundary conditions should be able to provide equilibrium to the system. In this example, the beam is supported at each end in such a way that it can freely rotate and translate vertically, it cannot resist horizontal movement

and. Y means Yes there is support at coordinate X-Y, 1 means it is fixed in global X-direction and 2 means fixed in global Y-direction.



```
CoorBOUNDSE
File Edit View
| -EnterWithKeywords-
EnterNewBoundaryCoordinatesYorN:
Y
BoundaryCoordinatesX-Y:
0.00,0.00
FixedDirection:
1
EnterNewBoundaryCoordinatesYorN:
Y
BoundaryCoordinatesX-Y:
0.00,0.00
FixedDirection:
2
EnterNewBoundaryCoordinatesYorN:
Y
BoundaryCoordinatesX-Y:
3000.00,0.00
FixedDirection:
2
EnterNewBoundaryCoordinatesYorN:
N
```

### **CoorLoadSE.TXT**

Nodal load data is inputted. As shown in below, the coordinate where the load is applied is defined and the direction of the load which is perpendicular to the direction of the member. The load value is in N. The program has also the capabilities to support multiple loading points.

```
CoorLoadSE
File Edit View
-EnterWithKeywords-
EnterNewLoadCoordinatesYorN:
Y
LoadCoordinatesX-Y:
1000.000000000000,0.0000000000
LoadDirection:
2
LoadValue:
-0.4000E+06
EnterNewLoadCoordinatesYorN:
Y
LoadCoordinatesX-Y:
2000.000000000000,0.0000000000
LoadDirection:
2
LoadValue:
-0.4000E+06
EnterNewLoadCoordinatesYorN:
N
```

### Current\_PlasticDamageParam.TXT

```
Current_PlasticDamageParam
File Edit View
-EnterWithKeywords-
MaterialModels_1Reduce3D_2Direct1DSugano_3Direct1DSaatchi:
2
DirectUniaxialModelPostpeakCalibrationFactor:
XXX
CurrentCompressionPlasticityParameter:
XXX
CurrentTensionPlasticityParameter:
XXX
CurrentCompressionDamageParameter:
XXX
CurrentTensionDamageParameter:
XXX
```

### SEC.TXT





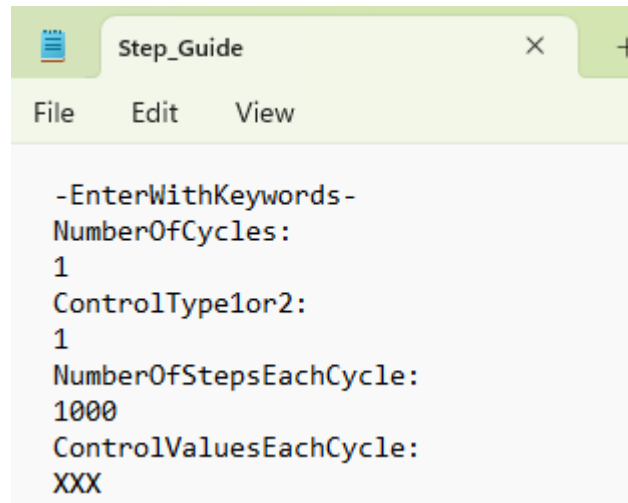
```
ReinforcementSE
File Edit View
-EnterWithKeywords-
NumberOfRebarProperties:
    2
NumberOfRebarsInTheGroup:
    2
RebarElasticityModulusOfTheGroup:
    42000
RebarYieldStressOfTheGroup:
    689.0
RebarHardeningModulusOfTheGroup:
    1000.0
RebarAreaAndLocationInEachGroup:
    286.4
    -75.00, -125.00
    286.4
    75.00, -125.00
NumberOfRebarsInTheGroup:
    2
RebarElasticityModulusOfTheGroup:
    200000.0000000000
RebarYieldStressOfTheGroup:
    480.000000000000
RebarHardeningModulusOfTheGroup:
    600.0
RebarAreaAndLocationInEachGroup:
    78.5
    -75.00, 125.00
    78.5
    75.00, 125.00
ApplyAllElementsYorN:
Y
NumberOfRebarGroupsUsedInEachElement:
    1
RebarGroupNoForEachElement:
    1
EnterStirrupsYorN:
Y
AverageSpacingOfStirrups:
    100
AreaOfStirrupsWithinEachSpacing:
    78.5
ReportReinforcementPlasticReturn:
N
```

**Solution\_ParameterSE.TXT**

```
Solution_ParameterSE
File Edit View

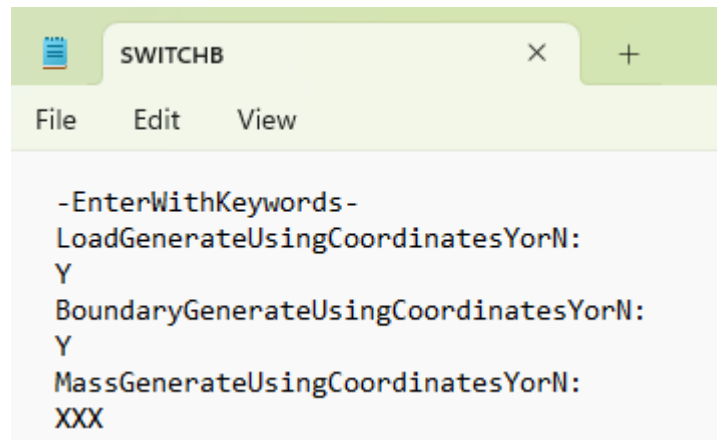
-EnterWithKeywords-
ElementType:
  1
NumIntPoint:
  3
SectionWidthIntegPoint:
  3
SectionHeightIntegPoint:
  12
AnalysisTypeNoShear0Shear1:
  1
AnalysisTypeStatic1Dynamic2Both3:
  1
ControlTypeLoad1Displacement2:
  2
ControlNodeCoordinates:
  2000.000000000000000,0.000000000000000
ControlNodeNumber:
  22
ControlDirection:
  2
StepSize:
  -1.000000000000000
StepNumberLimit:
  56
PlasticReturn_type_1CuttingPlane_2CPP:
  1
AlgorithmStabilizationYorN:
  N
DenominatorAmplificationFactor:
  1.000000000000000
PenaltyFactorLagrangian:
  0.000000000000000E+000
PlasticReturnIterationLimit:
  1000
ViscosityRate_0Independent_1ViscoPlastic_2ViscosRegularization:
  0
ViscoPlasticRetardationTime:
  0.000000000000000E+000
ViscoPlasticTimeIncrement:
  0.000000000000000E+000
```

Step\_Guide.TXT



```
-EnterWithKeywords-  
NumberOfCycles:  
1  
ControlType1or2:  
1  
NumberOfStepsEachCycle:  
1000  
ControlValuesEachCycle:  
XXX
```

**SWITCHB.TXT**



```
-EnterWithKeywords-  
LoadGenerateUsingCoordinatesYorN:  
Y  
BoundaryGenerateUsingCoordinatesYorN:  
Y  
MassGenerateUsingCoordinatesYorN:  
XXX
```

### A1.3.2. Input check

```

INPUT_CHECK - Notepad
File Edit Format View Help
| *****Start Time*****
| 17 : 57 : 56 : 534
|
|-----|
| ***Enter the Names of Plasticity Related Output files***
|
| ***Choose from the below list of Possible Output files***
|
| ***List of Possible Output files***
|
| to be addressed at ListOutputFileSE.txt
|
|         ---Lamda.DAC---
|         ---STATIC_DISPLACEMENTS.DAC---
|         ---DEP_X.DAC---
|         ---DEP_Y.DAC---
|         ---ROT_Z.DAC---
|
|         ---PLASTIC_RETURN_LOG_FILE.DAC---
|         ---InstantDrawFiles---
|         ---SURFACE_AND_RETURN.TXT---
|         ---StressConvergenceChase---
|
|-----|
| Number of pieces along an element          3
| Number of pieces along width b of the Cross-section      3
| Number of pieces along height h of the Cross-section     12
|
| COORDINATES OF NODES
| NOD      X(mm)      Y(mm)
| 1         0.000000    0.000000
| 2        100.000000    0.000000
| 3        200.000000    0.000000
| 4        300.000000    0.000000
| 5        400.000000    0.000000
| 6        500.000000    0.000000
| 7        600.000000    0.000000
| 8        700.000000    0.000000
| 9        800.000000    0.000000
| 10       900.000000    0.000000
| 11      1000.000000    0.000000
| 12      1100.000000    0.000000
| 13      1200.000000    0.000000
| 14      1300.000000    0.000000
| 15      1400.000000    0.000000
| 16      1500.000000    0.000000
| 17      1600.000000    0.000000
| 18      1700.000000    0.000000
| 19      1800.000000    0.000000
| 20      1900.000000    0.000000
| 21      2000.000000    0.000000
| 22      2100.000000    0.000000
| 23      2200.000000    0.000000
| 24      2300.000000    0.000000
| 25      2400.000000    0.000000
| 26      2500.000000    0.000000
| 27      2600.000000    0.000000
| 28      2700.000000    0.000000
| 29      2800.000000    0.000000
| 30      2900.000000    0.000000
| 31      3000.000000    0.000000
|
| ELEMENT   I END      J END      LENGTH (mm)
| 1         1         2         100.0000000
| 2         2         3         100.0000000
| 3         3         4         100.0000000
| 4         4         5         100.0000000
| 5         5         6         100.0000000
| 6         6         7         100.0000000
| 7         7         8         100.0000000
| 8         8         9         100.0000000
| 9         9        10         100.0000000
| 10        10       11         100.0000000
| 11        11       12         100.0000000
| 12        12       13         100.0000000
| 13        13       14         100.0000000
|
| <

```

INPUT\_CHECK - Notepad

```

File Edit Format View Help
-----
13          13          14          100.00000000
14          14          15          100.00000000
15          15          16          100.00000000
16          16          17          100.00000000
17          17          18          100.00000000
18          18          19          100.00000000
19          19          20          100.00000000
20          20          21          100.00000000
21          21          22          100.00000000
22          22          23          100.00000000
23          23          24          100.00000000
24          24          25          100.00000000
25          25          26          100.00000000
26          26          27          100.00000000
27          27          28          100.00000000
28          28          29          100.00000000
29          29          30          100.00000000
30          30          31          100.00000000

Loads are generated using Coordinates
Load No    11          in direction  2          applied at  1000.00    0.00
Load No    21          in direction  2          applied at  2000.00    0.00
-----

Boundary Conditions are generated using Coordinates
BC applied in direction  1          at    0.00    0.00
BC applied in direction  2          at    0.00    0.00
BC applied in direction  2          at  3000.00    0.00
-----

Multiple-Point Constraints are imposed directly to nodes
-----

FactorIntersectTensionCompressionSurface  1.5000000000000000

PROPERTIES OF SOLID

Ec          nu          fc          ft          ko          eps_c    P_type    al_p
N/mm2
0.3200E+05  0.15  -46.0000  2.0000  0.1400  -0.002200  1  0.150

          Kbu          G
          N/mm2          N/mm2
          15238.0952380952          13913.0434782609

Factor to make sure Tension Surface and Mentrey-Willam Intersects
1.5000000000000000
-----

P_type=1 Linear | P_type=2 Higher order Potential func (al_p=2 Quadratic)
T_type=1 Rankine surface | T_type=2 Mixed surface with Cut-off

-----
-----If T_Type =1 -----***Suggested numbers***-----
ksi_t0= 1.45*ft/afc | But we read si_to | So enter approximately  1.45
-----
-----If T_Type =2 -----***Suggested numbers***-----
ksi_m0=-2.5/afc | But we read si_mo | So enter approximately -2.5
ksi_t0= 1.45*ft/afc | But we read si_to | So enter approximately  1.45
Ro_t0 =1.05 /afc | But we read o_to | So enter approximately  1.05
      0<mkf<1 | rate_vkm<1
-----

T_type    ksi_m0    ksi_t0    Ro_t0    n3    Fdamc    Fdamt
1          0.0000    0.0000    0.0000    0.2700    0.0000    0.000000

Isotropic Analysis Type 0 | Anisotropic Analysis Type 1
IA_type =          0

gama1=  0.000000000000000E+000
gama2=  0.000000000000000E+000
-----

Output NOT generated for any Plastic return scenario for the Concrete Beam
<

```

INPUT\_CHECK - Notepad

File Edit Format View Help

Output NOT generated for any Plastic return scenario for the Concrete Beam

```

-----
Number of Reinforcement Groups with different Properties          2
Number of Reinforcement Bars in Group      1 is                2
-----For the Reinforcement Group-----
Er = 42000.0000000000
sig_y = 689.0000000000
Hr = 1000.0000000000

Number of Reinforcement Bars in Group      2 is                2
-----For the Reinforcement Group-----
Er = 200000.0000000000
sig_y = 480.0000000000
Hr = 600.0000000000

Number of total re-bars within the Cross-section          4
Properties of the Reinforcement
Mem = 1
Num Location x Location y Area
1 -75.0000 -125.0000 .2864E+03
2 75.0000 -125.0000 .2864E+03
3 -75.0000 125.0000 .7850E+02
4 75.0000 125.0000 .7850E+02
-----
Mem = 2
Num Location x Location y Area
1 -75.0000 -125.0000 .2864E+03
2 75.0000 -125.0000 .2864E+03
3 -75.0000 125.0000 .7850E+02
4 75.0000 125.0000 .7850E+02
-----
Mem = 3
Num Location x Location y Area
1 -75.0000 -125.0000 .2864E+03
2 75.0000 -125.0000 .2864E+03
3 -75.0000 125.0000 .7850E+02
4 75.0000 125.0000 .7850E+02
-----
Mem = 4
Num Location x Location y Area
1 -75.0000 -125.0000 .2864E+03
2 75.0000 -125.0000 .2864E+03
3 -75.0000 125.0000 .7850E+02
4 75.0000 125.0000 .7850E+02
-----
Mem = 5
Num Location x Location y Area
1 -75.0000 -125.0000 .2864E+03
2 75.0000 -125.0000 .2864E+03
3 -75.0000 125.0000 .7850E+02
4 75.0000 125.0000 .7850E+02
-----
Mem = 6
Num Location x Location y Area
1 -75.0000 -125.0000 .2864E+03
2 75.0000 -125.0000 .2864E+03
3 -75.0000 125.0000 .7850E+02
4 75.0000 125.0000 .7850E+02
-----
Mem = 7
Num Location x Location y Area
1 -75.0000 -125.0000 .2864E+03
2 75.0000 -125.0000 .2864E+03
3 -75.0000 125.0000 .7850E+02
4 75.0000 125.0000 .7850E+02
-----
Mem = 8
Num Location x Location y Area
1 -75.0000 -125.0000 .2864E+03
2 75.0000 -125.0000 .2864E+03
3 -75.0000 125.0000 .7850E+02
4 75.0000 125.0000 .7850E+02
-----
Mem = 9
Num Location x Location y Area
1 -75.0000 -125.0000 .2864E+03

```

INPUT\_CHECK - Notepad

```

File Edit Format View Help
1 -75.0000 -125.0000 .2864E+03
2 75.0000 -125.0000 .2864E+03
3 -75.0000 125.0000 .7850E+02
4 75.0000 125.0000 .7850E+02
-----
Mem = 10
Num Location x Location y Area
1 -75.0000 -125.0000 .2864E+03
2 75.0000 -125.0000 .2864E+03
3 -75.0000 125.0000 .7850E+02
4 75.0000 125.0000 .7850E+02
-----
Mem = 11
Num Location x Location y Area
1 -75.0000 -125.0000 .2864E+03
2 75.0000 -125.0000 .2864E+03
3 -75.0000 125.0000 .7850E+02
4 75.0000 125.0000 .7850E+02
-----
Mem = 12
Num Location x Location y Area
1 -75.0000 -125.0000 .2864E+03
2 75.0000 -125.0000 .2864E+03
3 -75.0000 125.0000 .7850E+02
4 75.0000 125.0000 .7850E+02
-----
Mem = 13
Num Location x Location y Area
1 -75.0000 -125.0000 .2864E+03
2 75.0000 -125.0000 .2864E+03
3 -75.0000 125.0000 .7850E+02
4 75.0000 125.0000 .7850E+02
-----
Mem = 14
Num Location x Location y Area
1 -75.0000 -125.0000 .2864E+03
2 75.0000 -125.0000 .2864E+03
3 -75.0000 125.0000 .7850E+02
4 75.0000 125.0000 .7850E+02
-----
Mem = 15
Num Location x Location y Area
1 -75.0000 -125.0000 .2864E+03
2 75.0000 -125.0000 .2864E+03
3 -75.0000 125.0000 .7850E+02
4 75.0000 125.0000 .7850E+02
-----
Mem = 16
Num Location x Location y Area
1 -75.0000 -125.0000 .2864E+03
2 75.0000 -125.0000 .2864E+03
3 -75.0000 125.0000 .7850E+02
4 75.0000 125.0000 .7850E+02
-----
Mem = 17
Num Location x Location y Area
1 -75.0000 -125.0000 .2864E+03
2 75.0000 -125.0000 .2864E+03
3 -75.0000 125.0000 .7850E+02
4 75.0000 125.0000 .7850E+02
-----
Mem = 18
Num Location x Location y Area
1 -75.0000 -125.0000 .2864E+03
2 75.0000 -125.0000 .2864E+03
3 -75.0000 125.0000 .7850E+02
4 75.0000 125.0000 .7850E+02
-----
Mem = 19
Num Location x Location y Area
1 -75.0000 -125.0000 .2864E+03
2 75.0000 -125.0000 .2864E+03
3 -75.0000 125.0000 .7850E+02
4 75.0000 125.0000 .7850E+02
-----
Mem = 20
Num Location x Location y Area

```



INPUT\_CHECK - Notepad

```

File Edit Format View Help
-----
Num Location x Location y Area
1 -75.0000 -125.0000 .2864E+03
2 75.0000 -125.0000 .2864E+03
3 -75.0000 125.0000 .7850E+02
4 75.0000 125.0000 .7850E+02
-----
Mem = 21
Num Location x Location y Area
1 -75.0000 -125.0000 .2864E+03
2 75.0000 -125.0000 .2864E+03
3 -75.0000 125.0000 .7850E+02
4 75.0000 125.0000 .7850E+02
-----
Mem = 22
Num Location x Location y Area
1 -75.0000 -125.0000 .2864E+03
2 75.0000 -125.0000 .2864E+03
3 -75.0000 125.0000 .7850E+02
4 75.0000 125.0000 .7850E+02
-----
Mem = 23
Num Location x Location y Area
1 -75.0000 -125.0000 .2864E+03
2 75.0000 -125.0000 .2864E+03
3 -75.0000 125.0000 .7850E+02
4 75.0000 125.0000 .7850E+02
-----
Mem = 24
Num Location x Location y Area
1 -75.0000 -125.0000 .2864E+03
2 75.0000 -125.0000 .2864E+03
3 -75.0000 125.0000 .7850E+02
4 75.0000 125.0000 .7850E+02
-----
Mem = 25
Num Location x Location y Area
1 -75.0000 -125.0000 .2864E+03
2 75.0000 -125.0000 .2864E+03
3 -75.0000 125.0000 .7850E+02
4 75.0000 125.0000 .7850E+02
-----
Mem = 26
Num Location x Location y Area
1 -75.0000 -125.0000 .2864E+03
2 75.0000 -125.0000 .2864E+03
3 -75.0000 125.0000 .7850E+02
4 75.0000 125.0000 .7850E+02
-----
Mem = 27
Num Location x Location y Area
1 -75.0000 -125.0000 .2864E+03
2 75.0000 -125.0000 .2864E+03
3 -75.0000 125.0000 .7850E+02
4 75.0000 125.0000 .7850E+02
-----
Mem = 28
Num Location x Location y Area
1 -75.0000 -125.0000 .2864E+03
2 75.0000 -125.0000 .2864E+03
3 -75.0000 125.0000 .7850E+02
4 75.0000 125.0000 .7850E+02
-----
Mem = 29
Num Location x Location y Area
1 -75.0000 -125.0000 .2864E+03
2 75.0000 -125.0000 .2864E+03
3 -75.0000 125.0000 .7850E+02
4 75.0000 125.0000 .7850E+02
-----
Mem = 30
Num Location x Location y Area
1 -75.0000 -125.0000 .2864E+03
2 75.0000 -125.0000 .2864E+03
3 -75.0000 125.0000 .7850E+02
4 75.0000 125.0000 .7850E+02
-----
*****

```

output NOT generated for any Plastic return scenario for the Reinforcement

-----

CROSS-SECTIONAL PROPERTIES including Reinforcement

Mem	EA mm2	EIX mm4
1	.20E+10	.1517E+14
2	.20E+10	.1517E+14
3	.20E+10	.1517E+14
4	.20E+10	.1517E+14
5	.20E+10	.1517E+14
6	.20E+10	.1517E+14
7	.20E+10	.1517E+14
8	.20E+10	.1517E+14
9	.20E+10	.1517E+14
10	.20E+10	.1517E+14
11	.20E+10	.1517E+14
12	.20E+10	.1517E+14
13	.20E+10	.1517E+14
14	.20E+10	.1517E+14
15	.20E+10	.1517E+14
16	.20E+10	.1517E+14
17	.20E+10	.1517E+14
18	.20E+10	.1517E+14
19	.20E+10	.1517E+14
20	.20E+10	.1517E+14
21	.20E+10	.1517E+14
22	.20E+10	.1517E+14
23	.20E+10	.1517E+14
24	.20E+10	.1517E+14
25	.20E+10	.1517E+14
26	.20E+10	.1517E+14
27	.20E+10	.1517E+14
28	.20E+10	.1517E+14
29	.20E+10	.1517E+14
30	.20E+10	.1517E+14

-----

BOUNDARY CONDITIONS

FIXED NODE	FIXED DIRECTION
1	GLOBAL X DIRECTION
1	GLOBAL Y DIRECTION
31	GLOBAL Y DIRECTION

NODAL LOADS

NODE	LOADING TYPE	DIRECTION	P N	M Nmm
11	CONCENTRATED P	GLOBAL Y	-.4000E+06	
21	CONCENTRATED P	GLOBAL Y	-.4000E+06	

-----

CONSTANT NODAL LOADS

NODE	LOADING TYPE	DIRECTION	CP N	CM Nmm
------	--------------	-----------	---------	-----------

Analysis type: 0 for No Shear| 1 for Including Shear  
S\_type = 1 selected

Analysis type: 1 for Static only| 2 for Dynamic only| 3 for Both  
1 selected

-----

The results are produced for 0 number of files

-----

MaterialModels\_1Reduce3D\_2Direct1DSugano\_3Direct1DSaatchi 2  
 DirectUniaxialModelPostpeakCalibrationFactor 4.000000000000  
 CurrentCompressionPlasticityParameter 0.000000000000E+000

<

```

Analysis type: 1 for Static only| 2 for Dynamic only| 3 for Both
              1 selected
-----

The results are produced for          0 number of files
-----

MaterialModels_1Reduce3D_2Direct1DSugano_3Direct1DSaatchi          2
DirectUniaxialModelPostpeakCalibrationFactor  4.000000000000000
CurrentCompressionPlasticityParameter  0.000000000000000E+000
CurrentTensionPlasticityParameter  0.000000000000000E+000
CurrentCompressionDamageParameter  0.000000000000000E+000
CurrentTensionDamageParameter  0.000000000000000E+000
-----

Analysis Control type: Enter 1 for Load Control or Enter 2 for Displacement Con
trol          2
The control node number          21

Enter the direction: Enter 1 for X Enter 2 for Y Enter 3 for Z Rot
Control direction =          2 selected
Enter the step increment size -1.000000000000000
How many steps do you want to continue          56
-----

Plastic return type: 1 for Cutting_plane | 2 for Closest Point Projection | 3 f
or Premono-Willam          1

Iteration limit to terminate plastic return          1000

Enter| 0 rate-independent | 1 visco-plastic | 2 viscous regularization
0

Enter GlobalAlgorithm_ErrorMargin 9.999999974752427E-007
-----

Enter PlasticityAlgorithm_ErrorMargin 9.999999747378752E-005

Number of cycles          1
C_type=          1
*****End of Static Analysis*****
          17 :          58 :          5 :          614

```

### A1.3.3. Output files

- DEP\_X, DEP\_Y records deflections values along x and y-axis of the node selected in Solution\_Parameters at the end of each step.
- Lamda is the factor to describe the amount of force that was required to have a respective deflection. This is later multiplied by the nodal load to get the Force-displacement graph.
- ELEM\_MATRIX, ROT\_Z, STATIC\_DISPLACEMENTS and TRANS are additional outputs that describe the behavior of each element at the end of each step in the program run.

## DEP\_X

DEP\_X - Notepad  
File Edit Format View Help

```
4.116360761585035E-002  
0.281169969664856  
0.475288304387282  
0.660083511869108  
0.849770900731120  
1.04381453507716  
1.25990743901444  
1.44377342296885  
1.63062470403253  
1.81879036133263  
2.00827489418673  
2.19940612704558  
2.39159662271163  
2.58442776833779  
2.77809747443275  
3.02398472350313  
3.21759855711076  
3.41072775949631  
3.60393982894572  
3.79705520395285  
3.99018975164665  
4.18255284535900  
4.37574775825882  
4.56933888515711  
4.76394860223566  
4.95862031357919  
5.15357591370966  
5.34935805888747  
5.54539436315886  
5.74249395136966  
5.93957526199708  
6.13664574627503  
6.33273039611004  
6.52907005430857  
6.72514164015284  
6.92108211161198  
7.11695990782442  
7.31287644277021  
7.50884339940883  
7.70471492175009  
7.90141222653260  
8.07648945507242  
8.00377464173763  
8.09672455762467  
8.21446570308397  
8.34712346252341  
8.48308350782568  
8.63472553621486  
8.79151523849347  
8.94532580982648  
9.08989554839292  
9.17256684959701  
9.31725612313173  
9.47128992497105  
9.62709548353896  
9.78072772281064
```

# DEP\_Y

```
DEP_Y - Notepad
File Edit Format View Help
-1.0000000000000000
-2.0000000000000000
-3.0000000000000000
-4.0000000000000000
-5.0000000000000000
-6.0000000000000000
-7.0000000000000000
-8.0000000000000000
-9.0000000000000000
-10.0000000000000000
-11.0000000000000000
-12.0000000000000000
-13.0000000000000000
-14.0000000000000000
-15.0000000000000000
-16.0000000000000000
-17.0000000000000000
-18.0000000000000000
-19.0000000000000000
-20.0000000000000000
-21.0000000000000000
-22.0000000000000000
-23.0000000000000000
-24.0000000000000000
-25.0000000000000000
-26.0000000000000000
-27.0000000000000000
-28.0000000000000000
-29.0000000000000000
-30.0000000000000000
-31.0000000000000000
-32.0000000000000000
-33.0000000000000000
-34.0000000000000000
-35.0000000000000000
-36.0000000000000000
-37.0000000000000000
-38.0000000000000000
-39.0000000000000000
-40.0000000000000000
-41.0000000000000000
-42.0000000000000000
-43.0000000000000000
-44.0000000000000000
-45.0000000000000000
-46.0000000000000000
-47.0000000000000000
-48.0000000000000000
-49.0000000000000000
-50.0000000000000000
-51.0000000000000000
-52.0000000000000000
-53.0000000000000000
-54.0000000000000000
-55.0000000000000000
-56.0000000000000000
```











## Lamda

Lamda - Notepad

File Edit Format View Help

3.026151795936299E-002  
1.996746076184712E-002  
2.343848437473522E-002  
2.750770044120694E-002  
3.117517606565595E-002  
3.465216345500333E-002  
3.507234575133015E-002  
3.965969447371862E-002  
4.402446298672098E-002  
4.835264820132004E-002  
5.261396877999554E-002  
5.677747503316505E-002  
6.088229844716924E-002  
6.497551875164372E-002  
6.906997202796113E-002  
7.123012840642685E-002  
7.574303048126209E-002  
8.016962333672198E-002  
8.454638113389007E-002  
8.891965941844954E-002  
9.328723266437623E-002  
9.771461162930026E-002  
0.102076625740984  
0.106424929432713  
0.110707405661653  
0.115030361214868  
0.119357406246238  
0.123671359392945  
0.127987710736448  
0.132255785562777  
0.136566259462535  
0.140883276001475  
0.145259772887259  
0.149595363999529  
0.153935104310575  
0.158277158193428  
0.162622762603217  
0.166969205911870  
0.171316678378569  
0.175670326588737  
0.179981334427542  
0.184000160933673  
0.152277902335646  
0.162754510403297  
0.170882558993183  
0.177977023535912  
0.183457059816014  
0.187852218237966  
0.191979439099481  
0.195808698278724  
0.199040445179729  
0.199769454865642  
0.204195875931989  
0.208199773296550  
0.212149712781701  
0.216047925576607

## ROT\_Z

ROT\_Z - Notepad

File Edit Format View Help

6.440896968388597E-004  
1.578599022215223E-003  
2.343978710228557E-003  
3.054257752236703E-003  
3.716582273811857E-003  
4.335040023802476E-003  
4.686985222349597E-003  
5.276635414337285E-003  
5.876572615792627E-003  
6.478951396467797E-003  
7.077916441224118E-003  
7.670768764672552E-003  
8.255695232728580E-003  
8.834278181304490E-003  
9.408448409411827E-003  
9.763250968144101E-003  
1.034388449189690E-002  
1.093501018577020E-002  
1.153116932107992E-002  
1.212990080917528E-002  
1.272955023949256E-002  
1.332949114321517E-002  
1.392921852520180E-002  
1.452821746456425E-002  
1.512650274612290E-002  
1.572343189958957E-002  
1.631951542883192E-002  
1.691452646761788E-002  
1.750875390073846E-002  
1.810260274153054E-002  
1.869604706784478E-002  
1.928937202306326E-002  
1.988338019518126E-002  
2.047800421574057E-002  
2.107329878601371E-002  
2.166914003147511E-002  
2.226545828475297E-002  
2.286202343364902E-002  
2.345874979736177E-002  
2.405581705768581E-002  
2.465306458236774E-002  
2.528177156295101E-002  
2.664833960173943E-002  
2.754906943941359E-002  
2.847029829633195E-002  
2.939127868871120E-002  
3.010797935444333E-002  
3.079431801019134E-002  
3.145906998634029E-002  
3.209374979635106E-002  
3.267905539797734E-002  
3.286993654740209E-002  
3.344417269512690E-002  
3.404347211767455E-002  
3.464858846561663E-002  
3.525107843537614E-002

# STATIC\_DISPLACEMENTS

STATIC_DISPLACEMENTS - Notepad					STATIC_DISPLACEMENTS - Notepad				
File	Edit	Format	View	Help	File	Edit	Format	View	Help
NODAL DISPLACEMENTS	STEP	1			NODAL DISPLACEMENTS	STEP	3		
NODE	X	Y	rZ		NODE	X	Y	rZ	
1	0.00E+00	0.00E+00	-0.11E-02		1	0.00E+00	0.00E+00	-0.31E-02	
2	0.19E-05	-0.11E+00	-0.11E-02		2	0.14E-05	-0.31E+00	-0.31E-02	
3	0.75E-05	-0.23E+00	-0.11E-02		3	0.58E-05	-0.63E+00	-0.31E-02	
4	0.17E-04	-0.34E+00	-0.11E-02		4	0.13E-04	-0.94E+00	-0.31E-02	
5	0.30E-04	-0.45E+00	-0.11E-02		5	0.23E-04	-0.13E+01	-0.31E-02	
6	0.47E-04	-0.55E+00	-0.10E-02		6	0.36E-04	-0.16E+01	-0.30E-02	
7	0.81E-04	-0.66E+00	-0.98E-03		7	0.64E-04	-0.19E+01	-0.30E-02	
8	0.27E-03	-0.75E+00	-0.92E-03		8	0.23E-03	-0.22E+01	-0.30E-02	
9	0.97E-03	-0.84E+00	-0.85E-03		9	0.14E-02	-0.25E+01	-0.29E-02	
10	0.26E-02	-0.93E+00	-0.76E-03		10	0.13E-01	-0.27E+01	-0.27E-02	
11	0.54E-02	-0.10E+01	-0.64E-03		11	0.45E-01	-0.30E+01	-0.23E-02	
12	0.90E-02	-0.11E+01	-0.52E-03		12	0.88E-01	-0.32E+01	-0.19E-02	
13	0.13E-01	-0.11E+01	-0.39E-03		13	0.13E+00	-0.34E+01	-0.14E-02	
14	0.16E-01	-0.11E+01	-0.26E-03		14	0.17E+00	-0.35E+01	-0.94E-03	
15	0.20E-01	-0.12E+01	-0.13E-03		15	0.22E+00	-0.36E+01	-0.47E-03	
16	0.23E-01	-0.12E+01	0.26E-17		16	0.26E+00	-0.36E+01	0.10E-16	
17	0.27E-01	-0.12E+01	0.13E-03		17	0.30E+00	-0.36E+01	0.47E-03	
18	0.30E-01	-0.11E+01	0.26E-03		18	0.35E+00	-0.35E+01	0.94E-03	
19	0.34E-01	-0.11E+01	0.39E-03		19	0.39E+00	-0.34E+01	0.14E-02	
20	0.38E-01	-0.11E+01	0.52E-03		20	0.43E+00	-0.32E+01	0.19E-02	
21	0.41E-01	-0.10E+01	0.64E-03		21	0.48E+00	-0.30E+01	0.23E-02	
22	0.44E-01	-0.93E+00	0.76E-03		22	0.51E+00	-0.27E+01	0.27E-02	
23	0.46E-01	-0.84E+00	0.85E-03		23	0.52E+00	-0.25E+01	0.29E-02	
24	0.46E-01	-0.75E+00	0.92E-03		24	0.52E+00	-0.22E+01	0.30E-02	
25	0.46E-01	-0.66E+00	0.98E-03		25	0.52E+00	-0.19E+01	0.30E-02	
26	0.47E-01	-0.55E+00	0.10E-02		26	0.52E+00	-0.16E+01	0.30E-02	
27	0.47E-01	-0.45E+00	0.11E-02		27	0.52E+00	-0.13E+01	0.31E-02	
28	0.47E-01	-0.34E+00	0.11E-02		28	0.52E+00	-0.94E+00	0.31E-02	
29	0.47E-01	-0.23E+00	0.11E-02		29	0.52E+00	-0.63E+00	0.31E-02	
30	0.47E-01	-0.11E+00	0.11E-02		30	0.52E+00	-0.31E+00	0.31E-02	
31	0.47E-01	0.00E+00	0.11E-02		31	0.52E+00	0.00E+00	0.31E-02	

NODAL DISPLACEMENTS	STEP	2			NODAL DISPLACEMENTS	STEP	4		
NODE	X	Y	rZ		NODE	X	Y	rZ	
1	0.00E+00	0.00E+00	-0.21E-02		1	0.00E+00	0.00E+00	-0.42E-02	
2	0.12E-05	-0.21E+00	-0.21E-02		2	0.17E-05	-0.42E+00	-0.42E-02	
3	0.49E-05	-0.42E+00	-0.21E-02		3	0.68E-05	-0.84E+00	-0.42E-02	
4	0.11E-04	-0.63E+00	-0.21E-02		4	0.15E-04	-0.13E+01	-0.41E-02	
5	0.20E-04	-0.84E+00	-0.21E-02		5	0.27E-04	-0.17E+01	-0.41E-02	
6	0.31E-04	-0.10E+01	-0.20E-02		6	0.42E-04	-0.21E+01	-0.41E-02	
7	0.57E-04	-0.12E+01	-0.20E-02		7	0.94E-04	-0.25E+01	-0.40E-02	
8	0.22E-03	-0.14E+01	-0.20E-02		8	0.62E-03	-0.29E+01	-0.40E-02	
9	0.86E-03	-0.16E+01	-0.19E-02		9	0.49E-02	-0.33E+01	-0.39E-02	
10	0.45E-02	-0.18E+01	-0.18E-02		10	0.28E-01	-0.37E+01	-0.36E-02	
11	0.22E-01	-0.20E+01	-0.16E-02		11	0.76E-01	-0.40E+01	-0.31E-02	
12	0.48E-01	-0.21E+01	-0.13E-02		12	0.13E+00	-0.43E+01	-0.24E-02	
13	0.74E-01	-0.23E+01	-0.95E-03		13	0.19E+00	-0.45E+01	-0.18E-02	
14	0.10E+00	-0.23E+01	-0.63E-03		14	0.25E+00	-0.46E+01	-0.12E-02	
15	0.13E+00	-0.24E+01	-0.32E-03		15	0.31E+00	-0.47E+01	-0.61E-03	
16	0.15E+00	-0.24E+01	0.71E-17		16	0.37E+00	-0.48E+01	0.12E-16	
17	0.18E+00	-0.24E+01	0.32E-03		17	0.43E+00	-0.47E+01	0.61E-03	
18	0.20E+00	-0.23E+01	0.63E-03		18	0.48E+00	-0.46E+01	0.12E-02	
19	0.23E+00	-0.23E+01	0.95E-03		19	0.54E+00	-0.45E+01	0.18E-02	
20	0.26E+00	-0.21E+01	0.13E-02		20	0.60E+00	-0.43E+01	0.24E-02	
21	0.28E+00	-0.20E+01	0.16E-02		21	0.66E+00	-0.40E+01	0.31E-02	
22	0.30E+00	-0.18E+01	0.18E-02		22	0.71E+00	-0.37E+01	0.36E-02	
23	0.30E+00	-0.16E+01	0.19E-02		23	0.73E+00	-0.33E+01	0.39E-02	
24	0.30E+00	-0.14E+01	0.20E-02		24	0.74E+00	-0.29E+01	0.40E-02	
25	0.30E+00	-0.12E+01	0.20E-02		25	0.74E+00	-0.25E+01	0.40E-02	
26	0.30E+00	-0.10E+01	0.20E-02		26	0.74E+00	-0.21E+01	0.41E-02	
27	0.30E+00	-0.84E+00	0.21E-02		27	0.74E+00	-0.17E+01	0.41E-02	
28	0.30E+00	-0.63E+00	0.21E-02		28	0.74E+00	-0.13E+01	0.41E-02	
29	0.30E+00	-0.42E+00	0.21E-02		29	0.74E+00	-0.84E+00	0.42E-02	
30	0.30E+00	-0.21E+00	0.21E-02		30	0.74E+00	-0.42E+00	0.42E-02	
31	0.30E+00	0.00E+00	0.21E-02		31	0.74E+00	0.00E+00	0.42E-02	

NODAL DISPLACEMENTS	STEP	3			NODAL DISPLACEMENTS	STEP	5		
NODE	X	Y	rZ		NODE	X	Y	rZ	
1	0.00E+00	0.00E+00	-0.21E-02		1	0.00E+00	0.00E+00	-0.42E-02	
2	0.12E-05	-0.21E+00	-0.21E-02		2	0.17E-05	-0.42E+00	-0.42E-02	
3	0.49E-05	-0.42E+00	-0.21E-02		3	0.68E-05	-0.84E+00	-0.42E-02	
4	0.11E-04	-0.63E+00	-0.21E-02		4	0.15E-04	-0.13E+01	-0.41E-02	
5	0.20E-04	-0.84E+00	-0.21E-02		5	0.27E-04	-0.17E+01	-0.41E-02	
6	0.31E-04	-0.10E+01	-0.20E-02		6	0.42E-04	-0.21E+01	-0.41E-02	
7	0.57E-04	-0.12E+01	-0.20E-02		7	0.94E-04	-0.25E+01	-0.40E-02	
8	0.22E-03	-0.14E+01	-0.20E-02		8	0.62E-03	-0.29E+01	-0.40E-02	
9	0.86E-03	-0.16E+01	-0.19E-02		9	0.49E-02	-0.33E+01	-0.39E-02	
10	0.45E-02	-0.18E+01	-0.18E-02		10	0.28E-01	-0.37E+01	-0.36E-02	
11	0.22E-01	-0.20E+01	-0.16E-02		11	0.76E-01	-0.40E+01	-0.31E-02	
12	0.48E-01	-0.21E+01	-0.13E-02		12	0.13E+00	-0.43E+01	-0.24E-02	
13	0.74E-01	-0.23E+01	-0.95E-03		13	0.19E+00	-0.45E+01	-0.18E-02	
14	0.10E+00	-0.23E+01	-0.63E-03		14	0.25E+00	-0.46E+01	-0.12E-02	
15	0.13E+00	-0.24E+01	-0.32E-03		15	0.31E+00	-0.47E+01	-0.61E-03	
16	0.15E+00	-0.24E+01	0.71E-17		16	0.37E+00	-0.48E+01	0.12E-16	
17	0.18E+00	-0.24E+01	0.32E-03		17	0.43E+00	-0.47E+01	0.61E-03	
18	0.20E+00	-0.23E+01	0.63E-03		18	0.48E+00	-0.46E+01	0.12E-02	
19	0.23E+00	-0.23E+01	0.95E-03		19	0.54E+00	-0.45E+01	0.18E-02	
20	0.26E+00	-0.21E+01	0.13E-02		20	0.60E+00	-0.43E+01	0.24E-02	
21	0.28E+00	-0.20E+01	0.16E-02		21	0.66E+00	-0.40E+01	0.31E-02	
22	0.30E+00	-0.18E+01	0.18E-02		22	0.71E+00	-0.37E+01	0.36E-02	
23	0.30E+00	-0.16E+01	0.19E-02		23	0.73E+00	-0.33E+01	0.39E-02	
24	0.30E+00	-0.14E+01	0.20E-02		24	0.74E+00	-0.29E+01	0.40E-02	
25	0.30E+00	-0.12E+01	0.20E-02		25	0.74E+00	-0.25E+01	0.40E-02	
26	0.30E+00	-0.10E+01	0.20E-02		26	0.74E+00	-0.21E+01	0.41E-02	
27	0.30E+00	-0.84E+00	0.21E-02		27	0.74E+00	-0.17E+01	0.41E-02	
28	0.30E+00	-0.63E+00	0.21E-02		28	0.74E+00	-0.13E+01	0.41E-02	
29	0.30E+00	-0.42E+00	0.21E-02		29	0.74E+00	-0.84E+00	0.42E-02	
30	0.30E+00	-0.21E+00	0.21E-02		30	0.74E+00	-0.42E+00	0.42E-02	
31	0.30E+00	0.00E+00	0.21E-02		31	0.74E+00	0.00E+00	0.42E-02	

STATIC\_DISPLACEMENTS - Notepad

File	Edit	Format	View	Help
NODAL DISPLACEMENTS				STEP
NODE	X	Y	rZ	5
1	0.00E+00	0.00E+00	-0.52E-02	
2	0.19E-05	-0.53E+00	-0.52E-02	
3	0.77E-05	-0.11E+01	-0.52E-02	
4	0.17E-04	-0.16E+01	-0.52E-02	
5	0.31E-04	-0.21E+01	-0.52E-02	
6	0.48E-04	-0.26E+01	-0.51E-02	
7	0.25E-03	-0.31E+01	-0.51E-02	
8	0.20E-02	-0.36E+01	-0.50E-02	
9	0.13E-01	-0.41E+01	-0.48E-02	
10	0.51E-01	-0.46E+01	-0.44E-02	
11	0.11E+00	-0.50E+01	-0.37E-02	
12	0.19E+00	-0.53E+01	-0.30E-02	
13	0.26E+00	-0.56E+01	-0.22E-02	
14	0.33E+00	-0.58E+01	-0.15E-02	
15	0.41E+00	-0.59E+01	-0.74E-03	
16	0.48E+00	-0.59E+01	0.12E-16	
17	0.56E+00	-0.59E+01	0.74E-03	
18	0.63E+00	-0.58E+01	0.15E-02	
19	0.70E+00	-0.56E+01	0.22E-02	
20	0.78E+00	-0.53E+01	0.30E-02	
21	0.85E+00	-0.50E+01	0.37E-02	
22	0.91E+00	-0.46E+01	0.44E-02	
23	0.95E+00	-0.41E+01	0.48E-02	
24	0.96E+00	-0.36E+01	0.50E-02	
25	0.96E+00	-0.31E+01	0.51E-02	
26	0.96E+00	-0.26E+01	0.51E-02	
27	0.96E+00	-0.21E+01	0.52E-02	
28	0.96E+00	-0.16E+01	0.52E-02	
29	0.96E+00	-0.11E+01	0.52E-02	
30	0.96E+00	-0.53E+00	0.52E-02	
31	0.96E+00	0.00E+00	0.52E-02	

NODAL DISPLACEMENTS				STEP
NODE	X	Y	rZ	6
1	0.00E+00	0.00E+00	-0.63E-02	
2	0.21E-05	-0.64E+00	-0.63E-02	
3	0.85E-05	-0.13E+01	-0.63E-02	
4	0.19E-04	-0.19E+01	-0.63E-02	
5	0.34E-04	-0.25E+01	-0.63E-02	
6	0.83E-04	-0.32E+01	-0.62E-02	
7	0.67E-03	-0.38E+01	-0.62E-02	
8	0.56E-02	-0.44E+01	-0.60E-02	
9	0.30E-01	-0.50E+01	-0.57E-02	
10	0.84E-01	-0.55E+01	-0.51E-02	
11	0.16E+00	-0.60E+01	-0.43E-02	
12	0.25E+00	-0.64E+01	-0.35E-02	
13	0.34E+00	-0.67E+01	-0.26E-02	
14	0.43E+00	-0.69E+01	-0.17E-02	
15	0.51E+00	-0.70E+01	-0.87E-03	
16	0.60E+00	-0.71E+01	0.13E-16	
17	0.69E+00	-0.70E+01	0.87E-03	
18	0.78E+00	-0.69E+01	0.17E-02	
19	0.87E+00	-0.67E+01	0.26E-02	
20	0.96E+00	-0.64E+01	0.35E-02	
21	0.10E+01	-0.60E+01	0.43E-02	
22	0.11E+01	-0.55E+01	0.51E-02	
23	0.12E+01	-0.50E+01	0.57E-02	
24	0.12E+01	-0.44E+01	0.60E-02	
25	0.12E+01	-0.38E+01	0.62E-02	
26	0.12E+01	-0.32E+01	0.62E-02	
27	0.12E+01	-0.25E+01	0.63E-02	
28	0.12E+01	-0.19E+01	0.63E-02	
29	0.12E+01	-0.13E+01	0.63E-02	
30	0.12E+01	-0.64E+00	0.63E-02	
31	0.12E+01	0.00E+00	0.63E-02	

NODAL DISPLACEMENTS STEP 7

STATIC\_DISPLACEMENTS - Notepad

File	Edit	Format	View	Help
NODAL DISPLACEMENTS				STEP
NODE	X	Y	rZ	7
1	0.00E+00	0.00E+00	-0.75E-02	
2	0.22E-05	-0.76E+00	-0.75E-02	
3	0.86E-05	-0.15E+01	-0.75E-02	
4	0.19E-04	-0.23E+01	-0.75E-02	
5	0.34E-04	-0.30E+01	-0.75E-02	
6	0.14E-03	-0.38E+01	-0.74E-02	
7	0.23E-02	-0.45E+01	-0.73E-02	
8	0.37E-01	-0.52E+01	-0.69E-02	
9	0.99E-01	-0.59E+01	-0.63E-02	
10	0.18E+00	-0.65E+01	-0.56E-02	
11	0.27E+00	-0.70E+01	-0.47E-02	
12	0.37E+00	-0.74E+01	-0.37E-02	
13	0.47E+00	-0.77E+01	-0.28E-02	
14	0.57E+00	-0.80E+01	-0.19E-02	
15	0.67E+00	-0.81E+01	-0.94E-03	
16	0.76E+00	-0.82E+01	0.74E-17	
17	0.86E+00	-0.81E+01	0.94E-03	
18	0.96E+00	-0.80E+01	0.19E-02	
19	0.11E+01	-0.77E+01	0.28E-02	
20	0.12E+01	-0.74E+01	0.37E-02	
21	0.13E+01	-0.70E+01	0.47E-02	
22	0.14E+01	-0.65E+01	0.56E-02	
23	0.14E+01	-0.59E+01	0.63E-02	
24	0.15E+01	-0.52E+01	0.69E-02	
25	0.15E+01	-0.45E+01	0.73E-02	
26	0.15E+01	-0.38E+01	0.74E-02	
27	0.15E+01	-0.30E+01	0.75E-02	
28	0.15E+01	-0.23E+01	0.75E-02	
29	0.15E+01	-0.15E+01	0.75E-02	
30	0.15E+01	-0.76E+00	0.75E-02	
31	0.15E+01	0.00E+00	0.75E-02	

NODAL DISPLACEMENTS				STEP
NODE	X	Y	rZ	8
1	0.00E+00	0.00E+00	-0.87E-02	
2	0.24E-05	-0.87E+00	-0.87E-02	
3	0.97E-05	-0.17E+01	-0.86E-02	
4	0.22E-04	-0.26E+01	-0.86E-02	
5	0.39E-04	-0.35E+01	-0.86E-02	
6	0.32E-03	-0.43E+01	-0.85E-02	
7	0.56E-02	-0.52E+01	-0.84E-02	
8	0.54E-01	-0.60E+01	-0.79E-02	
9	0.13E+00	-0.67E+01	-0.71E-02	
10	0.22E+00	-0.74E+01	-0.63E-02	
11	0.33E+00	-0.80E+01	-0.53E-02	
12	0.44E+00	-0.85E+01	-0.42E-02	
13	0.55E+00	-0.88E+01	-0.32E-02	
14	0.66E+00	-0.91E+01	-0.21E-02	
15	0.77E+00	-0.93E+01	-0.11E-02	
16	0.88E+00	-0.93E+01	0.12E-16	
17	0.10E+01	-0.93E+01	0.11E-02	
18	0.11E+01	-0.91E+01	0.21E-02	
19	0.12E+01	-0.88E+01	0.32E-02	
20	0.13E+01	-0.85E+01	0.42E-02	
21	0.14E+01	-0.80E+01	0.53E-02	
22	0.15E+01	-0.74E+01	0.63E-02	
23	0.16E+01	-0.67E+01	0.71E-02	
24	0.17E+01	-0.60E+01	0.79E-02	
25	0.18E+01	-0.52E+01	0.84E-02	
26	0.18E+01	-0.43E+01	0.85E-02	
27	0.18E+01	-0.35E+01	0.86E-02	
28	0.18E+01	-0.26E+01	0.86E-02	
29	0.18E+01	-0.17E+01	0.86E-02	
30	0.18E+01	-0.87E+00	0.87E-02	
31	0.18E+01	0.00E+00	0.87E-02	

STATIC\_DISPLACEMENTS - Notepad

File Edit Format View Help

NODAL DISPLACEMENTS STEP 9			
NODE	X	Y	rZ
1	0.00E+00	0.00E+00	-0.98E-02
2	0.27E-05	-0.98E+00	-0.98E-02
3	0.11E-04	-0.20E+01	-0.98E-02
4	0.24E-04	-0.29E+01	-0.97E-02
5	0.65E-04	-0.39E+01	-0.97E-02
6	0.72E-03	-0.49E+01	-0.96E-02
7	0.11E-01	-0.58E+01	-0.94E-02
8	0.72E-01	-0.68E+01	-0.88E-02
9	0.16E+00	-0.76E+01	-0.80E-02
10	0.26E+00	-0.84E+01	-0.70E-02
11	0.38E+00	-0.90E+01	-0.59E-02
12	0.51E+00	-0.95E+01	-0.47E-02
13	0.63E+00	-0.99E+01	-0.35E-02
14	0.76E+00	-0.10E+02	-0.24E-02
15	0.88E+00	-0.10E+02	-0.12E-02
16	0.10E+01	-0.10E+02	0.15E-16
17	0.11E+01	-0.10E+02	0.12E-02
18	0.13E+01	-0.10E+02	0.24E-02
19	0.14E+01	-0.99E+01	0.35E-02
20	0.15E+01	-0.95E+01	0.47E-02
21	0.16E+01	-0.90E+01	0.59E-02
22	0.17E+01	-0.84E+01	0.70E-02
23	0.19E+01	-0.76E+01	0.80E-02
24	0.19E+01	-0.68E+01	0.88E-02
25	0.20E+01	-0.58E+01	0.94E-02
26	0.20E+01	-0.49E+01	0.96E-02
27	0.20E+01	-0.39E+01	0.97E-02
28	0.20E+01	-0.29E+01	0.97E-02
29	0.20E+01	-0.20E+01	0.98E-02
30	0.20E+01	-0.98E+00	0.98E-02
31	0.20E+01	0.00E+00	0.98E-02

NODAL DISPLACEMENTS STEP 10			
NODE	X	Y	rZ
1	0.00E+00	0.00E+00	-0.11E-01
2	0.30E-05	-0.11E+01	-0.11E-01
3	0.12E-04	-0.22E+01	-0.11E-01
4	0.27E-04	-0.33E+01	-0.11E-01
5	0.12E-03	-0.44E+01	-0.11E-01
6	0.16E-02	-0.55E+01	-0.11E-01
7	0.20E-01	-0.65E+01	-0.10E-01
8	0.92E-01	-0.75E+01	-0.97E-02
9	0.19E+00	-0.85E+01	-0.88E-02
10	0.30E+00	-0.93E+01	-0.77E-02
11	0.44E+00	-0.10E+02	-0.65E-02
12	0.57E+00	-0.11E+02	-0.52E-02
13	0.71E+00	-0.11E+02	-0.39E-02
14	0.85E+00	-0.11E+02	-0.26E-02
15	0.99E+00	-0.12E+02	-0.13E-02
16	0.11E+01	-0.12E+02	0.19E-16
17	0.13E+01	-0.12E+02	0.13E-02
18	0.14E+01	-0.11E+02	0.26E-02
19	0.15E+01	-0.11E+02	0.39E-02
20	0.17E+01	-0.11E+02	0.52E-02
21	0.18E+01	-0.10E+02	0.65E-02
22	0.19E+01	-0.93E+01	0.77E-02
23	0.21E+01	-0.85E+01	0.88E-02
24	0.22E+01	-0.75E+01	0.97E-02
25	0.22E+01	-0.65E+01	0.10E-01
26	0.23E+01	-0.55E+01	0.11E-01
27	0.23E+01	-0.44E+01	0.11E-01
28	0.23E+01	-0.33E+01	0.11E-01
29	0.23E+01	-0.22E+01	0.11E-01
30	0.23E+01	-0.11E+01	0.11E-01
31	0.23E+01	0.00E+00	0.11E-01

NODAL DISPLACEMENTS STEP 13

STATIC\_DISPLACEMENTS - Notepad

File Edit Format View Help

NODAL DISPLACEMENTS STEP 11			
NODE	X	Y	rZ
1	0.00E+00	0.00E+00	-0.12E-01
2	0.32E-05	-0.12E+01	-0.12E-01
3	0.13E-04	-0.24E+01	-0.12E-01
4	0.29E-04	-0.36E+01	-0.12E-01
5	0.23E-03	-0.48E+01	-0.12E-01
6	0.34E-02	-0.60E+01	-0.12E-01
7	0.32E-01	-0.72E+01	-0.11E-01
8	0.11E+00	-0.83E+01	-0.11E-01
9	0.22E+00	-0.93E+01	-0.96E-02
10	0.35E+00	-0.10E+02	-0.84E-02
11	0.49E+00	-0.11E+02	-0.71E-02
12	0.64E+00	-0.12E+02	-0.57E-02
13	0.80E+00	-0.12E+02	-0.42E-02
14	0.95E+00	-0.12E+02	-0.28E-02
15	0.11E+01	-0.13E+02	-0.14E-02
16	0.13E+01	-0.13E+02	0.18E-16
17	0.14E+01	-0.13E+02	0.14E-02
18	0.16E+01	-0.12E+02	0.28E-02
19	0.17E+01	-0.12E+02	0.42E-02
20	0.19E+01	-0.12E+02	0.57E-02
21	0.20E+01	-0.11E+02	0.71E-02
22	0.22E+01	-0.10E+02	0.84E-02
23	0.23E+01	-0.93E+01	0.96E-02
24	0.24E+01	-0.83E+01	0.11E-01
25	0.25E+01	-0.72E+01	0.11E-01
26	0.25E+01	-0.60E+01	0.12E-01
27	0.25E+01	-0.48E+01	0.12E-01
28	0.25E+01	-0.36E+01	0.12E-01
29	0.25E+01	-0.24E+01	0.12E-01
30	0.25E+01	-0.12E+01	0.12E-01
31	0.25E+01	0.00E+00	0.12E-01

NODAL DISPLACEMENTS STEP 12			
NODE	X	Y	rZ
1	0.00E+00	0.00E+00	-0.13E-01
2	0.35E-05	-0.13E+01	-0.13E-01
3	0.14E-04	-0.26E+01	-0.13E-01
4	0.38E-04	-0.40E+01	-0.13E-01
5	0.45E-03	-0.53E+01	-0.13E-01
6	0.69E-02	-0.66E+01	-0.13E-01
7	0.47E-01	-0.79E+01	-0.12E-01
8	0.14E+00	-0.91E+01	-0.12E-01
9	0.26E+00	-0.10E+02	-0.10E-01
10	0.40E+00	-0.11E+02	-0.91E-02
11	0.55E+00	-0.12E+02	-0.77E-02
12	0.72E+00	-0.13E+02	-0.61E-02
13	0.88E+00	-0.13E+02	-0.46E-02
14	0.10E+01	-0.14E+02	-0.31E-02
15	0.12E+01	-0.14E+02	-0.15E-02
16	0.14E+01	-0.14E+02	0.18E-16
17	0.15E+01	-0.14E+02	0.15E-02
18	0.17E+01	-0.14E+02	0.31E-02
19	0.19E+01	-0.13E+02	0.46E-02
20	0.20E+01	-0.13E+02	0.61E-02
21	0.22E+01	-0.12E+02	0.77E-02
22	0.24E+01	-0.11E+02	0.91E-02
23	0.25E+01	-0.10E+02	0.10E-01
24	0.26E+01	-0.91E+01	0.12E-01
25	0.27E+01	-0.79E+01	0.12E-01
26	0.27E+01	-0.66E+01	0.13E-01
27	0.28E+01	-0.53E+01	0.13E-01
28	0.28E+01	-0.40E+01	0.13E-01
29	0.28E+01	-0.26E+01	0.13E-01
30	0.28E+01	-0.13E+01	0.13E-01
31	0.28E+01	0.00E+00	0.13E-01

NODAL DISPLACEMENTS STEP 13

STATIC\_DISPLACEMENTS - Notepad

File Edit Format View Help

NODAL DISPLACEMENTS STEP 13			
NODE	X	Y	rZ
1	0.00E+00	0.00E+00	-0.14E-01
2	0.37E-05	-0.14E+01	-0.14E-01
3	0.15E-04	-0.29E+01	-0.14E-01
4	0.58E-04	-0.43E+01	-0.14E-01
5	0.86E-03	-0.58E+01	-0.14E-01
6	0.13E-01	-0.72E+01	-0.14E-01
7	0.66E-01	-0.85E+01	-0.13E-01
8	0.17E+00	-0.98E+01	-0.12E-01
9	0.30E+00	-0.11E+02	-0.11E-01
10	0.45E+00	-0.12E+02	-0.98E-02
11	0.62E+00	-0.13E+02	-0.83E-02
12	0.79E+00	-0.14E+02	-0.66E-02
13	0.97E+00	-0.14E+02	-0.50E-02
14	0.11E+01	-0.15E+02	-0.33E-02
15	0.13E+01	-0.15E+02	-0.17E-02
16	0.15E+01	-0.15E+02	0.17E-16
17	0.17E+01	-0.15E+02	0.17E-02
18	0.19E+01	-0.15E+02	0.33E-02
19	0.20E+01	-0.14E+02	0.50E-02
20	0.22E+01	-0.14E+02	0.66E-02
21	0.24E+01	-0.13E+02	0.83E-02
22	0.26E+01	-0.12E+02	0.98E-02
23	0.27E+01	-0.11E+02	0.11E-01
24	0.28E+01	-0.98E+01	0.12E-01
25	0.29E+01	-0.85E+01	0.13E-01
26	0.30E+01	-0.72E+01	0.14E-01
27	0.30E+01	-0.58E+01	0.14E-01
28	0.30E+01	-0.43E+01	0.14E-01
29	0.30E+01	-0.29E+01	0.14E-01
30	0.30E+01	-0.14E+01	0.14E-01
31	0.30E+01	0.00E+00	0.14E-01

NODAL DISPLACEMENTS STEP 14			
NODE	X	Y	rZ
1	0.00E+00	0.00E+00	-0.16E-01
2	0.40E-05	-0.16E+01	-0.16E-01
3	0.16E-04	-0.31E+01	-0.16E-01
4	0.80E-04	-0.47E+01	-0.15E-01
5	0.16E-02	-0.62E+01	-0.15E-01
6	0.22E-01	-0.78E+01	-0.15E-01
7	0.89E-01	-0.92E+01	-0.14E-01
8	0.20E+00	-0.11E+02	-0.13E-01
9	0.34E+00	-0.12E+02	-0.12E-01
10	0.50E+00	-0.13E+02	-0.11E-01
11	0.68E+00	-0.14E+02	-0.88E-02
12	0.87E+00	-0.15E+02	-0.71E-02
13	0.11E+01	-0.15E+02	-0.53E-02
14	0.13E+01	-0.16E+02	-0.35E-02
15	0.14E+01	-0.16E+02	-0.18E-02
16	0.16E+01	-0.16E+02	0.16E-16
17	0.18E+01	-0.16E+02	0.18E-02
18	0.20E+01	-0.16E+02	0.35E-02
19	0.22E+01	-0.15E+02	0.53E-02
20	0.24E+01	-0.15E+02	0.71E-02
21	0.26E+01	-0.14E+02	0.88E-02
22	0.28E+01	-0.13E+02	0.11E-01
23	0.29E+01	-0.12E+02	0.12E-01
24	0.31E+01	-0.11E+02	0.13E-01
25	0.32E+01	-0.92E+01	0.14E-01
26	0.32E+01	-0.78E+01	0.15E-01
27	0.33E+01	-0.62E+01	0.15E-01
28	0.33E+01	-0.47E+01	0.15E-01
29	0.33E+01	-0.31E+01	0.16E-01
30	0.33E+01	-0.16E+01	0.16E-01
31	0.33E+01	0.00E+00	0.16E-01

NODAL DISPLACEMENTS STEP 15			
NODE	X	Y	rZ
1	0.00E+00	0.00E+00	-0.17E-01
2	0.42E-05	-0.17E+01	-0.17E-01
3	0.17E-04	-0.34E+01	-0.17E-01
4	0.14E-03	-0.50E+01	-0.17E-01
5	0.30E-02	-0.67E+01	-0.17E-01
6	0.35E-01	-0.83E+01	-0.16E-01
7	0.11E+00	-0.99E+01	-0.15E-01
8	0.23E+00	-0.11E+02	-0.14E-01
9	0.38E+00	-0.13E+02	-0.13E-01
10	0.55E+00	-0.14E+02	-0.11E-01
11	0.75E+00	-0.15E+02	-0.94E-02
12	0.95E+00	-0.16E+02	-0.75E-02
13	0.12E+01	-0.17E+02	-0.56E-02
14	0.14E+01	-0.17E+02	-0.38E-02
15	0.16E+01	-0.17E+02	-0.19E-02
16	0.18E+01	-0.17E+02	0.15E-16
17	0.20E+01	-0.17E+02	0.19E-02
18	0.22E+01	-0.17E+02	0.38E-02
19	0.24E+01	-0.17E+02	0.56E-02
20	0.26E+01	-0.16E+02	0.75E-02
21	0.28E+01	-0.15E+02	0.94E-02
22	0.30E+01	-0.14E+02	0.11E-01
23	0.31E+01	-0.13E+02	0.13E-01
24	0.33E+01	-0.11E+02	0.14E-01
25	0.34E+01	-0.99E+01	0.15E-01
26	0.35E+01	-0.83E+01	0.16E-01

NODAL DISPLACEMENTS STEP 16			
NODE	X	Y	rZ
1	0.00E+00	0.00E+00	-0.18E-01
2	0.44E-05	-0.18E+01	-0.18E-01
3	0.17E-04	-0.37E+01	-0.18E-01
4	0.24E-03	-0.55E+01	-0.18E-01
5	0.40E-01	-0.73E+01	-0.18E-01
6	0.13E+00	-0.91E+01	-0.17E-01
7	0.24E+00	-0.11E+02	-0.16E-01
8	0.37E+00	-0.12E+02	-0.15E-01
9	0.53E+00	-0.14E+02	-0.13E-01
10	0.71E+00	-0.15E+02	-0.12E-01
11	0.91E+00	-0.16E+02	-0.98E-02
12	0.11E+01	-0.17E+02	-0.78E-02
13	0.13E+01	-0.18E+02	-0.59E-02
14	0.15E+01	-0.18E+02	-0.39E-02
15	0.18E+01	-0.18E+02	-0.20E-02
16	0.20E+01	-0.18E+02	0.18E-13
17	0.22E+01	-0.18E+02	0.20E-02
18	0.24E+01	-0.18E+02	0.39E-02
19	0.26E+01	-0.18E+02	0.59E-02
20	0.28E+01	-0.17E+02	0.78E-02
21	0.30E+01	-0.16E+02	0.98E-02
22	0.32E+01	-0.15E+02	0.12E-01
23	0.34E+01	-0.14E+02	0.13E-01
24	0.36E+01	-0.12E+02	0.15E-01
25	0.37E+01	-0.11E+02	0.16E-01
26	0.38E+01	-0.91E+01	0.17E-01
27	0.39E+01	-0.73E+01	0.18E-01
28	0.39E+01	-0.55E+01	0.18E-01
29	0.39E+01	-0.37E+01	0.18E-01
30	0.39E+01	-0.18E+01	0.18E-01
31	0.39E+01	0.00E+00	0.18E-01

NODAL DISPLACEMENTS STEP 19			
NODE	X	Y	rZ
1	0.00E+00	0.00E+00	-0.22E-01
2	0.52E-05	-0.22E+01	-0.22E-01
3	0.21E-04	-0.44E+01	-0.22E-01
4	0.81E-03	-0.66E+01	-0.22E-01
5	0.67E-01	-0.87E+01	-0.21E-01
6	0.18E+00	-0.11E+02	-0.20E-01
7	0.31E+00	-0.13E+02	-0.19E-01
8	0.47E+00	-0.15E+02	-0.17E-01
9	0.65E+00	-0.16E+02	-0.16E-01
10	0.87E+00	-0.18E+02	-0.14E-01
11	0.11E+01	-0.19E+02	-0.12E-01
12	0.14E+01	-0.20E+02	-0.92E-02
13	0.16E+01	-0.21E+02	-0.69E-02
14	0.19E+01	-0.21E+02	-0.46E-02
15	0.21E+01	-0.22E+02	-0.23E-02
16	0.24E+01	-0.22E+02	-0.33E-14
17	0.26E+01	-0.22E+02	0.23E-02
18	0.29E+01	-0.21E+02	0.46E-02
19	0.31E+01	-0.21E+02	0.69E-02
20	0.34E+01	-0.20E+02	0.92E-02
21	0.36E+01	-0.19E+02	0.12E-01
22	0.38E+01	-0.18E+02	0.14E-01
23	0.41E+01	-0.16E+02	0.16E-01
24	0.42E+01	-0.15E+02	0.17E-01
25	0.44E+01	-0.13E+02	0.19E-01
26	0.45E+01	-0.11E+02	0.20E-01
27	0.46E+01	-0.87E+01	0.21E-01
28	0.47E+01	-0.66E+01	0.22E-01
29	0.47E+01	-0.44E+01	0.22E-01
30	0.47E+01	-0.22E+01	0.22E-01
31	0.47E+01	0.00E+00	0.22E-01

NODE	X	Y	rZ
1	0.00E+00	0.00E+00	-0.20E-01
2	0.46E-05	-0.20E+01	-0.20E-01
3	0.19E-04	-0.39E+01	-0.20E-01
4	0.36E-03	-0.59E+01	-0.19E-01
5	0.52E-01	-0.78E+01	-0.19E-01
6	0.15E+00	-0.97E+01	-0.18E-01
7	0.27E+00	-0.11E+02	-0.17E-01
8	0.41E+00	-0.13E+02	-0.16E-01
9	0.57E+00	-0.15E+02	-0.14E-01
10	0.76E+00	-0.16E+02	-0.12E-01
11	0.98E+00	-0.17E+02	-0.10E-01
12	0.12E+01	-0.18E+02	-0.83E-02
13	0.14E+01	-0.19E+02	-0.62E-02
14	0.16E+01	-0.19E+02	-0.41E-02
15	0.19E+01	-0.19E+02	-0.21E-02
16	0.21E+01	-0.20E+02	-0.14E-13
17	0.23E+01	-0.19E+02	0.21E-02
18	0.25E+01	-0.19E+02	0.41E-02
19	0.28E+01	-0.19E+02	0.62E-02
20	0.30E+01	-0.18E+02	0.83E-02
21	0.32E+01	-0.17E+02	0.10E-01
22	0.34E+01	-0.16E+02	0.12E-01
23	0.36E+01	-0.15E+02	0.14E-01
24	0.38E+01	-0.13E+02	0.16E-01
25	0.39E+01	-0.11E+02	0.17E-01
26	0.40E+01	-0.97E+01	0.18E-01
27	0.41E+01	-0.78E+01	0.19E-01
28	0.42E+01	-0.59E+01	0.19E-01
29	0.42E+01	-0.39E+01	0.20E-01
30	0.42E+01	-0.20E+01	0.20E-01
31	0.42E+01	0.00E+00	0.20E-01

NODE	X	Y	rZ
1	0.00E+00	0.00E+00	-0.23E-01
2	0.55E-05	-0.23E+01	-0.23E-01
3	0.34E-04	-0.46E+01	-0.23E-01
4	0.12E-02	-0.69E+01	-0.23E-01
5	0.73E-01	-0.92E+01	-0.22E-01
6	0.19E+00	-0.11E+02	-0.21E-01
7	0.33E+00	-0.13E+02	-0.20E-01
8	0.50E+00	-0.15E+02	-0.18E-01
9	0.69E+00	-0.17E+02	-0.16E-01
10	0.92E+00	-0.19E+02	-0.14E-01
11	0.12E+01	-0.20E+02	-0.12E-01
12	0.14E+01	-0.21E+02	-0.97E-02
13	0.17E+01	-0.22E+02	-0.73E-02
14	0.20E+01	-0.23E+02	-0.49E-02
15	0.22E+01	-0.23E+02	-0.24E-02
16	0.25E+01	-0.23E+02	-0.15E-14
17	0.27E+01	-0.23E+02	0.24E-02
18	0.30E+01	-0.23E+02	0.49E-02
19	0.33E+01	-0.22E+02	0.73E-02
20	0.35E+01	-0.21E+02	0.97E-02
21	0.38E+01	-0.20E+02	0.12E-01
22	0.40E+01	-0.19E+02	0.14E-01
23	0.43E+01	-0.17E+02	0.16E-01
24	0.45E+01	-0.15E+02	0.18E-01
25	0.46E+01	-0.13E+02	0.20E-01
26	0.48E+01	-0.11E+02	0.21E-01
27	0.49E+01	-0.92E+01	0.22E-01
28	0.50E+01	-0.69E+01	0.23E-01
29	0.50E+01	-0.46E+01	0.23E-01
30	0.50E+01	-0.23E+01	0.23E-01
31	0.50E+01	0.00E+00	0.23E-01

NODE	X	Y	rZ
1	0.00E+00	0.00E+00	-0.21E-01
2	0.49E-05	-0.21E+01	-0.21E-01
3	0.20E-04	-0.42E+01	-0.21E-01
4	0.53E-03	-0.62E+01	-0.21E-01
5	0.60E-01	-0.83E+01	-0.20E-01
6	0.16E+00	-0.10E+02	-0.19E-01
7	0.29E+00	-0.12E+02	-0.18E-01
8	0.44E+00	-0.14E+02	-0.16E-01
9	0.62E+00	-0.15E+02	-0.15E-01
10	0.82E+00	-0.17E+02	-0.13E-01
11	0.10E+01	-0.18E+02	-0.11E-01
12	0.13E+01	-0.19E+02	-0.87E-02
13	0.15E+01	-0.20E+02	-0.66E-02
14	0.18E+01	-0.20E+02	-0.44E-02
15	0.20E+01	-0.21E+02	-0.22E-02
16	0.22E+01	-0.21E+02	-0.70E-14
17	0.25E+01	-0.21E+02	0.22E-02
18	0.27E+01	-0.20E+02	0.44E-02
19	0.29E+01	-0.20E+02	0.66E-02
20	0.32E+01	-0.19E+02	0.87E-02
21	0.34E+01	-0.18E+02	0.11E-01
22	0.36E+01	-0.17E+02	0.13E-01
23	0.38E+01	-0.15E+02	0.15E-01
24	0.40E+01	-0.14E+02	0.16E-01
25	0.42E+01	-0.12E+02	0.18E-01
26	0.43E+01	-0.10E+02	0.19E-01

NODE	X	Y	rZ
1	0.00E+00	0.00E+00	-0.24E-01
2	0.57E-05	-0.24E+01	-0.24E-01
3	0.48E-04	-0.49E+01	-0.24E-01
4	0.19E-02	-0.73E+01	-0.24E-01
5	0.80E-01	-0.97E+01	-0.23E-01
6	0.20E+00	-0.12E+02	-0.22E-01
7	0.35E+00	-0.14E+02	-0.21E-01
8	0.53E+00	-0.16E+02	-0.19E-01
9	0.73E+00	-0.18E+02	-0.17E-01
10	0.97E+00	-0.20E+02	-0.15E-01
11	0.12E+01	-0.21E+02	-0.13E-01
12	0.15E+01	-0.22E+02	-0.10E-01
13	0.18E+01	-0.23E+02	-0.76E-02
14	0.21E+01	-0.24E+02	-0.51E-02
15	0.23E+01	-0.24E+02	-0.25E-02
16	0.26E+01	-0.24E+02	-0.44E-15
17	0.29E+01	-0.24E+02	0.25E-02
18	0.32E+01	-0.24E+02	0.51E-02
19	0.34E+01	-0.23E+02	0.76E-02
20	0.37E+01	-0.22E+02	0.10E-01
21	0.40E+01	-0.21E+02	0.13E-01
22	0.43E+01	-0.20E+02	0.15E-01
23	0.45E+01	-0.18E+02	0.17E-01
24	0.47E+01	-0.16E+02	0.19E-01
25	0.49E+01	-0.14E+02	0.21E-01
26	0.50E+01	-0.12E+02	0.22E-01

STATIC_DISPLACEMENTS - Notepad				STATIC_DISPLACEMENTS - Notepad				STATIC_DISPLACEMENTS - Notepad			
File Edit Format View Help				File Edit Format View Help				File Edit Format View Help			
NODAL DISPLACEMENTS STEP 22				NODAL DISPLACEMENTS STEP 25				NODAL DISPLACEMENTS STEP 28			
NODE	X	Y	rZ	NODE	X	Y	rZ	NODE	X	Y	rZ
1	0.00E+00	0.00E+00	-0.25E-01	1	0.00E+00	0.00E+00	-0.29E-01	1	0.00E+00	0.00E+00	-0.33E-01
2	0.60E-05	-0.26E+01	-0.25E-01	2	0.68E-05	-0.29E+01	-0.29E-01	2	0.76E-05	-0.33E+01	-0.33E-01
3	0.61E-04	-0.51E+01	-0.25E-01	3	0.14E-03	-0.58E+01	-0.29E-01	3	0.27E-03	-0.65E+01	-0.33E-01
4	0.29E-02	-0.76E+01	-0.25E-01	4	0.91E-02	-0.87E+01	-0.29E-01	4	0.23E-01	-0.98E+01	-0.32E-01
5	0.86E-01	-0.10E+02	-0.24E-01	5	0.11E+00	-0.12E+02	-0.28E-01	5	0.14E+00	-0.13E+02	-0.31E-01
6	0.21E+00	-0.13E+02	-0.23E-01	6	0.25E+00	-0.14E+02	-0.26E-01	6	0.30E+00	-0.16E+02	-0.30E-01
7	0.37E+00	-0.15E+02	-0.22E-01	7	0.43E+00	-0.17E+02	-0.25E-01	7	0.50E+00	-0.19E+02	-0.28E-01
8	0.56E+00	-0.17E+02	-0.20E-01	8	0.64E+00	-0.19E+02	-0.23E-01	8	0.74E+00	-0.22E+02	-0.26E-01
9	0.77E+00	-0.19E+02	-0.18E-01	9	0.89E+00	-0.21E+02	-0.21E-01	9	0.10E+01	-0.24E+02	-0.23E-01
10	0.10E+01	-0.21E+02	-0.16E-01	10	0.12E+01	-0.23E+02	-0.18E-01	10	0.13E+01	-0.26E+02	-0.20E-01
11	0.13E+01	-0.22E+02	-0.13E-01	11	0.15E+01	-0.25E+02	-0.15E-01	11	0.17E+01	-0.28E+02	-0.17E-01
12	0.16E+01	-0.23E+02	-0.11E-01	12	0.18E+01	-0.26E+02	-0.12E-01	12	0.20E+01	-0.30E+02	-0.14E-01
13	0.19E+01	-0.24E+02	-0.08E-02	13	0.21E+01	-0.27E+02	-0.91E-02	13	0.24E+01	-0.31E+02	-0.10E-01
14	0.22E+01	-0.25E+02	-0.53E-02	14	0.25E+01	-0.28E+02	-0.61E-02	14	0.28E+01	-0.32E+02	-0.68E-02
15	0.24E+01	-0.25E+02	-0.27E-02	15	0.28E+01	-0.29E+02	-0.30E-02	15	0.31E+01	-0.32E+02	-0.34E-02
16	0.27E+01	-0.25E+02	0.13E-15	16	0.31E+01	-0.29E+02	0.79E-15	16	0.35E+01	-0.32E+02	0.89E-15
17	0.30E+01	-0.25E+02	0.27E-02	17	0.34E+01	-0.29E+02	0.30E-02	17	0.39E+01	-0.32E+02	0.34E-02
18	0.33E+01	-0.25E+02	0.53E-02	18	0.38E+01	-0.28E+02	0.61E-02	18	0.42E+01	-0.32E+02	0.68E-02
19	0.36E+01	-0.24E+02	0.80E-02	19	0.41E+01	-0.27E+02	0.91E-02	19	0.46E+01	-0.31E+02	0.10E-01
20	0.39E+01	-0.23E+02	0.11E-01	20	0.44E+01	-0.26E+02	0.12E-01	20	0.50E+01	-0.30E+02	0.14E-01
21	0.42E+01	-0.22E+02	0.13E-01	21	0.48E+01	-0.25E+02	0.15E-01	21	0.53E+01	-0.28E+02	0.17E-01
22	0.45E+01	-0.21E+02	0.16E-01	22	0.51E+01	-0.23E+02	0.18E-01	22	0.57E+01	-0.26E+02	0.20E-01
23	0.47E+01	-0.19E+02	0.18E-01	23	0.54E+01	-0.21E+02	0.21E-01	23	0.60E+01	-0.24E+02	0.23E-01
24	0.49E+01	-0.17E+02	0.20E-01	24	0.56E+01	-0.19E+02	0.23E-01	24	0.63E+01	-0.22E+02	0.26E-01
25	0.51E+01	-0.15E+02	0.22E-01	25	0.58E+01	-0.17E+02	0.25E-01	25	0.65E+01	-0.19E+02	0.28E-01
26	0.53E+01	-0.13E+02	0.23E-01	26	0.60E+01	-0.14E+02	0.26E-01	26	0.67E+01	-0.16E+02	0.30E-01
27	0.54E+01	-0.10E+02	0.24E-01	27	0.61E+01	-0.12E+02	0.28E-01	27	0.69E+01	-0.13E+02	0.31E-01
28	0.55E+01	-0.76E+01	0.25E-01	28	0.62E+01	-0.87E+01	0.29E-01	28	0.70E+01	-0.98E+01	0.32E-01
29	0.55E+01	-0.51E+01	0.25E-01	29	0.62E+01	-0.58E+01	0.29E-01	29	0.70E+01	-0.98E+01	0.32E-01
30	0.55E+01	-0.26E+01	0.25E-01	30	0.62E+01	-0.29E+01	0.29E-01	30	0.70E+01	-0.65E+01	0.33E-01
31	0.55E+01	0.00E+00	0.25E-01	31	0.62E+01	0.00E+00	0.29E-01	31	0.70E+01	-0.33E+01	0.33E-01



File Edit Format View Help    File Edit Format View Help    File Edit Format View Help

NODAL DISPLACEMENTS    STEP    31				NODAL DISPLACEMENTS    STEP    34				NODAL DISPLACEMENTS    STEP    37			
NODE	X	Y	rZ	NODE	X	Y	rZ	NODE	X	Y	rZ
1	0.00E+00	0.00E+00	-0.36E-01	1	0.00E+00	0.00E+00	-0.40E-01	1	0.00E+00	0.00E+00	-0.43E-01
2	0.84E-05	-0.36E+01	-0.36E-01	2	0.92E-05	-0.40E+01	-0.40E-01	2	0.10E-04	-0.44E+01	-0.43E-01
3	0.53E-03	-0.73E+01	-0.36E-01	3	0.10E-02	-0.80E+01	-0.40E-01	3	0.21E-02	-0.87E+01	-0.43E-01
4	0.45E-01	-0.11E+02	-0.36E-01	4	0.67E-01	-0.12E+02	-0.39E-01	4	0.87E-01	-0.13E+02	-0.42E-01
5	0.17E+00	-0.14E+02	-0.34E-01	5	0.21E+00	-0.16E+02	-0.38E-01	5	0.25E+00	-0.17E+02	-0.41E-01
6	0.36E+00	-0.18E+02	-0.33E-01	6	0.41E+00	-0.19E+02	-0.36E-01	6	0.46E+00	-0.21E+02	-0.39E-01
7	0.58E+00	-0.21E+02	-0.31E-01	7	0.65E+00	-0.23E+02	-0.34E-01	7	0.73E+00	-0.25E+02	-0.36E-01
8	0.84E+00	-0.24E+02	-0.28E-01	8	0.94E+00	-0.26E+02	-0.31E-01	8	0.10E+01	-0.28E+02	-0.34E-01
9	0.11E+01	-0.27E+02	-0.25E-01	9	0.13E+01	-0.29E+02	-0.28E-01	9	0.14E+01	-0.32E+02	-0.30E-01
10	0.15E+01	-0.29E+02	-0.22E-01	10	0.17E+01	-0.32E+02	-0.24E-01	10	0.18E+01	-0.35E+02	-0.26E-01
11	0.19E+01	-0.31E+02	-0.19E-01	11	0.21E+01	-0.34E+02	-0.20E-01	11	0.23E+01	-0.37E+02	-0.22E-01
12	0.23E+01	-0.33E+02	-0.15E-01	12	0.25E+01	-0.36E+02	-0.16E-01	12	0.28E+01	-0.39E+02	-0.18E-01
13	0.27E+01	-0.34E+02	-0.11E-01	13	0.30E+01	-0.37E+02	-0.12E-01	13	0.32E+01	-0.41E+02	-0.13E-01
14	0.31E+01	-0.35E+02	-0.75E-02	14	0.34E+01	-0.38E+02	-0.82E-02	14	0.37E+01	-0.42E+02	-0.89E-02
15	0.35E+01	-0.35E+02	-0.37E-02	15	0.39E+01	-0.39E+02	-0.41E-02	15	0.42E+01	-0.42E+02	-0.45E-02
16	0.39E+01	-0.36E+02	0.20E-13	16	0.43E+01	-0.39E+02	-0.83E-14	16	0.47E+01	-0.43E+02	0.32E-14
17	0.43E+01	-0.36E+02	0.37E-02	17	0.47E+01	-0.39E+02	0.41E-02	17	0.52E+01	-0.42E+02	0.45E-02
18	0.47E+01	-0.35E+02	0.75E-02	18	0.52E+01	-0.38E+02	0.82E-02	18	0.57E+01	-0.42E+02	0.89E-02
19	0.51E+01	-0.34E+02	0.11E-01	19	0.56E+01	-0.37E+02	0.12E-01	19	0.61E+01	-0.41E+02	0.13E-01
20	0.55E+01	-0.33E+02	0.15E-01	20	0.61E+01	-0.36E+02	0.16E-01	20	0.66E+01	-0.39E+02	0.18E-01
21	0.59E+01	-0.31E+02	0.19E-01	21	0.65E+01	-0.34E+02	0.20E-01	21	0.71E+01	-0.37E+02	0.22E-01
22	0.63E+01	-0.29E+02	0.22E-01	22	0.70E+01	-0.32E+02	0.24E-01	22	0.76E+01	-0.35E+02	0.26E-01
23	0.67E+01	-0.27E+02	0.25E-01	23	0.73E+01	-0.29E+02	0.28E-01	23	0.80E+01	-0.32E+02	0.30E-01
24	0.70E+01	-0.24E+02	0.28E-01	24	0.77E+01	-0.26E+02	0.31E-01	24	0.84E+01	-0.28E+02	0.34E-01
25	0.72E+01	-0.21E+02	0.31E-01	25	0.79E+01	-0.23E+02	0.34E-01	25	0.87E+01	-0.25E+02	0.36E-01
26	0.75E+01	-0.18E+02	0.33E-01	26	0.82E+01	-0.19E+02	0.36E-01	26	0.89E+01	-0.21E+02	0.39E-01
27	0.76E+01	-0.14E+02	0.34E-01	27	0.84E+01	-0.16E+02	0.38E-01	27	0.91E+01	-0.17E+02	0.41E-01
28	0.78E+01	-0.11E+02	0.36E-01	28	0.85E+01	-0.12E+02	0.39E-01	28	0.93E+01	-0.13E+02	0.42E-01
29	0.78E+01	-0.73E+01	0.36E-01	29	0.86E+01	-0.80E+01	0.40E-01	29	0.94E+01	-0.87E+01	0.43E-01
30	0.78E+01	-0.36E+01	0.36E-01	30	0.86E+01	-0.40E+01	0.40E-01	30	0.94E+01	-0.44E+01	0.43E-01
31	0.78E+01	0.00E+00	0.36E-01	31	0.86E+01	0.00E+00	0.40E-01	31	0.94E+01	0.00E+00	0.43E-01
-----											
NODAL DISPLACEMENTS    STEP    32				NODAL DISPLACEMENTS    STEP    35				NODAL DISPLACEMENTS    STEP    38			
NODE	X	Y	rZ	NODE	X	Y	rZ	NODE	X	Y	rZ
1	0.00E+00	0.00E+00	-0.37E-01	1	0.00E+00	0.00E+00	-0.41E-01	1	0.00E+00	0.00E+00	-0.45E-01
2	0.86E-05	-0.38E+01	-0.37E-01	2	0.94E-05	-0.41E+01	-0.41E-01	2	0.10E-04	-0.45E+01	-0.45E-01
3	0.64E-03	-0.75E+01	-0.37E-01	3	0.13E-02	-0.82E+01	-0.41E-01	3	0.28E-02	-0.89E+01	-0.45E-01
4	0.53E-01	-0.11E+02	-0.37E-01	4	0.74E-01	-0.12E+02	-0.40E-01	4	0.93E-01	-0.13E+02	-0.44E-01
5	0.19E+00	-0.15E+02	-0.35E-01	5	0.22E+00	-0.16E+02	-0.39E-01	5	0.26E+00	-0.18E+02	-0.42E-01
6	0.37E+00	-0.18E+02	-0.34E-01	6	0.43E+00	-0.20E+02	-0.37E-01	6	0.48E+00	-0.22E+02	-0.40E-01
7	0.60E+00	-0.22E+02	-0.32E-01	7	0.68E+00	-0.24E+02	-0.35E-01	7	0.75E+00	-0.26E+02	-0.37E-01
8	0.87E+00	-0.25E+02	-0.29E-01	8	0.97E+00	-0.27E+02	-0.32E-01	8	0.11E+01	-0.29E+02	-0.35E-01
9	0.12E+01	-0.27E+02	-0.26E-01	9	0.13E+01	-0.30E+02	-0.29E-01	9	0.14E+01	-0.33E+02	-0.31E-01
10	0.15E+01	-0.30E+02	-0.23E-01	10	0.17E+01	-0.33E+02	-0.25E-01	10	0.19E+01	-0.35E+02	-0.27E-01
11	0.19E+01	-0.32E+02	-0.19E-01	11	0.21E+01	-0.35E+02	-0.21E-01	11	0.23E+01	-0.38E+02	-0.23E-01
12	0.24E+01	-0.34E+02	-0.15E-01	12	0.26E+01	-0.37E+02	-0.17E-01	12	0.28E+01	-0.40E+02	-0.18E-01
13	0.28E+01	-0.35E+02	-0.12E-01	13	0.31E+01	-0.38E+02	-0.13E-01	13	0.33E+01	-0.42E+02	-0.14E-01
14	0.32E+01	-0.36E+02	-0.77E-02	14	0.35E+01	-0.39E+02	-0.84E-02	14	0.38E+01	-0.43E+02	-0.91E-02
15	0.36E+01	-0.37E+02	-0.39E-02	15	0.40E+01	-0.40E+02	-0.42E-02	15	0.43E+01	-0.43E+02	-0.46E-02
16	0.40E+01	-0.37E+02	-0.13E-13	16	0.44E+01	-0.40E+02	0.77E-14	16	0.48E+01	-0.44E+02	-0.61E-15
17	0.45E+01	-0.37E+02	0.39E-02	17	0.49E+01	-0.40E+02	0.42E-02	17	0.53E+01	-0.43E+02	0.46E-02
18	0.49E+01	-0.36E+02	0.77E-02	18	0.53E+01	-0.39E+02	0.84E-02	18	0.58E+01	-0.43E+02	0.91E-02
19	0.53E+01	-0.35E+02	0.12E-01	19	0.58E+01	-0.38E+02	0.13E-01	19	0.63E+01	-0.42E+02	0.14E-01
20	0.57E+01	-0.34E+02	0.15E-01	20	0.63E+01	-0.37E+02	0.17E-01	20	0.68E+01	-0.40E+02	0.18E-01
21	0.61E+01	-0.32E+02	0.19E-01	21	0.67E+01	-0.35E+02	0.21E-01	21	0.73E+01	-0.38E+02	0.23E-01
22	0.65E+01	-0.30E+02	0.23E-01	22	0.72E+01	-0.33E+02	0.25E-01	22	0.78E+01	-0.35E+02	0.27E-01
23	0.69E+01	-0.27E+02	0.26E-01	23	0.75E+01	-0.30E+02	0.29E-01	23	0.82E+01	-0.33E+02	0.31E-01
24	0.72E+01	-0.25E+02	0.29E-01	24	0.79E+01	-0.27E+02	0.32E-01	24	0.86E+01	-0.29E+02	0.35E-01
25	0.75E+01	-0.22E+02	0.32E-01	25	0.82E+01	-0.24E+02	0.35E-01	25	0.89E+01	-0.26E+02	0.37E-01
26	0.77E+01	-0.18E+02	0.34E-01	26	0.84E+01	-0.20E+02	0.37E-01	26	0.92E+01	-0.22E+02	0.40E-01
27	0.79E+01	-0.15E+02	0.35E-01	27	0.86E+01	-0.16E+02	0.39E-01	27	0.94E+01	-0.18E+02	0.42E-01
28	0.80E+01	-0.11E+02	0.37E-01	28	0.88E+01	-0.12E+02	0.40E-01	28	0.96E+01	-0.13E+02	0.44E-01
29	0.81E+01	-0.75E+01	0.37E-01	29	0.89E+01	-0.82E+01	0.41E-01	29	0.96E+01	-0.89E+01	0.45E-01
30	0.81E+01	-0.38E+01	0.37E-01	30	0.89E+01	-0.41E+01	0.41E-01	30	0.97E+01	-0.45E+01	0.45E-01
31	0.81E+01	0.00E+00	0.37E-01	31	0.89E+01	0.00E+00	0.41E-01	31	0.97E+01	0.00E+00	0.45E-01
-----											
NODAL DISPLACEMENTS    STEP    33				NODAL DISPLACEMENTS    STEP    36				NODAL DISPLACEMENTS    STEP    39			
NODE	X	Y	rZ	NODE	X	Y	rZ	NODE	X	Y	rZ
1	0.00E+00	0.00E+00	-0.39E-01	1	0.00E+00	0.00E+00	-0.42E-01	1	0.00E+00	0.00E+00	-0.46E-01
2	0.89E-05	-0.39E+01	-0.39E-01	2	0.97E-05	-0.42E+01	-0.42E-01	2	0.11E-04	-0.46E+01	-0.46E-01
3	0.82E-03	-0.77E+01	-0.39E-01	3	0.17E-02	-0.85E+01	-0.42E-01	3	0.36E-02	-0.92E+01	-0.46E-01
4	0.60E-01	-0.12E+02	-0.38E-01	4	0.80E-01	-0.13E+02	-0.41E-01	4	0.99E-01	-0.14E+02	-0.45E-01
5	0.20E+00	-0.15E+02	-0.37E-01	5	0.23E+00	-0.17E+02	-0.40E-01	5	0.27E+00	-0.18E+02	-0.43E-01
6	0.39E+00	-0.19E+02	-0.35E-01	6	0.44E+00	-0.21E+02	-0.38E-01	6	0.50E+00	-0.22E+02	-0.41E-01
7	0.63E+00	-0.22E+02	-0.33E-01	7	0.70E+00	-0.24E+02	-0.36E-01	7	0.77E+00	-0.26E+02	-0.38E-01
8	0.91E+00	-0.25E+02	-0.30E-01	8	0.10E+01	-0.28E+02	-0.33E-01	8	0.11E+01	-0.30E+02	-0.35E-01
9	0.12E+01	-0.28E+02	-0.27E-01	9	0.14E+01	-0.31E+02	-0.29E-01	9	0.15E+01	-0.33E+02	-0.32E-01
10	0.16E+01	-0.31E+02	-0.24E-01	10	0.18E+01	-0.34E+02	-0.26E-01	10	0.19E+01	-0.36E+02	-0.28E-01
11	0.20E+01	-0.33E+02	-0.20E-01	11	0.22E+01	-0.36E+02	-0.22E-01	11	0.24E+01	-0.39E+02	-0.23E-01
12	0.24E+01	-0.35E+02	-0.16E-01	12	0.27E+01	-0.38E+02	-0.17E-01	12	0.29E+01	-0.41E+02	-0.19E-01
13	0.29E+01	-0.36E+02	-0.12E-01	13	0.31E+01	-0.39E+02	-0.13E-01	13	0.34E+01	-0.43E+02	-0.14E-01
14	0.33E+01	-0.37E+02	-0.80E-02	14	0.36E+01	-0.41E+02	-0.87E-02	14	0.39E+01	-0.44E+02	-0.94E-02
15	0.37E+01	-0.38E+02	-0.40E-02	15	0.41E+01	-0.41E+02	-0.43E-02	15	0.44E+01	-0.45E+02	-0.47E-02
16	0.42E+01	-0.38E+02	0.14E-13	16	0.46E+01	-0.41E+02	-0.33E-14	16	0.50E+01	-0.45E+02	0.13E-14
17	0.46E+01	-0.38E+02	0.40E-02	17	0.46E+01	-0.41E+02	0.43E-02	17	0.55E+01	-0.45E+02	0.47E-02
18	0.50E+01	-0.37E+02	0.80E-02	18	0.50E+01	-0.41E+02	0.43E-02	18	0.60E+01	-0.44E+02	0.94E-02
19	0.55E+01	-0.36E+02	0.12E-01	19	0.55E+01	-0.41E+02	0.87E-02	19	0.65E+01	-0.43E+02	0.14E-01
20	0.59E+01	-0.35E+02	0.16E-01	20	0.60E+01	-0.39E+02	0.13E-01	20	0.70E+01	-0.41E+02	0.19E-01
21	0.63E+01	-0.33E+02	0.								

STATIC\_DISPLACEMENTS - Notepad

STATIC_DISPLACEMENTS - Notepad					STATIC_DISPLACEMENTS - Notepad						
File	Edit	Format	View	Help	File	Edit	Format	View	Help		
NODAL DISPLACEMENTS STEP 43					NODAL DISPLACEMENTS STEP 46						
NODE	X	Y	rZ		NODE	X	Y	rZ			
1	0.00E+00	0.00E+00	-0.47E-01	1	0.00E+00	0.00E+00	-0.50E-01	1	0.00E+00	0.00E+00	-0.53E-01
2	0.16E-04	-0.47E+01	-0.47E-01	2	0.26E-04	-0.50E+01	-0.50E-01	2	0.27E-04	-0.54E+01	-0.53E-01
3	0.46E-02	-0.94E+01	-0.47E-01	3	0.76E-02	-0.10E+02	-0.50E-01	3	0.89E-02	-0.11E+02	-0.53E-01
4	0.11E+00	-0.14E+02	-0.46E-01	4	0.12E+00	-0.15E+02	-0.49E-01	4	0.12E+00	-0.16E+02	-0.52E-01
5	0.28E+00	-0.19E+02	-0.44E-01	5	0.30E+00	-0.20E+02	-0.47E-01	5	0.31E+00	-0.21E+02	-0.50E-01
6	0.51E+00	-0.23E+02	-0.42E-01	6	0.55E+00	-0.25E+02	-0.45E-01	6	0.55E+00	-0.26E+02	-0.48E-01
7	0.80E+00	-0.27E+02	-0.39E-01	7	0.85E+00	-0.29E+02	-0.42E-01	7	0.85E+00	-0.31E+02	-0.45E-01
8	0.11E+01	-0.31E+02	-0.36E-01	8	0.12E+01	-0.33E+02	-0.39E-01	8	0.12E+01	-0.35E+02	-0.42E-01
9	0.15E+01	-0.34E+02	-0.33E-01	9	0.16E+01	-0.37E+02	-0.36E-01	9	0.21E+01	-0.43E+02	-0.34E-01
10	0.20E+01	-0.37E+02	-0.29E-01	10	0.21E+01	-0.40E+02	-0.31E-01	10	0.26E+01	-0.46E+02	-0.29E-01
11	0.25E+01	-0.40E+02	-0.24E-01	11	0.26E+01	-0.43E+02	-0.27E-01	11	0.32E+01	-0.49E+02	-0.24E-01
12	0.30E+01	-0.42E+02	-0.19E-01	12	0.31E+01	-0.45E+02	-0.21E-01	12	0.38E+01	-0.51E+02	-0.18E-01
13	0.35E+01	-0.44E+02	-0.14E-01	13	0.37E+01	-0.47E+02	-0.16E-01	13	0.43E+01	-0.52E+02	-0.12E-01
14	0.40E+01	-0.45E+02	-0.96E-02	14	0.42E+01	-0.49E+02	-0.11E-01	14	0.49E+01	-0.53E+02	-0.59E-02
15	0.46E+01	-0.46E+02	-0.48E-02	15	0.48E+01	-0.49E+02	-0.53E-02	15	0.55E+01	-0.53E+02	0.50E-15
16	0.51E+01	-0.46E+02	0.28E-15	16	0.53E+01	-0.50E+02	0.51E-15	16	0.61E+01	-0.53E+02	0.59E-02
17	0.56E+01	-0.46E+02	0.48E-02	17	0.58E+01	-0.49E+02	0.53E-02	17	0.66E+01	-0.52E+02	0.12E-01
18	0.61E+01	-0.45E+02	0.96E-02	18	0.64E+01	-0.49E+02	0.11E-01	18	0.72E+01	-0.51E+02	0.18E-01
19	0.67E+01	-0.44E+02	0.14E-01	19	0.69E+01	-0.47E+02	0.16E-01	19	0.78E+01	-0.49E+02	0.24E-01
20	0.72E+01	-0.42E+02	0.19E-01	20	0.75E+01	-0.45E+02	0.21E-01	20	0.83E+01	-0.46E+02	0.29E-01
21	0.77E+01	-0.40E+02	0.24E-01	21	0.80E+01	-0.43E+02	0.27E-01	21	0.89E+01	-0.43E+02	0.34E-01
22	0.82E+01	-0.37E+02	0.29E-01	22	0.85E+01	-0.40E+02	0.31E-01	22	0.93E+01	-0.39E+02	0.38E-01
23	0.86E+01	-0.34E+02	0.33E-01	23	0.90E+01	-0.37E+02	0.36E-01	23	0.98E+01	-0.35E+02	0.42E-01
24	0.90E+01	-0.31E+02	0.36E-01	24	0.94E+01	-0.33E+02	0.39E-01	24	0.10E+02	-0.31E+02	0.45E-01
25	0.94E+01	-0.27E+02	0.39E-01	25	0.98E+01	-0.29E+02	0.42E-01	25	0.10E+02	-0.26E+02	0.48E-01
26	0.97E+01	-0.23E+02	0.42E-01	26	0.10E+02	-0.25E+02	0.45E-01	26	0.11E+02	-0.21E+02	0.50E-01
27	0.99E+01	-0.19E+02	0.44E-01	27	0.10E+02	-0.20E+02	0.47E-01	27	0.11E+02	-0.16E+02	0.52E-01
28	0.10E+02	-0.14E+02	0.46E-01	28	0.10E+02	-0.15E+02	0.49E-01	28	0.11E+02	-0.11E+02	0.53E-01
29	0.10E+02	-0.94E+01	0.47E-01	29	0.11E+02	-0.10E+02	0.50E-01	29	0.11E+02	-0.54E+01	0.53E-01
30	0.10E+02	-0.47E+01	0.47E-01	30	0.11E+02	-0.50E+01	0.50E-01	30	0.11E+02	-0.54E+01	0.53E-01
31	0.10E+02	0.00E+00	0.47E-01	31	0.11E+02	0.00E+00	0.50E-01	31	0.11E+02	0.00E+00	0.53E-01
NODAL DISPLACEMENTS STEP 41					NODAL DISPLACEMENTS STEP 44						
NODE	X	Y	rZ		NODE	X	Y	rZ			
1	0.00E+00	0.00E+00	-0.48E-01	1	0.00E+00	0.00E+00	-0.51E-01	1	0.00E+00	0.00E+00	-0.55E-01
2	0.22E-04	-0.48E+01	-0.48E-01	2	0.26E-04	-0.51E+01	-0.51E-01	2	0.29E-04	-0.55E+01	-0.55E-01
3	0.60E-02	-0.97E+01	-0.48E-01	3	0.76E-02	-0.10E+02	-0.51E-01	3	0.11E-01	-0.11E+02	-0.54E-01
4	0.11E+00	-0.14E+02	-0.47E-01	4	0.12E+00	-0.15E+02	-0.50E-01	4	0.13E+00	-0.16E+02	-0.53E-01
5	0.29E+00	-0.19E+02	-0.45E-01	5	0.30E+00	-0.20E+02	-0.48E-01	5	0.31E+00	-0.22E+02	-0.51E-01
6	0.53E+00	-0.23E+02	-0.43E-01	6	0.55E+00	-0.25E+02	-0.46E-01	6	0.56E+00	-0.27E+02	-0.49E-01
7	0.82E+00	-0.28E+02	-0.40E-01	7	0.85E+00	-0.30E+02	-0.43E-01	7	0.87E+00	-0.31E+02	-0.46E-01
8	0.12E+01	-0.32E+02	-0.37E-01	8	0.12E+01	-0.34E+02	-0.40E-01	8	0.12E+01	-0.36E+02	-0.43E-01
9	0.16E+01	-0.35E+02	-0.34E-01	9	0.16E+01	-0.38E+02	-0.36E-01	9	0.16E+01	-0.40E+02	-0.39E-01
10	0.20E+01	-0.38E+02	-0.29E-01	10	0.21E+01	-0.41E+02	-0.32E-01	10	0.21E+01	-0.44E+02	-0.35E-01
11	0.25E+01	-0.41E+02	-0.25E-01	11	0.26E+01	-0.44E+02	-0.28E-01	11	0.27E+01	-0.47E+02	-0.30E-01
12	0.31E+01	-0.43E+02	-0.20E-01	12	0.32E+01	-0.46E+02	-0.22E-01	12	0.32E+01	-0.50E+02	-0.24E-01
13	0.36E+01	-0.45E+02	-0.15E-01	13	0.37E+01	-0.48E+02	-0.17E-01	13	0.38E+01	-0.52E+02	-0.18E-01
14	0.41E+01	-0.46E+02	-0.99E-02	14	0.43E+01	-0.50E+02	-0.11E-01	14	0.44E+01	-0.53E+02	-0.12E-01
15	0.47E+01	-0.47E+02	-0.49E-02	15	0.48E+01	-0.51E+02	-0.55E-02	15	0.50E+01	-0.54E+02	-0.60E-02
16	0.52E+01	-0.47E+02	0.70E-15	16	0.54E+01	-0.51E+02	0.49E-15	16	0.56E+01	-0.55E+02	0.50E-15
17	0.58E+01	-0.47E+02	0.49E-02	17	0.59E+01	-0.51E+02	0.55E-02	17	0.61E+01	-0.54E+02	0.60E-02
18	0.63E+01	-0.46E+02	0.99E-02	18	0.65E+01	-0.50E+02	0.11E-01	18	0.67E+01	-0.53E+02	0.12E-01
19	0.68E+01	-0.45E+02	0.15E-01	19	0.70E+01	-0.48E+02	0.17E-01	19	0.73E+01	-0.52E+02	0.18E-01
20	0.74E+01	-0.43E+02	0.20E-01	20	0.75E+01	-0.46E+02	0.22E-01	20	0.79E+01	-0.50E+02	0.24E-01
21	0.79E+01	-0.41E+02	0.25E-01	21	0.81E+01	-0.44E+02	0.28E-01	21	0.85E+01	-0.47E+02	0.30E-01
22	0.84E+01	-0.38E+02	0.29E-01	22	0.86E+01	-0.41E+02	0.32E-01	22	0.90E+01	-0.44E+02	0.35E-01
23	0.89E+01	-0.35E+02	0.34E-01	23	0.91E+01	-0.38E+02	0.36E-01	23	0.95E+01	-0.36E+02	0.43E-01
24	0.93E+01	-0.32E+02	0.37E-01	24	0.95E+01	-0.34E+02	0.40E-01	24	0.99E+01	-0.31E+02	0.46E-01
25	0.96E+01	-0.28E+02	0.40E-01	25	0.99E+01	-0.30E+02	0.43E-01	25	0.10E+02	-0.27E+02	0.49E-01
26	0.99E+01	-0.23E+02	0.43E-01	26	0.10E+02	-0.25E+02	0.46E-01	26	0.11E+02	-0.22E+02	0.51E-01
27	0.10E+02	-0.19E+02	0.45E-01	27	0.10E+02	-0.20E+02	0.48E-01	27	0.11E+02	-0.16E+02	0.53E-01
28	0.10E+02	-0.14E+02	0.47E-01	28	0.11E+02	-0.15E+02	0.50E-01	28	0.11E+02	-0.11E+02	0.54E-01
29	0.10E+02	-0.97E+01	0.48E-01	29	0.11E+02	-0.10E+02	0.51E-01	29	0.11E+02	-0.55E+01	0.55E-01
30	0.10E+02	-0.48E+01	0.48E-01	30	0.11E+02	-0.51E+01	0.51E-01	30	0.11E+02	-0.55E+01	0.55E-01
31	0.10E+02	0.00E+00	0.48E-01	31	0.11E+02	0.00E+00	0.51E-01	31	0.11E+02	0.00E+00	0.55E-01
NODAL DISPLACEMENTS STEP 42					NODAL DISPLACEMENTS STEP 45						
NODE	X	Y	rZ		NODE	X	Y	rZ			
1	0.00E+00	0.00E+00	-0.49E-01	1	0.00E+00	0.00E+00	-0.52E-01	1	0.00E+00	0.00E+00	-0.56E-01
2	0.28E-04	-0.50E+01	-0.49E-01	2	0.27E-04	-0.52E+01	-0.52E-01	2	0.35E-04	-0.56E+01	-0.56E-01
3	0.76E-02	-0.99E+01	-0.49E-01	3	0.77E-02	-0.10E+02	-0.52E-01	3	0.13E-01	-0.11E+02	-0.55E-01
4	0.12E+00	-0.15E+02	-0.48E-01	4	0.12E+00	-0.16E+02	-0.51E-01	4	0.13E+00	-0.17E+02	-0.54E-01
5	0.30E+00	-0.20E+02	-0.46E-01	5	0.30E+00	-0.21E+02	-0.49E-01	5	0.32E+00	-0.22E+02	-0.53E-01
6	0.54E+00	-0.24E+02	-0.44E-01	6	0.55E+00	-0.26E+02	-0.47E-01	6	0.57E+00	-0.27E+02	-0.50E-01
7	0.85E+00	-0.28E+02	-0.41E-01	7	0.85E+00	-0.30E+02	-0.44E-01	7	0.88E+00	-0.32E+02	-0.47E-01
8	0.12E+01	-0.32E+02	-0.38E-01	8	0.12E+01	-0.34E+02	-0.41E-01	8	0.13E+01	-0.37E+02	-0.44E-01
9	0.16E+01	-0.36E+02	-0.34E-01	9	0.16E+01	-0.38E+02	-0.37E-01	9	0.17E+01	-0.41E+02	-0.40E-01
10	0.21E+01	-0.39E+02	-0.30E-01	10	0.21E+01	-0.42E+02	-0.33E-01	10	0.22E+01	-0.45E+02	-0.36E-01
11	0.26E+01	-0.42E+02	-0.25E-01	11	0.26E+01	-0.45E+02	-0.28E-01	11	0.27E+01	-0.48E+02	-0.31E-01
12	0.31E+01	-0.44E+02	-0.20E-01	12	0.32E+01	-0.48E+02	-0.23E-01	12	0.33E+01	-0.51E+02	-0.25E-01
13	0.37E+01	-0.46E+02	-0.15E-01	13	0.37E+01	-0.50E+02	-0.17E-01	13	0.39E+01	-0.53E+02	-0.18E-01
14	0.42E+01	-0.47E+02	-0.10E-01	14	0.43E+01	-0.51E+02	-0.11E-01	14	0.45E+01	-0.54E+02	-0.12E-01
15	0.48E+01	-0.48E+02	-0.51E-02	15	0.49E+01	-0.52E+02	-0.57E-02	15	0.51E+01	-0.55E+02	-0.62E-02
16	0.53E+01	-0.48E+02	0.48E-15	16	0.54E+01	-0.52E+02	0.49E-15	16	0.57E+01	-0.56E+02	0.50E-15
17	0.59E+01	-0.48E+02	0.51E-02	17	0.60E+01	-0.52E+02	0.57E-02	17	0.63E+01	-0.55E+02	0.62E-02
18	0.64E+01	-0.47E+02	0.10E-01	18	0.65E+01	-0.51E+02	0.11E-01	18	0.69E+01	-0.54E+02	0.12E-01
19	0.70E+01	-0.46E+02	0.15E-01	19	0.71E+01	-0.50E+02	0.17E-01	19	0.74E+01	-0.53E+02	0.18E-01
20	0.75E+01	-0.44E+02	0.20E-01	20	0.77E+01	-0.48E+02	0.23E-01	20	0.80E+01	-0.51E+02	0.25E

File	Edit	Format	View	Help	File	Edit	Format	View	Help	File	Edit	Format	View	Help
NODAL DISPLACEMENTS STEP 49					NODAL DISPLACEMENTS STEP 52					NODAL DISPLACEMENTS STEP 55				
NODE	X	Y	rZ		NODE	X	Y	rZ		NODE	X	Y	rZ	
1	0.00E+00	0.00E+00	-0.57E-01		1	0.00E+00	0.00E+00	-0.60E-01		1	0.00E+00	0.00E+00	-0.64E-01	
2	0.41E-04	-0.57E+01	-0.57E-01		2	0.53E-04	-0.60E+01	-0.60E-01		2	0.79E-04	-0.64E+01	-0.64E-01	
3	0.15E-01	-0.11E+02	-0.57E-01		3	0.24E-01	-0.12E+02	-0.60E-01		3	0.34E-01	-0.13E+02	-0.63E-01	
4	0.14E+00	-0.17E+02	-0.55E-01		4	0.15E+00	-0.18E+02	-0.59E-01		4	0.17E+00	-0.19E+02	-0.62E-01	
5	0.33E+00	-0.22E+02	-0.54E-01		5	0.36E+00	-0.24E+02	-0.57E-01		5	0.39E+00	-0.25E+02	-0.60E-01	
6	0.59E+00	-0.28E+02	-0.51E-01		6	0.63E+00	-0.29E+02	-0.54E-01		6	0.67E+00	-0.31E+02	-0.57E-01	
7	0.90E+00	-0.33E+02	-0.48E-01		7	0.95E+00	-0.35E+02	-0.51E-01		7	0.10E+01	-0.37E+02	-0.54E-01	
8	0.13E+01	-0.37E+02	-0.45E-01		8	0.13E+01	-0.40E+02	-0.48E-01		8	0.14E+01	-0.42E+02	-0.51E-01	
9	0.17E+01	-0.42E+02	-0.41E-01		9	0.18E+01	-0.44E+02	-0.44E-01		9	0.19E+01	-0.47E+02	-0.46E-01	
10	0.22E+01	-0.46E+02	-0.36E-01		10	0.23E+01	-0.48E+02	-0.39E-01		10	0.24E+01	-0.51E+02	-0.41E-01	
11	0.27E+01	-0.49E+02	-0.31E-01		11	0.29E+01	-0.52E+02	-0.33E-01		11	0.31E+01	-0.55E+02	-0.35E-01	
12	0.33E+01	-0.52E+02	-0.25E-01		12	0.35E+01	-0.55E+02	-0.26E-01		12	0.37E+01	-0.58E+02	-0.28E-01	
13	0.40E+01	-0.54E+02	-0.19E-01		13	0.41E+01	-0.57E+02	-0.20E-01		13	0.44E+01	-0.61E+02	-0.21E-01	
14	0.46E+01	-0.56E+02	-0.13E-01		14	0.48E+01	-0.59E+02	-0.13E-01		14	0.50E+01	-0.62E+02	-0.14E-01	
15	0.52E+01	-0.57E+02	-0.03E-02		15	0.54E+01	-0.60E+02	-0.06E-02		15	0.57E+01	-0.63E+02	-0.05E-02	
16	0.58E+01	-0.57E+02	0.49E-15		16	0.60E+01	-0.60E+02	0.47E-15		16	0.63E+01	-0.64E+02	0.45E-15	
17	0.64E+01	-0.57E+02	0.63E-02		17	0.67E+01	-0.60E+02	0.66E-02		17	0.70E+01	-0.63E+02	0.69E-02	
18	0.70E+01	-0.56E+02	0.13E-01		18	0.73E+01	-0.59E+02	0.13E-01		18	0.77E+01	-0.62E+02	0.14E-01	
19	0.76E+01	-0.54E+02	0.19E-01		19	0.79E+01	-0.57E+02	0.20E-01		19	0.83E+01	-0.61E+02	0.21E-01	
20	0.82E+01	-0.52E+02	0.25E-01		20	0.85E+01	-0.55E+02	0.26E-01		20	0.90E+01	-0.58E+02	0.28E-01	
21	0.88E+01	-0.49E+02	0.31E-01		21	0.92E+01	-0.52E+02	0.33E-01		21	0.96E+01	-0.55E+02	0.35E-01	
22	0.93E+01	-0.46E+02	0.36E-01		22	0.98E+01	-0.48E+02	0.39E-01		22	0.10E+02	-0.51E+02	0.41E-01	
23	0.98E+01	-0.42E+02	0.41E-01		23	0.10E+02	-0.44E+02	0.44E-01		23	0.11E+02	-0.47E+02	0.46E-01	
24	0.10E+02	-0.37E+02	0.45E-01		24	0.11E+02	-0.40E+02	0.48E-01		24	0.11E+02	-0.47E+02	0.46E-01	
25	0.11E+02	-0.33E+02	0.48E-01		25	0.11E+02	-0.35E+02	0.51E-01		25	0.11E+02	-0.47E+02	0.46E-01	
26	0.11E+02	-0.28E+02	0.51E-01		26	0.11E+02	-0.29E+02	0.54E-01		26	0.11E+02	-0.42E+02	0.51E-01	
27	0.11E+02	-0.22E+02	0.54E-01		27	0.12E+02	-0.24E+02	0.57E-01		27	0.12E+02	-0.37E+02	0.54E-01	
28	0.11E+02	-0.17E+02	0.55E-01		28	0.12E+02	-0.18E+02	0.59E-01		28	0.12E+02	-0.31E+02	0.57E-01	
29	0.12E+02	-0.11E+02	0.57E-01		29	0.12E+02	-0.12E+02	0.60E-01		29	0.12E+02	-0.25E+02	0.60E-01	
30	0.12E+02	-0.05E+01	0.57E-01		30	0.12E+02	-0.06E+01	0.60E-01		30	0.12E+02	-0.19E+02	0.61E-01	
31	0.12E+02	0.00E+00	0.57E-01		31	0.12E+02	0.00E+00	0.60E-01		31	0.12E+02	0.00E+00	0.63E-01	
NODAL DISPLACEMENTS STEP 50					NODAL DISPLACEMENTS STEP 53					NODAL DISPLACEMENTS STEP 56				
NODE	X	Y	rZ		NODE	X	Y	rZ		NODE	X	Y	rZ	
1	0.00E+00	0.00E+00	-0.58E-01		1	0.00E+00	0.00E+00	-0.62E-01		1	0.00E+00	0.00E+00	-0.65E-01	
2	0.46E-04	-0.58E+01	-0.58E-01		2	0.59E-04	-0.62E+01	-0.61E-01		2	0.90E-04	-0.65E+01	-0.65E-01	
3	0.17E-01	-0.12E+02	-0.58E-01		3	0.27E-01	-0.12E+02	-0.61E-01		3	0.38E-01	-0.13E+02	-0.65E-01	
4	0.14E+00	-0.17E+02	-0.57E-01		4	0.16E+00	-0.18E+02	-0.60E-01		4	0.18E+00	-0.19E+02	-0.63E-01	
5	0.34E+00	-0.23E+02	-0.55E-01		5	0.37E+00	-0.24E+02	-0.58E-01		5	0.40E+00	-0.26E+02	-0.61E-01	
6	0.60E+00	-0.28E+02	-0.52E-01		6	0.64E+00	-0.30E+02	-0.55E-01		6	0.69E+00	-0.32E+02	-0.59E-01	
7	0.92E+00	-0.33E+02	-0.49E-01		7	0.97E+00	-0.35E+02	-0.52E-01		7	0.10E+01	-0.37E+02	-0.55E-01	
8	0.13E+01	-0.38E+02	-0.46E-01		8	0.14E+01	-0.40E+02	-0.49E-01		8	0.15E+01	-0.43E+02	-0.50E-01	
9	0.17E+01	-0.43E+02	-0.42E-01		9	0.18E+01	-0.45E+02	-0.44E-01		9	0.18E+01	-0.43E+02	-0.51E-01	
10	0.22E+01	-0.47E+02	-0.37E-01		10	0.23E+01	-0.49E+02	-0.40E-01		10	0.19E+01	-0.48E+02	-0.47E-01	
11	0.28E+01	-0.50E+02	-0.32E-01		11	0.29E+01	-0.53E+02	-0.33E-01		11	0.25E+01	-0.52E+02	-0.42E-01	
12	0.34E+01	-0.53E+02	-0.26E-01		12	0.36E+01	-0.56E+02	-0.27E-01		12	0.31E+01	-0.56E+02	-0.35E-01	
13	0.40E+01	-0.55E+02	-0.19E-01		13	0.42E+01	-0.58E+02	-0.20E-01		13	0.38E+01	-0.59E+02	-0.28E-01	
14	0.46E+01	-0.57E+02	-0.13E-01		14	0.49E+01	-0.60E+02	-0.13E-01		14	0.45E+01	-0.62E+02	-0.21E-01	
15	0.53E+01	-0.58E+02	-0.04E-02		15	0.55E+01	-0.61E+02	-0.06E-02		15	0.51E+01	-0.63E+02	-0.14E-01	
16	0.59E+01	-0.58E+02	0.45E-15		16	0.61E+01	-0.61E+02	0.47E-15		16	0.58E+01	-0.64E+02	-0.17E-02	
17	0.65E+01	-0.58E+02	0.64E-02		17	0.68E+01	-0.61E+02	0.67E-02		17	0.65E+01	-0.65E+02	0.45E-15	
18	0.71E+01	-0.57E+02	0.13E-01		18	0.74E+01	-0.60E+02	0.13E-01		18	0.71E+01	-0.64E+02	0.71E-02	
19	0.77E+01	-0.55E+02	0.19E-01		19	0.80E+01	-0.58E+02	0.20E-01		19	0.78E+01	-0.63E+02	0.14E-01	
20	0.83E+01	-0.53E+02	0.26E-01		20	0.87E+01	-0.56E+02	0.27E-01		20	0.84E+01	-0.62E+02	0.21E-01	
21	0.89E+01	-0.50E+02	0.32E-01		21	0.93E+01	-0.53E+02	0.33E-01		21	0.91E+01	-0.59E+02	0.28E-01	
22	0.95E+01	-0.47E+02	0.37E-01		22	0.99E+01	-0.49E+02	0.40E-01		22	0.98E+01	-0.56E+02	0.35E-01	
23	0.10E+02	-0.43E+02	0.42E-01		23	0.10E+02	-0.45E+02	0.44E-01		23	0.10E+02	-0.52E+02	0.42E-01	
24	0.10E+02	-0.38E+02	0.46E-01		24	0.11E+02	-0.40E+02	0.49E-01		24	0.11E+02	-0.48E+02	0.47E-01	
25	0.11E+02	-0.33E+02	0.49E-01		25	0.11E+02	-0.35E+02	0.52E-01		25	0.11E+02	-0.43E+02	0.51E-01	
26	0.11E+02	-0.28E+02	0.52E-01		26	0.12E+02	-0.30E+02	0.55E-01		26	0.12E+02	-0.37E+02	0.55E-01	
27	0.11E+02	-0.23E+02	0.55E-01		27	0.12E+02	-0.24E+02	0.58E-01		27	0.13E+02	-0.31E+02	0.59E-01	
28	0.12E+02	-0.17E+02	0.57E-01		28	0.12E+02	-0.18E+02	0.60E-01		28	0.13E+02	-0.25E+02	0.60E-01	
29	0.12E+02	-0.12E+02	0.58E-01		29	0.12E+02	-0.12E+02	0.61E-01		29	0.13E+02	-0.19E+02	0.62E-01	
30	0.12E+02	-0.06E+01	0.58E-01		30	0.12E+02	-0.06E+01	0.61E-01		30	0.13E+02	-0.13E+02	0.63E-01	
31	0.12E+02	0.00E+00	0.58E-01		31	0.12E+02	0.00E+00	0.62E-01		31	0.13E+02	0.00E+00	0.64E-01	
NODAL DISPLACEMENTS STEP 51					NODAL DISPLACEMENTS STEP 54					NODAL DISPLACEMENTS STEP 57				
NODE	X	Y	rZ		NODE	X	Y	rZ		NODE	X	Y	rZ	
1	0.00E+00	0.00E+00	-0.59E-01		1	0.00E+00	0.00E+00	-0.63E-01		1	0.00E+00	0.00E+00	-0.66E-01	
2	0.51E-04	-0.59E+01	-0.59E-01		2	0.68E-04	-0.63E+01	-0.63E-01		2	0.90E-04	-0.66E+01	-0.66E-01	
3	0.19E-01	-0.12E+02	-0.59E-01		3	0.31E-01	-0.13E+02	-0.62E-01		3	0.38E-01	-0.13E+02	-0.65E-01	
4	0.15E+00	-0.18E+02	-0.58E-01		4	0.17E+00	-0.19E+02	-0.61E-01		4	0.18E+00	-0.19E+02	-0.63E-01	
5	0.35E+00	-0.23E+02	-0.56E-01		5	0.38E+00	-0.25E+02	-0.59E-01		5	0.40E+00	-0.26E+02	-0.61E-01	
6	0.61E+00	-0.29E+02	-0.53E-01		6	0.65E+00	-0.31E+02	-0.56E-01		6	0.69E+00	-0.32E+02	-0.59E-01	
7	0.94E+00	-0.34E+02	-0.50E-01		7	0.10E+01	-0.36E+02	-0.53E-01		7	0.10E+01	-0.37E+02	-0.55E-01	
8	0.13E+01	-0.39E+02	-0.47E-01		8	0.14E+01	-0.41E+02	-0.50E-01		8	0.15E+01	-0.43E+02	-0.51E-01	
9	0.18E+01	-0.43E+02	-0.43E-01		9	0.19E+01	-0.46E+02	-0.45E-01		9	0.19E+01	-0.48E+02	-0.47E-01	
10	0.23E+01	-0.47E+02	-0.38E-01		10	0.24E+01	-0.50E+02	-0.40E-01		10	0.25E+01	-0.52E+02	-0.42E-01	
11	0.28E+01	-0.51E+02	-0.33E-01		11	0.30E+01	-0.54E+02	-0.34E-01		11	0.31E+01	-0.56E+02	-0.35E-01	
12	0.35E+01	-0.54E+02	-0.26E-01		12	0.37E+01	-0.57E+02	-0.27E-01		12	0.38E+01	-0.59E+02	-0.28E-01	
13	0.41E+01	-0.56E+02	-0.20E-01		13	0.43E+01	-0.59E+02	-0.20E-01		13	0.45E+01	-0.62E+02	-0.21E-01	
14	0.47E+01	-0.58E+02	-0.13E-01		14	0.49E+01	-0.61E+02	-0.14E-01		14	0.51E+01	-		







## A1.4. Example 2. Shear Wall Analysis

The specimen G-15 represent a single shear wall. The wall specimens were 3,500 mm in height, 200 mm thick and was 1,500 mm in length as shown in Figure 4-15. G-15 concrete dimensions and details of reinforcement configuration The nominal concrete compressive strength used for G15 was 40 MPa. An axial load of  $0.07 \cdot b_w \cdot l_w \cdot f'_c$  was applied at the top of the wall. #3 for vertical bars ( $f_{fu} = 1,412 \text{ MPa}$ ,  $E_f = 66.9 \text{ GPa}$ ,  $\varepsilon_{fu} = 2.11\%$ ,  $A_f = 71.3 \text{ mm}^2$ ) and spiral ties (for straight portions  $f_{fu} = 962 \text{ MPa}$ ,  $E_f = 52 \text{ GPa}$ ,  $\varepsilon_{fu} = 1.85\%$ ,  $A_f = 71.3 \text{ mm}^2$ ; for bent portions:  $f_{fu} = 500 \text{ MPa}$  and #4 for horizontal bars ( $f_{fu} = 1,392 \text{ MPa}$ ,  $E_f = 69.6 \text{ GPa}$ ,  $\varepsilon_{fu} = 2\%$ ,  $A_f = 126.7 \text{ mm}^2$ ).

### A1.4.1. Input files

#### GEOSE.TXT

The image shows two Notepad windows side-by-side. The left window, titled 'GEOSE - Notepad', contains the following text:

```

-EnterWithKeywords-
NumNodes:
35
NumElems:
34
NodeCoor:
0.0000 , 0.0000
0.0000 , 100.0000
0.0000 , 200.0000
0.0000 , 300.0000
0.0000 , 400.0000
0.0000 , 500.0000
0.0000 , 600.0000
0.0000 , 700.0000
0.0000 , 800.0000
0.0000 , 900.0000
0.0000 , 1000.0000
0.0000 , 1100.0000
0.0000 , 1200.0000
0.0000 , 1300.0000
0.0000 , 1400.0000
0.0000 , 1500.0000
0.0000 , 1600.0000
0.0000 , 1700.0000
0.0000 , 1800.0000
0.0000 , 1900.0000
0.0000 , 2000.0000
0.0000 , 2100.0000
0.0000 , 2200.0000
0.0000 , 2300.0000
0.0000 , 2400.0000
0.0000 , 2500.0000
0.0000 , 2600.0000
0.0000 , 2700.0000
0.0000 , 2800.0000
0.0000 , 2900.0000
0.0000 , 3000.0000
0.0000 , 3100.0000
0.0000 , 3200.0000
0.0000 , 3300.0000
0.0000 , 3400.0000

```

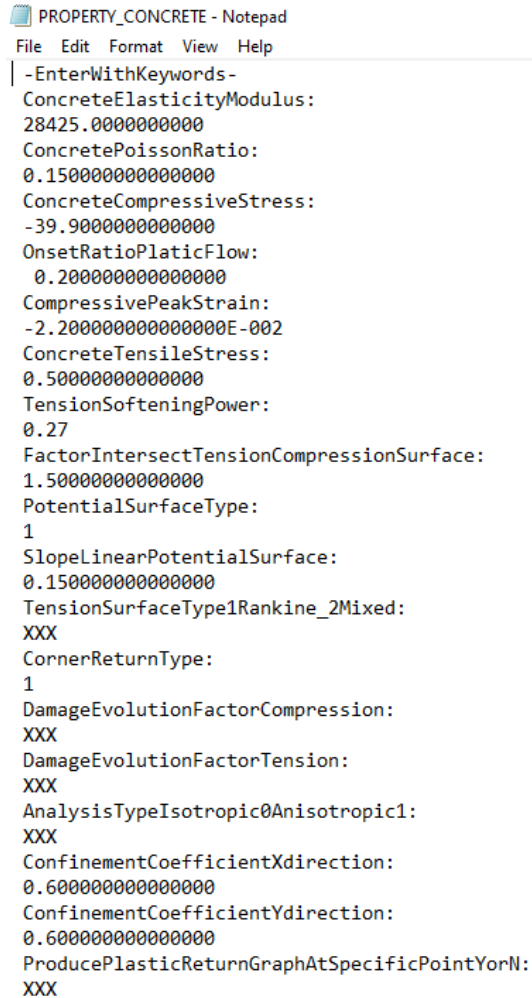
The right window, titled '\*GEOSE - Notepad', contains the following text:

```

ElemConnect:
1 , 2
2 , 3
3 , 4
4 , 5
5 , 6
6 , 7
7 , 8
8 , 9
9 , 10
10 , 11
11 , 12
12 , 13
13 , 14
14 , 15
15 , 16
16 , 17
17 , 18
18 , 19
19 , 20
20 , 21
21 , 22
22 , 23
23 , 24
24 , 25
25 , 26
26 , 27
27 , 28
28 , 29
29 , 30
30 , 31
31 , 32
32 , 33
33 , 34
34 , 35

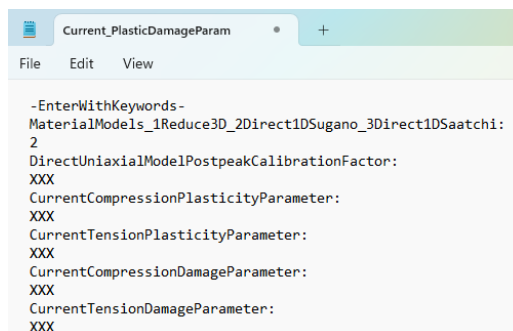
```

## PROPERTY\_CONCRETE.TXT



```
PROPERTY_CONCRETE - Notepad
File Edit Format View Help
-EnterWithKeywords-
ConcreteElasticityModulus:
28425.0000000000
ConcretePoissonRatio:
0.150000000000000
ConcreteCompressiveStress:
-39.9000000000000
OnsetRatioPlasticFlow:
0.200000000000000
CompressivePeakStrain:
-2.20000000000000E-002
ConcreteTensileStress:
0.500000000000000
TensionSofteningPower:
0.27
FactorIntersectTensionCompressionSurface:
1.500000000000000
PotentialSurfaceType:
1
SlopeLinearPotentialSurface:
0.150000000000000
TensionSurfaceType1Rankine_2Mixed:
XXX
CornerReturnType:
1
DamageEvolutionFactorCompression:
XXX
DamageEvolutionFactorTension:
XXX
AnalysisTypeIsotropic0Anisotropic1:
XXX
ConfinementCoefficientXdirection:
0.600000000000000
ConfinementCoefficientYdirection:
0.600000000000000
ProducePlasticReturnGraphAtSpecificPointYorN:
XXX
```

## Current\_PlasticDamageParam.TXT



```
Current_PlasticDamageParam
File Edit View
-EnterWithKeywords-
MaterialModels_1Reduce3D_2Direct1DSugano_3Direct1DSaatchi:
2
DirectUniaxialModelPostpeakCalibrationFactor:
XXX
CurrentCompressionPlasticityParameter:
XXX
CurrentTensionPlasticityParameter:
XXX
CurrentCompressionDamageParameter:
XXX
CurrentTensionDamageParameter:
XXX
```



## CoorLoadSE.TXT

```
CoorLoadSE - Notepad
File Edit Format View Help
-EnterWithKeywords-
EnterNewLoadCoordinatesYorN:
Y
LoadCoordinatesX-Y:
0.000000000000      3200.0000000000
LoadDirection:
1
LoadValue:
-1.000E+06
EnterNewLoadCoordinatesYorN:
N
```

## CoorBOUNDSE.TXT

```
CoorBOUNDSE - Notepad
File Edit Format View Help
-EnterWithKeywords-
EnterNewBoundaryCoordinatesYorN:
Y
BoundaryCoordinatesX-Y:
0.00  0.00
FixedDirection:
1
EnterNewBoundaryCoordinatesYorN:
Y
BoundaryCoordinatesX-Y:
0.00  0.00
FixedDirection:
2
EnterNewBoundaryCoordinatesYorN:
Y
BoundaryCoordinatesX-Y:
0.00  0.00
FixedDirection:
3
EnterNewBoundaryCoordinatesYorN:
N
```



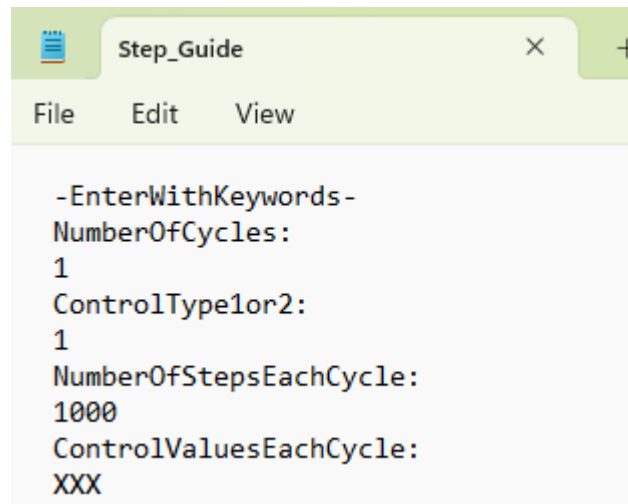
## ReinforcementSE.TXT

<pre> *ReinforcementSE - Notepad File Edit Format View Help -EnterWithKeywords- NumberOfRebarProperties:     1 NumberOfRebarsInTheGroup:     32 RebarElasticityModulusOfTheGroup:     66900 RebarYieldStressOfTheGroup:     250.0 RebarHardeningModulusOfTheGroup:     12000.0 RebarAreaAndLocationInEachGroup:     71.3 -75.00, -950.00     71.3000 75.00, -950.00     71.3000 -75.00, -900.00     71.3000 75.00, -900.00     71.3000 -75.00, -850.00     71.3000 75.00, -850.00     71.3000 -75.00, -800.00     71.3000 75.00, -800.00     71.3000 -75.00, -600.00     71.3000 75.00, -600.00     71.3000 -75.00, -400.00     71.3000 75.00, -400.00     71.3000 -75.00, -200.00     71.3000 75.00, -200.00     71.3000 -75.00, -100.00     71.3000 75.00, -100.00     71.3000 </pre>	<pre> *ReinforcementSE - Notepad File Edit Format View Help -75.00, 0.00     71.3000 75.00, 0.00     71.3000 -75.00, 200.00     71.3000 75.00, 200.00     71.3000 -75.00, 400.00     71.3000 75.00, 400.00     71.3000 -75.00, 600.00     71.3000 75.00, 600.00     71.3000 -75.00, 800.00     71.3000 75.00, 800.00     71.3000 -75.00, 850.00     71.3000 75.00, 850.00     71.3000 -75.00, 900.00     71.3000 75.00, 900.00     71.3000 -75.00, 950.00     71.3000 75.00, 950.00 ApplyAllElementsYorN: Y NumberOfRebarGroupsUsedInEachElement:     1 RebarGroupNoForEachElement:     1 EnterStirrupsYorN: Y AverageSpacingOfStirrups:     200.0 AreaOfStrirrupsWithinEachSpacing:     50.0 ReportReinforcementPlasticReturn: N </pre>
---	--

## Solution\_ParameterSE.TXT

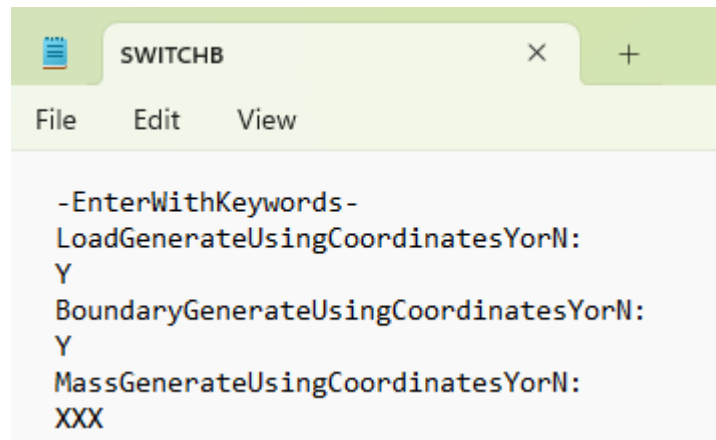
```
Solution_ParameterSE - Notepad
File Edit Format View Help
-EnterWithKeywords-
ElementType:
    1
NumIntPoint:
    3
SectionWidthIntegPoint:
    3
SectionHeightIntegPoint:
    12
AnalysisTypeNoShear0Shear1:
    0
AnalysisTypeStatic1Dynamic2Both3:
    1
ControlTypeLoad1Displacement2:
    2
ControlNodeCoordinates:
    0.000000000000000E+000,3200.00000000000
ControlNodeNumber:
    33
ControlDirection:
    1
StepSize:
    -1.000000000000000
StepNumberLimit:
    110
PlasticReturnType_1CuttingPlane_2CPP:
    1
AlgorithmStabilizationYorN:
    N
DenominatorAmplificationFactor:
    1.000000000000000
PenaltyFactorLagrangian:
    0.000000000000000E+000
PlasticReturnIterationLimit:
    1000
ViscosityRate_0Independent_1ViscoPlastic_2ViscosRegularization:
    0
ViscoPlasticRetardationTime:
    0.000000000000000E+000
ViscoPlasticTimeIncrement:
    0.000000000000000E+000
<
```

## Step\_Guide.TXT



```
-EnterWithKeywords-  
NumberOfCycles:  
1  
ControlType1or2:  
1  
NumberOfStepsEachCycle:  
1000  
ControlValuesEachCycle:  
XXX
```

## SWITCHB.TXT



```
-EnterWithKeywords-  
LoadGenerateUsingCoordinatesYorN:  
Y  
BoundaryGenerateUsingCoordinatesYorN:  
Y  
MassGenerateUsingCoordinatesYorN:  
XXX
```

## A1.3.2. Input check

```

INPUT_CHECK - Notepad
File Edit Format View Help
|*****Start Time*****
15 : 5 : 17 : 740
-----
***Enter the Names of Plasticity Related Output files***
***Choose from the below list of Possible Output files***
***List of Possible Output files***
to be addressed at ListOutputFileSE.txt
---Lamda.DAC---
---STATIC_DISPLACEMENTS.DAC---
---DEP_X.DAC---
---DEP_Y.DAC---
---ROT_Z.DAC---
---PLASTIC_RETURN_LOG_FILE.DAC---
---InstantDrawFiles---
---SURFACE_AND_RETURN.TXT---
---StressConvergenceChase---

Warning list mostly in 153
- Warning - No Intersection Rankine M-W
- Modification introduced to return to M-W directly

- Warning - No Intersection Rankine M-W
- Modification introduced to shift the Rankine surface with factor

- Warning - ro<epsilon
- In the M-W return algorithm Fp=0 is assigned directly

- Warning - ro<epsilon
- In the Rankine return algorithm Rankinep=0 is assigned directly

- Warning - ro<epsilon
- In the corner return algorithm Fp = Rankinep=0 is assigned directly

Warning - ro<epsilon
---- dFp_dro =0 is assigned ----

Warning - ro<epsilon
---- dRanFpa_dro =0 is assigned ----

Warning - K=dFp_dqp*dqp_dkapa*dkapa_dlam<0 for M-W
----K=0 is assigned ----

Warning - K_RanA= -dRanFpa_dqp*dqp_dkapa*dkapa_dlam<-100 for Rankine
---- K_RanA=-100 is assigned ----

WARNING - it_limit exceeded
-----

Number of pieces along an element 3
Number of pieces along width b of the Cross-section 3
Number of pieces along height h of the Cross-section 12

COORDINATES OF NODES
NOD X(mm) Y(mm)
1 0.000000 0.000000
2 0.000000 100.000000
3 0.000000 200.000000
4 0.000000 300.000000
5 0.000000 400.000000
6 0.000000 500.000000
7 0.000000 600.000000
8 0.000000 700.000000
9 0.000000 800.000000
10 0.000000 900.000000
11 0.000000 1000.000000
12 0.000000 1100.000000
13 0.000000 1200.000000

INPUT_CHECK - Notepad
File Edit Format View Help
14 0.000000 1300.000000
15 0.000000 1400.000000
16 0.000000 1500.000000
17 0.000000 1600.000000
18 0.000000 1700.000000
19 0.000000 1800.000000
20 0.000000 1900.000000
21 0.000000 2000.000000
22 0.000000 2100.000000
23 0.000000 2200.000000
24 0.000000 2300.000000
25 0.000000 2400.000000
26 0.000000 2500.000000
27 0.000000 2600.000000
28 0.000000 2700.000000
29 0.000000 2800.000000
30 0.000000 2900.000000
31 0.000000 3000.000000
32 0.000000 3100.000000
33 0.000000 3200.000000
34 0.000000 3300.000000
35 0.000000 3400.000000

ELEMENT I END J END LENGTH (mm)
1 1 2 100.0000000
2 2 3 100.0000000
3 3 4 100.0000000
4 4 5 100.0000000
5 5 6 100.0000000
6 6 7 100.0000000
7 7 8 100.0000000
8 8 9 100.0000000
9 9 10 100.0000000
10 10 11 100.0000000
11 11 12 100.0000000
12 12 13 100.0000000
13 13 14 100.0000000
14 14 15 100.0000000
15 15 16 100.0000000
16 16 17 100.0000000
17 17 18 100.0000000
18 18 19 100.0000000
19 19 20 100.0000000
20 20 21 100.0000000
21 21 22 100.0000000
22 22 23 100.0000000
23 23 24 100.0000000
24 24 25 100.0000000
25 25 26 100.0000000
26 26 27 100.0000000
27 27 28 100.0000000
28 28 29 100.0000000
29 29 30 100.0000000
30 30 31 100.0000000
31 31 32 100.0000000
32 32 33 100.0000000
33 33 34 100.0000000
34 34 35 100.0000000

Loads are generated using Coordinates
Load No 33 in direction 1 applied at 0.00 3200.00
-----

Boundary Conditions are generated using Coordinates
BC applied in direction 1 at 0.00 0.00
BC applied in direction 2 at 0.00 0.00
BC applied in direction 3 at 0.00 0.00
-----

Multiple-Point Constraints are imposed directly to nodes
-----

FactorIntersectTensionCompressionSurface 1.500000000000000

PROPERTIES OF SOLID

```

INPUT\_CHECK - Notepad

File Edit Format View Help

PROPERTIES OF SOLID

```
Ec      nu      fc      ft      ko      eps_c  P_type  al_p
N/mm2  N/mm2  N/mm2  N/mm2
0.2842E+05  0.15  -39.9000  0.5000  0.2000  -0.022000  1  0.150
```

```
Kbu      G
N/mm2    N/mm2
13535.7142857143  12358.6956521739
```

Factor to make sure Tension Surface and Mentrey-Willam Intersects  
1.5000000000000000

P\_type=1 Linear | P\_type=2 Higher order Potential func (al\_p=2 Quadratic)  
T\_type=1 Rankine surface | T\_type=2 Mixed surface with Cut-off

-----If T\_Type =1 -----\*\*\*Suggested numbers\*\*\*-----  
ksi\_t0= 1.45\*ft/afc | But we read si\_to | So enter approximately 1.45

-----If T\_Type =2 -----\*\*\*Suggested numbers\*\*\*-----  
ksi\_m0=-2.5/afc | But we read si\_mo | So enter approximately -2.5  
ksi\_t0= 1.45\*ft/afc | But we read si\_to | So enter approximately 1.45  
Ro\_t0 =1.05 /afc | But we read o\_to | So enter approximately 1.05  
0<mkf<1 | rate\_vkm<1

```
T_type  ksi_m0  ksi_t0  Ro_t0  n3  Fdamc  Fdamt
1  0.0000  0.0000  0.0000  0.2700  0.0000  0.000000
```

```
If ( TP_T>=0 ) then
  mcir = 0.1 * TP_T !The intersection tolerance
End If
```

```
If ( QI==0 ) then ! No modification needed
  QI=0
  modif_qst = 1.0
else if ( QI==1 .and. TP_T==0 ) then ! It is Ok to have no intersection
- Return to Mentrey - Willam
  QI=1
  modif_qst = 1.0
else if ( QI==1 .and. TP_T>0 ) then ! It is Ok to shift the Rankine
surface
  QI=0
  modif_qst = modif_qst2
End If
```

Isotropic Analysis Type 0 | Anisotropic Analysis Type 1  
IA\_type = 0

gama1= 0.6000000000000000

gama2= 0.6000000000000000

Output NOT generated for any Plastic return scenario for the Concrete Beam

Number of Reinforcement Groups with different Properties 1  
Number of Reinforcement Bars in Group 1 is 32

-----For the Reinforcement Group-----

```
Er = 66900.000000000000
sig_y = 250.000000000000
Hr = 12000.000000000000
```

Number of total re-bars within the Cross-section 32

Properties of the Reinforcement

```
Mem = 1
Num Location x Location y Area
1 -75.0000 -950.0000 .7130E+02
2 75.0000 -950.0000 .7130E+02
3 -75.0000 -900.0000 .7130E+02
4 75.0000 -900.0000 .7130E+02
5 -75.0000 -850.0000 .7130E+02
```

INPUT\_CHECK - Notepad

File Edit Format View Help

```
6 75.0000 -850.0000 .7130E+02
7 -75.0000 -800.0000 .7130E+02
8 75.0000 -800.0000 .7130E+02
9 -75.0000 -600.0000 .7130E+02
10 75.0000 -600.0000 .7130E+02
11 -75.0000 -400.0000 .7130E+02
12 75.0000 -400.0000 .7130E+02
13 -75.0000 -200.0000 .7130E+02
14 75.0000 -200.0000 .7130E+02
15 -75.0000 -100.0000 .7130E+02
16 75.0000 -100.0000 .7130E+02
17 -75.0000 0.0000 .7130E+02
18 75.0000 0.0000 .7130E+02
19 -75.0000 200.0000 .7130E+02
20 75.0000 200.0000 .7130E+02
21 -75.0000 400.0000 .7130E+02
22 75.0000 400.0000 .7130E+02
23 -75.0000 600.0000 .7130E+02
24 75.0000 600.0000 .7130E+02
25 -75.0000 800.0000 .7130E+02
26 75.0000 800.0000 .7130E+02
27 -75.0000 850.0000 .7130E+02
28 75.0000 850.0000 .7130E+02
29 -75.0000 900.0000 .7130E+02
30 75.0000 900.0000 .7130E+02
31 -75.0000 950.0000 .7130E+02
32 75.0000 950.0000 .7130E+02
```

```
Mem = 2
Num Location x Location y Area
1 -75.0000 -950.0000 .7130E+02
2 75.0000 -950.0000 .7130E+02
3 -75.0000 -900.0000 .7130E+02
4 75.0000 -900.0000 .7130E+02
5 -75.0000 -850.0000 .7130E+02
6 75.0000 -850.0000 .7130E+02
7 -75.0000 -800.0000 .7130E+02
8 75.0000 -800.0000 .7130E+02
9 -75.0000 -600.0000 .7130E+02
10 75.0000 -600.0000 .7130E+02
11 -75.0000 -400.0000 .7130E+02
12 75.0000 -400.0000 .7130E+02
13 -75.0000 -200.0000 .7130E+02
14 75.0000 -200.0000 .7130E+02
15 -75.0000 -100.0000 .7130E+02
16 75.0000 -100.0000 .7130E+02
17 -75.0000 0.0000 .7130E+02
18 75.0000 0.0000 .7130E+02
19 -75.0000 200.0000 .7130E+02
20 75.0000 200.0000 .7130E+02
21 -75.0000 400.0000 .7130E+02
22 75.0000 400.0000 .7130E+02
23 -75.0000 600.0000 .7130E+02
24 75.0000 600.0000 .7130E+02
25 -75.0000 800.0000 .7130E+02
26 75.0000 800.0000 .7130E+02
27 -75.0000 850.0000 .7130E+02
28 75.0000 850.0000 .7130E+02
29 -75.0000 900.0000 .7130E+02
30 75.0000 900.0000 .7130E+02
31 -75.0000 950.0000 .7130E+02
32 75.0000 950.0000 .7130E+02
```

```
Mem = 3
Num Location x Location y Area
1 -75.0000 -950.0000 .7130E+02
2 75.0000 -950.0000 .7130E+02
3 -75.0000 -900.0000 .7130E+02
4 75.0000 -900.0000 .7130E+02
5 -75.0000 -850.0000 .7130E+02
6 75.0000 -850.0000 .7130E+02
7 -75.0000 -800.0000 .7130E+02
8 75.0000 -800.0000 .7130E+02
9 -75.0000 -600.0000 .7130E+02
10 75.0000 -600.0000 .7130E+02
11 -75.0000 -400.0000 .7130E+02
12 75.0000 -400.0000 .7130E+02
```













INPUT\_CHECK - Notepad

```

File Edit Format View Help
29 -75.0000 900.0000 .7130E+02
30 75.0000 900.0000 .7130E+02
31 -75.0000 950.0000 .7130E+02
32 75.0000 950.0000 .7130E+02
-----
Mem = 34
Num Location x Location y Area
1 -75.0000 -950.0000 .7130E+02
2 75.0000 -950.0000 .7130E+02
3 -75.0000 -900.0000 .7130E+02
4 75.0000 -900.0000 .7130E+02
5 -75.0000 -850.0000 .7130E+02
6 75.0000 -850.0000 .7130E+02
7 -75.0000 -800.0000 .7130E+02
8 75.0000 -800.0000 .7130E+02
9 -75.0000 -600.0000 .7130E+02
10 75.0000 -600.0000 .7130E+02
11 -75.0000 -400.0000 .7130E+02
12 75.0000 -400.0000 .7130E+02
13 -75.0000 -200.0000 .7130E+02
14 75.0000 -200.0000 .7130E+02
15 -75.0000 -100.0000 .7130E+02
16 75.0000 -100.0000 .7130E+02
17 -75.0000 0.0000 .7130E+02
18 75.0000 0.0000 .7130E+02
19 -75.0000 200.0000 .7130E+02
20 75.0000 200.0000 .7130E+02
21 -75.0000 400.0000 .7130E+02
22 75.0000 400.0000 .7130E+02
23 -75.0000 600.0000 .7130E+02
24 75.0000 600.0000 .7130E+02
25 -75.0000 800.0000 .7130E+02
26 75.0000 800.0000 .7130E+02
27 -75.0000 850.0000 .7130E+02
28 75.0000 850.0000 .7130E+02
29 -75.0000 900.0000 .7130E+02
30 75.0000 900.0000 .7130E+02
31 -75.0000 950.0000 .7130E+02
32 75.0000 950.0000 .7130E+02
-----
*****

```

Output NOT generated for any Plastic return scenario for the Reinforcement

CROSS-SECTIONAL PROPERTIES including Reinforcement

```

Mem EA EIx
mm2 mm4
1 .12E+11 .3833E+16
2 .12E+11 .3833E+16
3 .12E+11 .3833E+16
4 .12E+11 .3833E+16
5 .12E+11 .3833E+16
6 .12E+11 .3833E+16
7 .12E+11 .3833E+16
8 .12E+11 .3833E+16
9 .12E+11 .3833E+16
10 .12E+11 .3833E+16
11 .12E+11 .3833E+16
12 .12E+11 .3833E+16
13 .12E+11 .3833E+16
14 .12E+11 .3833E+16
15 .12E+11 .3833E+16
16 .12E+11 .3833E+16
17 .12E+11 .3833E+16
18 .12E+11 .3833E+16
19 .12E+11 .3833E+16
20 .12E+11 .3833E+16
21 .12E+11 .3833E+16
22 .12E+11 .3833E+16
23 .12E+11 .3833E+16
24 .12E+11 .3833E+16
25 .12E+11 .3833E+16
26 .12E+11 .3833E+16
27 .12E+11 .3833E+16

```

INPUT\_CHECK - Notepad

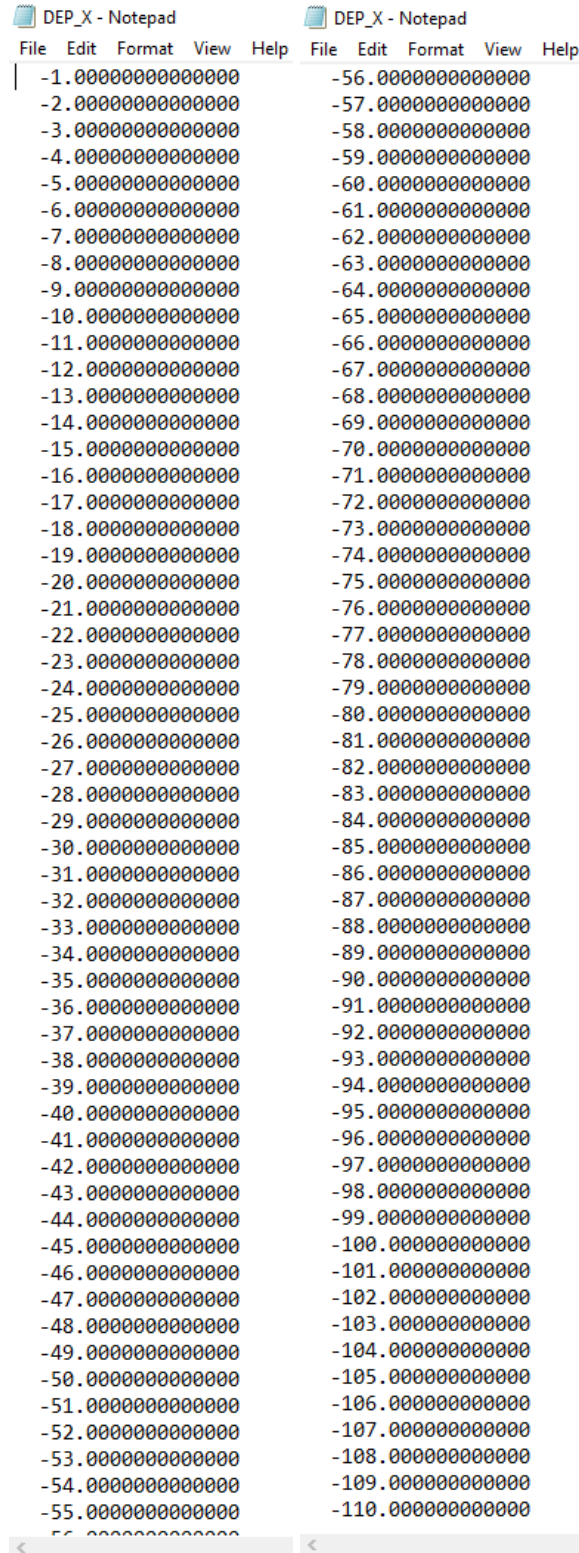
```

File Edit Format View Help
28 .12E+11 .3833E+16
29 .12E+11 .3833E+16
30 .12E+11 .3833E+16
31 .12E+11 .3833E+16
32 .12E+11 .3833E+16
33 .12E+11 .3833E+16
34 .12E+11 .3833E+16
-----
BOUNDARY CONDITIONS
FIXED NODE FIXED DIRECTION
1 GLOBAL X DIRECTION
1 GLOBAL Y DIRECTION
1 GLOBAL AROUND Z
-----
NODAL LOADS
NODE LOADING TYPE DIRECTION P M
N Nmm
33 CONCENTRATED P GLOBAL X -.1000E+07
-----
CONSTANT NODAL LOADS
NODE LOADING TYPE DIRECTION CP CM
N Nmm
36 CONCENTRATED P GLOBAL X -.7744E+07
-----
Analysis type: 0 for No Shear| 1 for Including Shear
S_type = 0 selected
-----
Analysis type: 1 for Static only| 2 for Dynamic only| 3 for Both
1 selected
-----
The results are produced for 0 number of files
-----
MaterialModels_1Reduce3D_2Direct1DSugano_3Direct1DSaatchi 2
DirectUniaxialModelPostpeakCalibrationFactor 4.000000000000000
CurrentCompressionPlasticityParameter 0.000000000000000E+000
CurrentTensionPlasticityParameter 0.000000000000000E+000
CurrentCompressionDamageParameter 0.000000000000000E+000
CurrentTensionDamageParameter 0.000000000000000E+000
-----
Analysis Control type: Enter 1 for Load Control or Enter 2 for Displacement Control
2
The control node number 33
Enter the direction: Enter 1 for X Enter 2 for Y Enter 3 for Z Rot
Control direction = 1 selected
Enter the step increment size -1.000000000000000
How many steps do you want to continue 110
-----
Plastic return type: 1 for Cutting_plane | 2 for Closest Point Projection | 3 for Premono-willam
1
Iteration limit to terminate plastic return 1000
Enter| 0 rate-independent | 1 visco-plastic | 2 viscous regularization
0
Enter GlobalAlgorithm_ErrorMargin 9.99999974752427E-007
-----
Enter PlasticityAlgorithm_ErrorMargin 9.999999747378752E-005
Identify First Point of Yield Yes or No NNNNNN

```

### A1.3.3. Output files

#### DEP\_X



```
DEP_X - Notepad DEP_X - Notepad
File Edit Format View Help File Edit Format View Help
-1.000000000000000 -56.0000000000000
-2.000000000000000 -57.0000000000000
-3.000000000000000 -58.0000000000000
-4.000000000000000 -59.0000000000000
-5.000000000000000 -60.0000000000000
-6.000000000000000 -61.0000000000000
-7.000000000000000 -62.0000000000000
-8.000000000000000 -63.0000000000000
-9.000000000000000 -64.0000000000000
-10.000000000000000 -65.0000000000000
-11.000000000000000 -66.0000000000000
-12.000000000000000 -67.0000000000000
-13.000000000000000 -68.0000000000000
-14.000000000000000 -69.0000000000000
-15.000000000000000 -70.0000000000000
-16.000000000000000 -71.0000000000000
-17.000000000000000 -72.0000000000000
-18.000000000000000 -73.0000000000000
-19.000000000000000 -74.0000000000000
-20.000000000000000 -75.0000000000000
-21.000000000000000 -76.0000000000000
-22.000000000000000 -77.0000000000000
-23.000000000000000 -78.0000000000000
-24.000000000000000 -79.0000000000000
-25.000000000000000 -80.0000000000000
-26.000000000000000 -81.0000000000000
-27.000000000000000 -82.0000000000000
-28.000000000000000 -83.0000000000000
-29.000000000000000 -84.0000000000000
-30.000000000000000 -85.0000000000000
-31.000000000000000 -86.0000000000000
-32.000000000000000 -87.0000000000000
-33.000000000000000 -88.0000000000000
-34.000000000000000 -89.0000000000000
-35.000000000000000 -90.0000000000000
-36.000000000000000 -91.0000000000000
-37.000000000000000 -92.0000000000000
-38.000000000000000 -93.0000000000000
-39.000000000000000 -94.0000000000000
-40.000000000000000 -95.0000000000000
-41.000000000000000 -96.0000000000000
-42.000000000000000 -97.0000000000000
-43.000000000000000 -98.0000000000000
-44.000000000000000 -99.0000000000000
-45.000000000000000 -100.0000000000000
-46.000000000000000 -101.0000000000000
-47.000000000000000 -102.0000000000000
-48.000000000000000 -103.0000000000000
-49.000000000000000 -104.0000000000000
-50.000000000000000 -105.0000000000000
-51.000000000000000 -106.0000000000000
-52.000000000000000 -107.0000000000000
-53.000000000000000 -108.0000000000000
-54.000000000000000 -109.0000000000000
-55.000000000000000 -110.0000000000000
```

# DEP\_Y

DEP_Y - Notepad					DEP_Y - Notepad				
File	Edit	Format	View	Help	File	Edit	Format	View	Help
0.	218519680305488				19.	6621067396785			
0.	518898208538416				20.	0310249912512			
0.	834691946124427				20.	4006837286345			
1.	16423269520403				20.	7709738895640			
1.	50687942655538				21.	1419320792486			
1.	91245850377095				21.	5133136206663			
2.	26190277792058				21.	8850352341584			
2.	61122513802492				22.	2575355001006			
2.	96064108167956				22.	6307303866503			
3.	31221653529996				23.	0042016706845			
3.	66714240848648				23.	3785348946866			
4.	02244673853188				23.	7537331768058			
4.	37674478602862				24.	1293767170414			
4.	72959997356000				24.	5055128412899			
5.	08086005290600				24.	8822902755629			
5.	42947337669351				25.	2597014412948			
5.	77537458941942				25.	6374149575646			
6.	11900269237763				26.	0153189477945			
6.	46213924042944				26.	3934026469557			
6.	80679077870283				26.	7716556261095			
7.	15305990987902				27.	1501194528335			
7.	49909763373337				27.	5289887922537			
7.	84503672467597				27.	9085639274088			
8.	19053213519114				28.	2883969023304			
8.	53670881293302				28.	6684911192073			
8.	88271513145134				29.	0489299342776			
9.	22937795744367				29.	4297204585102			
9.	57704335299749				29.	8108283972329			
9.	92546854505216				30.	1922141754196			
10.	2751046913317				30.	5742802295096			
10.	6266273411891				30.	9565047936304			
10.	9794374357234				31.	3388436410433			
11.	3337445878683				31.	7213559187849			
11.	6895708082919				32.	1041452644031			
12.	0465593644482				32.	4871893953242			
12.	4034055169366				32.	8705937119761			
12.	7608740901255				33.	2543470980973			
13.	1193561935343				33.	6383970895862			
13.	4783267673234				34.	0227062294655			
13.	8372974400300				34.	4073720798893			
14.	1967652570996				34.	7923677187577			
14.	5565627955638				35.	1775166859781			
14.	9173358718584				35.	5635131809629			
15.	2788812801688				35.	9490859453659			
15.	6411307292984				36.	3353191807010			
16.	0037167933535				36.	7217641345933			
16.	3669246475697				37.	1084707044926			
16.	7304067802865				37.	4954419826592			
17.	0946781979885				37.	8827115157613			
17.	4599837066177				38.	2702434492033			
17.	8257694529631				38.	6580123447799			
18.	1921632020512				39.	0460120527855			
18.	5590270293273				39.	4342529137323			
18.	9261276269649				39.	8227109536175			
19.	2939037319713				40.	2114048816135			
19.	6621067396785								





# Lamda

File	Edit	Format	View	Help	File	Edit	Format	View	Help
3.982005907311454E-002					0.340522257417418				
5.080139008028385E-002					0.343609643124238				
6.445748375818050E-002					0.346611689847167				
7.840020228290967E-002					0.349680214717752				
9.231142724173143E-002					0.352671453981940				
0.103020446153680					0.355652450129328				
0.119735843718785					0.358628080192758				
0.135563067957928					0.361675189102138				
0.149346194325985					0.364646662148347				
0.160837654778506					0.367609823909248				
0.170164792561552					0.370646550086432				
0.177738159006342					0.373596148506860				
0.184341392123987					0.376524859317402				
0.190243514889691					0.379450365180499				
0.195565317787944					0.382467879630854				
0.200564530253549					0.385401464084738				
0.205304362696819					0.388319358420917				
0.209847342223502					0.391232877052369				
0.214209581636490					0.394143006954067				
0.218458165967153					0.397051676297510				
0.222611020017062					0.399958133799057				
0.226649264218344					0.402956239324109				
0.230586165544964					0.405859276382893				
0.234440875019924					0.408751510042680				
0.238257480496113					0.411640103072555				
0.241979332172259					0.414521057474038				
0.245668438075724					0.417394097892638				
0.249284696263131					0.420265643032409				
0.252880644463160					0.423243363489574				
0.256433187804460					0.426125145363064				
0.259965758020640					0.428997719983080				
0.263446122616993					0.431869451020288				
0.266900919400100					0.434738536552065				
0.270311709506325					0.437600217330650				
0.273695637513041					0.440460690403632				
0.277050672849261					0.443313346864982				
0.280405449244699					0.446162047690757				
0.283711351424538					0.449009415224833				
0.287007557866514					0.451856860802963				
0.290257910451655					0.454699210828123				
0.293531590605185					0.457538006248303				
0.296742676811883					0.460492788195595				
0.299953813784457					0.463230154702307				
0.303160256347790					0.466176092947282				
0.306365253341552					0.469028068321368				
0.309507957011752					0.471869751256229				
0.312682913027877					0.474702795043067				
0.315802793839501					0.477530804803337				
0.318959576894199					0.480355179316140				
0.322097815126249					0.483179154254799				
0.325165899293692					0.486002400832918				
0.328285608667896					0.488825740846721				
0.331342870874925					0.491647266916209				
0.334388970108233					0.494468279268447				
0.337485206024001					0.497288779847998				

**ROT\_Z**

File	Edit	Format	View	Help	File	Edit	Format	View	Help
3.803596383179463E-004					2.324009220481702E-002				
7.773052265675081E-004					2.365930484430896E-002				
1.195069954801453E-003					2.407876764717057E-002				
1.628054246214983E-003					2.449943349918759E-002				
2.074950958742188E-003					2.492030730300726E-002				
2.578227713989379E-003					2.534162098221235E-002				
3.041898527820628E-003					2.576326202159368E-002				
3.503133532920932E-003					2.618634606454093E-002				
3.958895646900580E-003					2.660968283725183E-002				
4.408386713619710E-003					2.703329659046787E-002				
4.849369238866603E-003					2.745837408487219E-002				
5.280545593234314E-003					2.788379597765035E-002				
5.704130053785160E-003					2.830958582766597E-002				
6.122507871906779E-003					2.873581251660740E-002				
6.535315538173454E-003					2.916333908208263E-002				
6.943419225011917E-003					2.959100385940897E-002				
7.346311587708159E-003					3.001881675755776E-002				
7.745847906194367E-003					3.044675722333236E-002				
8.144453323069257E-003					3.087481468303964E-002				
8.544487334214116E-003					3.130300096836441E-002				
8.945666300861814E-003					3.173136846019267E-002				
9.345694878860293E-003					3.216079981448846E-002				
9.744396372787264E-003					3.259031037102447E-002				
1.014214804013641E-002					3.301999679005529E-002				
1.054061628895735E-002					3.344995393100526E-002				
1.093827818485636E-002					3.388021283792842E-002				
1.133659580013368E-002					3.431079050487274E-002				
1.173571253151984E-002					3.474170818768904E-002				
1.213569498111468E-002					3.517368510431224E-002				
1.253694553613878E-002					3.560571523818248E-002				
1.294037819162807E-002					3.603783456903853E-002				
1.334511470004814E-002					3.647007341180955E-002				
1.375149326417089E-002					3.690248286474072E-002				
1.415910393001158E-002					3.733513749709879E-002				
1.456771534930596E-002					3.776806106493069E-002				
1.497592650539974E-002					3.820130318400027E-002				
1.538462787403991E-002					3.863487574322802E-002				
1.579385260778612E-002					3.906874772117307E-002				
1.620358420384663E-002					3.950290814349021E-002				
1.661297792288903E-002					3.993743560549726E-002				
1.702305888618517E-002					4.037232159471089E-002				
1.743300431742686E-002					4.080819382836297E-002				
1.784405178441419E-002					4.124348736115317E-002				
1.825598445672829E-002					4.167977719398252E-002				
1.866867757466232E-002					4.211614687130896E-002				
1.908123429647478E-002					4.255263509402370E-002				
1.949471175463560E-002					4.298933750121790E-002				
1.990814429459132E-002					4.342630405917753E-002				
2.032267231432626E-002					4.386355233430175E-002				
2.073821316337110E-002					4.430106236665621E-002				
2.115381093385593E-002					4.473882090319010E-002				
2.157046010248949E-002					4.517683726569766E-002				
2.198717023147676E-002					4.561511482121647E-002				
2.240405015754217E-002					4.605362782293029E-002				
2.282201687900056E-002					4.649237171425984E-002				
2.324009220481702E-002									

# STATIC\_DISPLACEMENTS

STATIC\_DISPLACEMENTS - Notepad

File	Edit	Format	View	Help
NODAL DISPLACEMENTS STEP 1				
NODE	X	Y	rZ	
1	0.00E+00	0.00E+00	0.00E+00	
2	-0.23E-02	0.31E-01	0.47E-04	
3	-0.92E-02	0.60E-01	0.90E-04	
4	-0.20E-01	0.87E-01	0.13E-03	
5	-0.35E-01	0.11E+00	0.17E-03	
6	-0.54E-01	0.13E+00	0.20E-03	
7	-0.76E-01	0.15E+00	0.23E-03	
8	-0.10E+00	0.17E+00	0.26E-03	
9	-0.13E+00	0.18E+00	0.29E-03	
10	-0.16E+00	0.20E+00	0.31E-03	
11	-0.19E+00	0.20E+00	0.32E-03	
12	-0.22E+00	0.21E+00	0.34E-03	
13	-0.26E+00	0.22E+00	0.35E-03	
14	-0.29E+00	0.22E+00	0.35E-03	
15	-0.33E+00	0.22E+00	0.36E-03	
16	-0.36E+00	0.22E+00	0.36E-03	
17	-0.40E+00	0.22E+00	0.36E-03	
18	-0.44E+00	0.22E+00	0.37E-03	
19	-0.47E+00	0.22E+00	0.37E-03	
20	-0.51E+00	0.22E+00	0.37E-03	
21	-0.55E+00	0.22E+00	0.37E-03	
22	-0.58E+00	0.22E+00	0.37E-03	
23	-0.62E+00	0.22E+00	0.37E-03	
24	-0.66E+00	0.22E+00	0.38E-03	
25	-0.70E+00	0.22E+00	0.38E-03	
26	-0.73E+00	0.22E+00	0.38E-03	
27	-0.77E+00	0.22E+00	0.38E-03	
28	-0.81E+00	0.22E+00	0.38E-03	
29	-0.85E+00	0.22E+00	0.38E-03	
30	-0.89E+00	0.22E+00	0.38E-03	
31	-0.92E+00	0.22E+00	0.38E-03	
32	-0.96E+00	0.22E+00	0.38E-03	
33	-0.10E+01	0.22E+00	0.38E-03	
34	-0.10E+01	0.22E+00	0.38E-03	
35	-0.11E+01	0.22E+00	0.38E-03	

NODAL DISPLACEMENTS STEP 2				
NODE	X	Y	rZ	
1	0.00E+00	0.00E+00	0.00E+00	
2	-0.41E-02	0.59E-01	0.81E-04	
3	-0.16E-01	0.12E+00	0.16E-03	
4	-0.35E-01	0.17E+00	0.23E-03	
5	-0.62E-01	0.22E+00	0.30E-03	
6	-0.95E-01	0.26E+00	0.37E-03	
7	-0.13E+00	0.31E+00	0.43E-03	
8	-0.18E+00	0.35E+00	0.48E-03	
9	-0.23E+00	0.38E+00	0.53E-03	
10	-0.29E+00	0.41E+00	0.58E-03	
11	-0.35E+00	0.44E+00	0.62E-03	
12	-0.41E+00	0.46E+00	0.66E-03	
13	-0.48E+00	0.48E+00	0.69E-03	
14	-0.55E+00	0.50E+00	0.71E-03	
15	-0.62E+00	0.51E+00	0.73E-03	
16	-0.69E+00	0.51E+00	0.74E-03	
17	-0.77E+00	0.52E+00	0.75E-03	
18	-0.84E+00	0.52E+00	0.76E-03	
19	-0.92E+00	0.52E+00	0.76E-03	
20	-0.10E+01	0.52E+00	0.76E-03	
21	-0.11E+01	0.52E+00	0.77E-03	
22	-0.11E+01	0.52E+00	0.77E-03	
23	-0.12E+01	0.52E+00	0.77E-03	
24	-0.13E+01	0.52E+00	0.77E-03	
25	-0.14E+01	0.52E+00	0.77E-03	
26	-0.15E+01	0.52E+00	0.77E-03	
27	-0.15E+01	0.52E+00	0.77E-03	
28	-0.16E+01	0.52E+00	0.78E-03	
29	-0.17E+01	0.52E+00	0.78E-03	

STATIC\_DISPLACEMENTS - Notepad

File	Edit	Format	View	Help
NODAL DISPLACEMENTS STEP 3				
NODE	X	Y	rZ	
1	0.00E+00	0.00E+00	0.00E+00	
2	-0.55E-02	0.83E-01	0.11E-03	
3	-0.22E-01	0.16E+00	0.22E-03	
4	-0.49E-01	0.24E+00	0.32E-03	
5	-0.85E-01	0.31E+00	0.42E-03	
6	-0.13E+00	0.38E+00	0.51E-03	
7	-0.19E+00	0.44E+00	0.59E-03	
8	-0.25E+00	0.50E+00	0.68E-03	
9	-0.32E+00	0.56E+00	0.75E-03	
10	-0.40E+00	0.61E+00	0.82E-03	
11	-0.49E+00	0.65E+00	0.89E-03	
12	-0.58E+00	0.69E+00	0.95E-03	
13	-0.67E+00	0.73E+00	0.10E-02	
14	-0.78E+00	0.76E+00	0.10E-02	
15	-0.88E+00	0.78E+00	0.11E-02	
16	-0.99E+00	0.80E+00	0.11E-02	
17	-0.11E+01	0.82E+00	0.11E-02	
18	-0.12E+01	0.83E+00	0.12E-02	
19	-0.13E+01	0.83E+00	0.12E-02	
20	-0.15E+01	0.83E+00	0.12E-02	
21	-0.16E+01	0.83E+00	0.12E-02	
22	-0.17E+01	0.83E+00	0.12E-02	
23	-0.18E+01	0.83E+00	0.12E-02	
24	-0.19E+01	0.83E+00	0.12E-02	
25	-0.20E+01	0.83E+00	0.12E-02	
26	-0.22E+01	0.83E+00	0.12E-02	
27	-0.23E+01	0.83E+00	0.12E-02	
28	-0.24E+01	0.83E+00	0.12E-02	
29	-0.25E+01	0.83E+00	0.12E-02	
30	-0.26E+01	0.83E+00	0.12E-02	
31	-0.28E+01	0.83E+00	0.12E-02	
32	-0.29E+01	0.83E+00	0.12E-02	
33	-0.30E+01	0.83E+00	0.12E-02	
34	-0.31E+01	0.83E+00	0.12E-02	
35	-0.32E+01	0.83E+00	0.12E-02	

NODAL DISPLACEMENTS STEP 4				
NODE	X	Y	rZ	
1	0.00E+00	0.00E+00	0.00E+00	
2	-0.69E-02	0.10E+00	0.14E-03	
3	-0.27E-01	0.20E+00	0.27E-03	
4	-0.61E-01	0.30E+00	0.40E-03	
5	-0.11E+00	0.39E+00	0.52E-03	
6	-0.17E+00	0.48E+00	0.64E-03	
7	-0.23E+00	0.56E+00	0.75E-03	
8	-0.32E+00	0.64E+00	0.86E-03	
9	-0.41E+00	0.72E+00	0.96E-03	
10	-0.51E+00	0.78E+00	0.11E-02	
11	-0.62E+00	0.85E+00	0.11E-02	
12	-0.73E+00	0.91E+00	0.12E-02	
13	-0.86E+00	0.96E+00	0.13E-02	
14	-0.99E+00	1.0E+01	0.14E-02	
15	-0.11E+01	0.10E+01	0.14E-02	
16	-0.13E+01	0.11E+01	0.15E-02	
17	-0.14E+01	0.11E+01	0.15E-02	
18	-0.16E+01	0.11E+01	0.15E-02	
19	-0.17E+01	0.11E+01	0.16E-02	
20	-0.19E+01	0.12E+01	0.16E-02	
21	-0.21E+01	0.12E+01	0.16E-02	

STATIC\_DISPLACEMENTS - Notepad

File	Edit	Format	View	Help
NODAL DISPLACEMENTS STEP 5				
NODE	X	Y	rZ	
1	0.00E+00	0.00E+00	0.00E+00	
2	-0.83E-02	0.12E+00	0.17E-03	
3	-0.33E-01	0.24E+00	0.32E-03	
4	-0.73E-01	0.36E+00	0.48E-03	
5	-0.13E+00	0.47E+00	0.63E-03	
6	-0.20E+00	0.58E+00	0.77E-03	
7	-0.28E+00	0.68E+00	0.90E-03	
8	-0.38E+00	0.78E+00	0.10E-02	
9	-0.49E+00	0.87E+00	0.12E-02	
10	-0.61E+00	0.95E+00	0.13E-02	
11	-0.74E+00	1.0E+01	0.14E-02	
12	-0.88E+00	0.11E+01	0.15E-02	
13	-0.10E+01	0.12E+01	0.16E-02	
14	-0.12E+01	0.12E+01	0.17E-02	
15	-0.14E+01	0.13E+01	0.17E-02	
16	-0.15E+01	0.14E+01	0.18E-02	
17	-0.17E+01	0.14E+01	0.19E-02	
18	-0.19E+01	0.14E+01	0.19E-02	
19	-0.21E+01	0.15E+01	0.20E-02	
20	-0.23E+01	0.15E+01	0.20E-02	
21	-0.25E+01	0.15E+01	0.20E-02	
22	-0.27E+01	0.15E+01	0.20E-02	
23	-0.29E+01	0.15E+01	0.21E-02	
24	-0.31E+01	0.15E+01	0.21E-02	
25	-0.33E+01	0.15E+01	0.21E-02	
26	-0.35E+01	0.15E+01	0.21E-02	
27	-0.38E+01	0.15E+01	0.21E-02	
28	-0.40E+01	0.15E+01	0.21E-02	
29	-0.42E+01	0.15E+01	0.21E-02	
30	-0.44E+01	0.15E+01	0.21E-02	
31	-0.46E+01	0.15E+01	0.21E-02	
32	-0.48E+01	0.15E+01	0.21E-02	
33	-0.50E+01	0.15E+01	0.21E-02	
34	-0.52E+01	0.15E+01	0.21E-02	
35	-0.54E+01	0.15E+01	0.21E-02	

NODAL DISPLACEMENTS STEP 6				
NODE	X	Y	rZ	
1	0.00E+00	0.00E+00	0.00E+00	
2	-0.93E-02	0.14E+00	0.19E-03	
3	-0.37E-01	0.28E+00	0.36E-03	
4	-0.82E-01	0.41E+00	0.54E-03	
5	-0.14E+00	0.53E+00	0.70E-03	
6	-0.22E+00	0.65E+00	0.86E-03	
7	-0.32E+00	0.77E+00	0.10E-02	
8	-0.43E+00	0.88E+00	0.12E-02	
9	-0.55E+00	0.99E+00	0.13E-02	
10	-0.69E+00	1.1E+01	0.14E-02	
11	-0.84E+00	0.12E+01	0.16E-02	
12	-0.10E+01	0.13E+01	0.17E-02	
13	-0.12E+01	0.14E+01	0.18E-02	
14	-0.14E+01	0.15E+01	0.19E-02	

STATIC\_DISPLACEMENTS - Notepad

File	Edit	Format	View	Help
14	-0.14E+01	0.15E+01	0.19E-02	
15	-0.16E+01	0.15E+01	0.20E-02	
16	-0.18E+01	0.16E+01	0.21E-02	
17	-0.20E+01	0.17E+01	0.22E-02	
18	-0.22E+01	0.17E+01	0.23E-02	
19	-0.24E+01	0.18E+01	0.24E-02	
20	-0.27E+01	0.18E+01	0.24E-02	
21	-0.29E+01	0.19E+01	0.25E-02	
22	-0.32E+01	0.19E+01	0.25E-02	
23	-0.34E+01	0.19E+01	0.25E-02	
24	-0.37E+01	0.19E+01	0.26E-02	
25	-0.39E+01	0.19E+01	0.26E-02	
26	-0.42E+01	0.19E+01	0.26E-02	
27	-0.45E+01	0.19E+01	0.26E-02	
28	-0.47E+01	0.19E+01	0.26E-02	
29	-0.50E+01	0.19E+01	0.26E-02	
30	-0.52E+01	0.19E+01	0.26E-02	
31	-0.55E+01	0.19E+01	0.26E-02	
32	-0.57E+01	0.19E+01	0.26E-02	
33	-0.60E+01	0.19E+01	0.26E-02	
34	-0.63E+01	0.19E+01	0.26E-02	
35	-0.65E+01	0.19E+01	0.26E-02	
-----				
NODAL DISPLACEMENTS			STEP	7
NODE	X	Y	rZ	
1	0.00E+00	0.00E+00	0.00E+00	
2	-0.11E-01	0.16E+00	0.21E-03	
3	-0.42E-01	0.32E+00	0.42E-03	
4	-0.94E-01	0.47E+00	0.62E-03	
5	-0.17E+00	0.61E+00	0.81E-03	
6	-0.26E+00	0.75E+00	0.99E-03	
7	-0.36E+00	0.89E+00	0.12E-02	
8	-0.49E+00	0.10E+01	0.13E-02	
9	-0.63E+00	0.11E+01	0.15E-02	
10	-0.79E+00	0.13E+01	0.17E-02	
11	-0.96E+00	0.14E+01	0.18E-02	
12	-0.12E+01	0.15E+01	0.20E-02	
13	-0.14E+01	0.16E+01	0.21E-02	
14	-0.16E+01	0.17E+01	0.22E-02	
15	-0.18E+01	0.18E+01	0.23E-02	
16	-0.20E+01	0.18E+01	0.24E-02	
17	-0.23E+01	0.19E+01	0.26E-02	
18	-0.25E+01	0.20E+01	0.26E-02	
19	-0.28E+01	0.21E+01	0.27E-02	
20	-0.31E+01	0.21E+01	0.28E-02	
21	-0.34E+01	0.22E+01	0.29E-02	
22	-0.37E+01	0.22E+01	0.29E-02	
23	-0.40E+01	0.22E+01	0.30E-02	
24	-0.43E+01	0.23E+01	0.30E-02	
25	-0.46E+01	0.23E+01	0.30E-02	
26	-0.49E+01	0.23E+01	0.30E-02	
27	-0.52E+01	0.23E+01	0.30E-02	
28	-0.55E+01	0.23E+01	0.30E-02	
29	-0.58E+01	0.23E+01	0.30E-02	
30	-0.61E+01	0.23E+01	0.30E-02	
31	-0.64E+01	0.23E+01	0.30E-02	
32	-0.67E+01	0.23E+01	0.30E-02	
33	-0.70E+01	0.23E+01	0.30E-02	
34	-0.73E+01	0.23E+01	0.30E-02	
35	-0.76E+01	0.23E+01	0.30E-02	
-----				
NODAL DISPLACEMENTS			STEP	8
NODE	X	Y	rZ	
1	0.00E+00	0.00E+00	0.00E+00	
2	-0.12E-01	0.18E+00	0.24E-03	
3	-0.48E-01	0.36E+00	0.48E-03	
4	-0.11E+00	0.53E+00	0.70E-03	
5	-0.19E+00	0.69E+00	0.92E-03	
6	-0.29E+00	0.85E+00	0.11E-02	

STATIC\_DISPLACEMENTS - Notepad

File	Edit	Format	View	Help
7	-0.41E+00	0.10E+01	0.13E-02	
8	-0.56E+00	0.12E+01	0.15E-02	
9	-0.72E+00	0.13E+01	0.17E-02	
10	-0.90E+00	0.14E+01	0.19E-02	
11	-0.11E+01	0.16E+01	0.21E-02	
12	-0.13E+01	0.17E+01	0.22E-02	
13	-0.15E+01	0.18E+01	0.24E-02	
14	-0.18E+01	0.19E+01	0.25E-02	
15	-0.20E+01	0.20E+01	0.27E-02	
16	-0.23E+01	0.21E+01	0.28E-02	
17	-0.26E+01	0.22E+01	0.29E-02	
18	-0.29E+01	0.23E+01	0.30E-02	
19	-0.32E+01	0.23E+01	0.31E-02	
20	-0.35E+01	0.24E+01	0.32E-02	
21	-0.38E+01	0.25E+01	0.33E-02	
22	-0.42E+01	0.25E+01	0.34E-02	
23	-0.45E+01	0.26E+01	0.34E-02	
24	-0.49E+01	0.26E+01	0.35E-02	
25	-0.52E+01	0.26E+01	0.35E-02	
26	-0.56E+01	0.26E+01	0.35E-02	
27	-0.59E+01	0.26E+01	0.35E-02	
28	-0.62E+01	0.26E+01	0.35E-02	
29	-0.66E+01	0.26E+01	0.35E-02	
30	-0.69E+01	0.26E+01	0.35E-02	
31	-0.73E+01	0.26E+01	0.35E-02	
32	-0.76E+01	0.26E+01	0.35E-02	
33	-0.80E+01	0.26E+01	0.35E-02	
34	-0.84E+01	0.26E+01	0.35E-02	
35	-0.87E+01	0.26E+01	0.35E-02	
-----				
NODAL DISPLACEMENTS			STEP	9
NODE	X	Y	rZ	
1	0.00E+00	0.00E+00	0.00E+00	
2	-0.14E-01	0.21E+00	0.28E-03	
3	-0.55E-01	0.41E+00	0.54E-03	
4	-0.12E+00	0.60E+00	0.79E-03	
5	-0.21E+00	0.79E+00	0.10E-02	
6	-0.33E+00	0.96E+00	0.13E-02	
7	-0.47E+00	0.11E+01	0.15E-02	
8	-0.63E+00	0.13E+01	0.17E-02	
9	-0.81E+00	0.15E+01	0.19E-02	
10	-0.10E+01	0.16E+01	0.21E-02	
11	-0.12E+01	0.17E+01	0.23E-02	
12	-0.15E+01	0.19E+01	0.25E-02	
13	-0.17E+01	0.20E+01	0.27E-02	
14	-0.20E+01	0.21E+01	0.28E-02	
15	-0.23E+01	0.22E+01	0.30E-02	
16	-0.26E+01	0.24E+01	0.31E-02	
17	-0.29E+01	0.25E+01	0.32E-02	
18	-0.32E+01	0.26E+01	0.34E-02	
19	-0.36E+01	0.26E+01	0.35E-02	
20	-0.39E+01	0.27E+01	0.36E-02	
21	-0.43E+01	0.28E+01	0.37E-02	
22	-0.47E+01	0.29E+01	0.38E-02	
23	-0.51E+01	0.29E+01	0.39E-02	
24	-0.54E+01	0.29E+01	0.39E-02	
25	-0.58E+01	0.30E+01	0.39E-02	
26	-0.62E+01	0.30E+01	0.39E-02	
27	-0.66E+01	0.30E+01	0.39E-02	
28	-0.70E+01	0.30E+01	0.40E-02	
29	-0.74E+01	0.30E+01	0.40E-02	
30	-0.78E+01	0.30E+01	0.40E-02	
31	-0.82E+01	0.30E+01	0.40E-02	
32	-0.86E+01	0.30E+01	0.40E-02	
33	-0.90E+01	0.30E+01	0.40E-02	
34	-0.94E+01	0.30E+01	0.40E-02	
35	-0.98E+01	0.30E+01	0.40E-02	
-----				
NODAL DISPLACEMENTS			STEP	10
NODE	X	Y	rZ	

STATIC\_DISPLACEMENTS - Notepad

File	Edit	Format	View	Help
1	0.00E+00	0.00E+00	0.00E+00	
2	-0.16E-01	0.24E+00	0.31E-03	
3	-0.62E-01	0.47E+00	0.61E-03	
4	-0.14E+00	0.68E+00	0.89E-03	
5	-0.24E+00	0.89E+00	0.12E-02	
6	-0.37E+00	0.11E+01	0.14E-02	
7	-0.52E+00	0.13E+01	0.17E-02	
8	-0.70E+00	0.15E+01	0.19E-02	
9	-0.91E+00	0.16E+01	0.21E-02	
10	-0.11E+01	0.18E+01	0.23E-02	
11	-0.14E+01	0.19E+01	0.26E-02	
12	-0.16E+01	0.21E+01	0.28E-02	
13	-0.19E+01	0.22E+01	0.29E-02	
14	-0.22E+01	0.24E+01	0.31E-02	
15	-0.25E+01	0.25E+01	0.33E-02	
16	-0.29E+01	0.26E+01	0.34E-02	
17	-0.32E+01	0.27E+01	0.36E-02	
18	-0.36E+01	0.28E+01	0.37E-02	
19	-0.40E+01	0.29E+01	0.39E-02	
20	-0.44E+01	0.30E+01	0.40E-02	
21	-0.48E+01	0.31E+01	0.41E-02	
22	-0.52E+01	0.32E+01	0.42E-02	
23	-0.56E+01	0.32E+01	0.43E-02	
24	-0.60E+01	0.33E+01	0.43E-02	
25	-0.65E+01	0.33E+01	0.44E-02	
26	-0.69E+01	0.33E+01	0.44E-02	
27	-0.74E+01	0.33E+01	0.44E-02	
28	-0.78E+01	0.33E+01	0.44E-02	
29	-0.82E+01	0.33E+01	0.44E-02	
30	-0.87E+01	0.33E+01	0.44E-02	
31	-0.91E+01	0.33E+01	0.44E-02	
32	-0.96E+01	0.33E+01	0.44E-02	
33	-0.10E+02	0.33E+01	0.44E-02	
34	-0.10E+02	0.33E+01	0.44E-02	
35	-0.11E+02	0.33E+01	0.44E-02	
-----				
NODAL DISPLACEMENTS			STEP	11
NODE	X	Y	rZ	
1	0.00E+00	0.00E+00	0.00E+00	
2	-0.18E-01	0.27E+00	0.35E-03	
3	-0.69E-01	0.53E+00	0.69E-03	
4	-0.15E+00	0.77E+00	0.10E-02	
5	-0.27E+00	0.10E+01	0.13E-02	
6	-0.41E+00	0.12E+01	0.16E-02	
7	-0.59E+00	0.14E+01	0.19E-02	
8	-0.79E+00	0.16E+01	0.21E-02	
9	-0.10E+01	0.18E+01	0.24E-02	
10	-0.13E+01	0.20E+01	0.26E-02	
11	-0.15E+01	0.22E+01	0.28E-02	
12	-0.18E+01	0.23E+01	0.30E-02	
13	-0.21E+01	0.25E+01	0.32E-02	
14	-0.25E+01	0.26E+01	0.34E-02	
15	-0.28E+01	0.28E+01	0.36E-02	
16	-0.32E+01	0.29E+01	0.38E-02	
17	-0.36E+01	0.30E+01	0.39E-02	
18	-0.40E+01	0.31E+01	0.41E-02	
19	-0.44E+01	0.32E+01	0.42E-02	
20	-0.48E+01	0.33E+01	0.44E-02	
21	-0.53E+01	0.34E+01	0.45E-02	
22	-0.57E+01	0.35E+01	0.46E-02	
23	-0.62E+01	0.36E+01	0.47E-02	
24	-0.67E+01	0.36E+01	0.47E-02	
25	-0.71E+01	0.36E+01	0.48E-02	
26	-0.76E+01	0.37E+01	0.48E-02	
27	-0.81E+01	0.37E+01	0.48E-02	
28	-0.86E+01	0.37E+01	0.48E-02	
29	-0.91E+01	0.37E+01	0.48E-02	
30	-0.95E+01	0.37E+01	0.48E-02	
31	-0.10E+02	0.37E+01	0.48E-02	
32	-0.11E+02	0.37E+01	0.48E-02	













# APPENDIX 2

## ReinCon3D6DOF User Guide

### A2.1. Data entry and solutions

Program accepts a group of input data files with .TXT extension and creates another group of output files with .DAC extension.

#### A2.1.1. Input files for static 3D model

The input files required for the 3D model analyses are:

- **Auto\_Mesh\_SOLID**
- **Auto\_Mesh\_STIRRUP**
- **coorGEO\_BAR**
- **PROPERTY\_CONCRETE**
- **CoorLoad**
- **DirectEndConditions**
- **PROPERTY\_BAR**
- **PROPERTY\_SOLID**
- **SEC\_BAR**
- **Solution\_Parameters**
- **Step\_Guide**
- **SWITCH\_A**
- **SWITCH\_B**

Longitudinal reinforcements are defined in **coorGEO\_BAR** by specifying the coordinates at both ends of the rebar while the stirrups (**Auto\_Mesh\_STIRRUPS**) are defined by the spacing between them. It is possible to define regions of stirrups. The dimensions of the reinforcements are inputted in **SEC\_BAR**.

Note that while inputting the rebars are registered and after comes the stirrups.

NumberOfBarsWithFollowingSection(Ordered) means the total number of one group of reinforcements in all the elements.

### **A2.1.2. Output files for static 3D model**

The output files created after the 3D model static analysis

- **Bar\_Coor\_Ini**
- **Bar\_Strain**
- **Bar\_Stress**
- **file1**
- **file2**
- **fileline1**
- **hile1**
- **hloads**
- **hnodes**
- **hsupports**
- **Solid\_Coor\_Ini**
- **Solid\_StrainXX, Solid\_StrainXY, Solid\_StrainXZ, Solid\_StrainYY, Solid\_StrainYZ, Solid\_StrainZZ**
- **INPUT\_CHECK**
- **Lamda**
- **U\_Y**

### **A2.2. Input files**

- **DirectEndConditions: Support Information**

-EnterWithKeywords-

FirstEnd\_0Free\_1Fixed\_2Pinned\_3Roller\_4Sliding:

SecondEnd\_0Free\_1Fixed\_2Pinned\_3Roller\_4Sliding:

EnterNewPlaneRestraintYorN:

EnterNewLineRestraintYorN:  
EnterNewPlaneConstraintYorN:  
EnterNewLineConstraintYorN:  
LineConstraint-X-Y-Z-CoordinatesAtBothEnds:  
LineConstraintDirection:  
LineConstraintMasterX-Y-Z-Coordinates:  
EnterNewLineConstraintYorN:

- **CoorLoad.TXT: Nodal loads**

-EnterWithKeywords-

EnterNewLoadCoordinatesYorN: Y for a new load  
LoadCoordinatesX-Y-Z: Coordinate at which the node is applied  
LoadDirection: Direction of the nodal loading (1 or 2)  
LoadValue: Value of the nodal loading  
EnterNewLoadCoordinatesYorN: If there is no loading information put N

- **Auto\_Mesh\_SOLID.TXT: Structural geometry information**

-EnterWithKeywords-

NumberOfPiecesSeperatesWidthX:  
EnterWidthsX:  
NumberOfSeperationsEachWidthX:  
NumberOfPiecesSeperatesWidthY:  
EnterWidthsY:  
NumberOfSeperationsEachWidthY:  
NumberOfPiecesSeperatesWidthZ:  
EnterWidthsZ:  
NumberOfSeperationsEachWidthZ:

CrossSectionTrim\_YorN:

CoverTrim\_YorN:

- **Auto\_Mesh\_STIRRUP.TXT: Stirrup geometry information**

-EnterWithKeywords-

NumberOfStirrupRegions:

BeginningHeightToEndHeightEachRegion:

LowerBoundOfSpacingEachRegion:

- **PROPERTY\_SOLID.TXT: Properties of the concrete bulk**

-EnterWithKeywords-

ConcreteElasticityModulus:

ConcretePoissonRatio:

ConcreteCompressiveStress:

OnsetRatioPlasticFlow:

CompressivePeakStrain:

ConcreteTensileStress:

TensionSofteningPower:

FactorIntersectTensionCompressionSurface:

PotentialSurfaceType:

SlopeLinearPotentialSurface:

TensionSurfaceType1Rankine\_2Mixed:

CornerReturnType:

DamageEvolutionFactorCompression:

DamageEvolutionFactorTension:

AnalysisTypeIsotropic0Anisotropic1:

ProducePlasticReturnGraphAtSpecificPointYorN:

- **PROPERTY\_BAR.TXT: Properties of the reinforcements**

-EnterWithKeywords-

NumberOfBarsWithFollowingProperty(Ordered):

BarElasticityModulus:

BarYieldStressLimit:

BarHardeningModulus:

NumberOfBarsWithFollowingProperty(Ordered):

BarElasticityModulus:

BarYieldStressLimit:

BarHardeningModulus:

- **SEC\_BAR.TXT: Cross section of the reinforcements**

-EnterWithKeywords-

NumberOfBarsWithFollowingSection(Ordered):

WidthAndHeight:

NumberOfBarsWithFollowingSection(Ordered):

WidthAndHeight:

- **Step\_Guide.TXT: Setting the number of cycles**

-EnterWithKeywords-

NumberOfCycles:

ControlType1or2:

NumberOfStepsEachCycle:

- **SWITCH\_A.TXT: Activating option to consider during analysis**

-EnterWithKeywords-

AutoGenerateSolidMeshYorN:

AutoWrapYorN(RequiresAutoGenerateSolid):

ConnectRebarsUsingCoordinatesYorN:

AutoStirrupYorN(RequiresAutoGenerateSolid):

- **SWITCH\_B.TXT: Activating option to consider during analysis**

-EnterWithKeywords-

LoadGenerateUsingCoordinatesYorN:

BoundaryGenerateUsingCoordinatesYorN:

MPCGenerateUsingCoordinatesYorN:

DirectEndConditionsYorN:

- **Solution\_ParameterSE.TXT: Parameters needed for running**

-EnterWithKeywords-

ElementType:

PrevRunYorNorS:

NumberOfIntegrationPointsSolid:

NumberOfIntegrationPointsReinforcement:

NumberOfIntegrationPointsWrap:

ControlTypeLoad1Displacement2:

ControlNodeCoordinates:

ControlDirection:

StepSize:

StepNumberLimit:

HardeningType\_1volum\_2mixed:

HardeningUpdateLevel\_1GlobalStep\_2GlobalIteration\_3PlasticIteration:

PlasticReturnType\_1CuttingPlane\_2CPP:

TangentModulusType\_0Elastic\_1Plastic:

AlgorithmStabilizationYorN:

PlasticReturnIterationLimit:



ViscosityRate\_0Independent\_1ViscoPlastic\_2ViscosRegularization:

NumberOfStepsExtractGraphicalOutput:

AmplificationFactorForGraphicalOutput:

NumberOfCollectedOutputFiles:

CollectedOutputFileNames:

GlobalAlgorithm\_ErrorMargin:

PlasticityAlgorithm\_ErrorMargin:

IdentifyFirstPointofYieldYorN:

### **A2.3. Example 1. Beam Analysis**

The beam ISO30-1 is 200 mm wide and 300 mm high, as shown in Figure 4-8 to Figure 4-10, it is supported on a span of 3000 mm and is subjected to two equal loads symmetrically placed about the mid-span. The modulus of elasticity of concrete is 32 GPa and  $f_c=44$  MPa. Yielding stress for steel rebars is taken as 480 MPa, the ultimate strength is taken as 600 MPa and the modulus of elasticity is taken as 200 GPa. Conventional steel stirrups (10 mm diameter) is used in the non-constant moment zones, to prevent shear failure. The diameter of the reinforcement is maintained constant (19.1 mm diameter) and this beam is reinforced by two identical rebar as resumed in Figure 4-8.

#### **A1.3.1. Input files**

**Auto\_Mesh\_SOLID.TXT**

```
Auto_Mesh_SOLID - Notepad
File Edit Format View Help
-EnterWithKeywords-
NumberOfPiecesSeperatesWidthX:
4
EnterWidthsX:
25.0,75.0,75.0,25.0
NumberOfSeperationsEachWidthX:
1,1,1,1
NumberOfPiecesSeperatesWidthY:
4
EnterWidthsY:
25.0,125.0,125.0,25.0
NumberOfSeperationsEachWidthY:
1,1,1,1
NumberOfPiecesSeperatesWidthZ:
1
EnterWidthsZ:
3000.0
NumberOfSeperationsEachWidthZ:
30
CrossSectionTrim_YorN:
XXX
CrossSectionTrimRadiusXYplane:
XXX
CoverTrim_YorN:
XXX
CoverTrimRadiusXYplane:
XXX
```

**Auto\_Mesh\_STIRRUP.TXT**

```
Auto_Mesh_STIRRUP - Notepad
File Edit Format View Help
-EnterWithKeywords-
NumberOfStirrupRegions:
2
BeginningHeightToEndHeightEachRegion:
100.0,1000.0
2000.0,2900.0
LowerBoundOfSpacingEachRegion:
100.0
100.0
```

**CoorLoad.TXT**

```
CoorLoadSE
File Edit View
| -EnterWithKeywords-
EnterNewLoadCoordinatesYorN:
Y
LoadCoordinatesX-Y:
1000.000000000000,0.000000000000
LoadDirection:
2
LoadValue:
-0.4000E+06
EnterNewLoadCoordinatesYorN:
Y
LoadCoordinatesX-Y:
2000.000000000000,0.000000000000
LoadDirection:
2
LoadValue:
-0.4000E+06
EnterNewLoadCoordinatesYorN:
N
```

### SWITCH\_A.TXT

```
SWITCH_A - Notepad
File Edit Format View Help
-EnterWithKeywords-
AutoGenerateSolidMeshYorN:
Y
AutoWrapYorN(RequiresAutoGenerateSolid):
N
ConnectRebarsUsingCoordinatesYorN:
Y
AutoStirrupYorN(RequiresAutoGenerateSolid):
Y
```

### SWITCH\_B.TXT

```
SWITCH_B - Notepad
File Edit Format View Help
| -EnterWithKeywords-
LoadGenerateUsingCoordinatesYorN:
Y
BoundaryGenerateUsingCoordinatesYorN:
XXX
MPCGenerateUsingCoordinatesYorN:
XXX
DirectEndConditionsYorN:
Y
```

### DirectEndConditions.TXT

In order to analyze the system, the finite element solver requires boundary conditions to be defined. Boundary conditions should be able to provide equilibrium to the system. Additional to the conventional boundary conditions, an option to plane restrain the structure was introduced to be able to extend the member beyond supports providing an additional bond length. In this example, a constraint was used too to distribute the load between the nodes. This was done after it was constated that the tip load was causing stress concentration around a node hence convergence issues. The load node was the master coordinate the slave being a plane or line around it.

```
DirectEndConditions - Notepad
File Edit Format View Help
-EnterWithKeywords-
FirstEnd_1Fixed_2Pinned:
XXX
SecondEnd_0Free_1Fixed_2Sliding_3Roller:
XXX
EnterNewPlaneRestraintYorN:
Y
ApplyPlaneRestraint_NormalAxis_1X_2Y_3Z:
3
CoordinateOfRestraintPlaneOnSelectedAxis:
0
PlaneRestraintDirection:
1
EnterNewPlaneRestraintYorN:
Y
ApplyPlaneRestraint_NormalAxis_1X_2Y_3Z:
3
CoordinateOfRestraintPlaneOnSelectedAxis:
0
PlaneRestraintDirection:
2
EnterNewPlaneRestraintYorN:
Y
ApplyPlaneRestraint_NormalAxis_1X_2Y_3Z:
```

DirectEndConditions - Notepad

```
File Edit Format View Help
ApplyPlaneRestrstraint_NormalAxis_1X_2Y_3Z:
3
CoordinateOfRestrstraintPlaneOnSelectedAxis:
3000
PlaneRestrstraintDirection:
2
EnterNewLineRestrstraintYorN:
Y
LineRestrstraint-X-Y-Z-CoordinatesAtBothEnds:
0.0,150.0,0.0,200.0,150.0,0.0
LineRestrstraintDirection:
3
EnterNewPlaneConstraintYorN:
Y
ApplyPlaneConstraint_NormalAxis_1X_2Y_3Z:
3
CoordinateOfConstraintPlaneOnSelectedAxis:
1000.0
PlaneConstraintDirection:
2
PlaneConstraintMasterX-Y-Z-Coordinates:
100.0,300.0,1000.0
EnterNewPlaneConstraintYorN:
Y
ApplyPlaneConstraint_NormalAxis_1X_2Y_3Z:
3
CoordinateOfConstraintPlaneOnSelectedAxis:
2000.0
PlaneConstraintDirection:
2
PlaneConstraintMasterX-Y-Z-Coordinates:
100.0,300.0,2000.0
EnterNewLineConstraintYorN:
XXX
LineConstraint-X-Y-Z-CoordinatesAtBothEnds:
XXX
LineConstraintDirection:
XXX
LineConstraintMasterX-Y-Z-Coordinates:
XXX
```

## PROPERTY\_SOLID.TXT

```
PROPERTY_SOLID - Notepad
File Edit Format View Help
-EnterWithKeywords-
ConcreteElasticityModulus:
32.000E+03
ConcretePoissonRatio:
0.15
ConcreteCompressiveStress:
-46.0
OnsetRatioPlasticFlow:
0.005
CompressivePeakStrain:
-0.0022
ConcreteTensileStress:
2.0
TensionSofteningPower:
0.27
FactorIntersectTensionCompressionSurface:
1.5
PotentialSurfaceType:
1
SlopeLinearPotentialSurface:
0.15
OrderNonlinearPotentialSurface:
XXX
LimitVolumetricStressRatioForLinearKinkPotentialSurface:
XXX
ReductionRatePotentialSurfaceCoeFA:
XXX
ReductionRatePotentialSurfaceCoeFB:
XXX
SlopeBilinearPotentialSurface:
XXX
ReductionRatePotentialSurfaceCoeFB:
XXX
LimitVolumetricStressRatioForLinearKinkPotentialSurface:
XXX
OrderNonlinearPotentialSurface:
XXX
ReductionRatePotentialSurfaceCoeFB:
XXX
LimitVolumetricStressRatioForLinearKinkPotentialSurface:
XXX
TensionSurfaceType1Rankine_2Mixed:
XXX
MixedSurfaceCornerControlwith1KsiOr2Ro:
XXX
MixedSurfaceVolumetricStressLimit:
XXX
MixedSurfaceDeviatoricStressLimit:
XXX
TensionCornerVolumetricStressLimit:
XXX
TensionCornerDeviatoricStressLimit:
XXX
MixedSurfaceTetaAtCornerDeviatoricStressLimit:
XXX
CornerReturnTypeAssociative0orNon1:
XXX
DamageEvolutionFactorCompression:
XXX
DamageEvolutionFactorTension:
XXX
AnalysisTypeIsotropic0Anisotropic1:
XXX
SixAnisotropicDamageCoefficients:
XXX
ConfinementCoefficientYdirection:
XXX
ConfinementCoefficientZdirection:
XXX
ProducePlasticReturnGraphAtSpecificPointYorN:
XXX
Teta_select1:
XXX
Teta_select2:
XXX
ksi_select:
XXX
ShowIterationsInStressReturnYorN:
XXX
NumberOfGraphs:
XXX
ProducePlasticReturnGraphAtSpecificTimeYorN:
XXX
GlobalAnalysisStepNo:
XXX
```

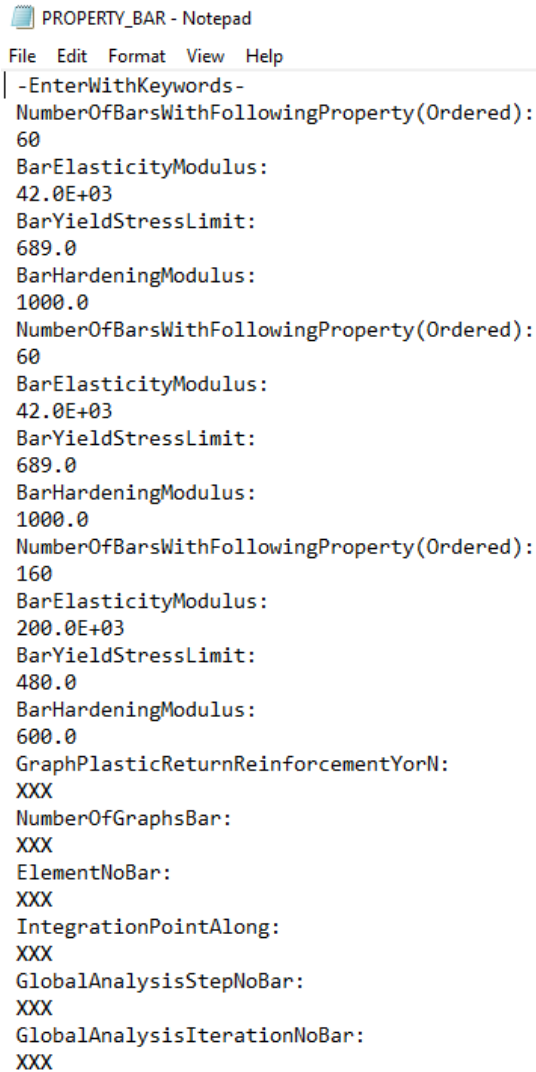
## coordGEO\_BAR.TXT

```
coordGEO_BAR - Notepad
File Edit Format View Help
-EnterWithKeywords-
EnterNewBarCoordinatesYorN:
Y
ConnectionType_0Direct_1Continuous:
1
X-Y-Z-CoordinatesAtBothEnds:
25.0,25.0,0.0,25.0,25.0,3000.0
EnterNewBarCoordinatesYorN:
Y
ConnectionType_0Direct_1Continuous:
1
X-Y-Z-CoordinatesAtBothEnds:
175.0,25.0,0.0,175.0,25.0,3000.0
EnterNewBarCoordinatesYorN:
Y
ConnectionType_0Direct_1Continuous:
1
X-Y-Z-CoordinatesAtBothEnds:
25.0,275.0,0.0,25.0,275.0,3000.0
EnterNewBarCoordinatesYorN:
Y
ConnectionType_0Direct_1Continuous:
1
X-Y-Z-CoordinatesAtBothEnds:
175.0,275.0,0.0,175.0,275.0,3000.0
EnterNewBarCoordinatesYorN:
N
```

## SEC\_BAR.TXT

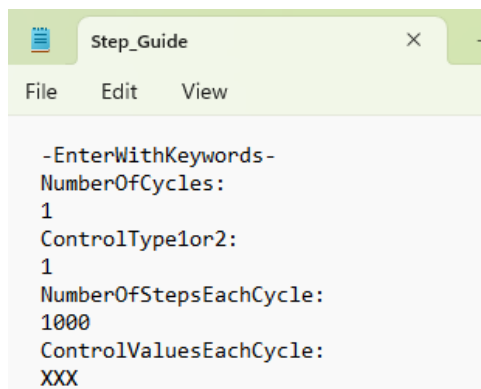
```
SEC_BAR - Notepad
File Edit Format View Help
-EnterWithKeywords-
NumberOfBarsWithFollowingSection(Ordered):
60
WidthAndHeight:
17.0,17.0
NumberOfBarsWithFollowingSection(Ordered):
60
WidthAndHeight:
8.90,8.90
NumberOfBarsWithFollowingSection(Ordered):
160
WidthAndHeight:
8.90,8.90
```

## PROPERTY\_BAR.TXT



PROPERTY\_BAR - Notepad  
File Edit Format View Help  
-EnterWithKeywords-  
NumberOfBarsWithFollowingProperty(Ordered):  
60  
BarElasticityModulus:  
42.0E+03  
BarYieldStressLimit:  
689.0  
BarHardeningModulus:  
1000.0  
NumberOfBarsWithFollowingProperty(Ordered):  
60  
BarElasticityModulus:  
42.0E+03  
BarYieldStressLimit:  
689.0  
BarHardeningModulus:  
1000.0  
NumberOfBarsWithFollowingProperty(Ordered):  
160  
BarElasticityModulus:  
200.0E+03  
BarYieldStressLimit:  
480.0  
BarHardeningModulus:  
600.0  
GraphPlasticReturnReinforcementYorN:  
XXX  
NumberOfGraphsBar:  
XXX  
ElementNoBar:  
XXX  
IntegrationPointAlong:  
XXX  
GlobalAnalysisStepNoBar:  
XXX  
GlobalAnalysisIterationNoBar:  
XXX

## Step\_Guide.TXT



Step\_Guide  
File Edit View  
-EnterWithKeywords-  
NumberOfCycles:  
1  
ControlType1or2:  
1  
NumberOfStepsEachCycle:  
1000  
ControlValuesEachCycle:  
XXX



## Solution\_Parameter.TXT

```
Solution_Parameters - Notepad
File Edit Format View Help
-EnterWithKeywords-
ElementType:
1
MeshGeneratedAutomaticallyYorN:
Y
PrevRunYorNorS:
N
LoadStepToStructureUpdate:
10
NumberOfIntegrationPointsSolid:
3
NumberOfIntegrationPointsReinforcement:
2
NumberOfIntegrationPointsWrap:
2
ControlTypeLoad1Displacement2:|
2
ControlNodeCoordinates:
100.0,300.0,1000.0
ControlNodeNumber:
XXX
ControlDirection:
2
StepSize:
-0.4
StepNumberLimit:
140
HardeningType_1volum_2mixed:
1
HardeningUpdateLevel_1GlobalStep_2GlobalIteration_3PlasticIteration:
1
<
```

```
Solution_Parameters - Notepad
File Edit Format View Help
PlasticReturnType_1CuttingPlane_2CPP:
1
TangentModulusType_0Elastic_1Plastic:
1
AlgorithmStabilizationYorN:
N
DenominatorAmplificationFactor:
XXX
PenaltyFactorLagrangian:
XXX
WeightinFactorForGeneralizedMidPointIntegration:
XXX
PlasticReturnIterationLimit:
1000
ViscosityRate_0Independent_1ViscoPlastic_2ViscosRegularization:
0
ViscoPlasticRetardationTime:
XXX
ViscoPlasticTimeIncrement:
XXX
ViscosRegularizationGlobalAlgorithmIterationLimit:
XXX
NumberOfStepsExtractGraphicalOutput:
10
AmplificationFactorForGraphicalOutput:
100.0
NumberOfCollectedOutputFiles:
2
CollectedOutputFileNames:
Lamda.DAC
U_Y.DAC
```



Mesh-size limit = 7.74193548387097

-----

Mesh-size limit = 3.87096774193548

Connectivity of Reinforcement beams using Coordinates

Element Connected between Nodes	7	and	32
Element Connected between Nodes	32	and	57
Element Connected between Nodes	57	and	82
Element Connected between Nodes	82	and	107
Element Connected between Nodes	107	and	132
Element Connected between Nodes	132	and	157
Element Connected between Nodes	157	and	182
Element Connected between Nodes	182	and	207
Element Connected between Nodes	207	and	232
Element Connected between Nodes	232	and	257
Element Connected between Nodes	257	and	282
Element Connected between Nodes	282	and	307
Element Connected between Nodes	307	and	332
Element Connected between Nodes	332	and	357
Element Connected between Nodes	357	and	382
Element Connected between Nodes	382	and	407
Element Connected between Nodes	407	and	432
Element Connected between Nodes	432	and	457
Element Connected between Nodes	457	and	482
Element Connected between Nodes	482	and	507
Element Connected between Nodes	507	and	532
Element Connected between Nodes	532	and	557
Element Connected between Nodes	557	and	582
Element Connected between Nodes	582	and	607
Element Connected between Nodes	607	and	632
Element Connected between Nodes	632	and	657
Element Connected between Nodes	657	and	682
Element Connected between Nodes	682	and	707
Element Connected between Nodes	707	and	732
Element Connected between Nodes	732	and	757
Element Connected between Nodes	9	and	34
Element Connected between Nodes	34	and	59
Element Connected between Nodes	59	and	84
Element Connected between Nodes	84	and	109
Element Connected between Nodes	109	and	134
Element Connected between Nodes	134	and	159
Element Connected between Nodes	159	and	184
Element Connected between Nodes	184	and	209
Element Connected between Nodes	209	and	234
Element Connected between Nodes	234	and	259
Element Connected between Nodes	259	and	284
Element Connected between Nodes	284	and	309
Element Connected between Nodes	309	and	334
Element Connected between Nodes	334	and	359
Element Connected between Nodes	359	and	384
Element Connected between Nodes	384	and	409
Element Connected between Nodes	409	and	434
Element Connected between Nodes	434	and	459
Element Connected between Nodes	459	and	484
Element Connected between Nodes	484	and	509

Element Connected between Nodes	484	and	509
Element Connected between Nodes	509	and	534
Element Connected between Nodes	534	and	559
Element Connected between Nodes	559	and	584
Element Connected between Nodes	584	and	609
Element Connected between Nodes	609	and	634
Element Connected between Nodes	634	and	659
Element Connected between Nodes	659	and	684
Element Connected between Nodes	684	and	709
Element Connected between Nodes	709	and	734
Element Connected between Nodes	734	and	759
Element Connected between Nodes	17	and	42
Element Connected between Nodes	42	and	67
Element Connected between Nodes	67	and	92
Element Connected between Nodes	92	and	117
Element Connected between Nodes	117	and	142
Element Connected between Nodes	142	and	167
Element Connected between Nodes	167	and	192
Element Connected between Nodes	192	and	217
Element Connected between Nodes	217	and	242
Element Connected between Nodes	242	and	267
Element Connected between Nodes	267	and	292
Element Connected between Nodes	292	and	317
Element Connected between Nodes	317	and	342
Element Connected between Nodes	342	and	367
Element Connected between Nodes	367	and	392
Element Connected between Nodes	392	and	417
Element Connected between Nodes	417	and	442
Element Connected between Nodes	442	and	467
Element Connected between Nodes	467	and	492
Element Connected between Nodes	492	and	517
Element Connected between Nodes	517	and	542
Element Connected between Nodes	542	and	567
Element Connected between Nodes	567	and	592
Element Connected between Nodes	592	and	617
Element Connected between Nodes	617	and	642
Element Connected between Nodes	642	and	667
Element Connected between Nodes	667	and	692
Element Connected between Nodes	692	and	717
Element Connected between Nodes	717	and	742
Element Connected between Nodes	742	and	767
Element Connected between Nodes	19	and	44
Element Connected between Nodes	44	and	69
Element Connected between Nodes	69	and	94
Element Connected between Nodes	94	and	119
Element Connected between Nodes	119	and	144
Element Connected between Nodes	144	and	169
Element Connected between Nodes	169	and	194
Element Connected between Nodes	194	and	219
Element Connected between Nodes	219	and	244
Element Connected between Nodes	244	and	269
Element Connected between Nodes	269	and	294
Element Connected between Nodes	294	and	319
Element Connected between Nodes	319	and	344
Element Connected between Nodes	344	and	369

```

Element Connected between Nodes 369 and 394
Element Connected between Nodes 394 and 419
Element Connected between Nodes 419 and 444
Element Connected between Nodes 444 and 469
Element Connected between Nodes 469 and 494
Element Connected between Nodes 494 and 519
Element Connected between Nodes 519 and 544
Element Connected between Nodes 544 and 569
Element Connected between Nodes 569 and 594
Element Connected between Nodes 594 and 619
Element Connected between Nodes 619 and 644
Element Connected between Nodes 644 and 669
Element Connected between Nodes 669 and 694
Element Connected between Nodes 694 and 719
Element Connected between Nodes 719 and 744
Element Connected between Nodes 744 and 769

```

Beam Element Mesh generation for Reinforcement - Completed

-----

```

Number of Stirrup Regions =          2

Stirrup No =          1
From height 100.000000000000 to height 1000.000000000000

Stirrup No =          1 covers          9 layers

Stirrup No =          2
From height 2000.000000000000 to height 2900.000000000000

Stirrup No =          2 covers          9 layers

Element Connected between Nodes      32 and      33
Element Connected between Nodes      33 and      34
Element Connected between Nodes      34 and      39
Element Connected between Nodes      39 and      44
Element Connected between Nodes      44 and      43
Element Connected between Nodes      43 and      42
Element Connected between Nodes      42 and      37
Element Connected between Nodes      37 and      32
Element Connected between Nodes      57 and      58
Element Connected between Nodes      58 and      59
Element Connected between Nodes      59 and      64
Element Connected between Nodes      64 and      69
Element Connected between Nodes      69 and      68
Element Connected between Nodes      68 and      67
Element Connected between Nodes      67 and      62
Element Connected between Nodes      62 and      57
Element Connected between Nodes      82 and      83
Element Connected between Nodes      83 and      84
Element Connected between Nodes      84 and      89
Element Connected between Nodes      89 and      94
Element Connected between Nodes      94 and      93
Element Connected between Nodes      93 and      92
Element Connected between Nodes      92 and      87
Element Connected between Nodes      87 and      82

```



INPUT\_CHECK - Notepad

File Edit Format View Help

```
Element Connected between Nodes      662 and      657
Element Connected between Nodes      682 and      683
Element Connected between Nodes      683 and      684
Element Connected between Nodes      684 and      689
Element Connected between Nodes      689 and      694
Element Connected between Nodes      694 and      693
Element Connected between Nodes      693 and      692
Element Connected between Nodes      692 and      687
Element Connected between Nodes      687 and      682
Element Connected between Nodes      707 and      708
Element Connected between Nodes      708 and      709
Element Connected between Nodes      709 and      714
Element Connected between Nodes      714 and      719
Element Connected between Nodes      719 and      718
Element Connected between Nodes      718 and      717
Element Connected between Nodes      717 and      712
Element Connected between Nodes      712 and      707
Element Connected between Nodes      732 and      733
Element Connected between Nodes      733 and      734
Element Connected between Nodes      734 and      739
Element Connected between Nodes      739 and      744
Element Connected between Nodes      744 and      743
Element Connected between Nodes      743 and      742
Element Connected between Nodes      742 and      737
Element Connected between Nodes      737 and      732
```

Mesh-size limit = 7.74193548387097

Loads are generated using Coordinates

```
Load No  273      in direction  2      applied at  100.00  300.00  1000.00
Load No  523      in direction  2      applied at  100.00  300.00  2000.00
```

\*\*\*\*\*

ConfinedLoadGenerateUsingCoordinatesYorN:

Y: CoorConfinedLoad.TXT --> CONFINED\_NODAL\_LOADS.TXT

\*\*\*\*\*

Confined Loads are generated using Coordinates

-----  
-----

Boundary Conditions are Directly imposed to Nodes

-----  
-----

Multiple-Point Constraints are imposed directly to nodes

-----  
-----

```
ApplyPlaneRestraint_NormalAxis_1X_2Y_3Z      3
CoordinateOfRestraintPlaneOnSelectedAxis  0.000000000000000E+000
PlaneRestraintDirection      1
ApplyPlaneRestraint_NormalAxis_1X_2Y_3Z      3
CoordinateOfRestraintPlaneOnSelectedAxis  0.000000000000000E+000
PlaneRestraintDirection      2
ApplyPlaneRestraint_NormalAxis_1X_2Y_3Z      3
CoordinateOfRestraintPlaneOnSelectedAxis  3000.000000000000
PlaneRestraintDirection      1
```

<

```

ApplyPlaneRestraint_NormalAxis_1X_2Y_3Z          3
CoordinateOfRestraintPlaneOnSelectedAxis          3000.000000000000
PlaneRestraintDirection                           2

LineRestraint-X-Y-Z-CoordinatesAtBothEnds
0.000000000000000E+000  150.0000000000000  0.000000000000000E+000
200.0000000000000  150.0000000000000  0.000000000000000E+000
LineRestraintDirection                             3

ApplyPlaneConstraint_NormalAxis_1X_2Y_3Z          3
CoordinateOfConstraintPlaneOnSelectedAxis          1000.000000000000
PlaneConstraintDirection                           2
PlaneConstraintMasterX-Y-Z-Coordinates
100.0000000000000  300.0000000000000  1000.0000000000000
ApplyPlaneConstraint_NormalAxis_1X_2Y_3Z          3
CoordinateOfConstraintPlaneOnSelectedAxis          2000.000000000000
PlaneConstraintDirection                           2
PlaneConstraintMasterX-Y-Z-Coordinates
100.0000000000000  300.0000000000000  2000.0000000000000
    
```

```

-----
Number of Nodes = 775
-----
Number of Solid elements = 480
Number of Shell elements = 0
Number of Bar elements = 280
-----
    
```

COORDINATES OF NODES

NOD	X(mm)	Y(mm)	Z(mm)
1	0.0000000	0.0000000	0.0000000
2	25.0000000	0.0000000	0.0000000
3	100.0000000	0.0000000	0.0000000
4	175.0000000	0.0000000	0.0000000
5	200.0000000	0.0000000	0.0000000
6	0.0000000	25.0000000	0.0000000
7	25.0000000	25.0000000	0.0000000
8	100.0000000	25.0000000	0.0000000
9	175.0000000	25.0000000	0.0000000
10	200.0000000	25.0000000	0.0000000
11	0.0000000	150.0000000	0.0000000
12	25.0000000	150.0000000	0.0000000
13	100.0000000	150.0000000	0.0000000
14	175.0000000	150.0000000	0.0000000
15	200.0000000	150.0000000	0.0000000
16	0.0000000	275.0000000	0.0000000
17	25.0000000	275.0000000	0.0000000
18	100.0000000	275.0000000	0.0000000
19	175.0000000	275.0000000	0.0000000
20	200.0000000	275.0000000	0.0000000
21	0.0000000	300.0000000	0.0000000
22	25.0000000	300.0000000	0.0000000



File	Edit	Format	View	Help
22	25.0000000	300.0000000	0.0000000	
23	100.0000000	300.0000000	0.0000000	
24	175.0000000	300.0000000	0.0000000	
25	200.0000000	300.0000000	0.0000000	
26	0.0000000	0.0000000	100.0000000	
27	25.0000000	0.0000000	100.0000000	
28	100.0000000	0.0000000	100.0000000	
29	175.0000000	0.0000000	100.0000000	
30	200.0000000	0.0000000	100.0000000	
31	0.0000000	25.0000000	100.0000000	
32	25.0000000	25.0000000	100.0000000	
33	100.0000000	25.0000000	100.0000000	
34	175.0000000	25.0000000	100.0000000	
35	200.0000000	25.0000000	100.0000000	
36	0.0000000	150.0000000	100.0000000	
37	25.0000000	150.0000000	100.0000000	
38	100.0000000	150.0000000	100.0000000	
39	175.0000000	150.0000000	100.0000000	
40	200.0000000	150.0000000	100.0000000	
41	0.0000000	275.0000000	100.0000000	
42	25.0000000	275.0000000	100.0000000	
43	100.0000000	275.0000000	100.0000000	
44	175.0000000	275.0000000	100.0000000	
45	200.0000000	275.0000000	100.0000000	
46	0.0000000	300.0000000	100.0000000	
47	25.0000000	300.0000000	100.0000000	
48	100.0000000	300.0000000	100.0000000	
49	175.0000000	300.0000000	100.0000000	
50	200.0000000	300.0000000	100.0000000	
51	0.0000000	0.0000000	200.0000000	
52	25.0000000	0.0000000	200.0000000	
53	100.0000000	0.0000000	200.0000000	
54	175.0000000	0.0000000	200.0000000	
55	200.0000000	0.0000000	200.0000000	
56	0.0000000	25.0000000	200.0000000	
57	25.0000000	25.0000000	200.0000000	
58	100.0000000	25.0000000	200.0000000	
59	175.0000000	25.0000000	200.0000000	
60	200.0000000	25.0000000	200.0000000	
61	0.0000000	150.0000000	200.0000000	
62	25.0000000	150.0000000	200.0000000	
63	100.0000000	150.0000000	200.0000000	
64	175.0000000	150.0000000	200.0000000	
65	200.0000000	150.0000000	200.0000000	
66	0.0000000	275.0000000	200.0000000	
67	25.0000000	275.0000000	200.0000000	
68	100.0000000	275.0000000	200.0000000	
69	175.0000000	275.0000000	200.0000000	
70	200.0000000	275.0000000	200.0000000	
71	0.0000000	300.0000000	200.0000000	
72	25.0000000	300.0000000	200.0000000	
73	100.0000000	300.0000000	200.0000000	
74	175.0000000	300.0000000	200.0000000	
75	200.0000000	300.0000000	200.0000000	
76	0.0000000	0.0000000	300.0000000	
77	25.0000000	0.0000000	300.0000000	

INPUT\_CHECK - Notepad

File	Edit	Format	View	Help
77	25.0000000	0.0000000	300.0000000	
78	100.0000000	0.0000000	300.0000000	
79	175.0000000	0.0000000	300.0000000	
80	200.0000000	0.0000000	300.0000000	
81	0.0000000	25.0000000	300.0000000	
82	25.0000000	25.0000000	300.0000000	
83	100.0000000	25.0000000	300.0000000	
84	175.0000000	25.0000000	300.0000000	
85	200.0000000	25.0000000	300.0000000	
86	0.0000000	150.0000000	300.0000000	
87	25.0000000	150.0000000	300.0000000	
88	100.0000000	150.0000000	300.0000000	
89	175.0000000	150.0000000	300.0000000	
90	200.0000000	150.0000000	300.0000000	
91	0.0000000	275.0000000	300.0000000	
92	25.0000000	275.0000000	300.0000000	
93	100.0000000	275.0000000	300.0000000	
94	175.0000000	275.0000000	300.0000000	
95	200.0000000	275.0000000	300.0000000	
96	0.0000000	300.0000000	300.0000000	
97	25.0000000	300.0000000	300.0000000	
98	100.0000000	300.0000000	300.0000000	
99	175.0000000	300.0000000	300.0000000	
100	200.0000000	300.0000000	300.0000000	
101	0.0000000	0.0000000	400.0000000	
102	25.0000000	0.0000000	400.0000000	
103	100.0000000	0.0000000	400.0000000	
104	175.0000000	0.0000000	400.0000000	
105	200.0000000	0.0000000	400.0000000	
106	0.0000000	25.0000000	400.0000000	
107	25.0000000	25.0000000	400.0000000	
108	100.0000000	25.0000000	400.0000000	
109	175.0000000	25.0000000	400.0000000	
110	200.0000000	25.0000000	400.0000000	
111	0.0000000	150.0000000	400.0000000	
112	25.0000000	150.0000000	400.0000000	
113	100.0000000	150.0000000	400.0000000	
114	175.0000000	150.0000000	400.0000000	
115	200.0000000	150.0000000	400.0000000	
116	0.0000000	275.0000000	400.0000000	
117	25.0000000	275.0000000	400.0000000	
118	100.0000000	275.0000000	400.0000000	
119	175.0000000	275.0000000	400.0000000	
120	200.0000000	275.0000000	400.0000000	
121	0.0000000	300.0000000	400.0000000	
122	25.0000000	300.0000000	400.0000000	
123	100.0000000	300.0000000	400.0000000	
124	175.0000000	300.0000000	400.0000000	
125	200.0000000	300.0000000	400.0000000	
126	0.0000000	0.0000000	500.0000000	
127	25.0000000	0.0000000	500.0000000	
128	100.0000000	0.0000000	500.0000000	
129	175.0000000	0.0000000	500.0000000	
130	200.0000000	0.0000000	500.0000000	
131	0.0000000	25.0000000	500.0000000	
132	25.0000000	25.0000000	500.0000000	

INPUT\_CHECK - Notepad

File	Edit	Format	View	Help
132	25.0000000	25.0000000	500.0000000	
133	100.0000000	25.0000000	500.0000000	
134	175.0000000	25.0000000	500.0000000	
135	200.0000000	25.0000000	500.0000000	
136	0.0000000	150.0000000	500.0000000	
137	25.0000000	150.0000000	500.0000000	
138	100.0000000	150.0000000	500.0000000	
139	175.0000000	150.0000000	500.0000000	
140	200.0000000	150.0000000	500.0000000	
141	0.0000000	275.0000000	500.0000000	
142	25.0000000	275.0000000	500.0000000	
143	100.0000000	275.0000000	500.0000000	
144	175.0000000	275.0000000	500.0000000	
145	200.0000000	275.0000000	500.0000000	
146	0.0000000	300.0000000	500.0000000	
147	25.0000000	300.0000000	500.0000000	
148	100.0000000	300.0000000	500.0000000	
149	175.0000000	300.0000000	500.0000000	
150	200.0000000	300.0000000	500.0000000	
151	0.0000000	0.0000000	600.0000000	
152	25.0000000	0.0000000	600.0000000	
153	100.0000000	0.0000000	600.0000000	
154	175.0000000	0.0000000	600.0000000	
155	200.0000000	0.0000000	600.0000000	
156	0.0000000	25.0000000	600.0000000	
157	25.0000000	25.0000000	600.0000000	
158	100.0000000	25.0000000	600.0000000	
159	175.0000000	25.0000000	600.0000000	
160	200.0000000	25.0000000	600.0000000	
161	0.0000000	150.0000000	600.0000000	
162	25.0000000	150.0000000	600.0000000	
163	100.0000000	150.0000000	600.0000000	
164	175.0000000	150.0000000	600.0000000	
165	200.0000000	150.0000000	600.0000000	
166	0.0000000	275.0000000	600.0000000	
167	25.0000000	275.0000000	600.0000000	
168	100.0000000	275.0000000	600.0000000	
169	175.0000000	275.0000000	600.0000000	
170	200.0000000	275.0000000	600.0000000	
171	0.0000000	300.0000000	600.0000000	
172	25.0000000	300.0000000	600.0000000	
173	100.0000000	300.0000000	600.0000000	
174	175.0000000	300.0000000	600.0000000	
175	200.0000000	300.0000000	600.0000000	
176	0.0000000	0.0000000	700.0000000	
177	25.0000000	0.0000000	700.0000000	
178	100.0000000	0.0000000	700.0000000	
179	175.0000000	0.0000000	700.0000000	
180	200.0000000	0.0000000	700.0000000	
181	0.0000000	25.0000000	700.0000000	
182	25.0000000	25.0000000	700.0000000	
183	100.0000000	25.0000000	700.0000000	
184	175.0000000	25.0000000	700.0000000	
185	200.0000000	25.0000000	700.0000000	
186	0.0000000	150.0000000	700.0000000	
187	25.0000000	150.0000000	700.0000000	

INPUT\_CHECK - Notepad

File	Edit	Format	View	Help
187	25.0000000	150.0000000	700.0000000	
188	100.0000000	150.0000000	700.0000000	
189	175.0000000	150.0000000	700.0000000	
190	200.0000000	150.0000000	700.0000000	
191	0.0000000	275.0000000	700.0000000	
192	25.0000000	275.0000000	700.0000000	
193	100.0000000	275.0000000	700.0000000	
194	175.0000000	275.0000000	700.0000000	
195	200.0000000	275.0000000	700.0000000	
196	0.0000000	300.0000000	700.0000000	
197	25.0000000	300.0000000	700.0000000	
198	100.0000000	300.0000000	700.0000000	
199	175.0000000	300.0000000	700.0000000	
200	200.0000000	300.0000000	700.0000000	
201	0.0000000	0.0000000	800.0000000	
202	25.0000000	0.0000000	800.0000000	
203	100.0000000	0.0000000	800.0000000	
204	175.0000000	0.0000000	800.0000000	
205	200.0000000	0.0000000	800.0000000	
206	0.0000000	25.0000000	800.0000000	
207	25.0000000	25.0000000	800.0000000	
208	100.0000000	25.0000000	800.0000000	
209	175.0000000	25.0000000	800.0000000	
210	200.0000000	25.0000000	800.0000000	
211	0.0000000	150.0000000	800.0000000	
212	25.0000000	150.0000000	800.0000000	
213	100.0000000	150.0000000	800.0000000	
214	175.0000000	150.0000000	800.0000000	
215	200.0000000	150.0000000	800.0000000	
216	0.0000000	275.0000000	800.0000000	
217	25.0000000	275.0000000	800.0000000	
218	100.0000000	275.0000000	800.0000000	
219	175.0000000	275.0000000	800.0000000	
220	200.0000000	275.0000000	800.0000000	
221	0.0000000	300.0000000	800.0000000	
222	25.0000000	300.0000000	800.0000000	
223	100.0000000	300.0000000	800.0000000	
224	175.0000000	300.0000000	800.0000000	
225	200.0000000	300.0000000	800.0000000	
226	0.0000000	0.0000000	900.0000000	
227	25.0000000	0.0000000	900.0000000	
228	100.0000000	0.0000000	900.0000000	
229	175.0000000	0.0000000	900.0000000	
230	200.0000000	0.0000000	900.0000000	
231	0.0000000	25.0000000	900.0000000	
232	25.0000000	25.0000000	900.0000000	
233	100.0000000	25.0000000	900.0000000	
234	175.0000000	25.0000000	900.0000000	
235	200.0000000	25.0000000	900.0000000	
236	0.0000000	150.0000000	900.0000000	
237	25.0000000	150.0000000	900.0000000	
238	100.0000000	150.0000000	900.0000000	
239	175.0000000	150.0000000	900.0000000	
240	200.0000000	150.0000000	900.0000000	
241	0.0000000	275.0000000	900.0000000	
242	25.0000000	275.0000000	900.0000000	

File	Edit	Format	View	Help
242	25.0000000	275.0000000	900.0000000	
243	100.0000000	275.0000000	900.0000000	
244	175.0000000	275.0000000	900.0000000	
245	200.0000000	275.0000000	900.0000000	
246	0.0000000	300.0000000	900.0000000	
247	25.0000000	300.0000000	900.0000000	
248	100.0000000	300.0000000	900.0000000	
249	175.0000000	300.0000000	900.0000000	
250	200.0000000	300.0000000	900.0000000	
251	0.0000000	0.0000000	1000.0000000	
252	25.0000000	0.0000000	1000.0000000	
253	100.0000000	0.0000000	1000.0000000	
254	175.0000000	0.0000000	1000.0000000	
255	200.0000000	0.0000000	1000.0000000	
256	0.0000000	25.0000000	1000.0000000	
257	25.0000000	25.0000000	1000.0000000	
258	100.0000000	25.0000000	1000.0000000	
259	175.0000000	25.0000000	1000.0000000	
260	200.0000000	25.0000000	1000.0000000	
261	0.0000000	150.0000000	1000.0000000	
262	25.0000000	150.0000000	1000.0000000	
263	100.0000000	150.0000000	1000.0000000	
264	175.0000000	150.0000000	1000.0000000	
265	200.0000000	150.0000000	1000.0000000	
266	0.0000000	275.0000000	1000.0000000	
267	25.0000000	275.0000000	1000.0000000	
268	100.0000000	275.0000000	1000.0000000	
269	175.0000000	275.0000000	1000.0000000	
270	200.0000000	275.0000000	1000.0000000	
271	0.0000000	300.0000000	1000.0000000	
272	25.0000000	300.0000000	1000.0000000	
273	100.0000000	300.0000000	1000.0000000	
274	175.0000000	300.0000000	1000.0000000	
275	200.0000000	300.0000000	1000.0000000	
276	0.0000000	0.0000000	1100.0000000	
277	25.0000000	0.0000000	1100.0000000	
278	100.0000000	0.0000000	1100.0000000	
279	175.0000000	0.0000000	1100.0000000	
280	200.0000000	0.0000000	1100.0000000	
281	0.0000000	25.0000000	1100.0000000	
282	25.0000000	25.0000000	1100.0000000	
283	100.0000000	25.0000000	1100.0000000	
284	175.0000000	25.0000000	1100.0000000	
285	200.0000000	25.0000000	1100.0000000	
286	0.0000000	150.0000000	1100.0000000	
287	25.0000000	150.0000000	1100.0000000	
288	100.0000000	150.0000000	1100.0000000	
289	175.0000000	150.0000000	1100.0000000	
290	200.0000000	150.0000000	1100.0000000	
291	0.0000000	275.0000000	1100.0000000	
292	25.0000000	275.0000000	1100.0000000	
293	100.0000000	275.0000000	1100.0000000	
294	175.0000000	275.0000000	1100.0000000	
295	200.0000000	275.0000000	1100.0000000	
296	0.0000000	300.0000000	1100.0000000	
297	25.0000000	300.0000000	1100.0000000	

File	Edit	Format	View	Help
297	25.0000000	300.0000000	1100.0000000	
298	100.0000000	300.0000000	1100.0000000	
299	175.0000000	300.0000000	1100.0000000	
300	200.0000000	300.0000000	1100.0000000	
301	0.0000000	0.0000000	1200.0000000	
302	25.0000000	0.0000000	1200.0000000	
303	100.0000000	0.0000000	1200.0000000	
304	175.0000000	0.0000000	1200.0000000	
305	200.0000000	0.0000000	1200.0000000	
306	0.0000000	25.0000000	1200.0000000	
307	25.0000000	25.0000000	1200.0000000	
308	100.0000000	25.0000000	1200.0000000	
309	175.0000000	25.0000000	1200.0000000	
310	200.0000000	25.0000000	1200.0000000	
311	0.0000000	150.0000000	1200.0000000	
312	25.0000000	150.0000000	1200.0000000	
313	100.0000000	150.0000000	1200.0000000	
314	175.0000000	150.0000000	1200.0000000	
315	200.0000000	150.0000000	1200.0000000	
316	0.0000000	275.0000000	1200.0000000	
317	25.0000000	275.0000000	1200.0000000	
318	100.0000000	275.0000000	1200.0000000	
319	175.0000000	275.0000000	1200.0000000	
320	200.0000000	275.0000000	1200.0000000	
321	0.0000000	300.0000000	1200.0000000	
322	25.0000000	300.0000000	1200.0000000	
323	100.0000000	300.0000000	1200.0000000	
324	175.0000000	300.0000000	1200.0000000	
325	200.0000000	300.0000000	1200.0000000	
326	0.0000000	0.0000000	1300.0000000	
327	25.0000000	0.0000000	1300.0000000	
328	100.0000000	0.0000000	1300.0000000	
329	175.0000000	0.0000000	1300.0000000	
330	200.0000000	0.0000000	1300.0000000	
331	0.0000000	25.0000000	1300.0000000	
332	25.0000000	25.0000000	1300.0000000	
333	100.0000000	25.0000000	1300.0000000	
334	175.0000000	25.0000000	1300.0000000	
335	200.0000000	25.0000000	1300.0000000	
336	0.0000000	150.0000000	1300.0000000	
337	25.0000000	150.0000000	1300.0000000	
338	100.0000000	150.0000000	1300.0000000	
339	175.0000000	150.0000000	1300.0000000	
340	200.0000000	150.0000000	1300.0000000	
341	0.0000000	275.0000000	1300.0000000	
342	25.0000000	275.0000000	1300.0000000	
343	100.0000000	275.0000000	1300.0000000	
344	175.0000000	275.0000000	1300.0000000	
345	200.0000000	275.0000000	1300.0000000	
346	0.0000000	300.0000000	1300.0000000	
347	25.0000000	300.0000000	1300.0000000	
348	100.0000000	300.0000000	1300.0000000	
349	175.0000000	300.0000000	1300.0000000	
350	200.0000000	300.0000000	1300.0000000	
351	0.0000000	0.0000000	1400.0000000	
352	25.0000000	0.0000000	1400.0000000	

INPUT\_CHECK - Notepad

File	Edit	Format	View	Help
352	25.0000000	0.0000000	1400.0000000	
353	100.0000000	0.0000000	1400.0000000	
354	175.0000000	0.0000000	1400.0000000	
355	200.0000000	0.0000000	1400.0000000	
356	0.0000000	25.0000000	1400.0000000	
357	25.0000000	25.0000000	1400.0000000	
358	100.0000000	25.0000000	1400.0000000	
359	175.0000000	25.0000000	1400.0000000	
360	200.0000000	25.0000000	1400.0000000	
361	0.0000000	150.0000000	1400.0000000	
362	25.0000000	150.0000000	1400.0000000	
363	100.0000000	150.0000000	1400.0000000	
364	175.0000000	150.0000000	1400.0000000	
365	200.0000000	150.0000000	1400.0000000	
366	0.0000000	275.0000000	1400.0000000	
367	25.0000000	275.0000000	1400.0000000	
368	100.0000000	275.0000000	1400.0000000	
369	175.0000000	275.0000000	1400.0000000	
370	200.0000000	275.0000000	1400.0000000	
371	0.0000000	300.0000000	1400.0000000	
372	25.0000000	300.0000000	1400.0000000	
373	100.0000000	300.0000000	1400.0000000	
374	175.0000000	300.0000000	1400.0000000	
375	200.0000000	300.0000000	1400.0000000	
376	0.0000000	0.0000000	1500.0000000	
377	25.0000000	0.0000000	1500.0000000	
378	100.0000000	0.0000000	1500.0000000	
379	175.0000000	0.0000000	1500.0000000	
380	200.0000000	0.0000000	1500.0000000	
381	0.0000000	25.0000000	1500.0000000	
382	25.0000000	25.0000000	1500.0000000	
383	100.0000000	25.0000000	1500.0000000	
384	175.0000000	25.0000000	1500.0000000	
385	200.0000000	25.0000000	1500.0000000	
386	0.0000000	150.0000000	1500.0000000	
387	25.0000000	150.0000000	1500.0000000	
388	100.0000000	150.0000000	1500.0000000	
389	175.0000000	150.0000000	1500.0000000	
390	200.0000000	150.0000000	1500.0000000	
391	0.0000000	275.0000000	1500.0000000	
392	25.0000000	275.0000000	1500.0000000	
393	100.0000000	275.0000000	1500.0000000	
394	175.0000000	275.0000000	1500.0000000	
395	200.0000000	275.0000000	1500.0000000	
396	0.0000000	300.0000000	1500.0000000	
397	25.0000000	300.0000000	1500.0000000	
398	100.0000000	300.0000000	1500.0000000	
399	175.0000000	300.0000000	1500.0000000	
400	200.0000000	300.0000000	1500.0000000	
401	0.0000000	0.0000000	1600.0000000	
402	25.0000000	0.0000000	1600.0000000	
403	100.0000000	0.0000000	1600.0000000	
404	175.0000000	0.0000000	1600.0000000	
405	200.0000000	0.0000000	1600.0000000	
406	0.0000000	25.0000000	1600.0000000	
407	25.0000000	25.0000000	1600.0000000	

File	Edit	Format	View	Help
407	25.0000000	25.0000000	1600.0000000	
408	100.0000000	25.0000000	1600.0000000	
409	175.0000000	25.0000000	1600.0000000	
410	200.0000000	25.0000000	1600.0000000	
411	0.0000000	150.0000000	1600.0000000	
412	25.0000000	150.0000000	1600.0000000	
413	100.0000000	150.0000000	1600.0000000	
414	175.0000000	150.0000000	1600.0000000	
415	200.0000000	150.0000000	1600.0000000	
416	0.0000000	275.0000000	1600.0000000	
417	25.0000000	275.0000000	1600.0000000	
418	100.0000000	275.0000000	1600.0000000	
419	175.0000000	275.0000000	1600.0000000	
420	200.0000000	275.0000000	1600.0000000	
421	0.0000000	300.0000000	1600.0000000	
422	25.0000000	300.0000000	1600.0000000	
423	100.0000000	300.0000000	1600.0000000	
424	175.0000000	300.0000000	1600.0000000	
425	200.0000000	300.0000000	1600.0000000	
426	0.0000000	0.0000000	1700.0000000	
427	25.0000000	0.0000000	1700.0000000	
428	100.0000000	0.0000000	1700.0000000	
429	175.0000000	0.0000000	1700.0000000	
430	200.0000000	0.0000000	1700.0000000	
431	0.0000000	25.0000000	1700.0000000	
432	25.0000000	25.0000000	1700.0000000	
433	100.0000000	25.0000000	1700.0000000	
434	175.0000000	25.0000000	1700.0000000	
435	200.0000000	25.0000000	1700.0000000	
436	0.0000000	150.0000000	1700.0000000	
437	25.0000000	150.0000000	1700.0000000	
438	100.0000000	150.0000000	1700.0000000	
439	175.0000000	150.0000000	1700.0000000	
440	200.0000000	150.0000000	1700.0000000	
441	0.0000000	275.0000000	1700.0000000	
442	25.0000000	275.0000000	1700.0000000	
443	100.0000000	275.0000000	1700.0000000	
444	175.0000000	275.0000000	1700.0000000	
445	200.0000000	275.0000000	1700.0000000	
446	0.0000000	300.0000000	1700.0000000	
447	25.0000000	300.0000000	1700.0000000	
448	100.0000000	300.0000000	1700.0000000	
449	175.0000000	300.0000000	1700.0000000	
450	200.0000000	300.0000000	1700.0000000	
451	0.0000000	0.0000000	1800.0000000	
452	25.0000000	0.0000000	1800.0000000	
453	100.0000000	0.0000000	1800.0000000	
454	175.0000000	0.0000000	1800.0000000	
455	200.0000000	0.0000000	1800.0000000	
456	0.0000000	25.0000000	1800.0000000	
457	25.0000000	25.0000000	1800.0000000	
458	100.0000000	25.0000000	1800.0000000	
459	175.0000000	25.0000000	1800.0000000	
460	200.0000000	25.0000000	1800.0000000	
461	0.0000000	150.0000000	1800.0000000	
462	25.0000000	150.0000000	1800.0000000	



File	Edit	Format	View	Help
721	0.0000000	300.0000000	2800.0000000	
722	25.0000000	300.0000000	2800.0000000	
723	100.0000000	300.0000000	2800.0000000	
724	175.0000000	300.0000000	2800.0000000	
725	200.0000000	300.0000000	2800.0000000	
726	0.0000000	0.0000000	2900.0000000	
727	25.0000000	0.0000000	2900.0000000	
728	100.0000000	0.0000000	2900.0000000	
729	175.0000000	0.0000000	2900.0000000	
730	200.0000000	0.0000000	2900.0000000	
731	0.0000000	25.0000000	2900.0000000	
732	25.0000000	25.0000000	2900.0000000	
733	100.0000000	25.0000000	2900.0000000	
734	175.0000000	25.0000000	2900.0000000	
735	200.0000000	25.0000000	2900.0000000	
736	0.0000000	150.0000000	2900.0000000	
737	25.0000000	150.0000000	2900.0000000	
738	100.0000000	150.0000000	2900.0000000	
739	175.0000000	150.0000000	2900.0000000	
740	200.0000000	150.0000000	2900.0000000	
741	0.0000000	275.0000000	2900.0000000	
742	25.0000000	275.0000000	2900.0000000	
743	100.0000000	275.0000000	2900.0000000	
744	175.0000000	275.0000000	2900.0000000	
745	200.0000000	275.0000000	2900.0000000	
746	0.0000000	300.0000000	2900.0000000	
747	25.0000000	300.0000000	2900.0000000	
748	100.0000000	300.0000000	2900.0000000	
749	175.0000000	300.0000000	2900.0000000	
750	200.0000000	300.0000000	2900.0000000	
751	0.0000000	0.0000000	3000.0000000	
752	25.0000000	0.0000000	3000.0000000	
753	100.0000000	0.0000000	3000.0000000	
754	175.0000000	0.0000000	3000.0000000	
755	200.0000000	0.0000000	3000.0000000	
756	0.0000000	25.0000000	3000.0000000	
757	25.0000000	25.0000000	3000.0000000	
758	100.0000000	25.0000000	3000.0000000	
759	175.0000000	25.0000000	3000.0000000	
760	200.0000000	25.0000000	3000.0000000	
761	0.0000000	150.0000000	3000.0000000	
762	25.0000000	150.0000000	3000.0000000	
763	100.0000000	150.0000000	3000.0000000	
764	175.0000000	150.0000000	3000.0000000	
765	200.0000000	150.0000000	3000.0000000	
766	0.0000000	275.0000000	3000.0000000	
767	25.0000000	275.0000000	3000.0000000	
768	100.0000000	275.0000000	3000.0000000	
769	175.0000000	275.0000000	3000.0000000	
770	200.0000000	275.0000000	3000.0000000	
771	0.0000000	300.0000000	3000.0000000	
772	25.0000000	300.0000000	3000.0000000	
773	100.0000000	300.0000000	3000.0000000	
774	175.0000000	300.0000000	3000.0000000	
775	200.0000000	300.0000000	3000.0000000	

SOLID TYPE ELEMENT

ELEMENT	I_END	J_END	K_END	L_END	M_END	N_END	O_END	P_END
1	1	2	7	6	26	27	32	31
2	2	3	8	7	27	28	33	32
3	3	4	9	8	28	29	34	33
4	4	5	10	9	29	30	35	34
5	6	7	12	11	31	32	37	36
6	7	8	13	12	32	33	38	37
7	8	9	14	13	33	34	39	38
8	9	10	15	14	34	35	40	39
9	11	12	17	16	36	37	42	41
10	12	13	18	17	37	38	43	42
11	13	14	19	18	38	39	44	43
12	14	15	20	19	39	40	45	44
13	16	17	22	21	41	42	47	46
14	17	18	23	22	42	43	48	47
15	18	19	24	23	43	44	49	48
16	19	20	25	24	44	45	50	49
17	26	27	32	31	51	52	57	56
18	27	28	33	32	52	53	58	57
19	28	29	34	33	53	54	59	58
20	29	30	35	34	54	55	60	59
21	31	32	37	36	56	57	62	61
22	32	33	38	37	57	58	63	62
23	33	34	39	38	58	59	64	63
24	34	35	40	39	59	60	65	64
25	36	37	42	41	61	62	67	66
26	37	38	43	42	62	63	68	67
27	38	39	44	43	63	64	69	68
28	39	40	45	44	64	65	70	69
29	41	42	47	46	66	67	72	71
30	42	43	48	47	67	68	73	72
31	43	44	49	48	68	69	74	73
32	44	45	50	49	69	70	75	74
33	51	52	57	56	76	77	82	81
34	52	53	58	57	77	78	83	82
35	53	54	59	58	78	79	84	83
36	54	55	60	59	79	80	85	84
37	56	57	62	61	81	82	87	86
38	57	58	63	62	82	83	88	87
39	58	59	64	63	83	84	89	88
40	59	60	65	64	84	85	90	89
41	61	62	67	66	86	87	92	91
42	62	63	68	67	87	88	93	92
43	63	64	69	68	88	89	94	93
44	64	65	70	69	89	90	95	94
45	66	67	72	71	91	92	97	96
46	67	68	73	72	92	93	98	97
47	68	69	74	73	93	94	99	98
48	69	70	75	74	94	95	100	99
49	76	77	82	81	101	102	107	106
50	77	78	83	82	102	103	108	107
51	78	79	84	83	103	104	109	108
52	79	80	85	84	104	105	110	109
53	81	82	87	86	106	107	112	111

INPUT\_CHECK - Notepad

File	Edit	Format	View	Help					
53		81	82	87	86	106	107	112	111
54		82	83	88	87	107	108	113	112
55		83	84	89	88	108	109	114	113
56		84	85	90	89	109	110	115	114
57		86	87	92	91	111	112	117	116
58		87	88	93	92	112	113	118	117
59		88	89	94	93	113	114	119	118
60		89	90	95	94	114	115	120	119
61		91	92	97	96	116	117	122	121
62		92	93	98	97	117	118	123	122
63		93	94	99	98	118	119	124	123
64		94	95	100	99	119	120	125	124
65		101	102	107	106	126	127	132	131
66		102	103	108	107	127	128	133	132
67		103	104	109	108	128	129	134	133
68		104	105	110	109	129	130	135	134
69		106	107	112	111	131	132	137	136
70		107	108	113	112	132	133	138	137
71		108	109	114	113	133	134	139	138
72		109	110	115	114	134	135	140	139
73		111	112	117	116	136	137	142	141
74		112	113	118	117	137	138	143	142
75		113	114	119	118	138	139	144	143
76		114	115	120	119	139	140	145	144
77		116	117	122	121	141	142	147	146
78		117	118	123	122	142	143	148	147
79		118	119	124	123	143	144	149	148
80		119	120	125	124	144	145	150	149
81		126	127	132	131	151	152	157	156
82		127	128	133	132	152	153	158	157
83		128	129	134	133	153	154	159	158
84		129	130	135	134	154	155	160	159
85		131	132	137	136	156	157	162	161
86		132	133	138	137	157	158	163	162
87		133	134	139	138	158	159	164	163
88		134	135	140	139	159	160	165	164
89		136	137	142	141	161	162	167	166
90		137	138	143	142	162	163	168	167
91		138	139	144	143	163	164	169	168
92		139	140	145	144	164	165	170	169
93		141	142	147	146	166	167	172	171
94		142	143	148	147	167	168	173	172
95		143	144	149	148	168	169	174	173
96		144	145	150	149	169	170	175	174
97		151	152	157	156	176	177	182	181
98		152	153	158	157	177	178	183	182
99		153	154	159	158	178	179	184	183
100		154	155	160	159	179	180	185	184
101		156	157	162	161	181	182	187	186
102		157	158	163	162	182	183	188	187
103		158	159	164	163	183	184	189	188
104		159	160	165	164	184	185	190	189
105		161	162	167	166	186	187	192	191
106		162	163	168	167	187	188	193	192
107		163	164	169	168	188	189	194	193
108		164	165	170	169	189	190	195	194

INPUT\_CHECK - Notepad

File	Edit	Format	View	Help												
108		164		165		170		169		189		190		195		194
109		166		167		172		171		191		192		197		196
110		167		168		173		172		192		193		198		197
111		168		169		174		173		193		194		199		198
112		169		170		175		174		194		195		200		199
113		176		177		182		181		201		202		207		206
114		177		178		183		182		202		203		208		207
115		178		179		184		183		203		204		209		208
116		179		180		185		184		204		205		210		209
117		181		182		187		186		206		207		212		211
118		182		183		188		187		207		208		213		212
119		183		184		189		188		208		209		214		213
120		184		185		190		189		209		210		215		214
121		186		187		192		191		211		212		217		216
122		187		188		193		192		212		213		218		217
123		188		189		194		193		213		214		219		218
124		189		190		195		194		214		215		220		219
125		191		192		197		196		216		217		222		221
126		192		193		198		197		217		218		223		222
127		193		194		199		198		218		219		224		223
128		194		195		200		199		219		220		225		224
129		201		202		207		206		226		227		232		231
130		202		203		208		207		227		228		233		232
131		203		204		209		208		228		229		234		233
132		204		205		210		209		229		230		235		234
133		206		207		212		211		231		232		237		236
134		207		208		213		212		232		233		238		237
135		208		209		214		213		233		234		239		238
136		209		210		215		214		234		235		240		239
137		211		212		217		216		236		237		242		241
138		212		213		218		217		237		238		243		242
139		213		214		219		218		238		239		244		243
140		214		215		220		219		239		240		245		244
141		216		217		222		221		241		242		247		246
142		217		218		223		222		242		243		248		247
143		218		219		224		223		243		244		249		248
144		219		220		225		224		244		245		250		249
145		226		227		232		231		251		252		257		256
146		227		228		233		232		252		253		258		257
147		228		229		234		233		253		254		259		258
148		229		230		235		234		254		255		260		259
149		231		232		237		236		256		257		262		261
150		232		233		238		237		257		258		263		262
151		233		234		239		238		258		259		264		263
152		234		235		240		239		259		260		265		264
153		236		237		242		241		261		262		267		266
154		237		238		243		242		262		263		268		267
155		238		239		244		243		263		264		269		268
156		239		240		245		244		264		265		270		269
157		241		242		247		246		266		267		272		271
158		242		243		248		247		267		268		273		272
159		243		244		249		248		268		269		274		273
160		244		245		250		249		269		270		275		274
161		251		252		257		256		276		277		282		281
162		252		253		258		257		277		278		283		282
163		253		254		259		258		278		279		284		283

INPUT\_CHECK - Notepad

File	Edit	Format	View	Help					
163		253	254	259	258	278	279	284	283
164		254	255	260	259	279	280	285	284
165		256	257	262	261	281	282	287	286
166		257	258	263	262	282	283	288	287
167		258	259	264	263	283	284	289	288
168		259	260	265	264	284	285	290	289
169		261	262	267	266	286	287	292	291
170		262	263	268	267	287	288	293	292
171		263	264	269	268	288	289	294	293
172		264	265	270	269	289	290	295	294
173		266	267	272	271	291	292	297	296
174		267	268	273	272	292	293	298	297
175		268	269	274	273	293	294	299	298
176		269	270	275	274	294	295	300	299
177		276	277	282	281	301	302	307	306
178		277	278	283	282	302	303	308	307
179		278	279	284	283	303	304	309	308
180		279	280	285	284	304	305	310	309
181		281	282	287	286	306	307	312	311
182		282	283	288	287	307	308	313	312
183		283	284	289	288	308	309	314	313
184		284	285	290	289	309	310	315	314
185		286	287	292	291	311	312	317	316
186		287	288	293	292	312	313	318	317
187		288	289	294	293	313	314	319	318
188		289	290	295	294	314	315	320	319
189		291	292	297	296	316	317	322	321
190		292	293	298	297	317	318	323	322
191		293	294	299	298	318	319	324	323
192		294	295	300	299	319	320	325	324
193		301	302	307	306	326	327	332	331
194		302	303	308	307	327	328	333	332
195		303	304	309	308	328	329	334	333
196		304	305	310	309	329	330	335	334
197		306	307	312	311	331	332	337	336
198		307	308	313	312	332	333	338	337
199		308	309	314	313	333	334	339	338
200		309	310	315	314	334	335	340	339
201		311	312	317	316	336	337	342	341
202		312	313	318	317	337	338	343	342
203		313	314	319	318	338	339	344	343
204		314	315	320	319	339	340	345	344
205		316	317	322	321	341	342	347	346
206		317	318	323	322	342	343	348	347
207		318	319	324	323	343	344	349	348
208		319	320	325	324	344	345	350	349
209		326	327	332	331	351	352	357	356
210		327	328	333	332	352	353	358	357
211		328	329	334	333	353	354	359	358
212		329	330	335	334	354	355	360	359
213		331	332	337	336	356	357	362	361
214		332	333	338	337	357	358	363	362
215		333	334	339	338	358	359	364	363
216		334	335	340	339	359	360	365	364
217		336	337	342	341	361	362	367	366
218		337	338	343	342	362	363	368	367

INPUT\_CHECK - Notepad

File	Edit	Format	View	Help					
218		337	338	343	342	362	363	368	367
219		338	339	344	343	363	364	369	368
220		339	340	345	344	364	365	370	369
221		341	342	347	346	366	367	372	371
222		342	343	348	347	367	368	373	372
223		343	344	349	348	368	369	374	373
224		344	345	350	349	369	370	375	374
225		351	352	357	356	376	377	382	381
226		352	353	358	357	377	378	383	382
227		353	354	359	358	378	379	384	383
228		354	355	360	359	379	380	385	384
229		356	357	362	361	381	382	387	386
230		357	358	363	362	382	383	388	387
231		358	359	364	363	383	384	389	388
232		359	360	365	364	384	385	390	389
233		361	362	367	366	386	387	392	391
234		362	363	368	367	387	388	393	392
235		363	364	369	368	388	389	394	393
236		364	365	370	369	389	390	395	394
237		366	367	372	371	391	392	397	396
238		367	368	373	372	392	393	398	397
239		368	369	374	373	393	394	399	398
240		369	370	375	374	394	395	400	399
241		376	377	382	381	401	402	407	406
242		377	378	383	382	402	403	408	407
243		378	379	384	383	403	404	409	408
244		379	380	385	384	404	405	410	409
245		381	382	387	386	406	407	412	411
246		382	383	388	387	407	408	413	412
247		383	384	389	388	408	409	414	413
248		384	385	390	389	409	410	415	414
249		386	387	392	391	411	412	417	416
250		387	388	393	392	412	413	418	417
251		388	389	394	393	413	414	419	418
252		389	390	395	394	414	415	420	419
253		391	392	397	396	416	417	422	421
254		392	393	398	397	417	418	423	422
255		393	394	399	398	418	419	424	423
256		394	395	400	399	419	420	425	424
257		401	402	407	406	426	427	432	431
258		402	403	408	407	427	428	433	432
259		403	404	409	408	428	429	434	433
260		404	405	410	409	429	430	435	434
261		406	407	412	411	431	432	437	436
262		407	408	413	412	432	433	438	437
263		408	409	414	413	433	434	439	438
264		409	410	415	414	434	435	440	439
265		411	412	417	416	436	437	442	441
266		412	413	418	417	437	438	443	442
267		413	414	419	418	438	439	444	443
268		414	415	420	419	439	440	445	444
269		416	417	422	421	441	442	447	446
270		417	418	423	422	442	443	448	447
271		418	419	424	423	443	444	449	448
272		419	420	425	424	444	445	450	449
273		420	421	426	425	445	446	451	450

INPUT\_CHECK - Notepad

File	Edit	Format	View	Help					
273		426	427	432	431	451	452	457	456
274		427	428	433	432	452	453	458	457
275		428	429	434	433	453	454	459	458
276		429	430	435	434	454	455	460	459
277		431	432	437	436	456	457	462	461
278		432	433	438	437	457	458	463	462
279		433	434	439	438	458	459	464	463
280		434	435	440	439	459	460	465	464
281		436	437	442	441	461	462	467	466
282		437	438	443	442	462	463	468	467
283		438	439	444	443	463	464	469	468
284		439	440	445	444	464	465	470	469
285		441	442	447	446	466	467	472	471
286		442	443	448	447	467	468	473	472
287		443	444	449	448	468	469	474	473
288		444	445	450	449	469	470	475	474
289		451	452	457	456	476	477	482	481
290		452	453	458	457	477	478	483	482
291		453	454	459	458	478	479	484	483
292		454	455	460	459	479	480	485	484
293		456	457	462	461	481	482	487	486
294		457	458	463	462	482	483	488	487
295		458	459	464	463	483	484	489	488
296		459	460	465	464	484	485	490	489
297		461	462	467	466	486	487	492	491
298		462	463	468	467	487	488	493	492
299		463	464	469	468	488	489	494	493
300		464	465	470	469	489	490	495	494
301		466	467	472	471	491	492	497	496
302		467	468	473	472	492	493	498	497
303		468	469	474	473	493	494	499	498
304		469	470	475	474	494	495	500	499
305		476	477	482	481	501	502	507	506
306		477	478	483	482	502	503	508	507
307		478	479	484	483	503	504	509	508
308		479	480	485	484	504	505	510	509
309		481	482	487	486	506	507	512	511
310		482	483	488	487	507	508	513	512
311		483	484	489	488	508	509	514	513
312		484	485	490	489	509	510	515	514
313		486	487	492	491	511	512	517	516
314		487	488	493	492	512	513	518	517
315		488	489	494	493	513	514	519	518
316		489	490	495	494	514	515	520	519
317		491	492	497	496	516	517	522	521
318		492	493	498	497	517	518	523	522
319		493	494	499	498	518	519	524	523
320		494	495	500	499	519	520	525	524
321		501	502	507	506	526	527	532	531
322		502	503	508	507	527	528	533	532
323		503	504	509	508	528	529	534	533
324		504	505	510	509	529	530	535	534
325		506	507	512	511	531	532	537	536
326		507	508	513	512	532	533	538	537
327		508	509	514	513	533	534	539	538
328		509	510	515	514	534	535	540	539

File	Edit	Format	View	Help					
328		509	510	515	514	534	535	540	539
329		511	512	517	516	536	537	542	541
330		512	513	518	517	537	538	543	542
331		513	514	519	518	538	539	544	543
332		514	515	520	519	539	540	545	544
333		516	517	522	521	541	542	547	546
334		517	518	523	522	542	543	548	547
335		518	519	524	523	543	544	549	548
336		519	520	525	524	544	545	550	549
337		526	527	532	531	551	552	557	556
338		527	528	533	532	552	553	558	557
339		528	529	534	533	553	554	559	558
340		529	530	535	534	554	555	560	559
341		531	532	537	536	556	557	562	561
342		532	533	538	537	557	558	563	562
343		533	534	539	538	558	559	564	563
344		534	535	540	539	559	560	565	564
345		536	537	542	541	561	562	567	566
346		537	538	543	542	562	563	568	567
347		538	539	544	543	563	564	569	568
348		539	540	545	544	564	565	570	569
349		541	542	547	546	566	567	572	571
350		542	543	548	547	567	568	573	572
351		543	544	549	548	568	569	574	573
352		544	545	550	549	569	570	575	574
353		551	552	557	556	576	577	582	581
354		552	553	558	557	577	578	583	582
355		553	554	559	558	578	579	584	583
356		554	555	560	559	579	580	585	584
357		556	557	562	561	581	582	587	586
358		557	558	563	562	582	583	588	587
359		558	559	564	563	583	584	589	588
360		559	560	565	564	584	585	590	589
361		561	562	567	566	586	587	592	591
362		562	563	568	567	587	588	593	592
363		563	564	569	568	588	589	594	593
364		564	565	570	569	589	590	595	594
365		566	567	572	571	591	592	597	596
366		567	568	573	572	592	593	598	597
367		568	569	574	573	593	594	599	598
368		569	570	575	574	594	595	600	599
369		576	577	582	581	601	602	607	606
370		577	578	583	582	602	603	608	607
371		578	579	584	583	603	604	609	608
372		579	580	585	584	604	605	610	609
373		581	582	587	586	606	607	612	611
374		582	583	588	587	607	608	613	612
375		583	584	589	588	608	609	614	613
376		584	585	590	589	609	610	615	614
377		586	587	592	591	611	612	617	616
378		587	588	593	592	612	613	618	617
379		588	589	594	593	613	614	619	618
380		589	590	595	594	614	615	620	619
381		591	592	597	596	616	617	622	621
382		592	593	598	597	617	618	623	622
383		593	594	599	598	618	619	624	623



INPUT\_CHECK - Notepad

File	Edit	Format	View	Help					
383		593	594	599	598	618	619	624	623
384		594	595	600	599	619	620	625	624
385		601	602	607	606	626	627	632	631
386		602	603	608	607	627	628	633	632
387		603	604	609	608	628	629	634	633
388		604	605	610	609	629	630	635	634
389		606	607	612	611	631	632	637	636
390		607	608	613	612	632	633	638	637
391		608	609	614	613	633	634	639	638
392		609	610	615	614	634	635	640	639
393		611	612	617	616	636	637	642	641
394		612	613	618	617	637	638	643	642
395		613	614	619	618	638	639	644	643
396		614	615	620	619	639	640	645	644
397		616	617	622	621	641	642	647	646
398		617	618	623	622	642	643	648	647
399		618	619	624	623	643	644	649	648
400		619	620	625	624	644	645	650	649
401		626	627	632	631	651	652	657	656
402		627	628	633	632	652	653	658	657
403		628	629	634	633	653	654	659	658
404		629	630	635	634	654	655	660	659
405		631	632	637	636	656	657	662	661
406		632	633	638	637	657	658	663	662
407		633	634	639	638	658	659	664	663
408		634	635	640	639	659	660	665	664
409		636	637	642	641	661	662	667	666
410		637	638	643	642	662	663	668	667
411		638	639	644	643	663	664	669	668
412		639	640	645	644	664	665	670	669
413		641	642	647	646	666	667	672	671
414		642	643	648	647	667	668	673	672
415		643	644	649	648	668	669	674	673
416		644	645	650	649	669	670	675	674
417		651	652	657	656	676	677	682	681
418		652	653	658	657	677	678	683	682
419		653	654	659	658	678	679	684	683
420		654	655	660	659	679	680	685	684
421		656	657	662	661	681	682	687	686
422		657	658	663	662	682	683	688	687
423		658	659	664	663	683	684	689	688
424		659	660	665	664	684	685	690	689
425		661	662	667	666	686	687	692	691
426		662	663	668	667	687	688	693	692
427		663	664	669	668	688	689	694	693
428		664	665	670	669	689	690	695	694
429		666	667	672	671	691	692	697	696
430		667	668	673	672	692	693	698	697
431		668	669	674	673	693	694	699	698
432		669	670	675	674	694	695	700	699
433		676	677	682	681	701	702	707	706
434		677	678	683	682	702	703	708	707
435		678	679	684	683	703	704	709	708
436		679	680	685	684	704	705	710	709
437		681	682	687	686	706	707	712	711
438		682	683	688	687	707	708	713	712

INPUT\_CHECK - Notepad

File	Edit	Format	View	Help					
438	682	683	688	687	707	708	713	712	
439	683	684	689	688	708	709	714	713	
440	684	685	690	689	709	710	715	714	
441	686	687	692	691	711	712	717	716	
442	687	688	693	692	712	713	718	717	
443	688	689	694	693	713	714	719	718	
444	689	690	695	694	714	715	720	719	
445	691	692	697	696	716	717	722	721	
446	692	693	698	697	717	718	723	722	
447	693	694	699	698	718	719	724	723	
448	694	695	700	699	719	720	725	724	
449	701	702	707	706	726	727	732	731	
450	702	703	708	707	727	728	733	732	
451	703	704	709	708	728	729	734	733	
452	704	705	710	709	729	730	735	734	
453	706	707	712	711	731	732	737	736	
454	707	708	713	712	732	733	738	737	
455	708	709	714	713	733	734	739	738	
456	709	710	715	714	734	735	740	739	
457	711	712	717	716	736	737	742	741	
458	712	713	718	717	737	738	743	742	
459	713	714	719	718	738	739	744	743	
460	714	715	720	719	739	740	745	744	
461	716	717	722	721	741	742	747	746	
462	717	718	723	722	742	743	748	747	
463	718	719	724	723	743	744	749	748	
464	719	720	725	724	744	745	750	749	
465	726	727	732	731	751	752	757	756	
466	727	728	733	732	752	753	758	757	
467	728	729	734	733	753	754	759	758	
468	729	730	735	734	754	755	760	759	
469	731	732	737	736	756	757	762	761	
470	732	733	738	737	757	758	763	762	
471	733	734	739	738	758	759	764	763	
472	734	735	740	739	759	760	765	764	
473	736	737	742	741	761	762	767	766	
474	737	738	743	742	762	763	768	767	
475	738	739	744	743	763	764	769	768	
476	739	740	745	744	764	765	770	769	
477	741	742	747	746	766	767	772	771	
478	742	743	748	747	767	768	773	772	
479	743	744	749	748	768	769	774	773	
480	744	745	750	749	769	770	775	774	

SHELL TYPE ELEMENT

ELEMENT	I END	J END	K END	L END
---------	-------	-------	-------	-------

BEAM TYPE ELEMENT

ELEMENT	I END	J END	LENGTH (mm)
1	7	32	100.00000000
2	32	57	100.00000000
3	57	82	100.00000000

INPUT\_CHECK - Notepad

File	Edit	Format	View	Help		
		3		57	82	100.00000000
		4		82	107	100.00000000
		5		107	132	100.00000000
		6		132	157	100.00000000
		7		157	182	100.00000000
		8		182	207	100.00000000
		9		207	232	100.00000000
		10		232	257	100.00000000
		11		257	282	100.00000000
		12		282	307	100.00000000
		13		307	332	100.00000000
		14		332	357	100.00000000
		15		357	382	100.00000000
		16		382	407	100.00000000
		17		407	432	100.00000000
		18		432	457	100.00000000
		19		457	482	100.00000000
		20		482	507	100.00000000
		21		507	532	100.00000000
		22		532	557	100.00000000
		23		557	582	100.00000000
		24		582	607	100.00000000
		25		607	632	100.00000000
		26		632	657	100.00000000
		27		657	682	100.00000000
		28		682	707	100.00000000
		29		707	732	100.00000000
		30		732	757	100.00000000
		31		9	34	100.00000000
		32		34	59	100.00000000
		33		59	84	100.00000000
		34		84	109	100.00000000
		35		109	134	100.00000000
		36		134	159	100.00000000
		37		159	184	100.00000000
		38		184	209	100.00000000
		39		209	234	100.00000000
		40		234	259	100.00000000
		41		259	284	100.00000000
		42		284	309	100.00000000
		43		309	334	100.00000000
		44		334	359	100.00000000
		45		359	384	100.00000000
		46		384	409	100.00000000
		47		409	434	100.00000000
		48		434	459	100.00000000
		49		459	484	100.00000000
		50		484	509	100.00000000
		51		509	534	100.00000000
		52		534	559	100.00000000
		53		559	584	100.00000000
		54		584	609	100.00000000
		55		609	634	100.00000000
		56		634	659	100.00000000
		57		659	684	100.00000000
		58		684	709	100.00000000

INPUT\_CHECK - Notepad

File	Edit	Format	View	Help
58		684		709
59		709		734
60		734		759
61		17		42
62		42		67
63		67		92
64		92		117
65		117		142
66		142		167
67		167		192
68		192		217
69		217		242
70		242		267
71		267		292
72		292		317
73		317		342
74		342		367
75		367		392
76		392		417
77		417		442
78		442		467
79		467		492
80		492		517
81		517		542
82		542		567
83		567		592
84		592		617
85		617		642
86		642		667
87		667		692
88		692		717
89		717		742
90		742		767
91		19		44
92		44		69
93		69		94
94		94		119
95		119		144
96		144		169
97		169		194
98		194		219
99		219		244
100		244		269
101		269		294
102		294		319
103		319		344
104		344		369
105		369		394
106		394		419
107		419		444
108		444		469
109		469		494
110		494		519
111		519		544
112		544		569
113		569		594

INPUT\_CHECK - Notepad

File	Edit	Format	View	Help	
113			569	594	100.00000000
114			594	619	100.00000000
115			619	644	100.00000000
116			644	669	100.00000000
117			669	694	100.00000000
118			694	719	100.00000000
119			719	744	100.00000000
120			744	769	100.00000000
121			32	33	75.00000000
122			33	34	75.00000000
123			34	39	125.00000000
124			39	44	125.00000000
125			44	43	75.00000000
126			43	42	75.00000000
127			42	37	125.00000000
128			37	32	125.00000000
129			57	58	75.00000000
130			58	59	75.00000000
131			59	64	125.00000000
132			64	69	125.00000000
133			69	68	75.00000000
134			68	67	75.00000000
135			67	62	125.00000000
136			62	57	125.00000000
137			82	83	75.00000000
138			83	84	75.00000000
139			84	89	125.00000000
140			89	94	125.00000000
141			94	93	75.00000000
142			93	92	75.00000000
143			92	87	125.00000000
144			87	82	125.00000000
145			107	108	75.00000000
146			108	109	75.00000000
147			109	114	125.00000000
148			114	119	125.00000000
149			119	118	75.00000000
150			118	117	75.00000000
151			117	112	125.00000000
152			112	107	125.00000000
153			132	133	75.00000000
154			133	134	75.00000000
155			134	139	125.00000000
156			139	144	125.00000000
157			144	143	75.00000000
158			143	142	75.00000000
159			142	137	125.00000000
160			137	132	125.00000000
161			157	158	75.00000000
162			158	159	75.00000000
163			159	164	125.00000000
164			164	169	125.00000000
165			169	168	75.00000000
166			168	167	75.00000000
167			167	162	125.00000000
168			168	167	125.00000000

INPUT\_CHECK - Notepad

File	Edit	Format	View	Help	
168			162	157	125.00000000
169			182	183	75.00000000
170			183	184	75.00000000
171			184	189	125.00000000
172			189	194	125.00000000
173			194	193	75.00000000
174			193	192	75.00000000
175			192	187	125.00000000
176			187	182	125.00000000
177			207	208	75.00000000
178			208	209	75.00000000
179			209	214	125.00000000
180			214	219	125.00000000
181			219	218	75.00000000
182			218	217	75.00000000
183			217	212	125.00000000
184			212	207	125.00000000
185			232	233	75.00000000
186			233	234	75.00000000
187			234	239	125.00000000
188			239	244	125.00000000
189			244	243	75.00000000
190			243	242	75.00000000
191			242	237	125.00000000
192			237	232	125.00000000
193			257	258	75.00000000
194			258	259	75.00000000
195			259	264	125.00000000
196			264	269	125.00000000
197			269	268	75.00000000
198			268	267	75.00000000
199			267	262	125.00000000
200			262	257	125.00000000
201			507	508	75.00000000
202			508	509	75.00000000
203			509	514	125.00000000
204			514	519	125.00000000
205			519	518	75.00000000
206			518	517	75.00000000
207			517	512	125.00000000
208			512	507	125.00000000
209			532	533	75.00000000
210			533	534	75.00000000
211			534	539	125.00000000
212			539	544	125.00000000
213			544	543	75.00000000
214			543	542	75.00000000
215			542	537	125.00000000
216			537	532	125.00000000
217			557	558	75.00000000
218			558	559	75.00000000
219			559	564	125.00000000
220			564	569	125.00000000
221			569	568	75.00000000
222			568	567	75.00000000
223			567	562	125.00000000

INPUT\_CHECK - Notepad

File	Edit	Format	View	Help			
223					567	562	125.00000000
224					562	557	125.00000000
225					582	583	75.00000000
226					583	584	75.00000000
227					584	589	125.00000000
228					589	594	125.00000000
229					594	593	75.00000000
230					593	592	75.00000000
231					592	587	125.00000000
232					587	582	125.00000000
233					607	608	75.00000000
234					608	609	75.00000000
235					609	614	125.00000000
236					614	619	125.00000000
237					619	618	75.00000000
238					618	617	75.00000000
239					617	612	125.00000000
240					612	607	125.00000000
241					632	633	75.00000000
242					633	634	75.00000000
243					634	639	125.00000000
244					639	644	125.00000000
245					644	643	75.00000000
246					643	642	75.00000000
247					642	637	125.00000000
248					637	632	125.00000000
249					657	658	75.00000000
250					658	659	75.00000000
251					659	664	125.00000000
252					664	669	125.00000000
253					669	668	75.00000000
254					668	667	75.00000000
255					667	662	125.00000000
256					662	657	125.00000000
257					682	683	75.00000000
258					683	684	75.00000000
259					684	689	125.00000000
260					689	694	125.00000000
261					694	693	75.00000000
262					693	692	75.00000000
263					692	687	125.00000000
264					687	682	125.00000000
265					707	708	75.00000000
266					708	709	75.00000000
267					709	714	125.00000000
268					714	719	125.00000000
269					719	718	75.00000000
270					718	717	75.00000000
271					717	712	125.00000000
272					712	707	125.00000000
273					732	733	75.00000000
274					733	734	75.00000000
275					734	739	125.00000000
276					739	744	125.00000000
277					744	743	75.00000000
278					743	742	75.00000000

INPUT\_CHECK - Notepad

File Edit Format View Help

278	743	742	75.00000000
279	742	737	125.00000000
280	737	732	125.00000000

-----  
BOUNDARY CONDITIONS

FIXED NODE      FIXED      DIRECTION

1	X	DIRECTON
2	X	DIRECTON
3	X	DIRECTON
4	X	DIRECTON
5	X	DIRECTON
6	X	DIRECTON
7	X	DIRECTON
8	X	DIRECTON
9	X	DIRECTON
10	X	DIRECTON
11	X	DIRECTON
12	X	DIRECTON
13	X	DIRECTON
14	X	DIRECTON
15	X	DIRECTON
16	X	DIRECTON
17	X	DIRECTON
18	X	DIRECTON
19	X	DIRECTON
20	X	DIRECTON
21	X	DIRECTON
22	X	DIRECTON
23	X	DIRECTON
24	X	DIRECTON
25	X	DIRECTON
1	Y	DIRECTON
2	Y	DIRECTON
3	Y	DIRECTON
4	Y	DIRECTON
5	Y	DIRECTON
6	Y	DIRECTON
7	Y	DIRECTON
8	Y	DIRECTON
9	Y	DIRECTON
10	Y	DIRECTON
11	Y	DIRECTON
12	Y	DIRECTON
13	Y	DIRECTON
14	Y	DIRECTON
15	Y	DIRECTON
16	Y	DIRECTON
17	Y	DIRECTON
18	Y	DIRECTON
19	Y	DIRECTON
20	Y	DIRECTON
21	Y	DIRECTON
22	Y	DIRECTON
23	Y	DIRECTON
24	Y	DIRECTON

INPUT\_CHECK - Notepad

File Edit Format View Help

24	Y	DIRECTON
25	Y	DIRECTON
751	X	DIRECTON
752	X	DIRECTON
753	X	DIRECTON
754	X	DIRECTON
755	X	DIRECTON
756	X	DIRECTON
757	X	DIRECTON
758	X	DIRECTON
759	X	DIRECTON
760	X	DIRECTON
761	X	DIRECTON
762	X	DIRECTON
763	X	DIRECTON
764	X	DIRECTON
765	X	DIRECTON
766	X	DIRECTON
767	X	DIRECTON
768	X	DIRECTON
769	X	DIRECTON
770	X	DIRECTON
771	X	DIRECTON
772	X	DIRECTON
773	X	DIRECTON
774	X	DIRECTON
775	X	DIRECTON
751	Y	DIRECTON
752	Y	DIRECTON
753	Y	DIRECTON
754	Y	DIRECTON
755	Y	DIRECTON
756	Y	DIRECTON
757	Y	DIRECTON
758	Y	DIRECTON
759	Y	DIRECTON
760	Y	DIRECTON
761	Y	DIRECTON
762	Y	DIRECTON
763	Y	DIRECTON
764	Y	DIRECTON
765	Y	DIRECTON
766	Y	DIRECTON
767	Y	DIRECTON
768	Y	DIRECTON
769	Y	DIRECTON
770	Y	DIRECTON
771	Y	DIRECTON
772	Y	DIRECTON
773	Y	DIRECTON
774	Y	DIRECTON
775	Y	DIRECTON
11	Z	DIRECTON
12	Z	DIRECTON
13	Z	DIRECTON
14	Z	DIRECTON



INPUT\_CHECK - Notepad

File Edit Format View Help

14 Z DIRECTON  
15 Z DIRECTON

NODAL LOADS				
NODE	LOADING TYPE	DIRECTION	P	M
			N	Nmm
273	CONCENTRATED P	GLOBAL Y	-.4000E+06	
523	CONCENTRATED P	GLOBAL Y	-.4000E+06	

CurrentCompressionPlasticityParameter 0.00000000000000E+000  
CurrentTensionPlasticityParameter 0.00000000000000E+000  
CurrentCompressionDamageParameter 0.00000000000000E+000  
CurrentTensionDamageParameter 0.00000000000000E+000

-----  
-----  
Number of Integration Points for Solid 3

Number of Integration Points for Reinforcement 2

Number of Integration Points for FRP Wrap 2

Analysis Control type: Enter 1 for Load Control or Enter 2 for Displacement Control  
2

The control node number 273

Direction: 1 for X | 2 for Y | 3 for Z | 4 for XRot | 5 for YRot | 6 for XRot  
Control direction = 2 selected

Enter the step increment size -0.4000000000000000

How many steps do you want to continue 140

-----  
-----  
Plastic return type: 1 for Cutting plane | 2 for Closest Point Projection  
1

Tangent Modulus: Enter 0 for Elastic Enter 1 for Elasto-plastic  
1

Iteration limit for plasticity algorithm incase it does not converge  
1000

-----  
-----  
0 For rate-independent | 1 For visco-plastic | 2 For viscous regularization  
0

<

```

INPUT_CHECK - Notepad
File Edit Format View Help
Enter number of steps for every graphical output      10
Enter amplification factor for graphical output 100.000000000000

The results are produced only for      2 files

The results are produced for Lamda.DAC

The results are produced for U_Y.DAC
Enter GlobalAlgorithm_ErrorMargin 9.99999974752427E-007
-----
Enter PlasticityAlgorithm_ErrorMargin 9.999999747378752E-005
-----
Number of cycles      1
C_type=      1
Number of steps in each cycles      1000
-----
ASR Volumetric strain = 0.000000000000000E+000
Contribution of ASR strain on the effective stress = 0.000000000000000E+000
Correlation of tension damage to compression damage 0.000000000000000E+000
-----
New Run is performed
-----

MPC CONSTRAINTS
  MASTER NOD   CONNECTED DOF   SLAVE NOD
    273         2         251
    273         2         252
    273         2         253
    273         2         254
    273         2         255
    273         2         256
    273         2         257
    273         2         258
    273         2         259
    273         2         260
    273         2         261
    273         2         262
    273         2         263
    273         2         264
    273         2         265
    273         2         266
    273         2         267
    273         2         268
    273         2         269
    273         2         270
    273         2         271
    273         2         272

```

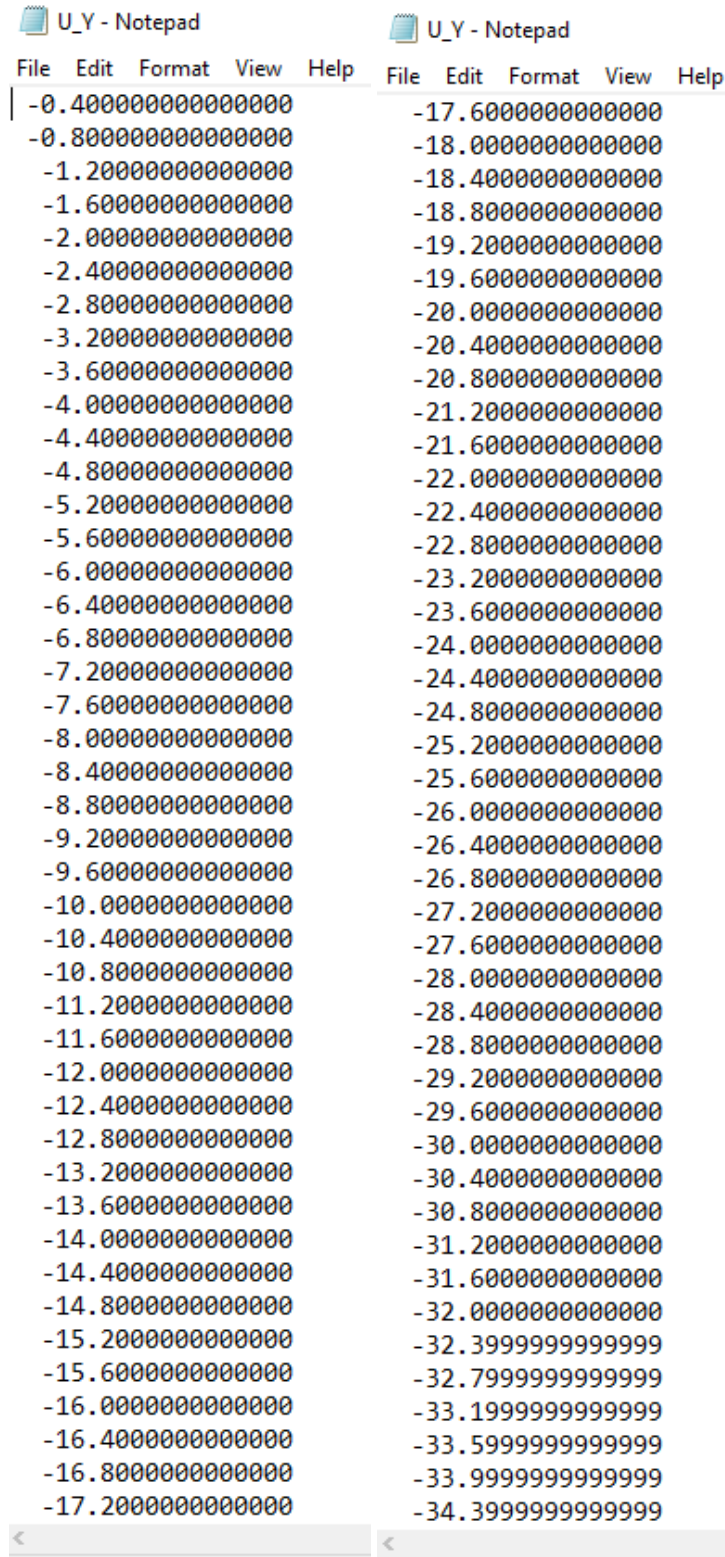
```

INPUT_CHECK - Notepad
File Edit Format View Help
273      2      255
273      2      256
273      2      257
273      2      258
273      2      259
273      2      260
273      2      261
273      2      262
273      2      263
273      2      264
273      2      265
273      2      266
273      2      267
273      2      268
273      2      269
273      2      270
273      2      271
273      2      272
273      2      274
273      2      275
523      2      501
523      2      502
523      2      503
523      2      504
523      2      505
523      2      506
523      2      507
523      2      508
523      2      509
523      2      510
523      2      511
523      2      512
523      2      513
523      2      514
523      2      515
523      2      516
523      2      517
523      2      518
523      2      519
523      2      520
523      2      521
523      2      522
523      2      524
523      2      525
-----
No further ASR loading
A_WEIGHT 0.000000000000000E+000
-----
No Smoothing

```

### A1.3.3. Output files

U\_Y



The image shows two Notepad windows side-by-side, both titled "U\_Y - Notepad". Each window has a menu bar with "File", "Edit", "Format", "View", and "Help". The left window contains a list of 35 numerical values starting from -0.4000000000000000 and increasing by 0.4 up to -17.2000000000000000. The right window contains a list of 34 numerical values starting from -17.6000000000000000 and increasing by 0.4 up to -34.3999999999999999. The values in the right window are rounded to 9 decimal places.

Window	Line	Value
U_Y - Notepad (Left)	1	-0.4000000000000000
	2	-0.8000000000000000
	3	-1.2000000000000000
	4	-1.6000000000000000
	5	-2.0000000000000000
	6	-2.4000000000000000
	7	-2.8000000000000000
	8	-3.2000000000000000
	9	-3.6000000000000000
	10	-4.0000000000000000
	11	-4.4000000000000000
	12	-4.8000000000000000
	13	-5.2000000000000000
	14	-5.6000000000000000
	15	-6.0000000000000000
	16	-6.4000000000000000
	17	-6.8000000000000000
	18	-7.2000000000000000
	19	-7.6000000000000000
	20	-8.0000000000000000
	21	-8.4000000000000000
	22	-8.8000000000000000
	23	-9.2000000000000000
	24	-9.6000000000000000
	25	-10.0000000000000000
	26	-10.4000000000000000
	27	-10.8000000000000000
	28	-11.2000000000000000
	29	-11.6000000000000000
	30	-12.0000000000000000
	31	-12.4000000000000000
	32	-12.8000000000000000
	33	-13.2000000000000000
	34	-13.6000000000000000
	35	-14.0000000000000000
U_Y - Notepad (Right)	1	-17.6000000000000000
	2	-18.0000000000000000
	3	-18.4000000000000000
	4	-18.8000000000000000
	5	-19.2000000000000000
	6	-19.6000000000000000
	7	-20.0000000000000000
	8	-20.4000000000000000
	9	-20.8000000000000000
	10	-21.2000000000000000
	11	-21.6000000000000000
	12	-22.0000000000000000
	13	-22.4000000000000000
	14	-22.8000000000000000
	15	-23.2000000000000000
	16	-23.6000000000000000
	17	-24.0000000000000000
	18	-24.4000000000000000
	19	-24.8000000000000000
	20	-25.2000000000000000
	21	-25.6000000000000000
	22	-26.0000000000000000
	23	-26.4000000000000000
	24	-26.8000000000000000
	25	-27.2000000000000000
	26	-27.6000000000000000
	27	-28.0000000000000000
	28	-28.4000000000000000
	29	-28.8000000000000000
	30	-29.2000000000000000
	31	-29.6000000000000000
	32	-30.0000000000000000
	33	-30.4000000000000000
	34	-30.8000000000000000
35	-31.2000000000000000	
36	-31.6000000000000000	
37	-32.0000000000000000	
38	-32.3999999999999999	
39	-32.7999999999999999	
40	-33.1999999999999999	
41	-33.5999999999999999	
42	-33.9999999999999999	
43	-34.3999999999999999	

# Lamda

Lamda - Notepad					Lamda - Notepad				
File	Edit	Format	View	Help	File	Edit	Format	View	Help
1.	744498814446482E-002				0.	107044739355935			
2.	692103819204879E-002				0.	108447783048950			
3.	251127129821774E-002				0.	109913876022766			
3.	659991751691873E-002				0.	111313974100190			
3.	950245430382231E-002				0.	112770912396734			
4.	196302121652758E-002				0.	114181409830162			
4.	433960616369986E-002				0.	115619724618058			
4.	666172938179439E-002				0.	117008591146658			
4.	893456010316080E-002				0.	118473873722783			
5.	115284760170831E-002				0.	119852281889457			
5.	334357580522630E-002				0.	121311786768985			
5.	548551010975797E-002				0.	122675840256735			
5.	726102655929892E-002				0.	124131501102614			
5.	891716701402835E-002				0.	125510120270440			
6.	055237486985624E-002				0.	126940069855015			
6.	217201423718734E-002				0.	128310276779950			
6.	377711843443569E-002				0.	129746720553124			
6.	537481370358063E-002				0.	131122575112253			
6.	695730825954122E-002				0.	132545054689177			
6.	853918463781056E-002				0.	133920781027581			
7.	008478993078962E-002				0.	135342853124630			
7.	162136866864716E-002				0.	136707802752236			
7.	314732167664331E-002				0.	138128366989171			
7.	469164161523466E-002				0.	139476257784828			
7.	621336008615585E-002				0.	140908866010611			
7.	773022635938807E-002				0.	142240402226569			
7.	921336616666119E-002				0.	143675605376452			
8.	072925706049619E-002				0.	144991010141916			
8.	220229779419128E-002				0.	146421127279070			
8.	367970072731845E-002				0.	147746781479762			
8.	517723067393550E-002				0.	149165845275052			
8.	666481728827077E-002				0.	150487090465904			
8.	814326938487130E-002				0.	151904232681837			
8.	959728574623819E-002				0.	153213821924986			
9.	107252333594330E-002				0.	154631657821385			
9.	253324126940481E-002				0.	155960006286652			
9.	399957493542889E-002				0.	157353600332789			
9.	544462944729035E-002				0.	158683241380335			
9.	689540265581779E-002				0.	160068397509881			
9.	836983339253071E-002				0.	161388730216399			
9.	980217088730557E-002				0.	162778731722319			
0.	101264935333923				0.	164107144155913			
0.	102698065397792				0.	165478552913535			